AD-763 338

PHYSICS AND CHEMISTRY OF GLASSES

NAVAL RESEARCH LABORATORY

PREPARED FOR
ADVANCED RESEARCH PROJECTS AGENCY

MAY 1973

NRL Memorandum Report 2590

Physics and Chemistry of Glasses

Robert J. Ginther and Russell D. Kirk
Central Materials Research Activity

John H. Konnert, George A. Ferguson, and Jerome Karle
Laboratory For The Structure of Matter

Stephen G. Bishop, David L. Griscom, and Dean L. Mitchell,
Anthony R. Ruffa, George H. Sigel, Jr., and P. Craig Taylor
Solid State Division

May 1973

NAVAL RESEARCH LABORATORY
Washington, D.C.

DOCUMENT CONTROL DATA - R & D

(Security classification of title, body of abstract and indexing annotation must be entered when the overall report is classified)

1. ORIGINATING ACTIVITY (Corporate author) Naval Research Laboratory Washington, D.C. 20375	2a. REPORT SECURITY CLASSIFICATION UNCLASSIFIED 2b. GROUP ---

3. REPORT TITLE

PHYSICS AND CHEMISTRY OF GLASSES

4. DESCRIPTIVE NOTES (Type of report and inclusive dates)

A final report.

5. AUTHOR(S) (First name, middle initial, last name)

Robert J. Ginther, Russell D. Kirk, John H. Konnert, George A. Ferguson, Jerome Karle, Stephen G. Bishop, David L. Griscom, Dean L. Mitchell, Anthony R. Ruffa, George H. Sigel, Jr., and P. Craig Taylor

6. REPORT DATE May 1973	7a. TOTAL NO. OF PAGES ~~214~~ 215	7b. NO. OF REFS 231

8a. CONTRACT OR GRANT NO. NRL Problem 64P03-07A b. PROJECT NO. ARPA Order No. 2029 (Formerly 418) c. Program Code No. 2D10 Program Element Code: 61101D d.	9a. ORIGINATOR'S REPORT NUMBER(S) NRL Memorandum Report 2590 9b. OTHER REPORT NO(S) (Any other numbers that may be assigned this report)

10. DISTRIBUTION STATEMENT

Approved for public release; distribution unlimited.

11. SUPPLEMENTARY NOTES	12. SPONSORING MILITARY ACTIVITY Advanced Research Projects Agency Washington, D.C. 20301

13. ABSTRACT

This report is a summary of glass research undertaken during a five year period (1967-72) under the sponsorship of the Advanced Research Projects Agency. Research areas which are reviewed include structure of glasses, synthesis and preparation of glasses, electronic structure of silica, ultraviolet spectra of silicate glasses, electron spin resonance in borate glasses, structural and electrical properties of chalcogenide glasses and ion bombardment effects on the strength of glass.

14 KEY WORDS	LINK A		LINK B		LINK C	
	ROLE	WT	ROLE	WT	ROLE	WT
Glass						
Structure of glass						
Radiation damage						
Optical properties						
Glass preparation						
Electron spin resonance						
Chalcogenide						
Ion implantation						

CONTENTS

Abstract ii
Foreword by J. H. Schulman iii

Paper I Effects of Impurities and Synthesis Atmosphere Upon the Optical Properties of Some Glasses 1

Paper II Diffraction Evidence for Tridymite-Like Ordering In Silica and Germania Glasses 35

Paper III Ultraviolet Spectra of Silicate Glasses - A Review of Some Experimental Evidence 42

Paper IV Models for Electronic Processes in SiO_2 89

Paper V ESR Studies of Radiation-Damage and Structure in Oxide Glasses: A Contemporary Overview With Illustrations From the Alkali Borate System 114

Paper VI Structural and Electrical Properties of Chalcogenide Glasses 169

Paper VII The Effects of Ion Implantation on the Strength of Fused Silica 199

ABSTRACT

This report is a summary of glass research undertaken during a five year period (1967-72) under the sponsorship of the Advanced Research Projects Agency. Research areas which are reviewed include structure of glasses, synthesis and preparation of glasses, electronic structure of silica, ultraviolet spectra of silicate glasses, electron spin resonance in borate glasses, structural and electrical properties of chalcogenide glasses and ion bombardment effects on the strength of glass.

PROBLEM STATUS

Final Report

AUTHORIZATION

NRL Problem P03-07A
Project ARPA Order 2029
(Formerly ARPA Order 418)

FOREWORD

In asking ARPA to help initiate a major program of glass study at NRL in 1966, it was pointed out that "the challenging scientific questions involved in the structure of glass and the tremendous technological potential of glassy materials justify a greatly increased national level of research effort on non-periodic solids...Glass has an enormous range of properties, which can be combined and varied almost at will; moreover it can be fabricated in virtually any size or shape and formed to any degree of precision that may be desired... Within the past decade or two a transformation has begun on the traditional view of glass as a fragile and brittle material, useful primarily because of its transparency and chemical inertness. Research on the chemistry and physics of glass has shown that an astonishing variety of electronic, chemical, and physical changes can be initiated and controlled to produce materials with a wide variety of interesting properties--photosensitivity, luminescence, electronic conductivity, and even flexibility... The full potential of glass is a long way from being realized, progress is far slower than in the field of crystalline materials; this is due, in part, to the relatively small number of organizations and individuals engaged in research on non-periodic solids".

ARPA support of this proposal permitted the Laboratory to mount a substantial research effort on the relationship of the optical and spectroscopic properties of inorganic oxide-based glasses to their composition and structure. A comprehensive approach to these problems was undertaken with a research team that included synthetic inorganic and analytical chemists, and experimental and theoretical physicists--all of whom had been thoroughly familiar with basic concepts derived from studies of color centers and luminescence of crystalline solids, among them ultra-high purity preparation and careful characterization of samples.

This report summarizes most of the results of the six year ARPA-sponsored research program, which began with the demonstration that the near-ultraviolet absorption of ordinary silicate glasses was an extrinsic phenomenon due to alliovalent impurities, principally iron. These studies have been extended to other problems of the glassy state year by year, and have culminated in the recent finding that silica (and perhaps all other) glass is much more ordered than has generally been believed, and that this glass consists of micro-crystalline regions of at least 20A in dimensions having the trydimite structure. In between these investigations lay many that shed light on the spectroscopy of oxide glasses, on their radiation-sensitivity and the radiation-induced centers produced in them, on their mechanical properties, and on the structure and electrical properties of chalcogenide glasses.

The reports by others in 1969 of switching and memory effects in chalcogenide glasses touched off feverish interest in the glassy state of matter by technologists and theoretical physicists alike--confirming NRL's assessment of the scientific challenges and technical promise of the glassy state. Glass and glassy-state phenomena are now recognized by the broad scientists community as challenging scientific problems, and research on these subjects is much more widespread and sophisticated. We are grateful for ARPA's support in the days when this had not yet come to pass.

J. H. SCHULMAN
Deputy Director of Research

EFFECTS OF IMPURITIES AND SYNTHESIS ATMOSPHERE UPON THE OPTICAL PROPERTIES OF SOME GLASSES

R. J. Ginther and R. D. Kirk

ABSTRACT

The effect of impurities upon the ultraviolet absorption of silicate glasses has been investigated. Differences in ultraviolet absorption of soda-silica glass as a function of the melting atmosphere are shown to be due to a valence change of iron impurity. In samples of low iron content not exhibiting this difference, other absorbing impurities have been identified from their luminescence properties. Copper and sulfur are shown to produce yellow luminescence in glass melted in reducing atmospheres, and Pt^{4+} has been identified as the source of red luminescence in glass melted in air in platinum crucibles. The study of platinum crucible corrosion by glass has been extended to laser glasses. Corrosion is shown to be a function of both the melting atmosphere and the glass composition and a new laser glass has been developed which is particularly resistant to platinum contamination. Preliminary results of the development of colorless, devitrification-resistant aluminate glasses are presented.

INTRODUCTION

Oxide type glasses have useful transmission in the wavelength range of about 180 nm to about 5μm. Their high softening temperatures, structural strength, and relative ease of fabrication in suitable sizes and shapes make them preferred materials for many applications. For the shortest wavelengths of this range, fused silica alone is employed, but its very high melting temperature with attendant high fabrication cost and size limitations favors the use of more complex glasses of lower melting temperature whenever possible. The latter materials generally exhibit a short wavelength absorption edge near 320 nm. While a significant portion of the poorer transmission of the complex glasses is caused by absorption due to nonbridging oxygen ions introduced by the alkali and alkaline earth ions used as fluxes or glass modifiers (1), impurity ions also contribute to the increased absorption. In the infrared region the transmission of silicate glasses generally does not extend beyond about 4 μm because of a vibrational absorption of the silica component. The use of either germanium oxide or alumina as the glass former in place of silica extends the useful transmission to around 5 μm. However, in oxide glasses the presence of hydroxyl groups produces the OH^- absorption band at about 3 μm. The influence of other common impurities upon transmission in this wavelength range does not seem to have been reported.

Fused silica having good transmission at wavelengths shorter than about 200 nm is a very pure material, but complex glasses are generally much less pure. For applications of the latter materials which require a high purity such as ultraviolet transmitting glasses, glass fibers for optical communications, scintillators, dosimeters, and lasers, pure glass synthesis is complicated by the necessity of obtaining a relatively large number of pure raw materials, most of which are not as readily purified as is silica. Consequently, whenever possible, studies of the role of impurities upon the optical properties of glass are made with a simple model glass such as soda-silica in order to simplify preparation problems, However, in the development of optical glasses for practical applications more complex glasses are required in order to obtain optimum properties and insure chemical durability. In the latter case the severe raw material purification problem cannot be avoided, and the preparations obtained are seldom as pure as those of the model glass.

Impurities can be introduced into glass preparations from the melting atmosphere and crucible as well as from the raw materials. Platinum is the most inert crucible material for silicate glasses, but melts made in such crucibles can be contaminated not only by platinum, but by impurities in the crucible such as iron and copper. Unpurified air atmospheres are a further source of contamination. Copper is reported to be a common contaminant from air (2), and water vapor in air is of concern in the preparation of infrared transmitting glasses. Another source of contamination in glass synthesis is impurities evolved from hot furnace ceramics. Contamination from hot ceramics can be minimized by using a locally heated system such as a cold wall induction furnace which employs the platinum melting crucible as a susceptor. Such a furnace also permits a choice of melting atmospheres. Its disadvantage is a crucible temperature which is generally higher than the temperature needed to melt the glass, a system which favors glass contamination by the crucible.

The detection and determination of trace impurities responsible for deleterious absorption in glass is a formidable problem. In a succeeding section it will be shown that Fe^{3+} and Cu^{+} in the fractional ppm range affect the ultraviolet absorption of sode-silica glass, and the tolerable levels for contaminants such as Cu, Fe, Ni, Cr, and Co in glass fiber optical waveguides have been set in the 0.05 - 0.002 ppm range (2). Methods for trace element determination in glass have been reviewed (3) and include colorimetric chemical analysis, emission and spark source mass spectrometry, electron spin resonance, and nuclear activation analysis. A general qualitative analysis by any method is seldom useful for the identification of impurities in the range of interest. A more successful procedure is to make an assumption that a particular ion is the source of an unwanted optical property, based usually on available information derived from the properties of glasses heavily doped with that ion, to set up a sensitive method for its determination, and to compare the optical properties of the glass of interest with a series of pure glasses doped with low concentrations of the suspected impurity.

In the following sections work related to the synthesis of pure glasses and the identification of the optical properties due to trace impurities are reviewed. Interest in pure glasses originated in an earlier program of the development of glass scintillators (4). In this work melting in a reducing atmosphere was required in order to maintain a cerium activator as the Ce^{3+} ion, and a superior ultraviolet transmission of the undoped base glass was noted when melting was conducted in the reducing atmosphere rather than in air. In later work with a thermoluminescent dosimeter glass the same improvement in transmission of the base glass was obtained as a function of the melting atmosphere, and best thermoluminescent response of the doped glass was found with reducing atmosphere melts even though the glass, a terbium activated lithium aluminosilicate, had no deliberately added components whose valence would be affected by the melting atmosphere (5). These observations were the occasions for the study of the effect of melting atmospheres on a soda-silica glass and the identification of the impurities responsible for its atmosphere dependent properties. The identification of platinum as one of these impurities combined with the known ability of platinum particles to damage laser glass led to a study of the platinum contamination of this material and the development of an essentially platinum-free laser glass. The final section reports some results of a present program concerned with aluminate glasses. These glasses are of interest for their transmission in the 3-5 μm region, and because they exhibit a particularly severe problem of platinum contamination.

SODA-SILICA GLASSES

The difference in the ultraviolet transmission of glass as a function of the melting atmosphere noted previously has been observed by others and two explantions have been proposed. Hensler (6) suggested that excess oxygen in the form of peroxide and superoxide ions produced by melting in oxidizing atmospheres contributes an absorption in the ultraviolet. An alternate explanation is that the difference may be connected with the oxidation state of metallic impurities (7). This is based on the fact that both the positions and extinction coefficients of transition metal ion absorptions are determined by their valence states. A clear choice between these explantions had not been possible since available preparations had not been of sufficient purity to establish the intrinsic absorption spectrum of the glass. Accordingly the study of the optical properties of a pure 1.0 Na_2O - 3.0 SiO_2 glass has been made (8).

Samples were prepared by melting both in air and reducing atmospheres. The raw materials used were recrystallized reagent grade Na_2CO_3 and SiO_2 prepared by the hydrolysis of ethylorthosilicate. The iron contents of most preparations of these materials were in the range of 0.5 ppm by wt. as determined by colorimetric analysis. Both undoped glasses and glasses doped with from 1.0 - 1000 ppm of iron were melted under both oxidizing and reducing conditions in platinum crucibles and their absorption spectra measured. Ferric ion content of the doped glasses was determined from EPR measurements, and the Fe^{3+} content of the undoped air melted glass was obtained from both the EPR and optical absorption spectra. Further experimental details are contained in Ref. (8).

Figures 1 and 2 illustrate the absorption spectra of the glasses melted in air and in the reducing atmosphere. Stronger absorption in the air melted glasses is evident, even in the undoped samples. Iron absorption in the air melted glasses is due to a Fe^{3+} band peaking at about 225 nm. The absorption in the glasses melted in the reducing atmosphere is from both Fe^{2+} and Fe^{3+} ions. From EPR data it was possible to determine the Fe^{3+} content of the reduced glasses and obtain the molar extinction coefficients for both Fe^{2+} and Fe^{3+} ions. By subtracting the Fe^{3+} contribution from the absorption spectra of the reduced glasses and the base glass contributions from the spectra of the glasses melted in both atmospheres, the absorption of both Fe^{2+} and Fe^{3+} ions and their molar extinction coefficients were obtained as shown in Fig. 3 The optical absorption and EPR data employed in obtaining the above results are in Table I.

Both EPR and absorption data indicated a Fe^{3+} content of about 6 ppm in the undoped air melted glass despite the fact that the iron content of the raw materials predicted a much lower concentration. A much purer air melted sample was obtained from carefully prepared raw materials which were subsequently handled very carefully in blending and then melted only one hour in a cold wall induction furnace. Iron could not be detected in this glass by either optical absorption, EPR, or with a spark source mass spectrograph operated with an iron background of 0.2 ppm. The absorption spectrum of this sample together with the spectra of earlier air melted glass and glass melted in the reducing atmosphere are shown in Fig. 4. The absorption of the air melted and reduced glasses are identical.

The above results indicate that the ultraviolet absorption of pure soda-silica glass is independent of the melting atmosphere and that previously measured differences can be attributed to a variation of the valence state of impurities. While a number of transition metal ions might be expected to produce an absorption variation as a function of melting atmosphere if present in sufficient concentration, iron appears to be the only impurity encountered which produced a measurable absorption difference.

The above observation is based on transmission measurements of samples of up to a few millimeters in thickness. However, in even the purest samples, the presence of other absorbing ions was demonstrated by a very weak luminescence under ultraviolet light. The identity of the impurities responsible for this luminescence has been revealed by comparing the optical properties of the pure samples with those of samples deliberately doped with ions suspected to be the luminescence sources (9).

Fig. 5 shows the emission spectra of soda-silica glass melted both in air and in a reducing atmosphere. The red luminescence in the air melted sample is due to platinum. It was obtained with only samples melted in platinum crucibles or with glasses melted in ceramic crucibles with deliberate platinum doping. Luminescence in glass due to platinum had been reported previously (10), but the valence state of the platinum ion had not been determined. The points superimposed on the spectrum of the air melted glass represent the emission of a preparation of K_2PtCl_6, the luminescence of which was first reported by Douglas et. al. (11). The exact coincidence of the spectra leads to the conclusion that the red luminescence of the glass is due and EPR data employed in obtaining the above results are in Table I.

Both EPR and absorption data indicated a Fe^{3+} content of about 6 ppm in the undoped air melted glass despite the fact that the iron content of the raw materials predicted a much lower concentration. A much purer air melted sample was obtained from carefully prepared raw materials which were subsequently handled very carefully in blending and then melted only one hour in a cold wall induction furnace. Iron could not be detected in this glass by either optical absorption, EPR, or with a spark source mass spectrograph operated with an iron background of 0.2 ppm. The absorption spectrum of this sample together with the spectra of earlier air melted glass and glass melted in the reducing atmosphere are shown in Fig. 4. The absorption of the air melted and reduced glasses are identical.

The above results indicate that the ultraviolet absorption of pure soda-silica glass is independent of the melting atmosphere and that previously measured differences can be attributed to a variation of the valence state of impurities. While a number of transition metal ions might be expected to produce an absorption variation as a function of melting atmosphere if present in sufficient concentration, iron appears to be the only impurity encountered which produced a measurable absorption difference.

The above observation is based on transmission measurements of samples of up to a few millimeters in thickness. However, in even the purest samples, the presence of other absorbing ions was demonstrated by a very weak luminescence under ultraviolet light. The identity of the impurities responsible for this luminescence has been revealed by comparing the optical properties of the pure samples with those of samples deliberately doped with ions suspected to be the luminescence sources (9).

Fig. 5 shows the emission spectra of soda-silica glass melted both in air and in a reducing atmosphere. The red luminescence in the air melted sample is due to platinum. It was obtained with only samples melted in platinum crucibles or with glasses melted in ceramic crucibles with deliberate platinum doping. Luminescence in glass due to platinum had been reported previously (10), but the valence state of the platinum ion had not been determined. The points superimposed on the spectrum of the air melted glass represent the emission of a preparation of K_2PtCl_6, the luminescence of which was first reported by Douglas et. al. (11). The exact coincidence of the spectra leads to the conclusion that the red luminescence of the glass is due to the Pt^{4+} ion.

The contaminant suspected as the source of the yellow luminescence of the glass melted under reducing conditions was copper. Copper doped samples were found to have similar emission spectra, but the spectra were broad and had no unique features which would make an identification based on this property alone convincing. Copper doped samples melted in reducing atmospheres were more efficient than those melted in air, demonstrating that the luminescent activator was the Cu^{+} ion in agreement with the work of Karapetyan (12). Further corroboration of the role of the Cu^{+} ion as an activator of the yellow luminescence of the undoped glass was obtained from the excitation spectra of Fig. 6.

The main excitation of the undoped glass and of the samples doped with up to 10^{-5} Cu is in a band which is still increasing at 240 nm, the wavelength limit of the measuring equipment (9). This confirms the identification of copper as a source of the yellow luminescence, but the small peak at 285 nm is not due to copper, and the shift of the main excitation peak to shorter wavelengths with the higher copper concentrations was unexpected.

The shift of the excitation peak and the saturation of the emission intensity with increasing copper content shown in Fig. 6 are due to the presence of Cu^{2+} ions. This was determined from the absorption spectra of Figs. 7 and 8. In the air melted glass, Cu^{2+} ion is seen to produce an absorption with a peak at about 235 nm, and this peak is present in the spectra of the glasses melted in the reducing atmosphere whose copper concentrations are those of the samples exhibiting the shift of the excitation peak. The Cu^{2+} ion absorbs the shorter wavelength ultraviolet in the excitation measurement without producing luminescence, rendering the longer wavelengths relatively more effective in exciting the glass and producing a shift of the measured peak. The ultraviolet absorption spectra of Cu^{+} and Cu^{2+} ions are remarkably similar to those of Fe^{2+} and Fe^{3+} ions, suggesting that the absorbing centers are similar complex species involving ions of the matrix glass.

The copper content of the undoped glass was obtained from determinations made with colorimetry, mass spectrographic analysis, and from electron spin resonance which detects on Cu^{2+} ions. Results are shown in Table II. The higher copper content of the air melted glass is believed to be due to greater contamination suffered in the melting process. Copper contamination of glass melts from impurities in platinum crucibles was found to be more severe in oxidizing than in reducing atmospheres.

The impurity responsible for the 285 nm excitation peak proved to be sulfur. Sulfur doping of soda-silica glass produced a yellow luminescence, and the excitation spectra of Fig. 9 clearly show the 285 nm excitation peak to be a function of sulfur concentration. Preparation conditions, doping with sodium sulfate and melting in a reducing atmosphere, suggests that the luminescent center is the S^{2-} ion. This ion has not been previously reported as an activator of luminescence. The S_2^- ion is known as a luminescent activator of both glass and crystals (13), but this ion produces a very different emission spectrum and requires a much higher doping level in glass than the concentration which would be present in the rather pure soda-silica samples.

A limited amount of work with more complex alkali, alkaline earth silicate and aluminosilicate glasses demonstrated the copper and platinum contamination of these materials as well. When melted in a reducing atmosphere the undoped alkali, alkaline earth silicates luminesced yellow and the aluminosilicates blue. Both these emissions were from copper impurities. A luminescence due to sulfur was not found. Air melting all these glasses in platinum crucibles produced the red luminescence of the Pt^{4+} ion. Subsequent remelting of air melted samples in a reducing atmosphere produced gray glasses containing metallic platinum particles, suggesting that reduction of dissolved ionic platinum can be a source of metallic platinum particles in laser and other optical glasses.

LASER GLASSES

While platinum is widely used as a container material in glass melting, it is recognized that this practice can result in contamination of the glass by platinum particles (14). These platinum particles have been found to have a destructive effect in the Q-switched operation of laser glass, and extensive programs for the production of platinum-free laser glass have been pursued (15). It has been shown that the most important contaminating mechanism is the atmospheric oxidation of the platinum crucible followed by a vapor phase transport and reduction of the platinum oxide to produce platinum particles in the melt (15). In addition the reversible solution and reprecipitation of platinum particles in a glass melt has been reported (16).

Laser glass is currently melted in platinum in a nitrogen atmosphere, and available inspection techniques cannot detect platinum particles in this product. However, this glass has been found to contain from 2-5 ppm of platinum. Undoubtedly the most of this platinum is present as PtO_2 dissolved in the glass and is innocuous in laser operation. Analytical procedures are not able to distinguish between oxidized and metallic platinum in glass, so that the preparation of material with a much lower total platinum content would provide greater assurance of the absence of damaging platinum particles. The work described in the last section showed that air melting of soda-silica glass produced dissolved platinum with attendant luminescence, but that melting in a reducing atmosphere did not. Moreover, mass spectrographic analysis, sensitive to 50 ppb of platinum was unable to detect this element in bulk portions of the glass melted in the reducing atmosphere. Accordingly the application of this melting technique to laser glass has been pursued (17).

Samples of commercial-type aluminosilicate and barium crown glasses were melted in nonoxidizing atmospheres in the cold wall induction furnace, and while the inner or bulk portions were platinum free, the surfaces were contaminated with deposits of bright lacy platinum consistent with the reported appearance of platinum contamination resulting from the crucible oxidation mechanism (15). The melts were not stirred, but in a production process these deposits would be stirred into the glass to produce damaging particles. While such deposits had not been noticed on soda-silica glass, careful examination of this material revealed similar platinum contamination. The results of melting the laser glasses are shown in Table III.

The lesser contamination of the barium crown glass as compared to the aluminosilicate indicated an effect of the glass composition, and this effect was corroborated by subsequent work with an alkali-free aluminosilicate and with soda-silica glass. The results are shown in Table IV. This table indicates that the simple elimination of alkali will not provide a solution to the contamination problem, but that contamination can probably be avoided by maintaining a high ratio of silica to alkaline components if the glass can be melted at 1400°C. However, the 1:5 and 1:6 soda-silica glasses did not produce uniform glass at even the 1500°C melting temperature.

The lacy nature of the platinum deposits combined with their dependence upon the glass composition and melting temperature suggests that the contaminating mechanism is the oxidation process, but that oxygen can be contributed to the atmosphere by dissociable volatile components of the glass melt. In the glasses prepared these components are the alkali and alkaline earth oxides whose relative volatility and stability are associated with the melting and boiling points and free energies of formation shown in Tables V and VI. The available data suggested that increasing volatility and decreasing stability of vapor are in the order (MgO + CaO), SrO, BaO, Li_2O, Na_2O, K_2O. This order plus the importance of the total concentration of alkaline components learned from the soda-silica glasses permits an interpretation of the contamination of the complex laser glasses. The composition of these glasses and the ratio of the alkaline to the acidic components are shown in Table VII. While the aluminosilicate glasses contain desirable alkaline components, the ratio of alkaline to acidic materials is very high. The barium crown glass has a much more favorable ratio, but employs more volatile and less stable alkaline compounds. Potassium is probably particularly harmful.

Work with the soda-silica glasses suggested that contamination could be minimized in a glass having an alkaline to acidic component ratio of 1·5 if this glass could be melted at 1400°C. The development of a laser glass of this ratio therefore was undertaken with the assumption that such a glass would require a relatively large number of components in order to achieve the low melting temperature. Synthesis was restricted to the use of those alkali and alkaline earth compounds expected to be least volatile and most stable and proceeded with the compositions of Table VIII.

In glass number 1, the ratio of total alkali oxide to alkaline earth oxide was chosen as 1:4 in the expectation that a low melting point would be favored by a high proportion of alkali oxide. The known tendency of lithium silicate glasses toward devitrification led to a choice of the proportions 1 Li_2O - 3 Na_2O. The proportions 1 MgO - 2 CaO is that of an eutectic between these materials, which might be of assistance in minimizing the melting temperature. The Al_2O_3 content of 1.0% is typical of silicate crown glasses. This glass melted at 1400°C, appeared platinum-free, but had a few undissolved seeds and many bubbles. Increasing its alumina content to that of glass number 2 eliminated the seeds, but not the bubbles. Providing the calcium as calcium fluoride, a common fining agent, greatly reduced the bubble content, and glass number 3 is believed to be a practical composition. Introduction of dopant ions such as cerium and neodymium to produce laser glass presented no additional problems.

A comparison of the platinum contamination of this glass with that of the aluminosilicate and barium crown type laser glasses made under the same conditions are shown in Table IX. The aluminosilicate and barium crown compositions are those of Table VII, the Resistant glass is number 3 from Table VIII, and Resistant D is the same glass doped with 0.1% Ce_2O_3 and 0.5% Nd_2O_3. The surface platinum concentration is in micrograms collected from a surface area of about 10 cm^2. Volume or bulk platinum is in parts per million by wt. No platinum was detected in any bulk sample. The sensitivity of the neutron activation technique is lower for bulk samples of calcium containing glasses than for barium crown. Surface platinum was detected on the resistant glass only with the mass spectrograph and at a level very close to the sensitivity limit of this instrument.

The new composition provides an improvement in platinum contamination resistance of a factor of 50-500. All glasses were prepared by a process which very likely maximizes platinum contamination. The small sample size, about 20 g., provides a high ratio of exposed platinum surface to the volume of the melt, and the induction heating technique heats this surface to a higher temperature than that of the melt. The production of larger batches in a resistance heated furnace should lead to even less contamination.

ALUMINATE GLASSES

Glasses derived from calcium aluminate are known to transmit in the 3-5 micron range and to have the high melting characteristics and high strength of silicate glasses which do not transmit beyond 4 microns. However, aluminates are difficult to synthesize because of devitrification problems, suffer severe platinum contamination which restricts at least their visible and ultraviolet transmission, and in common with silicate glasses usually have a strong absorption near 3 microns due to OH^- ions. The elimination of this OH^- ion absorption by remelting the glass in vacuum in graphite crucibles has been reported (18), so the solution of the devitrification and platinum corrosion problems would be expected to lead to more useful infrared transmitting glass.

Florence et. al. (19) have shown that among the most devitrification resistant aluminate glasses are those which contain components such as MgO, BaO, BeO, La_2O_3, PbO, GeO_2 or SiO_2 in addition to CaO and Al_2O_3, but that in all but the SiO_2 containing glasses devitrification is a severe problem even with samples that are rapidly quenched by casting from the melt. Incorporation of 6% SiO_2 eliminated devitrification, but reduced the infrared transmission beyond 4 microns. BeO also improved devitrification resistance but adversely affected transmission. Some complex glasses containing GeO_2 were also prepared, but the ability of GeO_2 to prevent devitrification was not mentioned. The use of alkalis and Fe_2O_3 in prevention of devitrification has also been reported (20), but elements such as alkalis, Fe, Pb, and Ge cannot be used in glasses to be remelted in vacuum in graphite crucibles. Florence also noted that aluminate glasses were colored amber to brown due to melting in platinum (19).

In a current exploration of the properties of aluminate glasses, more devitrification resistant compositions have been obtained, and the color due to platinum has been eliminated. Twenty gram samples of aluminate glasses have been melted in platinum crucibles in several atmospheres and allowed to cool in the melting crucibles. Of previously reported compositions containing MgO, BaO, CaO, Al_2O_3, GeO_2, SiO_2, La_2O_3, only those containing SiO_2 failed to exhibit severe crystallization. A new molar composition 6.8% MgO, 53.7% CaO, 7.9% BaO and 31.6% Al_2O_3 proved superior to any previously reported for the MgO, CaO, BaO, Al_2O_3 system. A composition 8.6% MgO, 49.2% CaO, 6.7% BaO, 29.1% Al_2O_3 and 6.4% SiO_2 was completely devitrification resistant as expected, and a germanium analog containing GeO_2 instead of SiO_2 was nearly equally good. A new composition containing 9.2% MgO, 48.0% CaO, 7.7% BaO, 32.4% Al_2O_3 and 2.7% Y_2O_3 was about as good as the germanium glass. The infrared absorption of the GeO_2 and Y_2O_3 containing glasses are yet to be determined.

Melting in nonoxidizing atmospheres produced colorless glasses with the above four compositions. A comparison of the transmission of the MgO, CaO, BaO, Al_2O_3 glass melted in air with that of a sample melted in a reducing atmosphere is shown in Fig. 10. The poorer transmission of the air melted sample in the visible and ultraviolet is due to dissolved platinum, the absorption in both glasses at 3 microns is from the OH^- band. The reason for the poorer transmission of the air melted glass at the longest wavelength is not known. The reduction of the OH^- band by the reducing atmosphere melting was greater than expected since the atmosphere used was not the dryest obtainable in the cold wall furnace. It is possible that further improvements in the atmosphere control could eliminate the OH^- band and the necessity for remelting in graphite crucibles in vacuum.

The earlier work with laser glasses provided compositional guidelines for the preparation of platinum-free glass. A ratio of alkaline to acidic components of about 1:5 was found useful. Such a ratio cannot be achieved in the aluminate glasses since the glass forming region is limited to compositions near a 1:1 ratio. In most samples of aluminate glass prepared by melting in nonoxidizing atmospheres, metallic platinum contamination was observed by inspection with a low power microscope. While in silicate glasses platinum deposits were found only on the surfaces of glass melts, in aluminate glasses crystals of platinum were observed in interior portions as well Some observations on the platinum contamination as a function of the melting atmosphere are shown in Table X. The formation of these platinum deposits was found to be independent of the presence of silicon, germanium, or yttrium, except that no germanium containing samples were melted in atmospheres containing CO.

The brown and yellow colors are due to dissolved platinum. With only a high purity argon atmosphere was platinum contamination not observed. However, in light of the fact that the aluminate glass compositions are not considered favorable for platinum contamination resistance, the effectiveness of the argon atmosphere awaits confirmation by sensitive chemical analyses.

SUMMARY

Work on the synthesis of pure glasses and the determination of the effects of impurities upon the optical properties of some glasses has been reviewed. The near ultraviolet absorption of silicate glasses has been shown to be due to impurities, particularly iron, and iron has been demonstrated as the source of the variation of the ultraviolet absorption of these glasses as a function of melting atmosphere. Copper, sulfur, and platinum has been identified as absorbing impurities from luminescence studies. Platinum contamination from glass melting crucibles has been found to be a function of both the glass composition and melting atmosphere, and a new nearly platinum-free laser glass has been developed. New compositions and melting procedures have been obtained for infrared transmitting aluminate glasses which are resistant to both devitrification and platinum contamination.

REFERENCES

1. J. M. Stevels, Proceedings of The 11th International Congress on Pure and Applied Chemistry 5, 519 (1953).

2. C. K. Kim, S. S. Voris, and W. G. French, Glass Technol. 7, 128 (1971).

3. D. E. Campbell and P. B. Adams, Glass Technol. 10, 29 (1969).

4. R. J. Ginther and J. H. Schulman, IRE Trans. on Nuclear Science NS-5, 92 (1958).

   R. J. Ginther, IRE Trans. on Nuclear Science, NS-7, 28 (1960).

5. R. J. Ginther, in Luminescence Dosimetry; Ed., F.H. Attix, Proceedings of International Conference on Luminescence Dosimetry, Stanford University, Stanford, California 1965. (AEC Symposium Series 8, 1967) p. 118.

6. J. R. Hensler, in Advances in Glass Technology Part 2, Eds., F. B. Matson and G.E. Rindone (Plenum Press, New York, 1963) p. 25.

7. A. M. Bishay, Phys. Chem. Glasses 2, 26 (1961). H. L. Smith and A. J. Cohen, Phys. Chem. Glasses 4, 173 (1963).

8. G. H. Sigel and R. J. Ginther, Glass Technol. 9, 66 (1968).

9. R. J. Ginther and R. D. Kirk, J. Non-Crystalline Solids 6, 89 (1971).

10. G. E. Rindone, in Luminescence of Inorganic Solids, Ed., P. Goldberg. (Academic Press, New York, 1966) p. 425. C. Hirayama and F. E. Camp, J. Electrochem. Soc. 115, 1275 (1968).

11. I. N. Douglas, J. V. Nicholas, and B.G. Wyburn, J. Chem. Phys. 48, 1415 (1968).

12. G. O. Karapetyan, Izv. Akad. Nauk. SSSR, Ser. Fiz. 25, 539 (1961).

13. J. H. Schulman and R. D. Kirk, Solid State Commun. 2, 105 (1964).

R. D. Kirk, J. H. Schulman, and H. B. Rosenstock, Solid State Commun. 3, 235 (1965).

14. G. E. Rindone and J. L. Rhoads, J. Am. Ceram. Soc. 39, 173 (1956).

15. R. F. Woodcock, Final Report of Office of Naval Research Contract NONR 4656(00) August 1969.

16. Ye. I. Galant and N. A. Vyaz'mina, Opt. Mekh. Prom. 2, 26 (1960).

17. R. J. Ginther, J. Non-Crystalline Solids 6, 294 (1971).

18. J. R. Davy, U. S. Patent 3,338,694 (1967).

A. J. Worrall, Infrared Phys. 8, 49 (1968).

19. J. M. Florence, F. W. Glaze, and M. H. Black, J. Res. Natl. Bur. Standards, 55, 231 (1955).

20. H. C. Hafner, N. J. Kreidl, and R. A. Weidel, J. Am. Ceram. Soc. 41, 315 (1958).

TABLE I

Correlation of Optical Absorption and Electron Spin Resonance Intensity in Iron-Doped 1.0 Na_2O - 3.0 SiO_2 Glasses

Iron Doping Level (ppm)	Melting Atmosphere	Optical Absorption* Coefficient at 225 nm (cm^{-1}) (1 mm thickness)	Normalized Electron Spin Resonance** Intensity at g = 4.28 due to Fe^{3+}
0	Air	4.9	5.9
10	Air	13.2	15.0
100	Air	93.0	105
1000	Air	920	1000
0	Reducing	0.0	0.0
10	Reducing	3.1	1.1
100	Reducing	14.0	4.0
1000	Reducing	82.0	14.1

* Optical background level taken as that of an undoped glass melted in a reducing atmosphere with negligible iron absorption. Wavelength of 225 nm corresponds to center of Fe^{3+} absorption band.

** EPR intensity normalized to ppm of Fe^{3+} at 1000 ppm.

TABLE II

Copper Content of Undoped Glass

Analytical Method	Air Melted Glass	Glass Melted in Reducing Atmosphere
EPR	2×10^{-6}	
Colorimeter	$1.5 \pm 0.2 \times 10^{-6}$	$0.5 \pm 0.1 \times 10^{-6}$
Mass Spectrograph		0.4×10^{-6}

TABLE III

Platinum Contamination of Glass Surfaces

Glass	Melting Atmosphere	Melting Temperature °C	Microscopic Observation of Platinum	Sample Weight Grams	Weight of Platinum Determined, Micrograms
Aluminosilicate	CO	1400	Present	7.2	3.
Aluminosilicate	90% CO - 10% CO_2	1400	Present	9.9	10.5
Aluminosilicate	50% CO - 50% CO_2	1400	Present	10.0	25.
Aluminosilicate	CO_2	1400	Present	8.3	3.
Barium Crown	90% CO - 10% CO_2	1400	Present	15.4	< 1.
Barium Crown	Argon	1400	Present	12.0	< 1.

TABLE IV

Surface Contamination of Glasses

Glass	Melting Temperature °C	Microscopic Observation of Platinum	Sample Weight Grams	Weight of Platinum Determined, Micrograms
Calcium, magnesium aluminosilicate	1400	Present	15.4	< 1.
$1Na_2O-3SiO_2$	1400	Present	12.0	11.
$1Na_2O-4SiO_2$	1400	Present	12.0	4.
$1Na_2O-5SiO_2$	1400	Absent	12.0	< 1.
$1Na_2O-6SiO_2$	1400	Absent	12.0	< 1.
$1Na_2O-5SiO_2$	1500	Present	12.0	15.
$1Na_2O-6SiO_2$	1500	Present	12.0	5.

TABLE V

Melting and Boiling Points of Alkali and Alkaline Earth Oxides

Compound	Melting Point °K	Boiling Point °K
Li_2O	2000	
Na_2O	1190	< 2500
K_2O	(980)	
MgO	3173	
CaO	2873	3800
SrO	2703	
BaO	2196	3000

TABLE VI

Free Energy Change for Reaction

$R+\frac{1}{2}O_2 \rightarrow RO$

or $2R+\frac{1}{2}O_2 \rightarrow R_2O$

Compound	ΔF°_T (Calories, 1500°K)
K_2O	- 15,400
Na_2O	- 36,600
Li_2O	- 89,500
BaO	- 99,000
SrO	- 106,000
MgO	- 101,700
CaO	- 114,500

TABLE VII

Glass Compositions
(Mole %)

Glass	Li_2O	Na_2O	K_2O	MgO	CaO	BaO	Al_2O_3	SiO_2	M_2O+MO	to	$2Al_2O_3+SiO_2$
1 Alumino-silicate	27.3				11.4		2.7	58.6	1	:	1.65
2 Alumino-silicate				10.9	30.7		8.9	49.5	1	:	1.62
3 Barium Crown	2.5	7.5	7.6			2.5	1.3	78.6	1	:	4.04

TABLE VIII

Compositions of Contamination Resistant Glasses
(Mole %)

Glass	Li_2O	Na_2O	MgO	CaO	CaF_2	Al_2O_3	SiO_2
1	3.3	10.0	1.1	2.2		1.0	82.4
2	3.4	10.3	1.2	2.3		3.2	79.6
3	3.4	10.3	1.2		2.3	3.2	79.6

TABLE IX

Platinum Contamination of Glasses

Sample			Surface			Volume	
	Micro-scopic	Colori-metric	Emission Spectro-graph	Mass Spectro-graph	Neutron Acti-vation	Mass Spectro-graph	Neutron Acti-vation
Aluminosilicate	Present	10.5				< .05	
Barium Crown	Present	< 1.			4.9	< .05	< .003
Resistant	Absent	< 1.	< 0.1	.02	< 0.3	< .05	< .03
Resistant-D	Absent		< 0.1	.02	< 0.3		

TABLE X

Platinum Contamination of Aluminate Glasses

Melting Atmosphere	Color of Glass	Metallic Platinum Contamination	
		Melt Surface	Interior of Melt
Air	Brown	Absent	Absent
90%CO-10%CO_2	Colorless	Present	Present
90%A-10%CO	Colorless	Absent	Present
90%A-10%CO_2	Yellow	Absent	Absent
100%A	Colorless	Absent	Absent

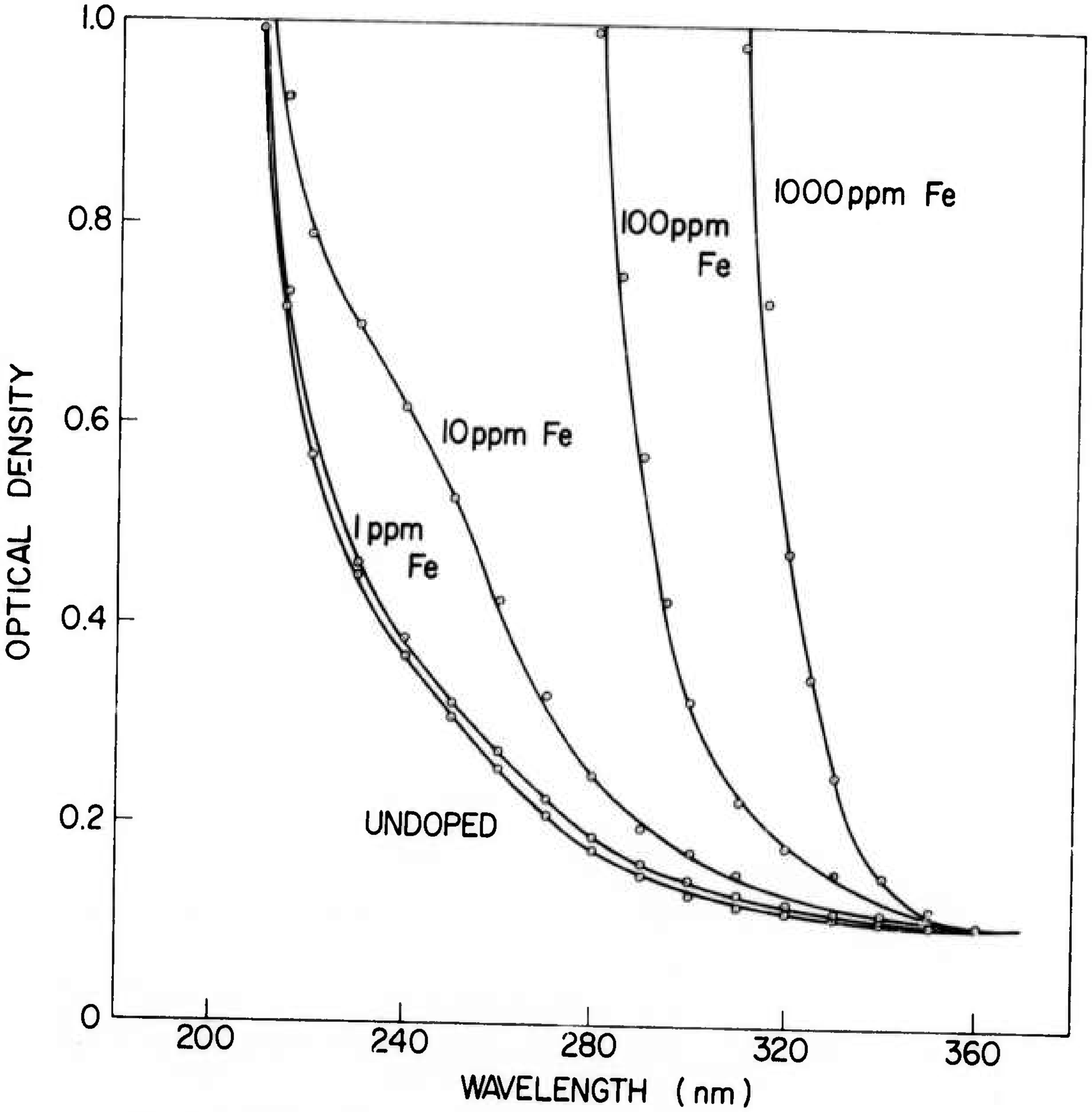

Fig. 1 - Absorption spectra of iron doped glasses melted in air.
Sample thickness 1 mm.

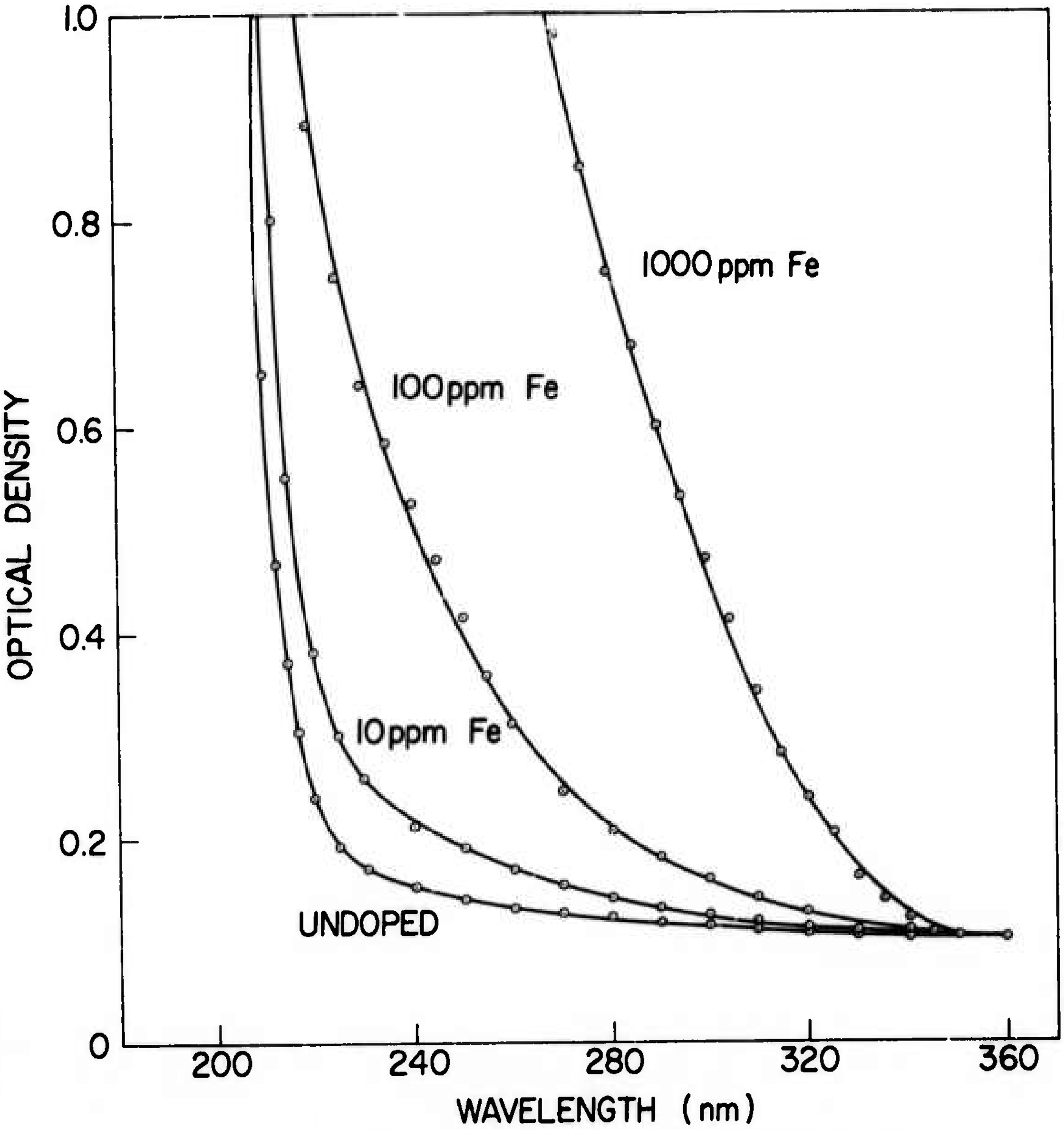

Fig. 2 - Absorption spectra of iron doped glasses melted in reducing atmosphere. Sample thickness 1 mm.

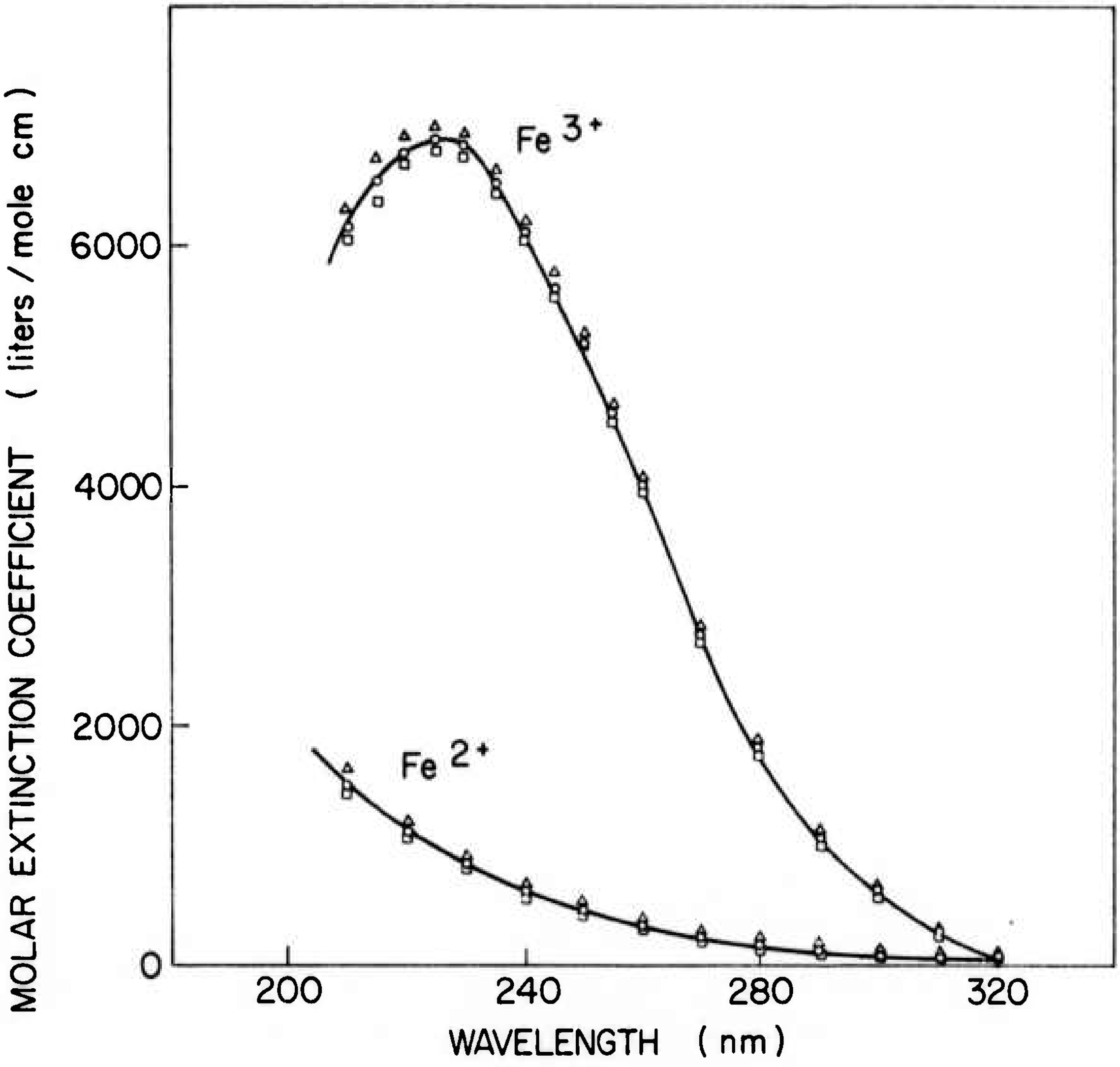

Fig. 3 - Molar extinction coefficients for ferric and ferrous ions in soda-silica glass.

Δ	1000 ppm iron
0	100 ppm iron
☐	10 ppm iron

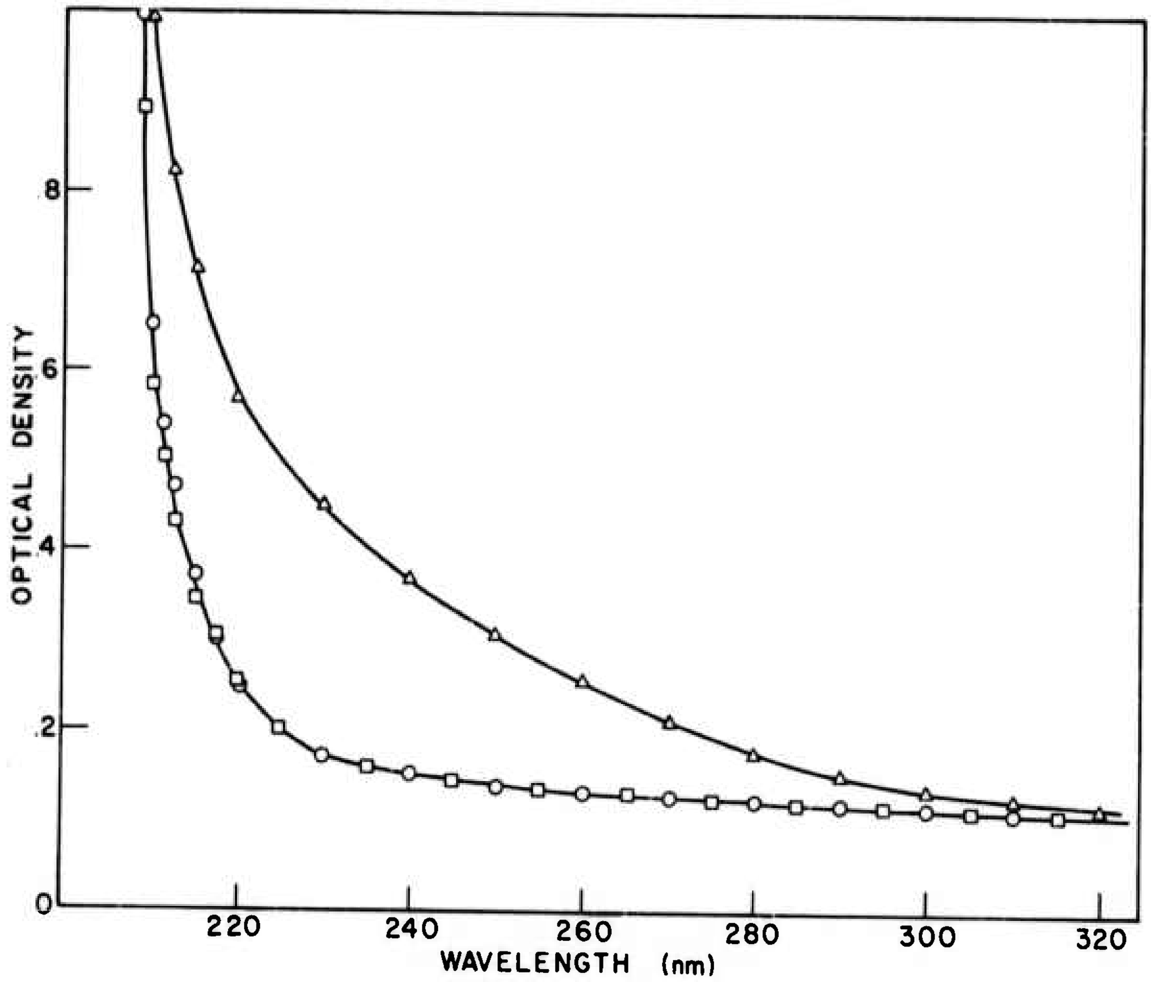

Fig. 4 - Ultravioleted absorption of undoped soda-silica glass melted in air and in reducing atmosphere.

Δ	Air-melted
0	Melted in reducing atmosphere
□	Air-melted, high purity

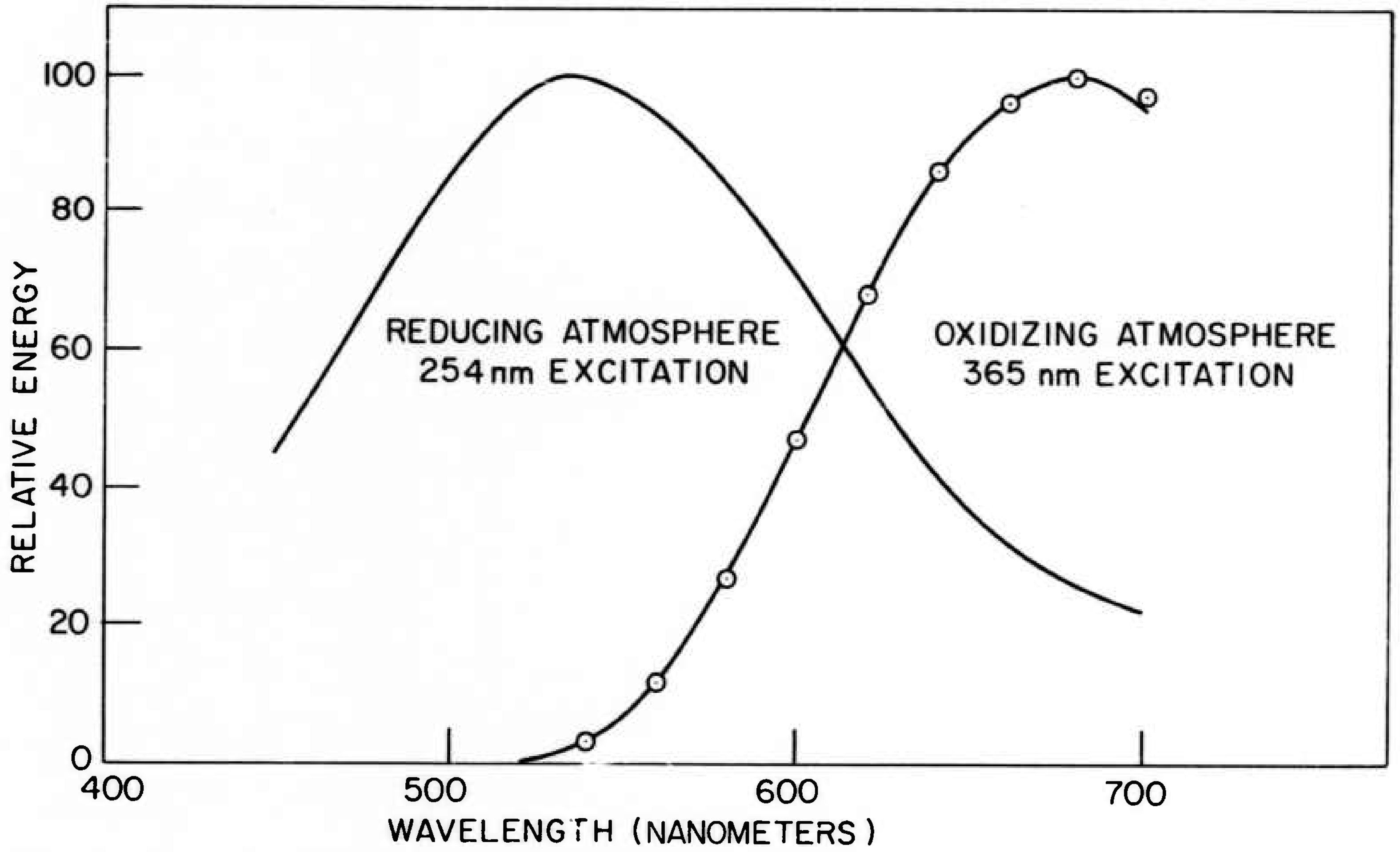

Fig. 5 - Emission spectra of undoped glasses

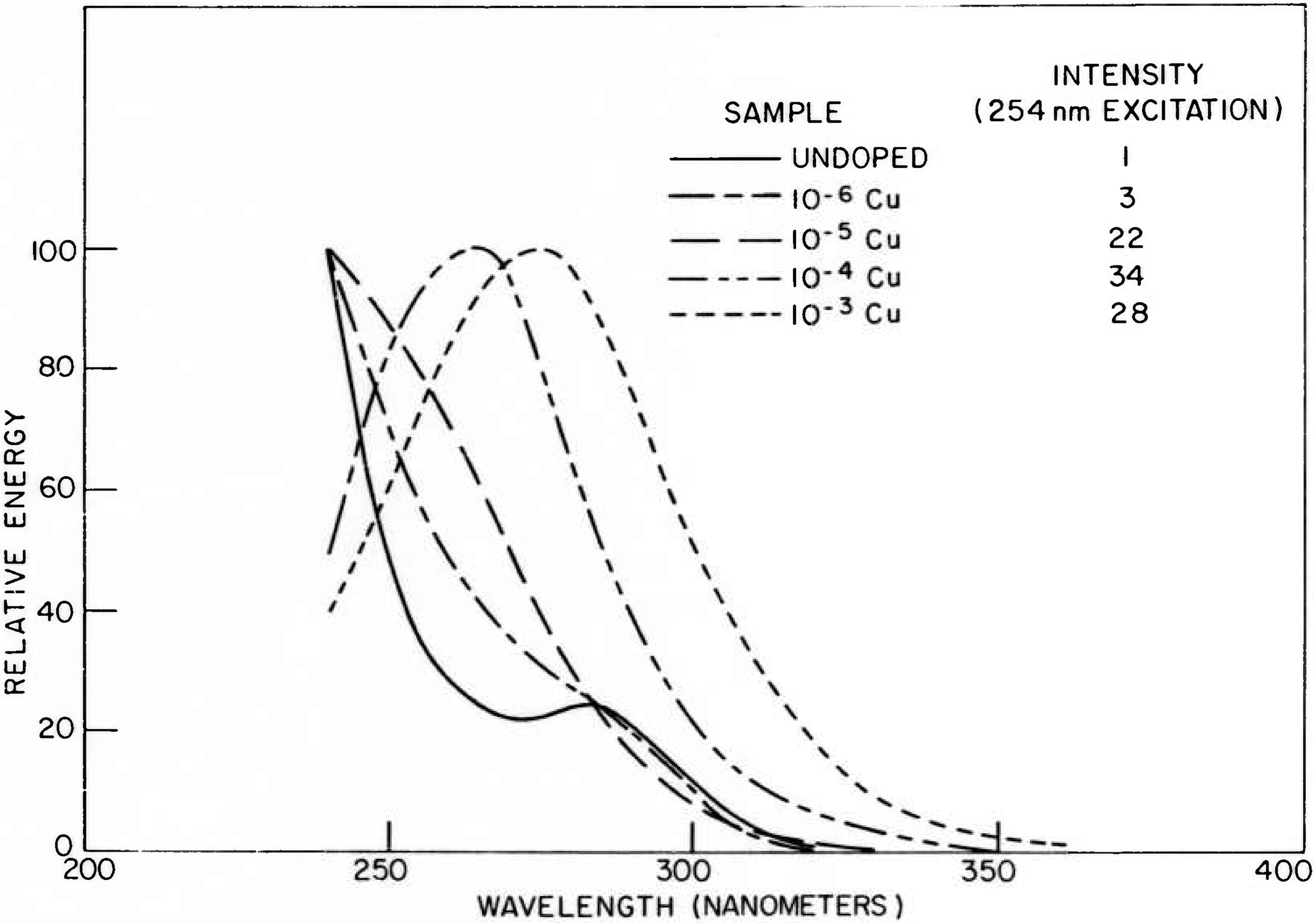

Fig. 6 - Excitation spectra of copper doped glasses

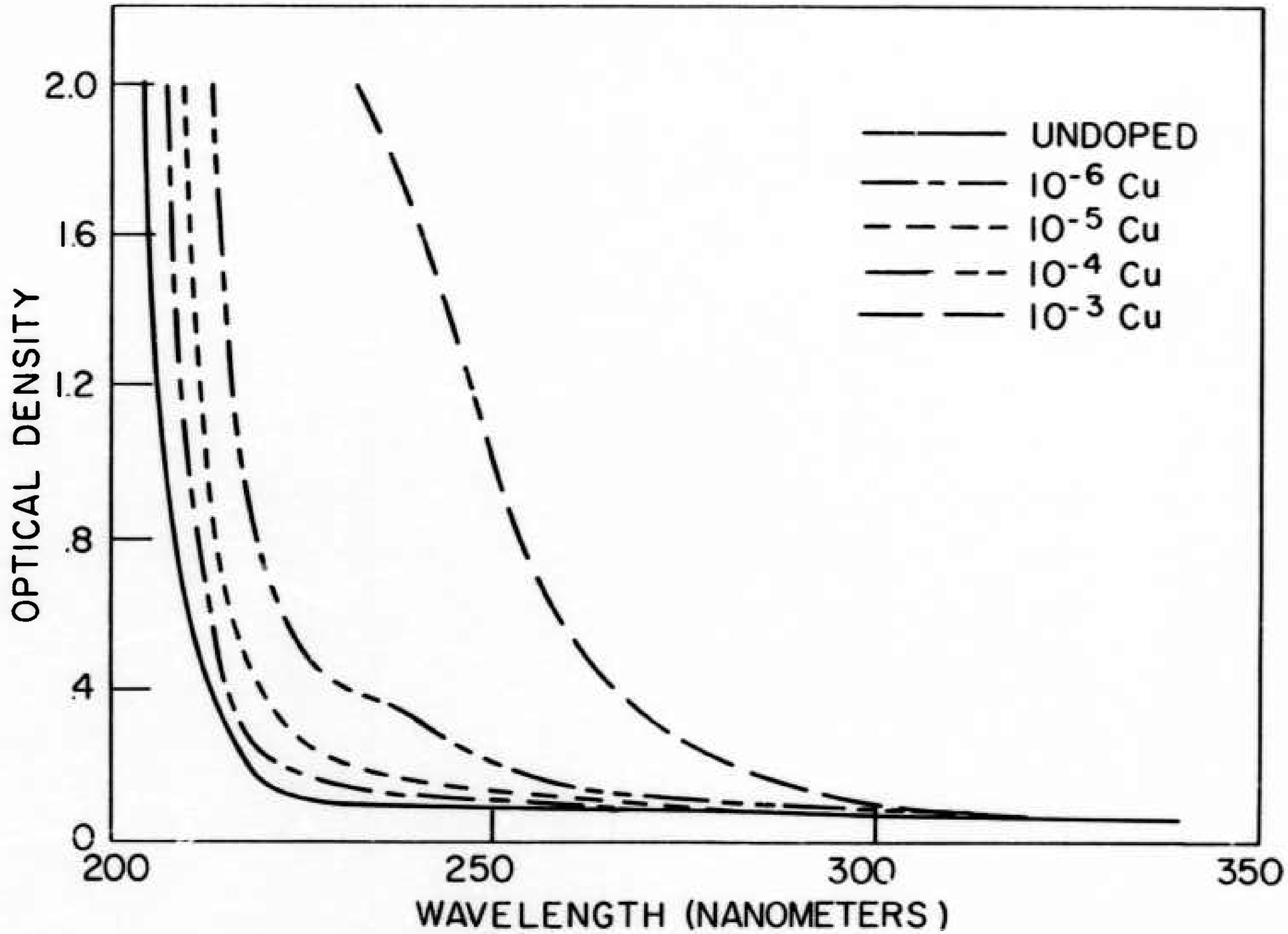

Fig. 7 - Absorption spectra of copper doped glasses melted in reducing atmosphere

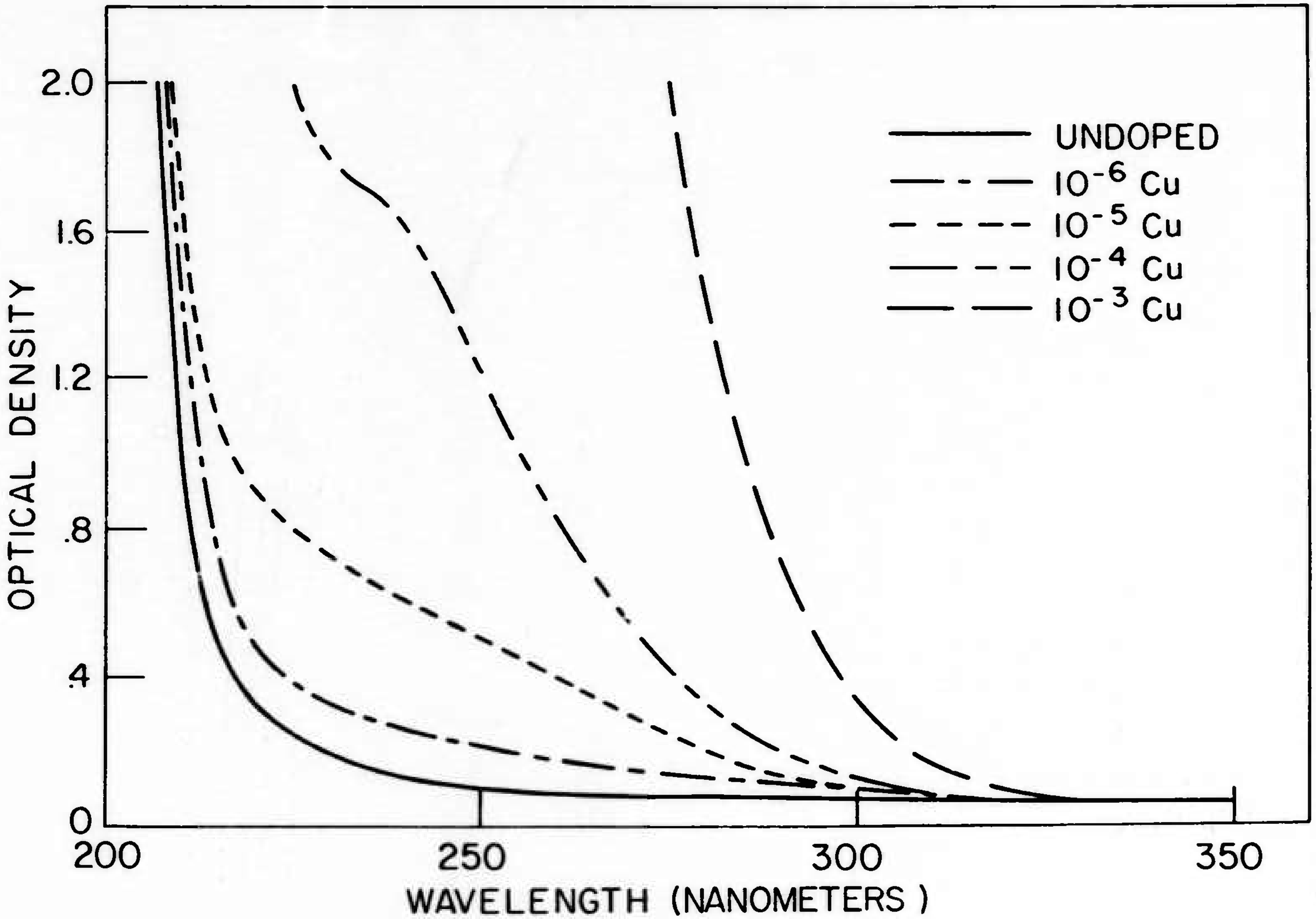

Fig. 8 - Absorption spectra of copper doped glasses melted in air

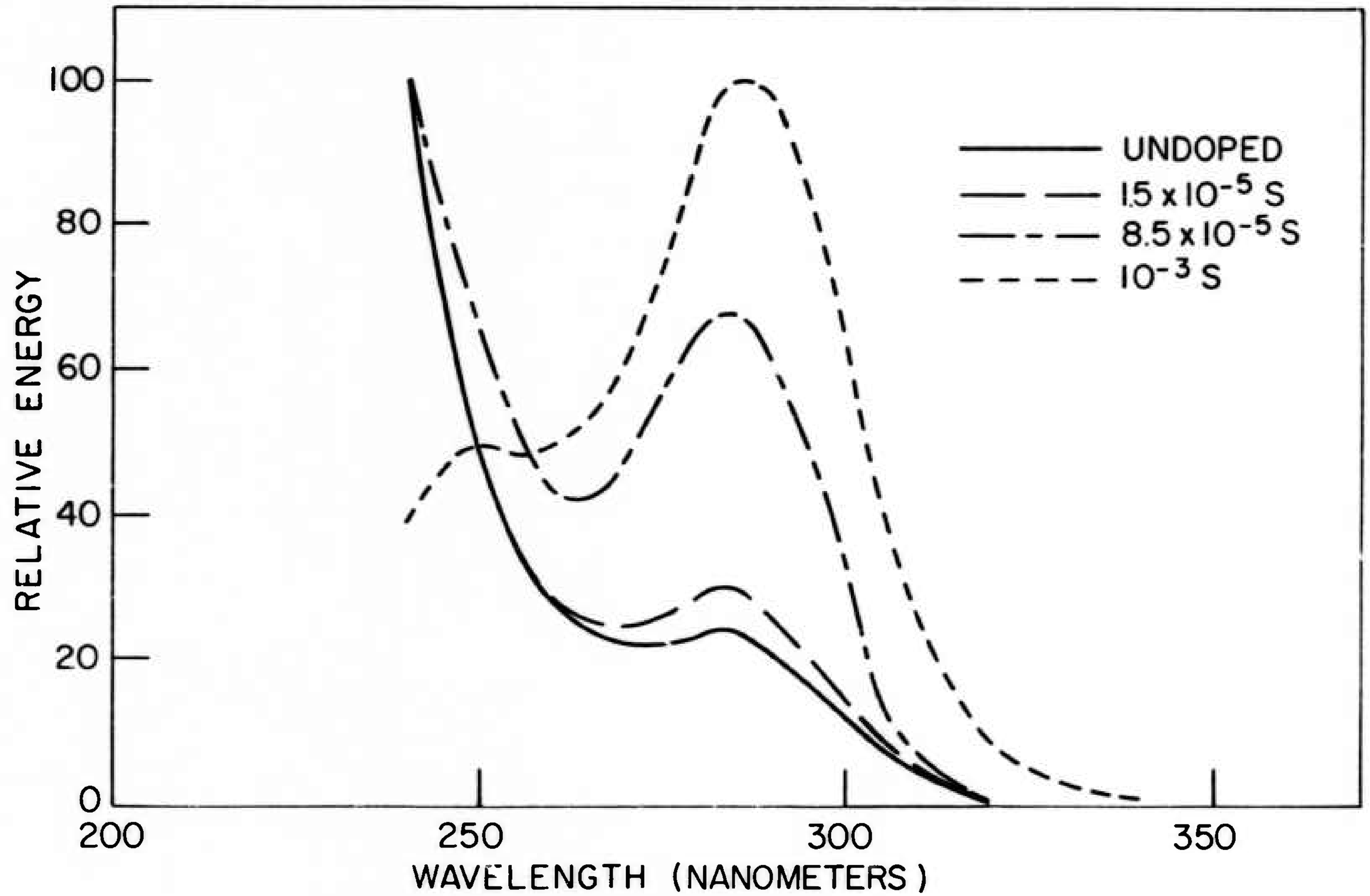

Fig. 9 - Excitation spectra of sulfur doped glasses

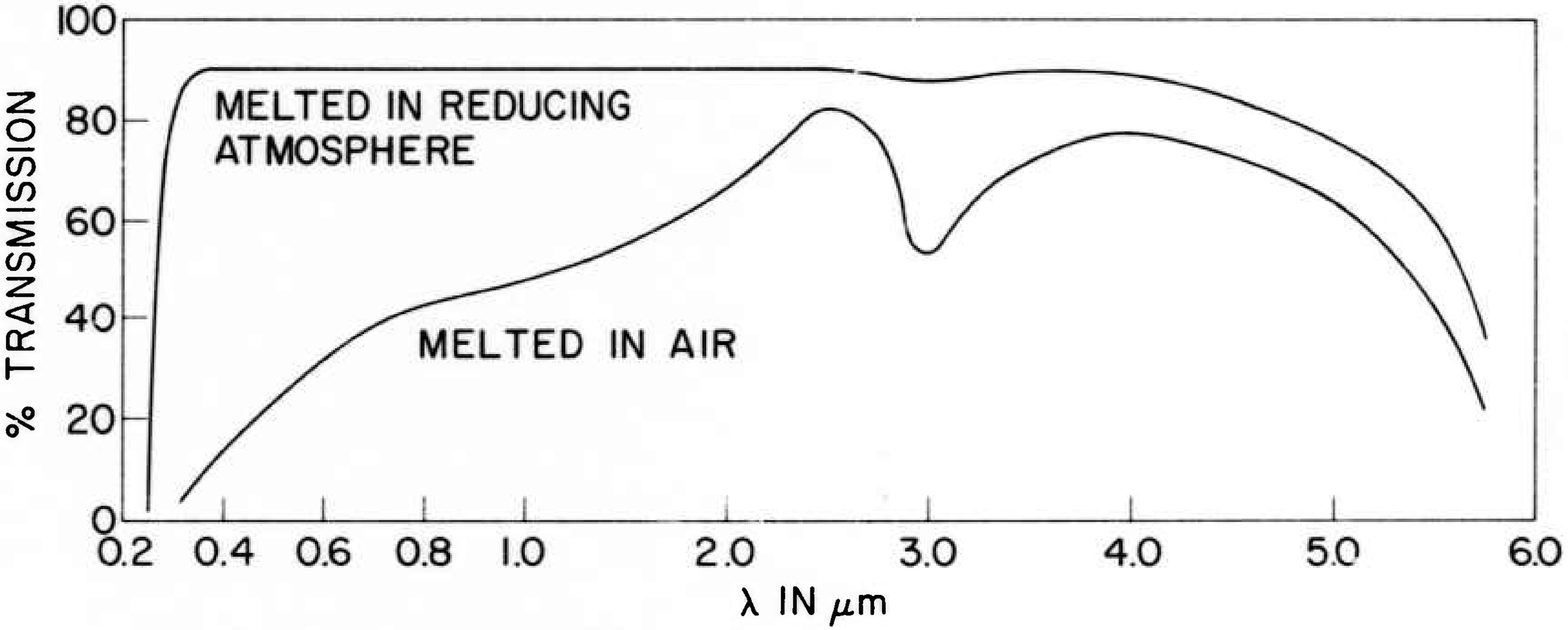

Fig. 10 - Transmission of 2 mm thickness of aluminate glasses melted in air and in reducing atmosphere. Note change of wavelength scale at 1.0 μm.

DIFFRACTION EVIDENCE FOR TRIDYMITE-LIKE ORDERING IN SILICA AND GERMANIA GLASSES

John Konnert, George A. Ferguson, Jerome Karle

The nature of the atomic arrangements in glass is currently the subject of considerable debate. In one model, the glass is described as a "random network" (1) in which only the shortest interatomic distances correspond to those in a crystalline phase. In another model, the glass is depicted as composed of small regions of crystalline-like order that are bonded together in essentially random orientations (2). The diffraction patterns of glasses have generally been interpreted as supporting the "random network" model.

It was felt, however, that certain inaccuracies both in the data collection and data processing could be masking important structural information that could prove useful in differentiating among models. The main sources of error in analyzing the diffraction data are:

1. Insufficient accuracy of the raw data experimental measurements.

2. Inaccurate separation of the interatomic distance contribution to the total intensity.

3. Experimental limitations on the range of the data collection.

Problem 1. is, of course, solved by collecting the data to a high degree of statistical accuracy, a time-consuming, but straight-forward, procedure. The latter two problems have been solved by the imposition of constraints on the resultant radial distribution function (RDF) (3). A procedure similar to that developed in the field of electron diffraction of gases is employed to separate from the total intensity that portion, i(s), containing the interatomic distance information (4). The experimental limitation of the data, the truncation problem, has been solved by recognizing that only the several shortest distances occurring in the sample are sufficiently ordered to contribute appreciably to the diffraction pattern at the experimental limit of data collection. These short distance (SD) contributions may be removed from i(s) by requiring that the resultant RDF be free from spurious details at small and large r. The equation utilized is:

$$r^2D(r) = 4\pi r^2(\rho(r) - \rho_o) =$$

$$\frac{2\pi}{r}\int_0^{S_{max}} s\left[Ki(s) - \sum_{SD} \frac{N_{ij}f_if_j \exp(-\ell_{ij}^2 s^2/2)\cdot \sin sr_{ij}}{sr_{ij}\sum_{uc} f^2}\right] \cdot \sin sr \, ds \qquad + \text{SD contributions}$$

where $s = (4\pi r^2 \sin\theta/\lambda)$, λ is the wavelength, 2θ is the angle between the incident and diffracted beam, K places the intensity on an absolute scale, r_{ij} is the distance between the ith and jth atoms, N_{ij} is the coordination number, ℓ_{ij} is the disorder parameter, UC is the unit of composition (SiO_2 or GeO_2), s_{max} is the experimental limit of data collection, the f's are the atomic scattering factors, ρ_o is the density parameter, and $4\pi r^2\rho(r)$ is the probability weighted by the scattering factors of finding atoms in the sample separated by r in the distance interval (r, r+dr).

This newly developed data reduction procedure has been employed with diffraction data obtained from silica glass and germania glass. X-ray diffraction data were collected with MoK_α radiation using samples formed both from fusing quartz and fusing the vapor phase hydrolysis products of pure silicon compounds ("infrasil" and "suprasil", prepared by Amersil Inc.). All data sets produced nearly identical RDF curves. Neutron diffraction data were collected with 0.84 A neutrons at the National Bureau of Standards using "suprasil" and germania glass samples prepared by Mr. Robert Ginther of the Naval Research Laboratory. The RDF's are illustrated in Fig. 1. Significant features are present out to at least 20 A, features that are not consistent with the popular "random network" model.

There exist several polymorphs of silica with varying densities; 2.20 g/cc for the glass, 2.31 g/cc for tridymite, 2.32 g/cc for cristobalite, 2.49 gm/cc for kestite, 2.65 g/cc for quartz, 3.01 g/cc for coesite, and 4.28 g/cc for stishovite. These densities suggest that tridymite and cristobalite might be related to the predominant atomic arrangements in the glass. Germania has been observed to exist in three polymorphs; the glass with a density of 3.65 g/cc, a quartz type structure with a density of 4.2 g/cc, and a rutile structure with a density of 6.2 g/cc. Significantly, the ratio of the densities of germania glass to quartz-like germania is the same as the ratio of the densities of tridymite to quartz.

RDF's were calculated for the crystalline forms by broadening the Bragg maxima in the powder diffraction patterns to correspond to an 11 A particle size for 3/4 of the sample and a 20 A size for 1/4. The crystalline structural parameters for quartz (5) and cristobalite (6) are well known from crystal structure analysis and were used to calculate the powder diffraction pattern. Tridymite, however, forms highly twinned crystals and the precise structure has not yet been obtained. Evidence for the bonding topology is provided by a high-temperature structure (7). For this reason a powder diffraction pattern was collected experimentally on a sample that possessed orthorhombic diffraction symmetry with cell dimensions of a = 81.97 A, b = 9.94 A, and c = 17.23 A.

In Fig. 1 the RDF's are illustrated. It can be seen that the x-ray RDF for silica glass is quite similar to the RDF obtained from the powdered tridymite, but considerably different from those obtained from cristobalite and quartz. The RDF for germania glass from neutron diffraction is very similar to the RDF for silica glass from x-ray diffraction. Since the Ge and O atoms scatter neutrons with approximately the same relative efficiency as Si and O atoms scatter x-rays, the RDF's strongly suggest that silica glass, germania glass, and tridymite possess very similar short-range order.

The diffraction data for the glasses are consistent with a structure in which nearly all of the atoms are within tridymite-like regions of dimensions up to at least 20 A. If this interpretation is correct, it requires that these regions be bonded efficiently together in a manner analagous to twinned crystals, but with a fairly large number of relative orientations and small distortions that result in isotropic macroscopic properties. The junctures between the ordered regions could then be related to differences in the inner regions of the RDF's of silica glass and tridymite-like particles.

In summary, the development of procedures for obtaining RDF's with a high degree of accuracy has resulted in the observation of structural details that were heretofore unobtainable. These details imply a great similarity between glasses and crystals on the atomic level.

References

1. W. H. Zachariasen, J. Am. Chem. Soc. 54, 3841(1932).
2. N. Valenkov and E. Porai-Koshits, Z. Krist. 91, 195(1936).
3. I. L. Karle and J. Karle, J. Chem. Phys. 17, 1052(1949); 18, 957, 963(1950).
4. P. D'Antonio, C. George, A. H. Lowrey and J. Karle, J. Chem. Phys. 55, 1071(1971).
5. R. A. Young and Ben Post, Acta Cryst. 15, 337(1962).
6. W. A. Dollase, Zeit. Krist. 121, 369(1965).
7. W. A. Dollase, Acta Cryst. 23, 617(1967).

Publications

Tridymite-Like Structure in Silica Glass, J. H. Konnert and J. Karle, Nature Physical Science 236, 92(1972).

Crystalline Ordering in Silica and Germania Glasses, J. H. Konnert, J. Karle and G. A. Ferguson, Science (in publication).

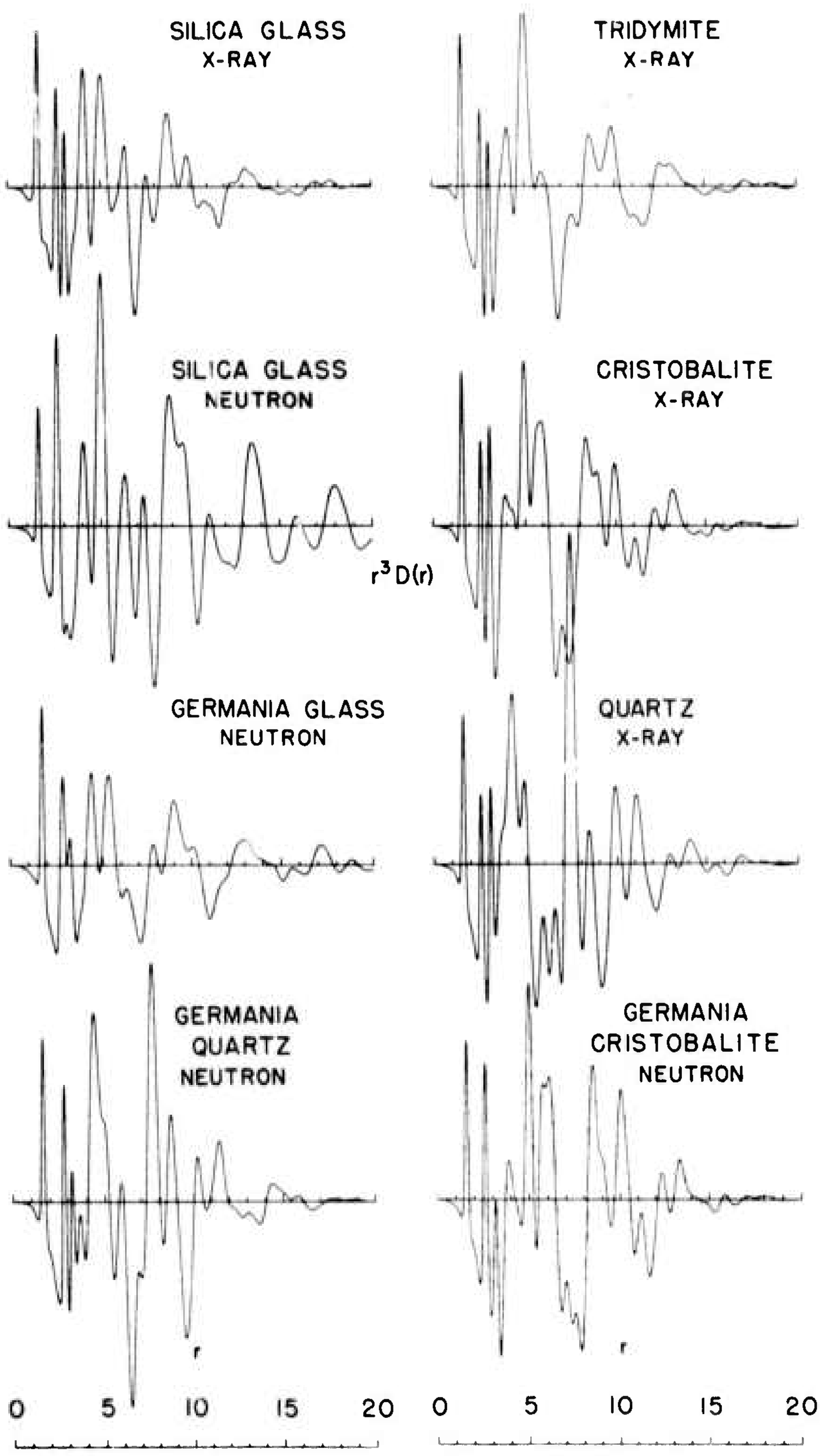

Fig. 1 - Radial distribution functions for silica and germania glasses and comparison functions derived from the broadened power patterns of crystalline polymorphs

ULTRAVIOLET SPECTRA OF SILICATE GLASSES

A REVIEW OF SOME EXPERIMENTAL EVIDENCE

G. H. Sigel Jr.

ABSTRACT

Ultraviolet spectroscopy is a useful experimental tool for the determination of the electronic structure of glasses. This paper discusses the ultraviolet spectra of SiO_2 and high purity silicate glasses. It considers in turn, absorption intrinsic to the Si-O network, the effects of network modifiers, impurity induced absorption, luminescence and radiation damage, both permanent and transient, in the wavelength region extending from 90 to 350 nm.

I INTRODUCTION

Recent technological advances in areas such as fiber communications, laser rods and windows, integrated optics, and electronic devices have focussed attention on the preparation and characterization of high purity glasses. One field of particular significance is the ultraviolet spectroscopy of SiO_2 and silicate glasses. The far u.v. is the region of the fundamental electronic absorption of the glasses. It is in the u.v. that both substitutional and modifying impurities exhibit their strongest absorption. In addition u.v. excitation normally produces luminescence in silicate glasses. Finally the basic radiation-induced defect centers in silicates exhibit absorption bands in the u.v. region.

This paper summarizes the results of an effort aimed at characterizing the ultraviolet spectra of high purity SiO_2 and simple silicate glasses. It considers in turn, intrinsic absorption, impurity-induced absorption, luminescence and radiation-induced absorption, both permanent and transient, which occur in the region extending from

90 to 350 nm. The purpose of the paper is not to give a comprehensive review of the ultraviolet spectra of glasses, but whenever possible, references have been made to previous work in the field.

II EXPERIMENTAL

Materials Preparation

Fused silica samples of Corning 7940 and 7943, Suprasil and Dynasil were used for this investigation as well as Sawyer crystalline quartz.

The alkali and aluminum-doped silica samples which were used were prepared by E. Lell while at Bausch and Lomb, Inc., using a flame fusion technique described elsewhere(1). Flame photometric determinations of the alkali content were made(2) since considerable loss can occur during preparation.

The alkali silicate glasses were prepared by R. J. Ginther of the NRL Central Materials Staff. Transition metal content of the best melts was less than 0.5 ppm. ESR, colormetric analyses, and mass spectrographic analyses were used to select both the purest starting materials as well as finished glasses.

Thin glass films were prepared using an MRC r-f sputtering unit. Target materials were selected from those glasses mentioned above.

Measurements

Ultraviolet absorption measurements above 200 nm were made on a Cary 14 spectrometer. Samples were mounted in an optical dewar whose temperature could be varied from room to liquid helium temperature. Below 200 nm, McPherson model 225 and 235 vacuum u.v. instruments were used to make reflectance and absorbance measurements respectively. A special reflectometer designed by Berning et al(3) was used.

Samples were irradiated with 50 kV x rays, 2 MeV electrons, and pulsed 600 keV electrons. The pulsed irradiations were performed using a Febetron 706 accelerator. Samples were maintained at constant temperature (300°, 77° or 4.2°K) and radiation induced coloration was measured by observing the attenuation of monochromatic light passed through the region of the sample in which the incident electrons were stopped. The experimental setup is shown in Figure 1. and has been described by Williams et al(4).

The apparatus was designed to measure transient radiation effects in optical materials.

ESR measurements were made using Varian E-3 and E-9 spectrometers operating at x band frequency.

III RESULTS AND DISCUSSION

A. Fundamental Ultraviolet Absorption of SiO_2

Fused silica and crystal α-quartz both consist of Si atoms tetrahedrally bonded to four O atoms, each O atom being common to (bridging) two such SiO_4 tetrahedra. The Si-O bond distance is roughly 1.61A in both materials. The Si-O-Si bond angle in crystal α-quartz is 144^o, but may vary in fused silica. Figure 2 shows the position of the u.v. edges of high purity crystalline quartz, fused silica and a silicate glass. The shift of the edge of silica relative to quartz is thought to occur because of the distribution of Si-O-Si bond angles in the glass, resulting in a variation in bond energies. However, the electronic absorption is primarily determined by the short range order. Phillip(5) was the first to measure the u.v. reflectance of crystalline quartz and fused silica and noted the similarity of the two. Figure 3 shows the reflectance spectra taken in our laboratory of high purity α-crystal quartz and fused silica. The similarity of the reflectance of the crystalline and glassy SiO_2 indicate that the absorption bands are not strongly dependent on the long range periodicity of the network. This suggests that the absorption arises from electronic transitions characteristic of the SiO_4 tetrahedron. The first absorption peak in SiO_2 does not occur until 120 nm (10.2 eV) although the transmission cutoff occurs at significantly lower energy (8.2 eV).

The necessity for some ordering even in the glass is suggested by measurements made on sputtered SiO_2 films. These films do not exhibit in reflectance any spectral structure such as found in the bulk silica samples. Rather they show an ever rising absorption edge near 8 eV. Since the films were prepared in argon, they may be slightly oxygen deficient. However Phillip(6) has recently shown that even SiO shows structure similar to SiO_2. It must be concluded that the failure to observe any structure in the films results from the lack of even very short range order in the films. Supporting this hypothesis was the evidence that annealing in vacuum at 750^oC partially restores the spectral structure of the u.v. reflectance of sputtered SiO_2 films.

Several theoretical papers (7-10) in the past few years have attempted interpretations of the fundamental absorption of SiO_2. There is not universal agreement at this time with regard to the electronic transitions involved. Loh(11) had proposed that the 10.2 eV peak was an exciton (i.e., a bound electron-hole pair) of the Si-O antibonding level and the 11.5 eV peak represented an interband transition. This tentative assignment was made by the comparison of the SiO_2 spectra with that of other semiconductors and insulators on the assumption that in general exciton transitions result in sharp peaks while interband transitions manifest themselves as either broad peaks or absorption edges. A valence bond model of Ruffa(7) for SiO_2 gives general support to this interpretation. Ruffa identified the sharp (120 nm) 10.2 eV peak with a Wannier exciton formed by the breaking of a single Si-O bond. The next broad peak at 108 nm (11.5 eV) was attributed to band-to-band transitions.

Reilly(8) employed a molecular orbital approach to interpret the valence levels of SiO_2, using hybrid orbitals of a Si-O-Si molecule. He observed that the highest filled valence band of SiO_2 is probably associated with the oxygen 2p valence electrons which do not participate in the Si-O bond. Since the similarity of the absorption of crystalline and amorphous forms of SiO_2 requires transitions which are insensitive to the Si-O-Si bond angle, the 10.2 eV peak was attributed to a transition to an exciton state with the hole orbital corresponding to the oxygen $2p_x$ orbital (i.e., the non-bonding oxygen orbital orthogonal to the SiO bonding orbital) and the electron orbital resembling the oxygen 3s. Possible explanations given for the 11.5 eV peak were that it corresponds either to a transition from the non-bonding oxygen p levels to the antibonding level or to the oxygen 2p-3d transition which is roughly 11 eV in the oxygen atom.

Bennett and Roth(9) have also employed the molecular orbital approach using the extended Huckel Theory to make their calculations on clusters of two and eight SiO_2 molecules. This technique calculated an energy gap of 13 eV compared to an experimental value of 11 eV. The removal of an oxygen atom was found to result in the introduction of several levels in the energy gap which appear to account for experimentally observed radiation bands.

Abarenkov et al(10) have used a semi-empirical method for the calculation of the electronic structure of vitreous germania and silica. The results of this calculation suggest a covalent model for bonding in silica. The similarity of energy levels calculated for chainlike and tetrahedrallike Si-O complexes is consistent with a disordered structure of silica. Finally the calculation predicts a shift in the fundamental edge of silica relative to crystalline quartz because of energy level shifts as the Si-O-Si angle changes.

The attempts of the theoreticians to explain the u.v. spectra of SiO_2 have been hampered by experimental uncertainties and lack of reliable experimental data. A controversy even exists over the interpretation of the x-ray analysis of the glass structure. Recent results by Konnert and Karle(12) show strong evidence for crystallites in fused silica, contrary to the findings of Mozzi and Warren(13). There are some observations which nevertheless can be made on the basis of the data available. First, the band gap of SiO_2 is approximately 10 electron volts. Photoemission measurements by DiStefano and Eastman(14) give a similar value as does x ray emission data.(15, 16) Secondly the fundamental absorption in bulk fused silica is not grossly affected by the presence of the disorder, suggesting that absorption is determined by processes within or between neighboring SiO_4 tetrahedra. Finally, in the presence of extreme disorder such as found in sputtered films, all recognizable structure vanishes.

B. Effects of Impurities on the Ultraviolet Absorption of SiO_2

1. Network Modifiers

As illustrated in Figure 2, alkali silicate glasses of high purity do not transmit below 200 nm. Sigel and Ginther(17) have shown that the fundamental absorption edge of an alkali silicate glass is well defined and not influenced by the reducing-oxidizing conditions during melting if it is sufficiently pure. During the present investigation thin films of high purity glasses ($3SiO_2$-$1NA_2O$, $3SiO_2$-$1K_2O$) were prepared by rf sputtering. Strong absorption was measured between 175 nm and 150 nm in the films and was attributed to the presence of alkali. This was confirmed by the author in a series of measurements on alkali doped silica(2). Optical absorption in the 150-200 nm region was found to be proportional to alkali concentration and independent of alkali type except for the degree of long wavelength tailing which increased in the order of Li, Na, K. The effect of the simultaneous doping of aluminum with the alkali on the ultraviolet absorption was suggestive that non-bridging oxygens (NBO) were the source of the absorption. Kats' and Stevels(18) and Lell(19) had previously seen evidence of alkali-aluminum pairing in glasses. Aluminum can substitute for silicon, requiring a nearby alkali for charge compensation, as shown schematically in

Fig. 4. If this scheme is correct, the resulting decrease in the concentration of NBO should produce a decrease in u.v. absorption in aluminum-alkali doped samples. This is confirmed by the data in Figure 4. Substitutional aluminum alone in SiO_2 did not produce any observable u.v. absorption in the silica in amounts up to .5%.

The effect of alkali on the ultraviolet absorption of silicate glasses was further measured in a series of reflectance measurements on silicate glasses of high alkali content. Significant changes relative to the SiO_2 reflectance were evident in all of the glasses. The spectra of the glasses were characterized by three reflection peaks at 145 nm (8.5 eV), 130 nm (9.3 eV), and 108 nm (11.5 eV). In simple binary silicates a band centered near 8.5 eV was observed which has been associated with non-bridging oxygen absorption (Figure 5). This band is responsible for the poorer transmission of alkali silicate glasses compared to SiO_2 and is apparently the same absorption seen in the alkali doped silica samples. Since no reflectance measurements were possible on the alkali-doped fused silica samples due to size limitations, commercial fused silica with poor ultraviolet transmission (Infrasil) was used for reflectance measurements. This material showed evidence of the 8.5 eV absorption band. Plazoder(20) has shown reflectance data for what was apparently impure α-quartz which also shows absorption at 8.5 eV (peak labeled A in his Figure 1), although it was not associated with an alkali induced defect.

Table 1 summarizes the reflectance data for the SiO_2 and silicate glasses which have been measured in the present work. All of the silicate glasses exhibited the 8.5 eV absorption. The type of network modifier, including both alkali and alkaline earth metals, did not appear to influence the position of this band as much as it did the halfwidth. This is evident in Figure 5 in which the tail of sodium silicate glass extends to higher wavelengths than the lithium glass.

The 11.5 eV (108 nm) reflectance peak which is found in SiO_2 was observed in all of the silicate glasses. This observation suggests two possibilities: (1) there is still a sufficient number of SiO_4 tetrahedra remaining in the glasses to produce the absorption characteristic of the bridging network, or (2) the 11.5 eV band arises from transitions involving atomic levels unperturbed by the addition of alkali. More theoretical and experimental work is required to settle this question.

It would be desirable to have a calculation on the magnitude of the alkali-oxygen interaction in the silicate system and the degree to which the charge density of the Si-O bond is changed when the oxygen becomes non-bridging and a neighboring alkali is introduced. If the Si-O bond were sufficiently weakened by such an interaction one could predict the existence of a lower energy absorption such as observed here. One should probably also consider excitation of the alkali-oxygen bond as another possible contribution to the optical absorption. Experimentally the measurements should be carried out to higher energies in the silicate glasses to allow comparison with the data of SiO_2. Also a greater range of glass compositions is needed to determine whether the 10.2 eV band undergoes a shift to lower energies as the alkali content increases.

The data however has established that the introduction of network modifiers into SiO_2 produces an absorption band near 8.5 eV which is responsible for the shift of the u.v. edge of silicate glasses to longer wavelengths.

In summary, measurements on thin films, doped fused silica and bulk glasses, confirm that the introduction of alkali oxide into SiO_2 introduces an optical absorption band near 8.5 eV which shifts the fundamental edge of SiO_2 to longer wavelengths. The ability of the aluminum to suppress this absorption band and the relative insensitivity to alkali type suggest that the breakup of the Si-O-Si network with the generation of non-bridging oxygens is responsible for the absorption. The absorption bands at higher energies are still open to interpretation. The 11.5 eV band has been observed in each of the silicates measured regardless of composition. It may therefore be associated with a band to band transition characteristic of the SiO_2 tetrahedron.

2) Transition Metals - Iron

The 3d electrons of the transition metals and the 4f electrons of the rare earths can produce charge transfer spectra in the far u.v. which is sufficiently intense that a few ppm can easily be detected in a 2 cm thickness of glass. The most serious problem in high purity glasses is Fe^{3+} which absorbs strongly near 230 nm. Swarts and Cook(21), Steele and Douglas(22) and Sigel and Ginther(17) have studied this band in various silicates. Figure 6 shows the effect of Fe^{3+} on the u.v. transmission of 3 SiO_2- $1Na_2O$ glass. In conventional thicknesses (1-10mm), the effect of the iron absorption is to produce an edge shift. The iron can be eliminated by the use of extremely pure starting materials, special furnaces, and maintenance of clean room standards during preparation.

The evaluation of the ultraviolet absorption due to iron in silicate glasses is complicated by the overlap of the ferric and ferrous bands as well as the strong absorption of the glass host at wavelengths below 200 nm. The ESR resonance of Fe^{3+} at $g = 4.28$ in silicate glasses(24.25) was used to monitor Fe^{3+} concentration. Figure 7 shows the ESR sensitivity to iron present 1 to 1000 ppm concentrations. The undoped glass shows evidence of iron contamination of about 6 ppm.

Iron concentrations were finally reduced to levels below 0.5 ppm in 1 Na_2O - 3 SiO_2 glass. A mass spectrograph which operated with a background of .2 ppm of iron was unable to defect any traces of iron. For these pure glasses the ultraviolet absorption of air melted and reduced-melted glasses was the same.

Other types of high purity silicates including 1 K_2O-3 SiO_2, 1 Na_2O-1 CaO- 3 SiO_2 and 1 Na_2 O-1 Al_2O_3 - 3 SiO_2 were found to exhibit similar behavior. Figure 8 shows the U.V. edge for these low iron glasses.

3) Other Impurities

Traces of other impurities were detected in the glasses by the mass spectrography, ESR, and wet chemistry analyses. Among the major impurities (above 1 ppm) were included water vapor, aluminum, copper, platinum, titanium, calcium, magnesium and cerium. The ultraviolet absorption of each of these impurities were investigated as well as that arising from gallium, indium, and thallium. However none of these were found to absorb nearly so strongly as ferric and ferrous iron

Water vapor was detected by the presence of the O-H stretching band near 2.7 microns(26) as well as by the mass spectrograph. No evidence of any u.v. absorption due to water vapor could be detected in the samples.

Aluminum absorption was studied in alkali aluminosilicate glasses such as the $3SiO_2$-$1Al_2O_3$-$1Na_2O$ glass in Figure 6 as well as fused silica doped with only aluminum in concentrations ranging from .05 to .5 mole %. There was no evidence of any u.v. absorption due to aluminum and normally the u.v. transmission improved.

Copper was detected by its characteristic ESR signal(25) in silicate glasses. Ginther and Kirk(27) have discussed the absorption and luminescence observed in copper doped silicate glasses.

Titanium was doped into sodium silicate glass at concentrations of 25 and 50 ppm. It absorbs moderately at wavelengths below 250 nm with the peak of the absorption lying near 200 nm and being obscured by the edge of the glass.

Calcium and magnesium were introduced into the alkali silicate glasses in large quantities. They do not absorb at energies below that of the alkali absorption. Thus the edge of the alkali silicate glass is essentially identical with a alkali-alkaline earth silicate with equivalent alkali content.

Cerium oxide was used to polish the glasses and traces remaining on the surface account for its detection by chemical analysis.

The results of this study can be summarized as follows: the ultraviolet absorption of silicate glasses can be divided into three general areas 1) 350 nm to 200 nm - impurity absorption. 2) 200 nm to 150 nm - network modifier - induced absorption resulting from the breakup of the Si-O network, and 3) below 150 nm - fundamental electronic absorption characteristic of the Si-O network of the glass.

C. Ultraviolet Absorption Produced by Irradiation of Silicate Glasses

Defect center formation in glassy SiO_2 seems best explained by the simple ionization of the Si-O bond, with ensuing relaxation of the inter-nuclear separations of atoms in regions of local strains.(26-30) Irradiated high purity SiO_2 exhibits absorption bands at 5.3 and 5.8 eV which will be referred to here as the E_2' and E_1' bands using Weeks(31) notation. These centers have been associated with electrons trapped in dangling silicon orbitals projecting into oxygen vacancies or voids in the glass network and which may be locally charge compensated by the presence of protons. They produce a sharp ESR resonance at $g = 2.0006$ which has been observed in both crystalline quartz and fused silica. Hochstrasser and Antonini(32) have observed the same center on freshly exposed SiO_2 surfaces under ultra-high vacuum conditions. Hickmott(33) has investigated the E' centers in sputtered SiO_2 films. The author(34) has reported optical and ESR confirmation of E' centers in ion-implanted SiO_2. The profile of damage in the ion implanted SiO_2, measured by monitoring the E' ESR resonance after repeated etching in HF solution, confirms that ionization is sufficient for defect center formation. Irradiated SiO_2 also possesses a major absorption band near 7.6 eV which has been tentatively assigned to trapped holes on interstitial oxygens by Mitchell and Paige.(35) This band does not appear to have any paramagnetic analogue. Nelson and Weeks(29,36) observed additional structure between 6 and 8 eV in irradiated SiO_2.

The situation is more complicated in the silicate glasses. These exhibit at least three classes of radiation induced defect centers: (1) those characteristic of flaws in the basic Si-O network, which were mentioned above (2) those resulting from the presence of substitutional impurities, such as aluminum and germanium and (3) those arising from the addition of network modifiers which can rupture Si-O bonds, creating non-bridging oxygens in the process. Lell, Kreidl and Hensler(37) have reviewed the radiation effects in quartz, silica and silicate glasses and Bishay(38) recently has treated radiation damage in more complex glasses. Alkali silicate glasses normally possess major radiation induced bands near 450 nm and 650 nm which have been attributed by Stroud(39) and others(40,41) to trapped holes, as well as bands near 310 and 235 nm which have been associated with trapped electrons. The ESR spectra of alkali silicate glasses consist of several resonances near $g = 2$ which have been studied by several investigators, the most recent work being that of Mackey et al(42) and Scheurs.(43)

Permanent damage studies in pure SiO_2 were not pursued because of the extensive literature on the subject. However luminescence and transient damage measurements were carried out using pulsed electrons and are reported in the latter part of this paper.

1) Damage in Alkali Doped SiO_2

A systematic study(44) has been made on the effects of alkali content on the radiation damage of SiO_2. This is of particular interest because of the problems of charge build up in the SiO_2 layer of MOS devices, which may be partially related to the radiation enhanced diffusion of alkali ions.

The radiation induced optical absorption in alkali doped silica has been measured by Lell(19) out to energies of 6 eV. In the present work measurements have been extended to 8 eV when the transparency of the samples permitted, as shown in Figure 9. In addition ESR measurements were made on the same samples. The principal radiation bands are the 7.6 eV band and the E_1' and E_2' bands which overlap to produce a compound band between 5 and 6 eV. The E_2' band at 235 nm (5.3 eV) was found to be proportional to alkali concentrations at doping levels ranging from 0.01 to 0.5 mole percent. This center was interpreted to be an electron trapped in a tetrahedral silicon orbital in the vicinity of a proton. The strong dependence on alkali concentration which has been observed here suggests that the center is a more complex one involving non-bridging oxygens, alkali and protons, and may be a characteristic defect of an alkali silicate glass rather than SiO_2. Weeks(31) did note an apparent correlation with alkali impurity content of his samples.

The ESR data for an irradiated potassium doped sample is shown in Figure 10. At low power levels (dotted line in Figure 10) the E' resonance near $g = 2.0006$ was observed as well as a new resonance with lower than axial symmetry centered between $g = 2.020$ and $g = 2.000$ which was not observed in pure SiO_2. This latter resonance has been observed by Schreurs(43) in alkali silicate glasses and was attributed to a hole located on a Si-O tetrahedron with two non-bridging oxygens. In the present study, it was found that the amplitude of this resonance was directly proportional to alkali content in the lightly doped samples. This dependence of the resonance on alkali concentration and the observed variation of broadening with the type of alkali, support the hypothesis that the holes are trapped on non-bridging oxygens in the vicinity of an alkali ion.

The 7.6 eV band was present in the alkali doped samples but showed no correlation with alkali content and was relatively constant (± 15%) for a given dose in all of the samples regardless of alkali content. This is not surprising since it is a principal radiation band in high purity SiO_2 apparently arises from a defect characteristic of the Si-O network. It was noted earlier in the paper that non-bridging oxygens may be responsible for the ultraviolet absorption in the 6 to 8 eV region. Just as the introduction of alkali can break bonds and produce singly bonded oxygens, the impinging radiation may ionize strained Si-O bonds, thereby producing absorption in the same region of the spectrum.

The ESR hole resonance was observed to bleach very closely with the E_2' ultraviolet band between 0 and 300°C which suggests that they may be complementary centers in alkali silicate glasses, in the same manner that the E_1' and the 7.6 eV hole band are complementary in pure SiO_2. It has been suggested(43) that in silicate glasses a 475 nm optical absorption band is correlated with the hole resonance. The low oscillator strength of the visible absorption bands as well as the presence of aluminum impurity in the doped samples made it impossible to test this assignment.

The other resonance observed in the samples was the E' resonance. This relatively long relaxation time for this center makes it easy to saturate. The comparison of the solid and dotted curves in Figure 10 indicate the rapid fall-off of the E' resonance intensity with microwave power. The solid curve is typical of spectra measured for potassium silicate glasses. Previous papers have noted the presence of a resonance at lower g values than the g = 2.01 hole resonance which apparently arose from trapped electrons. As a result of the present study, it has been definitely established that this resonance is due to E' centers and that E' centers are present in alkali silicate glasses.

It is known that the simultaneous presence of aluminum and alkali in a silicate glass will produce strong visible coloration after irradiation. Lell(14) found that the doping of only aluminum into pure SiO_2 did not affect the radiation induced optical absorption bands. EPR measurements made in this laboratory on irradiated aluminum doped SiO_2 show only the E' center resonance that is seen the high purity material. However, the simultaneous presence of aluminum and alkali results in dramatic changes of the radiation induced spectra of SiO_2. The radiation induced optical absorption is shown in Figure 11. The absorption in the visible and near ultraviolet is much more intense in these samples than those containing only alkali. Obrien(45) suggested that the 460 nm and 620 nm absorption bands in smoky quartz arose from two transitions of the same aluminum hole center. The presence of these bands in irradiated high purity silicate glasses suggests that the substitutional perturbation of aluminum for silicon may simply result in an increase in the oscillator strength of the visible bands, and that the basic hole center involves a hole trapped at a non-bridging oxygen which can be bonded to either a silicon or an aluminum. When the aluminum is present, there is strong hyperfine interaction of the hole with the spin 5/2 of the aluminum nucleus, producing a six line splitting which has been described by Griffith, Owen, and Ward(46). Obrien and Pryce(47) proposed a trapped hole at an aluminum atom which substitutes for a silicon atom in the SiO_2 structure, with the hole located mainly on one of the four oxygens, and spending only three percent of its time on the aluminum. The EPR data of Mackey(48) on Al-hole centers in crystal quartz indicated a six line signal of equal intensity and spacing whose g values shifted slightly depending on whether hydrogen, lithium or sodium was available as a charge compensator. The present work on the glassy SiO_2 is in agreement with these results on crystalline quartz and in addition includes data on the Al(K) resonance which is shifted still further to lower g values than the Al(NA) and Al(Li) resonances. This data is shown in Figure 12.

Although the visible absorption bands and EPR resonance in the samples were obviously related to the presence of aluminum, there was no definite correlation with concentration. This might be expected since the formation of these centers requires that the aluminum enter first substitutionally, and secondly paired with an alkali. Experience with the alkali-aluminum doped samples indicated that the previous thermal history of the samples significantly affected their radiation character. Thus sample A with twice as much aluminum and alkali as sample B might show the same response to a given radiation dose.

2) Radiation Damage in High Purity Silicate Glasses

The radiation induced optical absorption of two binary silicates air melted in platinum crucibles is shown in Figure 13. The ultraviolet absorption edge of these glasses at 6 eV prevented measurements at higher energies. Similar spectra were obtained for more complex glasses such as soda lime and alkali-aluminosilicate glasses. All of the high purity silicates exhibited a strong radiation band near 5.4 eV (230 nm). The presence of the charge transfer bands of transition metal and rare earth impurities often causes problems in this region of the spectrum since the impinging radiation can change the valences of the ions. For example the irradiation of typical air melted silicate glasses usually results in a decrease in absorption below 250 nm because Fe^{3+} which strongly absorbs at 230 nm is converted to Fe^{2+} which has a much weaker absorption. By monitoring the EPR signal of ferric iron in silicate glass at $g = 4.28$, it was observed that the conversion of ferric to ferrous iron during x-irradiation proceeds much more rapidly than the initial build-up of the 5.4 eV defect center band. Therefore the use of high purity essentially iron free glasses was required for these experiments. A comparison of the energy, lineshape, growth character and the thermal annealing properties of the 5.4 eV radiation band in the silicate glasses indicate that it is the same as the ultraviolet band observed in the alkali doped SiO_2; namely, the E'_2 center absorption.

The EPR data of the irradiated silicate glasses also indicate the presence of E' centers. The E' resonance is normally resolved only in potassium silicate glasses because the broad hole resonance near $g = 2.01$ often swamps it out. The E' resonance also saturates well before the hole resonance. The EPR data is similar to that for the alkali doped silica shown in Figure 10. The resonance data of Schreurs(43) on irradiated alkali silicate glasses shows evidence of these E' centers. It is not surprising that such a defect center should be present in both SiO2 and alkali silicate glasses since in each case SiO_4 tetrahedra are present and the Si-O bond distance remains roughly 1.6A°. The defect is only dependent on this short range order and therefore might be expected in other silicates as well.

The two visible hole bands at 2 eV and 2.7 eV are also present in the high purity glasses. The low level of aluminum impurity in these glasses (≈ 1 ppm or less) suggests that these transitions may arise from a hole in the valance band of the non-bridging oxygen ion which may have either a silicon or aluminum bonded to it. The aluminum seems capable of enhancing the probability of these transitions. This indicates that the oscillator strength of the optical bands must increase in the presence of aluminum. This assumes of course a correlation between the $g = 2.01$ EPR resonance and the optical absorption bands.

The remaining radiation induced band in the glasses was near 4 eV (310 nm) and has been discussed elsewhere(18). This center appeared to be non-paramagnetic and the current study has not revealed any new information on this defect center.

In summary, the presence of alkali in the Si-O network has been related to the formation of several common radiation induced defect centers in alkali silicate glasses. The alkali indirectly produce the defect centers by creating non-bridging oxygens which then serve as charge trapping sites in the glass network. The irradiation of lightly doped SiO_2 was found to provide a useful technique for studying the formation of defect centers which often occur in more complex silicate glasses. In particular, the intensity of the E_2' band at 5.4 eV and the paramagnetic hole center near $g = 2.01$ have been shown to be directly proportional to alkali content. The E_2' band has also been shown to exist in high purity alkali silicate glasses. This center had previously only been identified in crystalline quartz and fused silica.

2) Transient Radiation Effects in SiO_2 and Silicate Glasses

A. SiO_2

Very few studies of transient radiation effects have been made on silicate glasses. Mace and Gill(49) and Holzrichter and Emmett(50) have observed shortlived coloration in the visible in commercial grade silica. Landry et al(51) have produced transient damage in silicate glasses using intense ultraviolet irradiation. Griscom and

Sigel(52) have reported the observation of transient E' centers in high purity crystalline quartz and fused silica. The latter work will be briefly summarized here.

In pure SiO_2 the only transient coloration observed was centered near 2150A°. The absence of any effects at wavelengths above 3000A° such as those reported elsewhere(50) suggests that the transient damage in the visible results from the presence of impurities. Figure 14 shows a comparison of the permanent damage (solid line) in pure SiO_2 with the transient coloration (points). The permanent band has previously been assigned to electrons trapped on dangling silicon orbitals and is referred to as the E_1' or C band. The low temperature irradiation of 7940 fused silica with electrons produces an additional u.v. band near 265 nm(28). This band is not observed in the pulsed irradiations. The transient damage in 7940 resembles the permanent damage in 7943 (water free material). The longer wavelength band may depend on the migration of H^+ or OH^- ions to existing E' centers. The ratio of the E' band to the 265 nm band was found to be constant in a given sample. The two bands were observed to bleach uniformly. Excitation into the 265 nm band also produces photoluminescence centered near 670 nm. Excitation into the E' band did not produce any observable emission.

The ultraviolet coloration following the electron pulse is also accompanied by an intense luminescence centered near 450 nm. The decay rate of the emission is similar to but not identical with that of the absorption as shown in Figure 15. The spectra of the emission is shown in Figure 16. It shifts to higher energies as the temperature increases.

Any model to be suggested to explain these data must take into account the following experimental observations:

1) Permanent damage (E' band) is observed near 215 nm in irradiated glassy SiO_2. ESR data indicates that it arises from an electron trapped on a sp^3 silicon orbital.

2) Permanent coloration in glassy SiO_2 is more efficient at low temperatures and is dependent on the purity of the sample. Crystal quartz shows little if any permanent E' coloration if reasonably pure.

3) An intense blue luminescence(53) results as these permanent E' centers are bleached thermally. The luminescence intensity can be related to the annihilation rate of the E' centers.

4) There is no evidence of luminescence when exciting into the E' band with u.v. light.

5) The production and annihilation of E' centers during fracture of SiO_2 under ultra high vacuum conditions(32) is also accompanied by a strong blue emission.

6) Pulsed electron irradiation of SiO_2 produces transient absorption centers near 215 nm accompanied by a blue emission with similar time decay characteristics.

7) Decay rates appear exponential for times greater than 200 μsec. The luminescence usually is 10 to 30% faster than the absorption depending on temperature.

8) The decay rates of the transient effects in the fused silica are faster than in α quartz, and are quite temperature sensitive (see Table 2).

9) The production of the transient absorption centers occurs with approximately the same efficiency in the glassy and crystalline materials.

10) The luminescence is not proportional to the rate of decay of the absorption as shown in Figure 15, but almost proportional to the absorption itself.

The similarity of both the transient absorption and emission data with that observed in the case of the permanent damage of SiO_2 suggest that transient E' centers are being created as shown schematically in Figure 17. The pumping radiation can break a Si-O bond. The principal electron trap will be a dangling sp^3 silicon orbital while the principal hole trap will be the non-bonding p orbitals of a non-bridging oxygen. Bond rehealing will take place under ideal conditions in less than a few milli-seconds. However the presence of strains or impurities can prevent bond rehealing and will result in permanent damage. The question of permanent vs transient centers reduces then to the availability of holes for recombination at E' sites. This seems consistent with all of the experimental observations.

The luminescence is more difficult to explain. The first question to be asked is whether it is intrinsic or results from the presence of impurities. The possibility of host sensitized luminescence and charge transfer from impurity centers can not be completely ruled out. However there is strong evidence suggesting that the luminescence is intrinsic and linked to the E' absorption band.

1) The emission was observed to be rather constant in intensity in a variety of silica samples 2) the lifetime of the emission is similar to the E' band lifetime over a wide range 3) thermoluminescence and fracture experiments link the presence of the emission with E' centers. This data is consistent with a mechanism whereby the emission results from the radiative recombination of holes which have been thermally activated out a continuous distribution of shallow traps with electrons at E' sites. The data also indicate that a substantial number of E' centers are annihilated non-radiatively. This model will be discussed in detail in a forthcoming paper.(54) It is summarized in Figure 18. Two types of hole traps are postulated, one of which results in radiative recombination. The kinetic equations obtained using this model are consistent with the behavior in both fused and crystalline quartz except at very low temperatures where another mechanism seems to operate. The ground state of the E' center (level E) lies in the forbidden gap with an energy level similar to an sp^3 hybridized level. The excited state (E*) of the E' level probably lies below the conduction band since excitation at 215 nm produces neither bleaching nor photocurrent. Decay back to the ground state is non radiative. The absorption at any time t is proportional to the number of occupied E levels in the gap. It is postulated that recombination of holes at E' sites produces the emission. However since the intensity I is not proportional $\frac{dNE'}{dt}$, the majority of the E' centers must be annihilated non-radiatively by recombination with holes in H_n sites, probably adjacent to E' centers, at any time t following the pulse. The radiative process results when holes (H_d) are thermally activated out of traps into the conduction band and migrate to an E' site. If the E' population is changing rapidly relative to the H_d concentration because of non-radiative effects, the emission will be roughly proportional to the absorption, especially at low temperatures. This 2 hole center model predicts a deviation of absorption and emission decay times with increasing lifetime which is also observed.

In summary, transient defect centers have been observed in pulse irradiated SiO_2. These appear identical to the E' centers produced by prolonged irradiation. The emission accompanying the decay of the absorption has been attributed to the recombination of migrating holes to E' sites. The experiment has shown that E' defects are easily formed even in crystalline SiO_2. It illustrates the dynamic equilibrium which is maintained during irradiation and has provided a loss mechanism for energetic radiation in SiO_2. The experiment also has important consequences when considering radiation hardening of electronic devices involving SiO_2 films. Because of the long lifetime of the transient damage in SiO_2, high electric fields may tend to sweep carriers away before recombination takes place. This would produce a much larger concentration of defect centers per unit dose than would be indicated by permanent damage studies. Finally the data is consistent with the mechanisms previously suggested for glassy SiO_2, namely that damage proceeds by the ionization of Si-O bonds, some of which do not reheal because of the presence of strained bonds or impurities.

Transient Damage in Silicate Glasses

Pulsed irradiations have also been made on alkali doped SiO_2 and high purity alkali silicate glasses. Short lived coloration was observed in all cases. However, contrary to the situation in SiO_2, silicate glasses show substantial permanent coloration per pulse which makes it impossible to measure point by point across a band. This behavior is consistent with the hypothesis that the introduction of alkali produces non-bridging oxygens which can serve as permanent hole traps. Further investigations are planned on the transient coloration of lightly doped silica and quartz.

D) Luminescence

Numerous luminescent centers have been reported in silicate glasses. Much of the data has been summarized in reviews by Weyl(55) and Rindone(56). Virtually all of the centers reported can be traced to the presence of impurities, primarily rare earths and transition metals. The problem to be discussed here is whether pure SiO_2 or high purity silicate glasses exhibit any luminescence which can be associated with intrinsic defects in the Si-O network.

It is well known that most fused silica fluoresces strongly in the blue when exposed to u.v. light. However, the high purity synthetic materials such as Corning 7940 and Suprasil show essentially no fluorescence. The impurity content of the well known luminescent activators such as copper, manganese and silver has been measured to be less than 50 parts per billion(57,58) in these materials. These materials also show no evidence of an absorption band near 5.13 eV (242 nm) which has been associated with germanium impurity (50,60) and which has been correlated with a 3.04 ev emission band(61).

In the present investigation, ultraviolet excitation at room temperature using both xenon and high pressure mercury sources failed to produce any recordable emission in the high purity SiO_2. At liquid nitrogen temperature, however, all samples exhibited a strong emission (Figure 19) band at 2.9 eV with an excitation peak near 4.2 eV. The band was present in both crystalline quartz and fused silica. The introduction of alkali, aluminum and germanium impurities did not influence the intensity or shape of the emission curve. Further work is needed to determine the mechanism responsible for the emission and to attempt a correlation with the luminescence observed in the pulsed electron experiments. Other emission bands were observed in some samples but not others, indicating impurity sensitization, for example, a weak 2.2 eV band in the 7940.

One other interesting emission has been observed. The low temperature irradiation of SiO_2 with 2 MeV electrons produces ultraviolet absorption bands(28) at 215 nm and 257 nm. The shorter wavelength band is the E' center. The other band has been linked to the presence of water in silica since Corning 7943 and Suprasil W do not exhibit this radiation band. In the present investigation, it was consistently observed that the ratio of the intensities of the two bands remained constant in a given sample, and that the two centers bleached uniformly. Ultraviolet excitation into this (4.9 eV) band produced an emission (Figure 20) at 1.0 eV (670nm) which is not observed in the unirradiated silica. Thermal bleaching of the band also produces the red emission. A shift of 1 eV of both the absorption (4.9 vs 5.9 eV) and emission (1.9 vs 2.9 eV) relative to the E' center indicates that a new level may be present in the forbidden gap because of the presence of either H^+ or OH^-. The evidence suggests that protons migrate to E' centers producing a lower energy band near 4.9 eV. This results in a sharp decrease in the intensity of the E' band. The relative ratio of the two bands will depend both on the water content of the sample and the temperature during irradiation.

Although most of the emission bands in SiO_2 result from impurities, the two bands discussed here seem to be the best candidates for association with intrinsic processes. Further work is in progress to further clarify the present situation.

IV Summary

A review has been presented of some spectroscopic investigations of silicate glasses in the ultraviolet. The intrinsic ultraviolet absorption of both SiO_2, doped SiO_2 and silicate glasses has been measured. The introduction of alkali into SiO_2 has been found to produce an optical absorption band near 8.5 eV which shifts the fundamental edge to longer wavelengths. The universal presence of the 11.5 eV band in both SiO_2 and silicate glasses suggests that it results from a transition characteristic of the SiO_4 tetrahedron. The presence of alkali in the Si-O network has been related to the formation of several common radiation-induced defect centers in alkali silicate glasses. In doped silica samples, the intensity of the E_2' band at 5.4 eV and the paramagnetic hole center near $g = 2.01$ have both been shown to be proportional to alkali content. The 5.4 eV band has also been observed in irradiated high purity silicate glasses. Transient E' centers have been observed in both high purity crystalline quartz and fused silica, and have been correlated with a blue emission. A two hole center model has been suggested to account for the kinetics of transient processes. Finally, two emission bands have been discussed which may result from processes or defects intrinsic to the SiO_2 network.

Acknowledgments

The author is indebted to Mr. R. J. Ginther of the Naval Research Laboratory for the preparation of the high purity silicate glasses and to Dr. E. Lell of Bausch and Lomb, Inc., Rochester, N.Y. for the doped fused silica samples. The author also wishes to acknowledge Dr. D. L. Griscom who helped with the measurement and data analysis of the transient radiation effects work.

List of Tables

Table 1 Energies of Reflection Peaks in Silicate Glasses.

Table 2 Temperature Dependence of Decay Times in Crystal Quartz.

TABLE I

Energies of Reflection Peaks in Silicate Glasses

Glass Type	Location of Reflection Peaks (eV)			
SiO_2 (crystal)	-	-	10.2	11.5
SiO_2 (glassy)	-	-	10.2	11.5
1 Li_2O-2 SiO_2	8.5	9.3	-	11.5
1 Na_2O-2 SiO_2	8.5	9.3	-	11.5
1 Na_2O-3 SiO_2	8.5	9.3	-	11.5
1 Na_2O-6 SiO_2	-	9.0*	-	11.5
1 Na_2O - 1 CaO-5 SiO_2	8.5	9.3	-	11.5
1 Na_2O-1 Al_2O-3 SiO_2	8.5	-	10.2	11.5

*This broad peak appears to result from contributions from 8.5 and 9.3 eV peaks.

TABLE 2

Temperature Dependence of Decay Times in Crystalline Quartz

Temperature (^oK)	Luminescence $\tau_{1/2}$ (μsec)	Absorption $\tau_{1/2}$ (μsec)
4.2	825 ± 10	1035 ± 10
77	700 ± 25	840 ± 20
300	3 - 150	---

REFERENCES

1. E. Lell, J. Am. Ceram. Soc. 43, (1960) 422.
2. G.H. Sigel, Jr., J. Phys. Chem. Solids 32, (1971) 2373.
3. P.H. Berning, G. Hass, and R.P. Madden, J. Opt. Soc. Am. 50, (1960) 586.
4. R.T. Williams, R.G. Fuller, M.N. Kabler, and V.H. Ritz, Rev. Sci. Inst. 40, (1969) 1361.
5. H.R. Phillip, Solid State Commun. 4, (1966) 73.
6. H.R. Phillip, J. Phys. Chem. Solids 32, (1971) 1935.
7. A.R. Ruffa, Phys. Stat. Sol. 29, (1968) 605.
8. M.H. Reilly, J. Phys. Chem. Solids 31, (1970) 1041.
9. A.J. Bennett and L.M. Roth, J. Phys. Chem. Solids 32, (1971) 1251, Phys. Rev. B4, (1971) 2686.
10. I.V. Abarenkov, A.V. Amosov, V.F. Bratsev, and D.M. Yudin, Phys. Stat. Sol. 2, (1970) 865.
11. E. Loh, Solid State Commun. 2, (1964) 269.
12. J.H. Konnert and J. Karle, Nature Phys. Sci. 236, (1972) 92.
13. R.L. Mozzi and B.E. Warren, J. Appl. Cryst. 2, (1969) 164.
14. T.H. Distefano and D.E. Eastman, Phys. Rev. Letters 27, (1971) 1560.
15. D.J. Nagel, in Advances in X-ray Analysis, 13 Plen Press, New York (1970) 182.
16. G. Wiech, in Soft X-ray Band Spectra, Academic Press, New York (1968) 59.
17. G.H. Sigel, Jr., and R.J. Ginther, J. Glass Tech. 9, (1968) 66.

18. A. Kats and J.M. Stevels, Phillips Res. Rep. 11, (1956) 115.

19. E. Lell, Phys. Chem. Glass 3, (1962) 84.

20. K. Platzoder, Phys. Stat. Sol. 29, (1968) K63.

21. E.I. Swarts and L.M. Cook, Proc. 7th Inter. Cong. Glass (1965) 23.

22. F.N. Steele and R.W. Douglas, Phys. Chem. Glasses 6, (1965) 246.

23. W.D. Johnston, J. Am. Cer. Soc. 47, (1964) 198.

24. T. Castner, G.S. Newell, W.C. Holton and C.P. Slichter, J. Phys. Chem. 32, (1960) 668.

25. R.H. Sands, Phys. Rev. 99, (1955) 1222.

26. I. Simon, in *Modern Aspects of the Vitreous State*, Vol. 1, Butterworths, London (1960) Chap. 6.

27. R.J. Ginther and R.D. Kirk, J. Non Crystalline Solids 6, (1971) 89.

28. G.W. Arnold and W.D. Compton, Phys. Rev. 116, (1959) 802.

29. C.M. Nelson and R.A. Weeks, J. Appl. Phys. 32, (1961) 883.

30. C.W. Gwyn, J. Appl. Phys. 40, (1969) 4886.

31. R.A. Weeks, J. Appl. Phys. 27, (1956) 1376, Phys. Rev. 130, (1963) 570.

32. G. Hochstrasser and J.F. Antonini, Surface Science 32, (1972) 644.

33. T.W. Hickmott, J. Appl. Phys. 42, (1971) 2543.

34. G.H. Sigel, Jr., Bull. Am. Phys. Soc. 17, (1972) 287.

35. E.W. Mitchell and E.G. Paige, Phil. Mag. 1, (1956) 1085.

36. R.A. Weeks, J. Am. Ceram. Soc. 53, (1970) 176.

37. E. Lell, N.J. Kreidl and J.R. Hensler, in *Progress in Ceramic Science*, Vol. 3, Pergamon Press, New York (1966) 1-93.

38. A. Bishay, J. Non-Cryst. Solids 3, (1970) 54.

39. J.S. Stroud, J. Chem. Phys. 37, (1962) 836.

40. J.H. Mackey, H.L. Smith and J. Nahum, J. Phys. Chem. Solids 27, (1966) 1773.

41. J.H. Mackey, H.L. Smith and A. Halperin, J. Phys. Chem. Solids 27, (1966) 1759.

42. J.H. Mackey, J.W. Boss and M. Kopp, Phys. Chem. Glasses 11, (1970) 205.

43. J.W. Schreurs, J. Chem. Phys. 47, (1967) 818.

44. G.H. Sigel, Jr., Proc. 9th Intern. Congr. Glass 1, (1971) 801.

45. M.C.M. Obrien, Proc. Roy. Soc. (London) A231, (1955) 404.

46. J.H.E. Griffith, J. Owen, and I.M. Ward, Nature 173, (1954) 439.

47. M.C.M. Obrien and M.H.L. Pryce, *Defects in Crystalline Solids*, London Physical Society (1954) 88.

48. J.H. Mackey, Jr., J. Chem. Phys. 39, (1963) 74.

49. P.N. Mace and D.H. Gill, IEEE Trans. Nucl. Science 14, (1967) 62.

50. J.F. Holzrichter and J.L. Emmett, J. Appl. Phys. 40, (1969) 159.

51. R.J. Landry, E. Snitzer and R.H. Bartram, J. Appl. Physics 42, (1971) 3827.

52. D.L. Griscom and G.H. Sigel, Jr., Bull. Am. Phys. Soc. 13, (1968) 1474, G.H. Sigel, Jr. and D.L. Griscom, Bull. Amer. Ceram. Soc. 48, (1969) 447.

53. N. Kristianpoller and I. Katz, J. Opt. Soc. Am. 60, (1970) 424.

54. G.H. Sigel, Jr., D.L. Griscom and M.H. Reilly (to be published).

55. W.A. Weyl, Coloured Glasses, Soc. of Glass Technology, Sheffield (1951).

56. G.E. Rindone, in Luminescence of Inorganic Solids, Academic Press (1966) 419.

57. Amersil, Inc., Brochure, Optical Fused Quartz and Fused Silica (1970) 4.

58. G. Hetherington and L.W. Bell, Phys. Chem. Glasses 8, (1967) 206.

59. V. Garino-Canina, Compt. Rend. 242, (1956) 1982.

60. A.J. Cohen, Phys. Rev. 105, (1957) 1151.

61. W.H. Turner and H.A. Lee, J. Chem. Phys. 44, (1966) 1428.

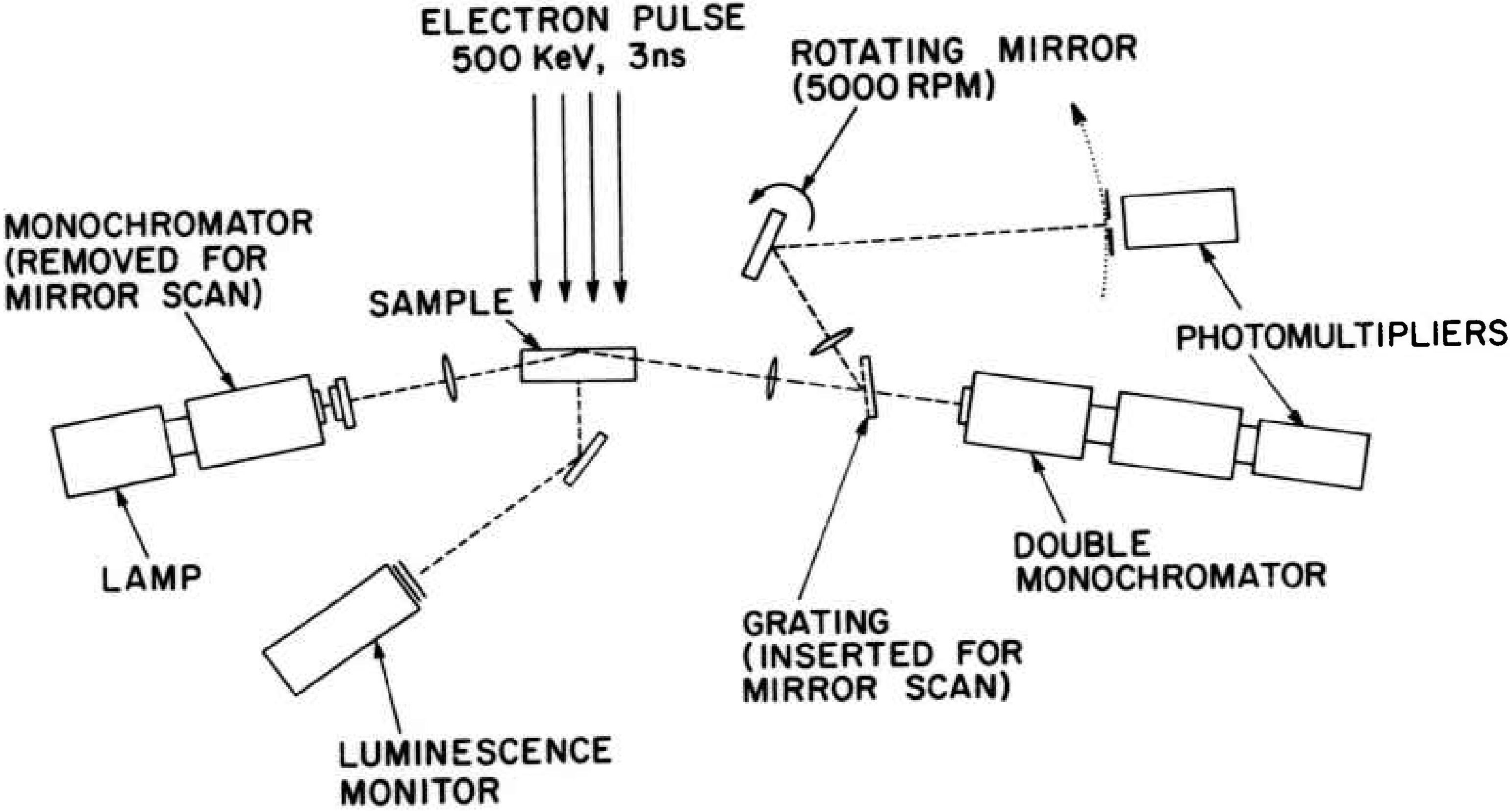

Fig. 1 - Schematic of apparatus used to measure transient absorption and emission. The system was designed to permit point by point or rapid scan measurements. (Courtesy of C. Marquardt)

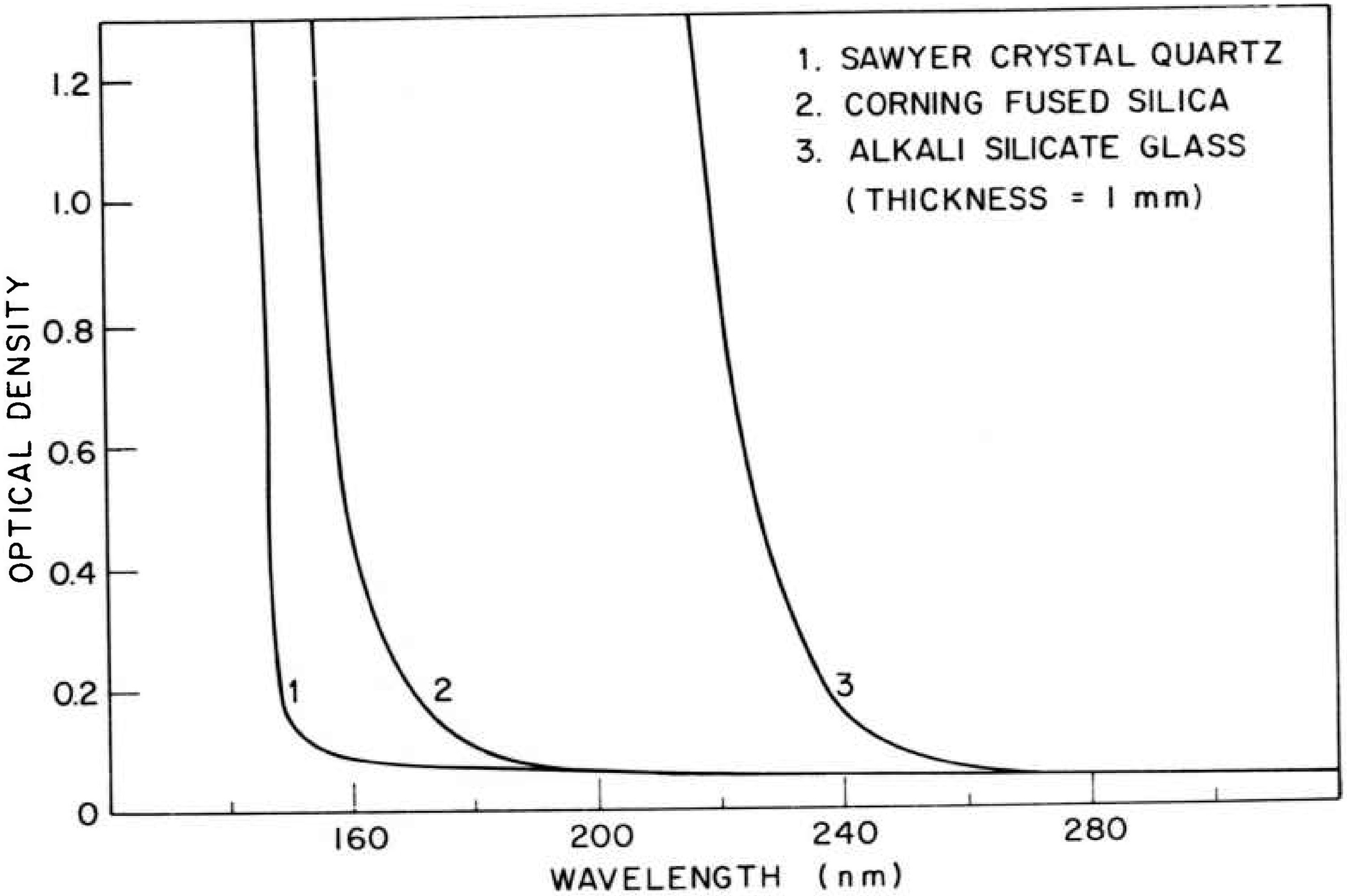

Fig. 2 - Position of ultraviolet absorption edges of high purity (1) crystalline quartz. (2) fused silica and (3) NRL 2 SiO_2 - NA_2O glass (samples of 1 mm thickness.

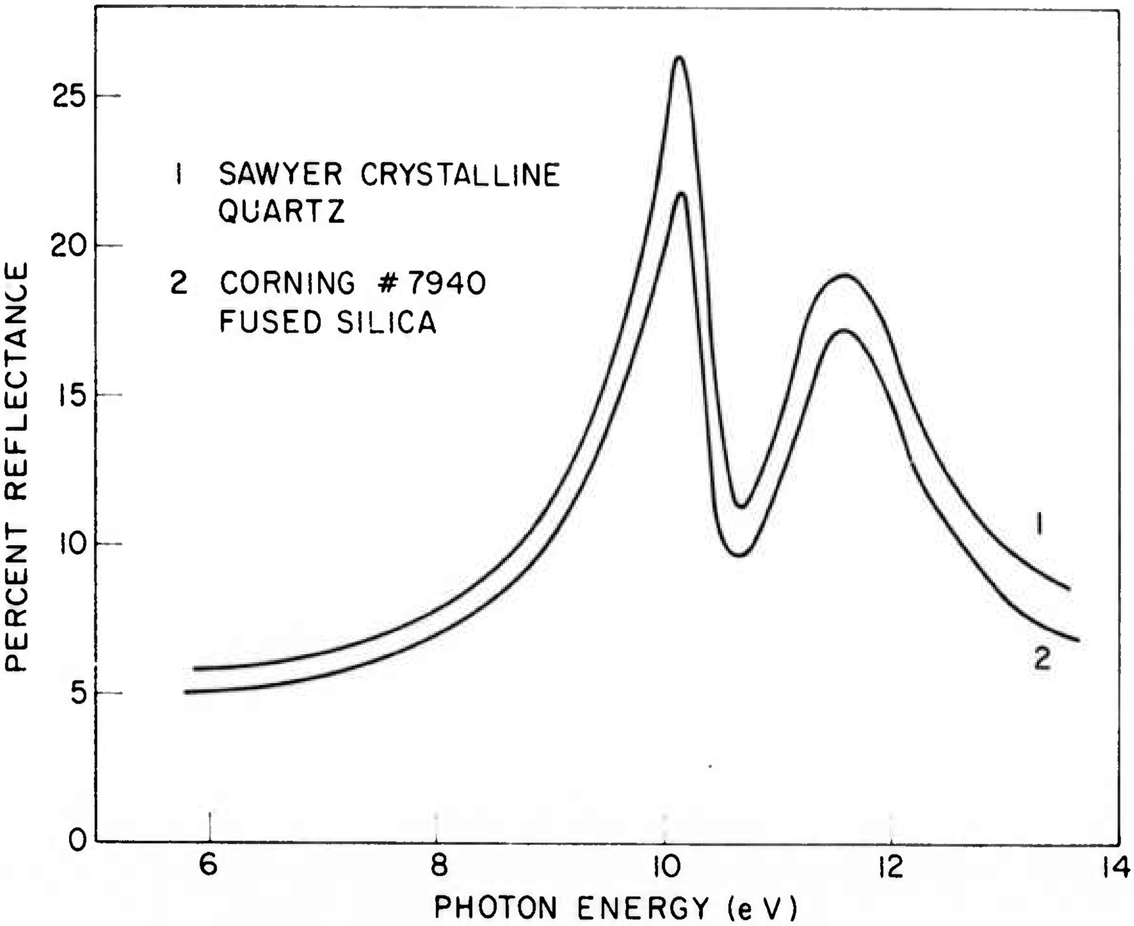

Fig. 3 - Vacuum ultraviolet reflectance of high purity (1) crystalline quartz and (2) fused silica showing the two lowest energy peaks at 10.2 eV and 11.5 eV. Additional peaks are observed at higher energies.

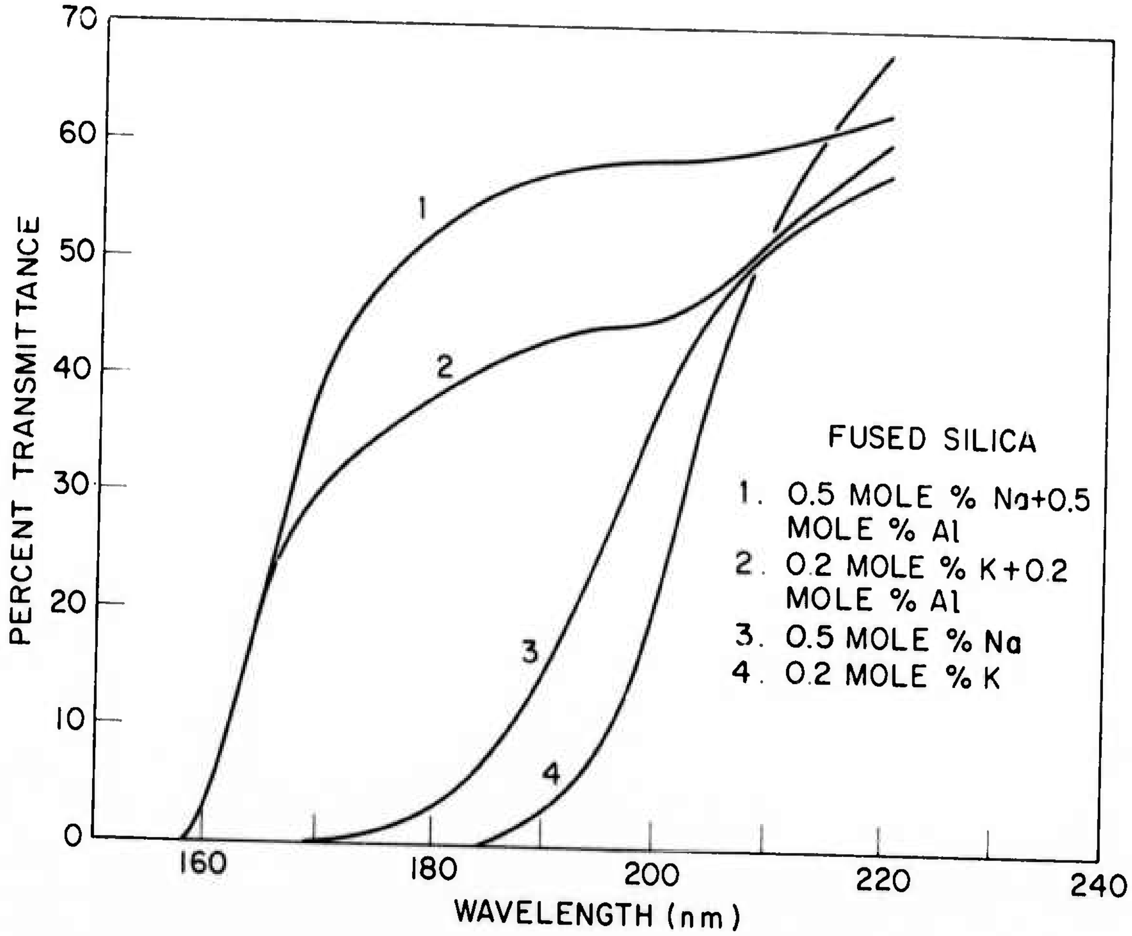

Fig. 4 - The effect of aluminum on the ultraviolet transmittance of alkali doped SiO_2. Samples codoped with aluminum and alkali showed weaker absorption in the 200 nm - 160 nm (6 - 8 eV) region probably because of the reduction of non-bridging oxygens by aluminum-alkali pairing in the network.

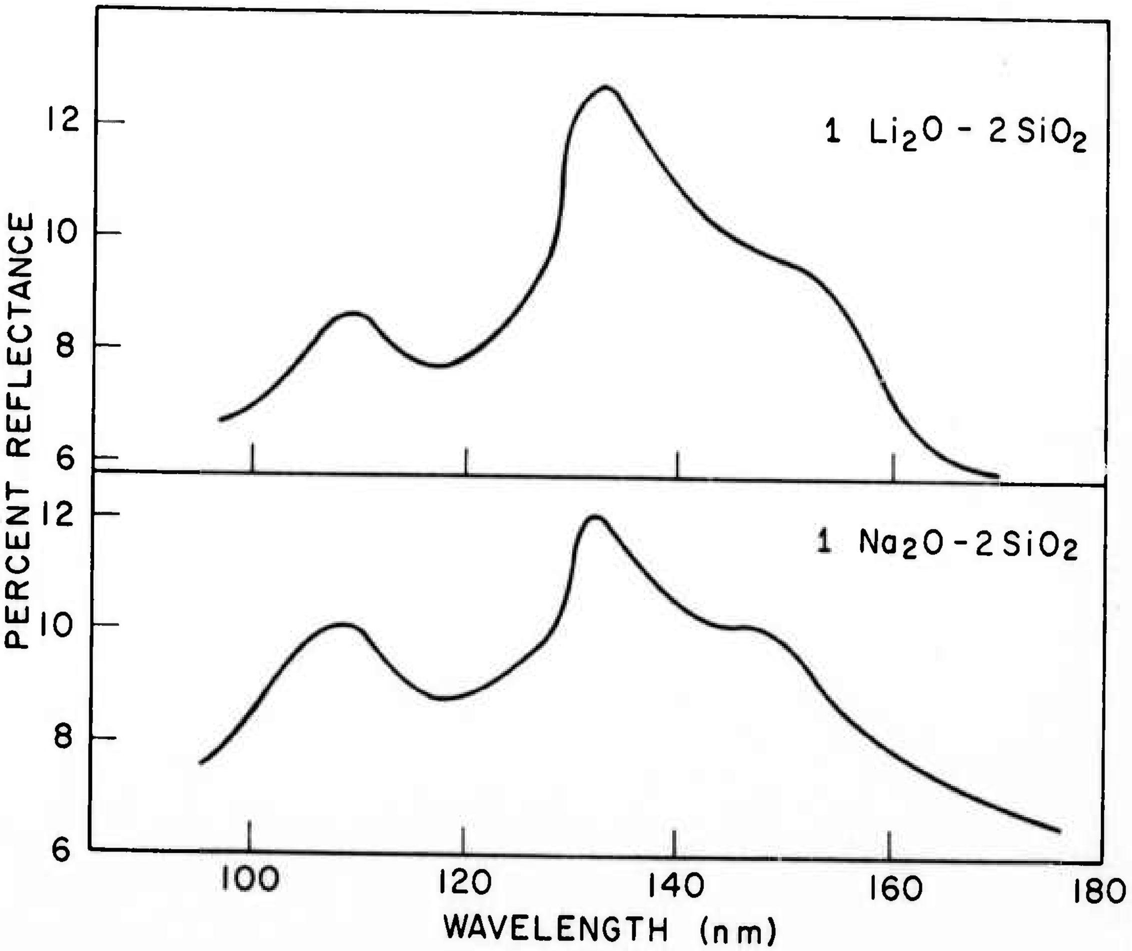

Fig. 5 - Reflectance spectra of two simple binary silicate glasses (upper) 1 Li_2 -2 SiO_2 (lower curve) 1 Na_2O-2 SiO_2. This data shows the similarity of the spectra regardless of the type of network modifier as well as the tailing of the low energy band.

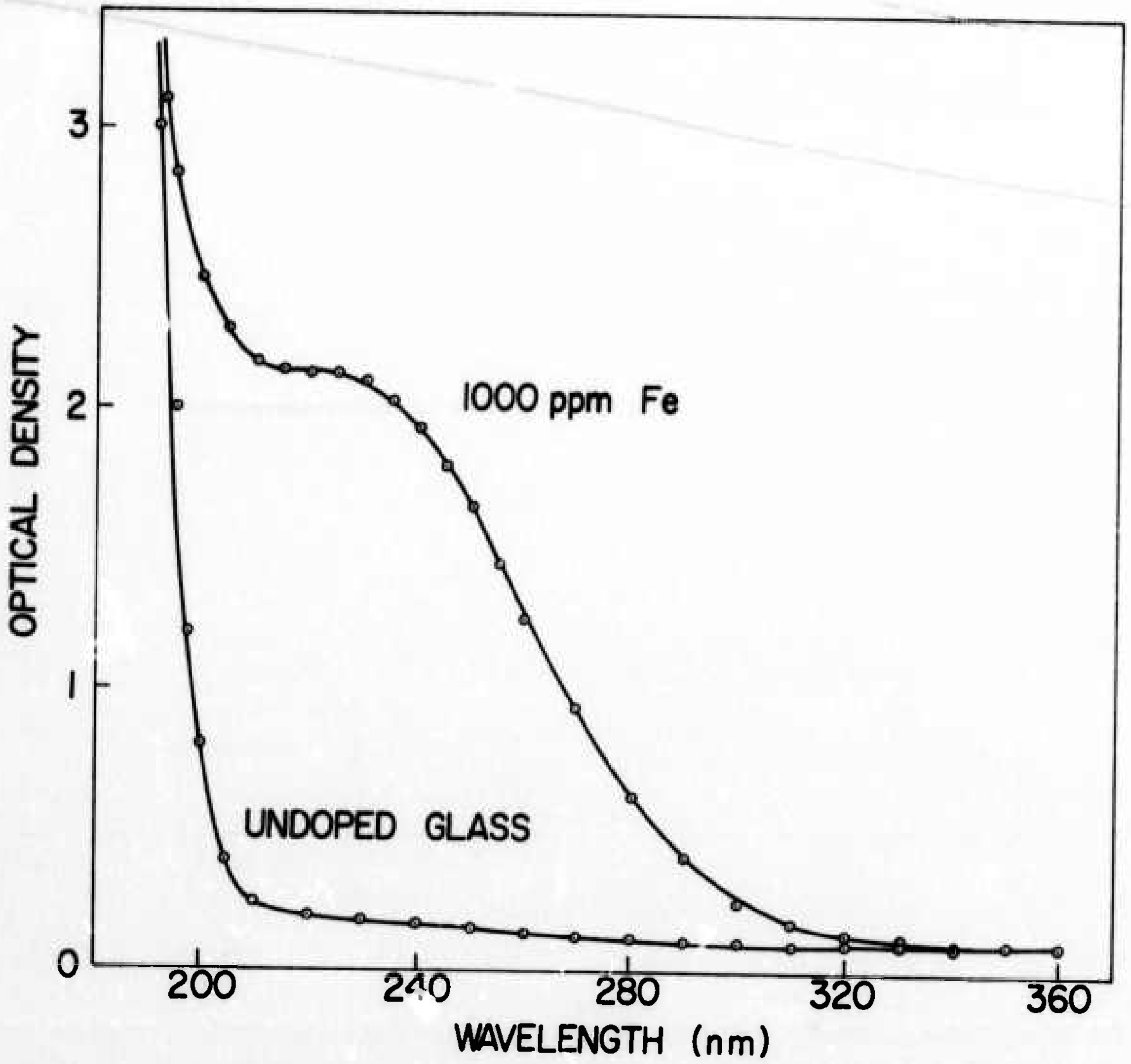

Fig. 6 - Ultraviolet absorption of undoped and iron-doped 3 SiO_2 -1 Na_2O glass melted in an oxidizing atmosphere (samples of 0.05 mm thickness).

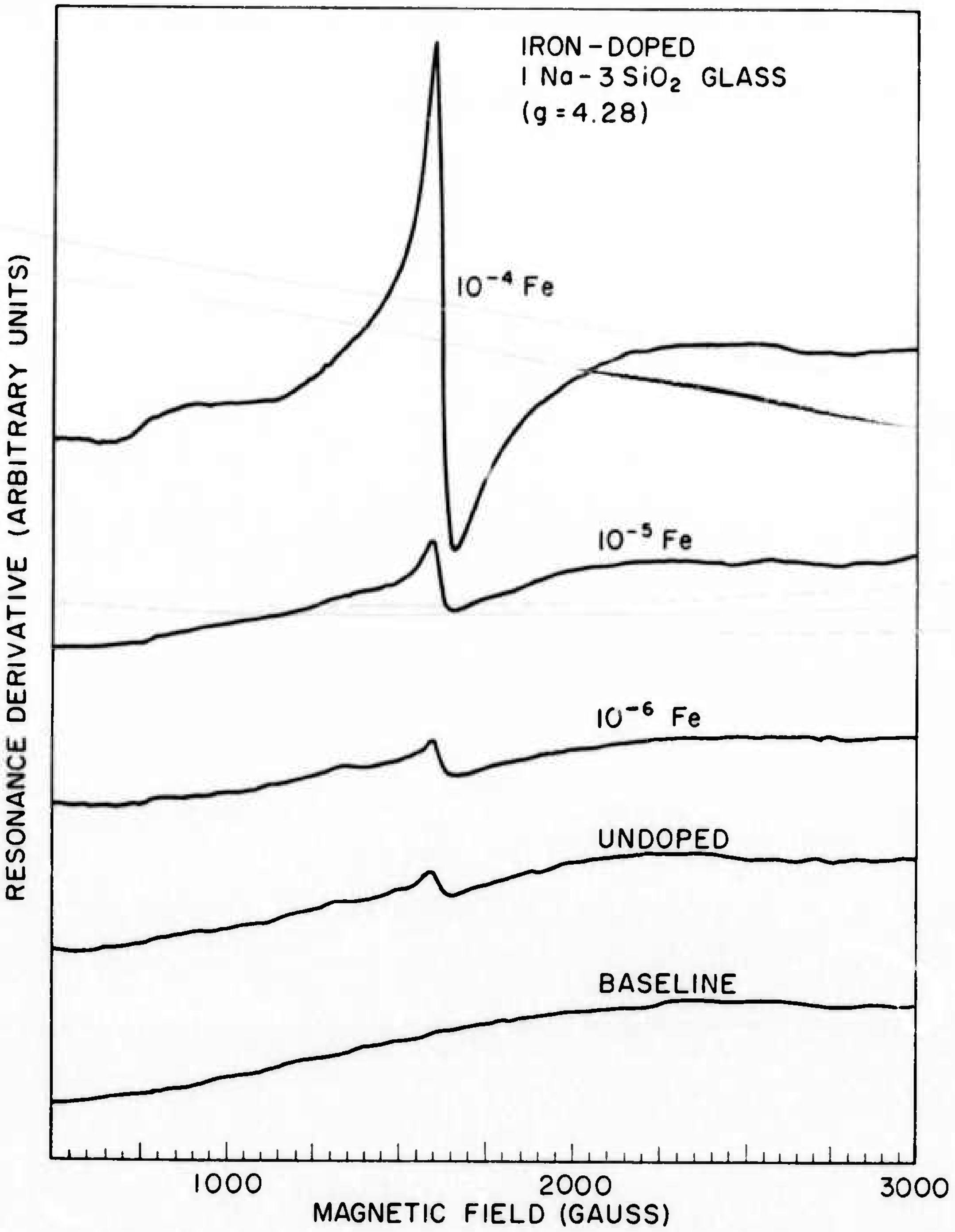

Fig. 7 - ESR signals from a series of iron-doped glasses indicating the sensitivity of the technique for detection of ferric iron.

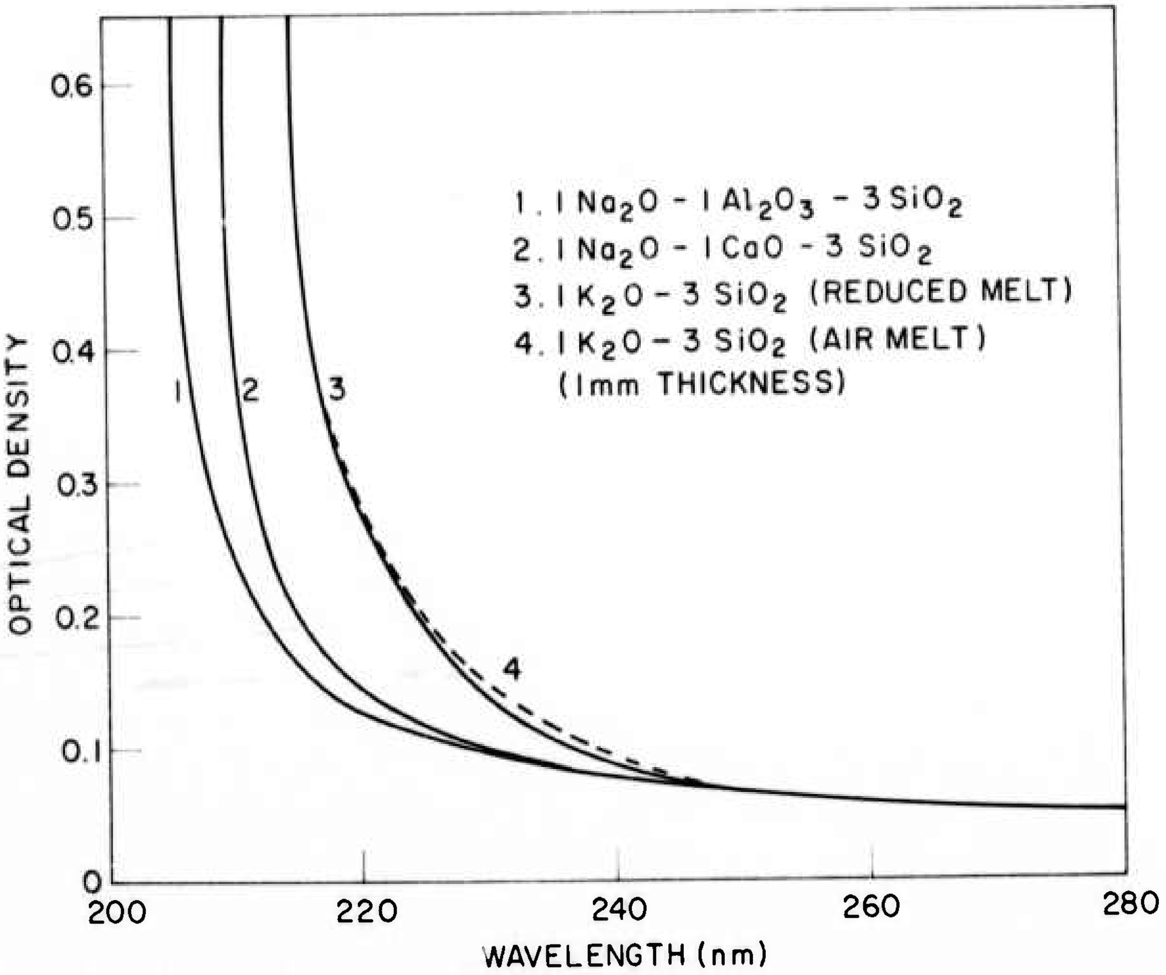

Fig. 8 - Location of ultraviolet edge for some typical high purity silicate glasses. The slight difference between air melted and reduced potassium silicate glass absorption is due to the presence of about 1 ppm iron.

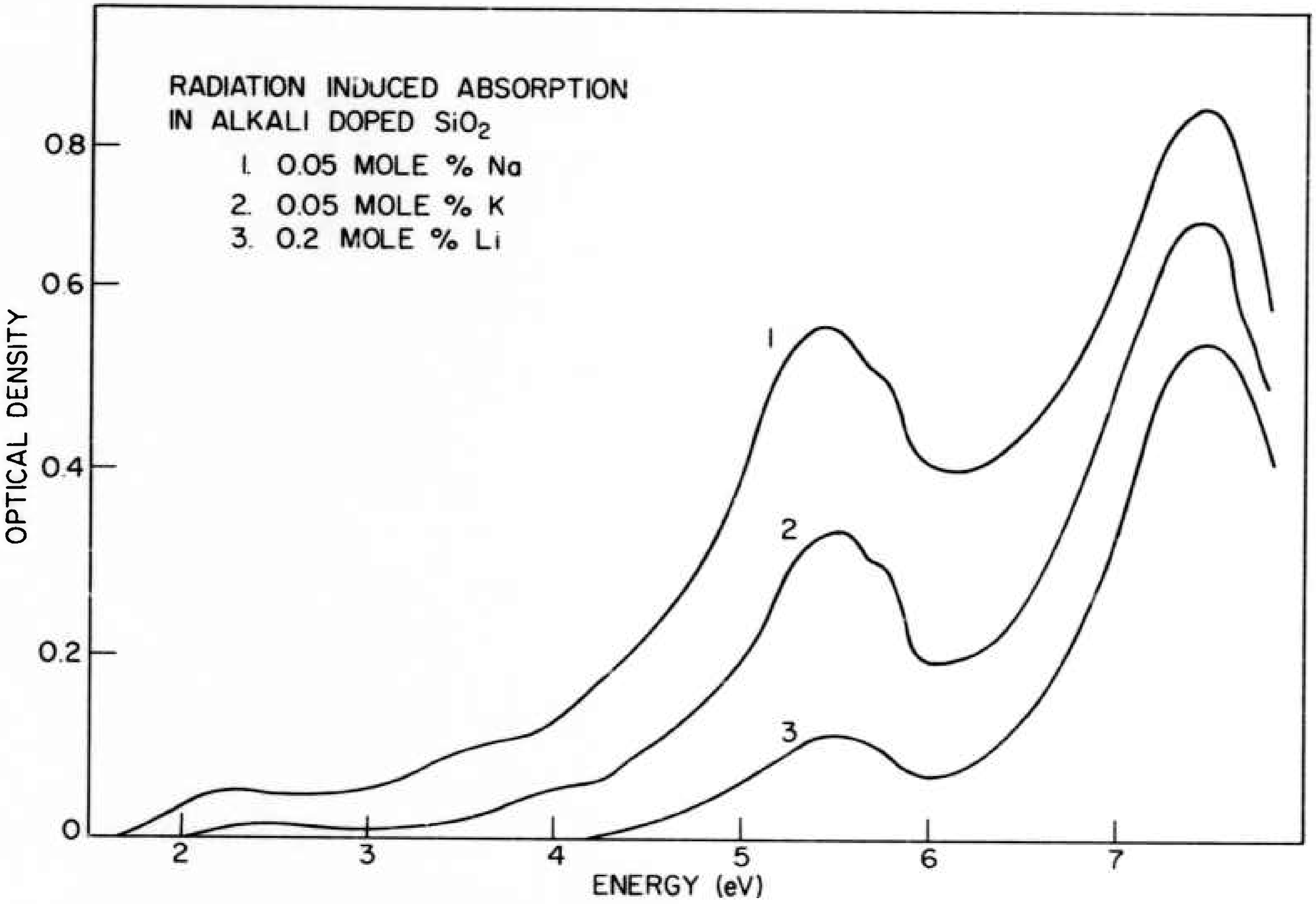

Fig. 9 - The radiation induced optical absorption in the alkali doped silica indicating the E_2' and E_1' bands at 5.4 and 5.8 eV and the hole band at 7.6 eV. The radiation dose is approximately 10^6R.

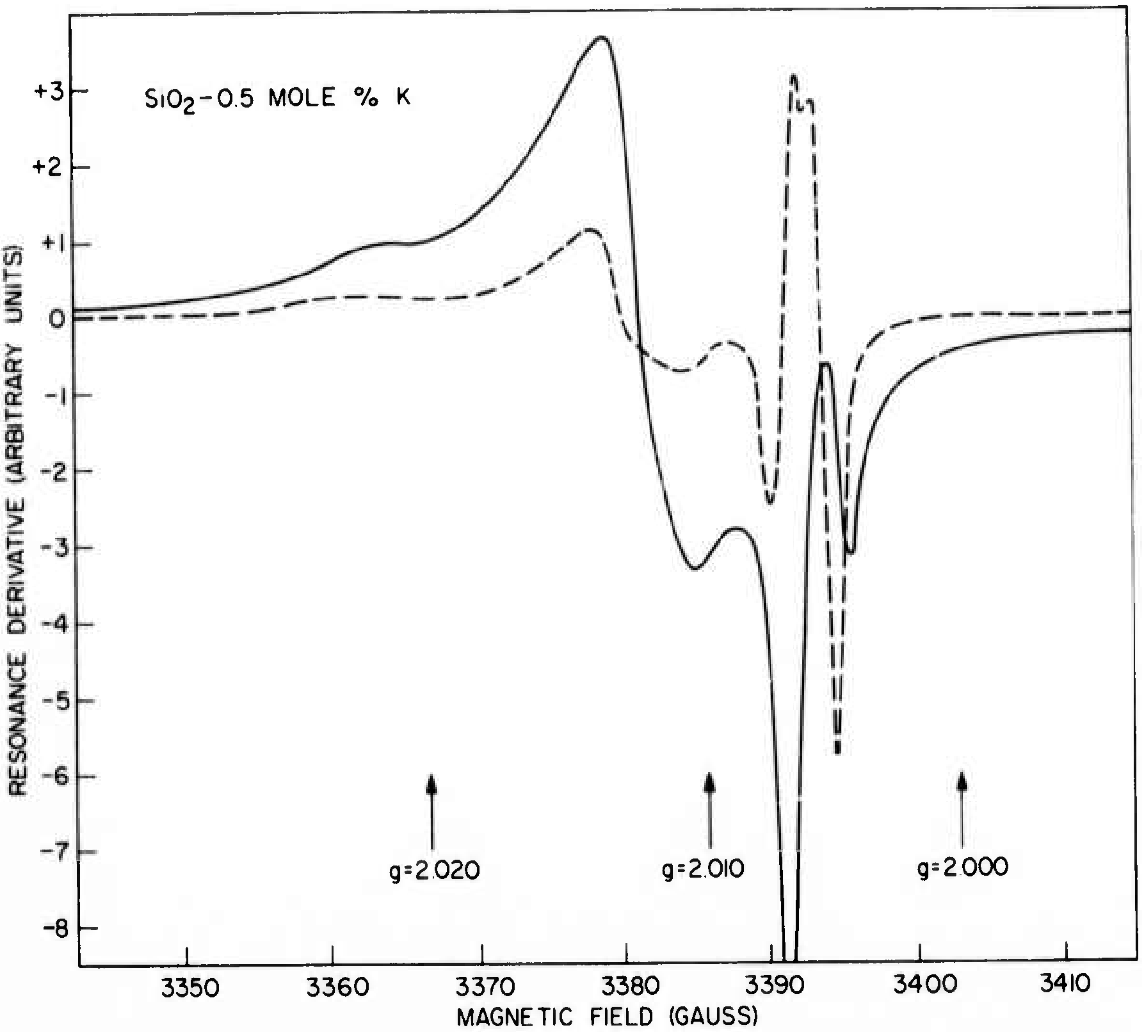

Fig. 10 - The EPR spectrum of an x-irradiated SiO$_2$ sample doped with 0.5 mole % potassium. The dotted curve was taken at 5 milliwatts power in the cavity and the solid curve at 100 milliwatts. The E' center at g = 2.0006 tends to saturate significantly with cavity power level. The remainder of the resonance results from the trapped hole center with lower than axial symmetry and having the principal g values of $g_1 = 2.003$, $g_2 = 2.009$, $g_3 = 2.019$.

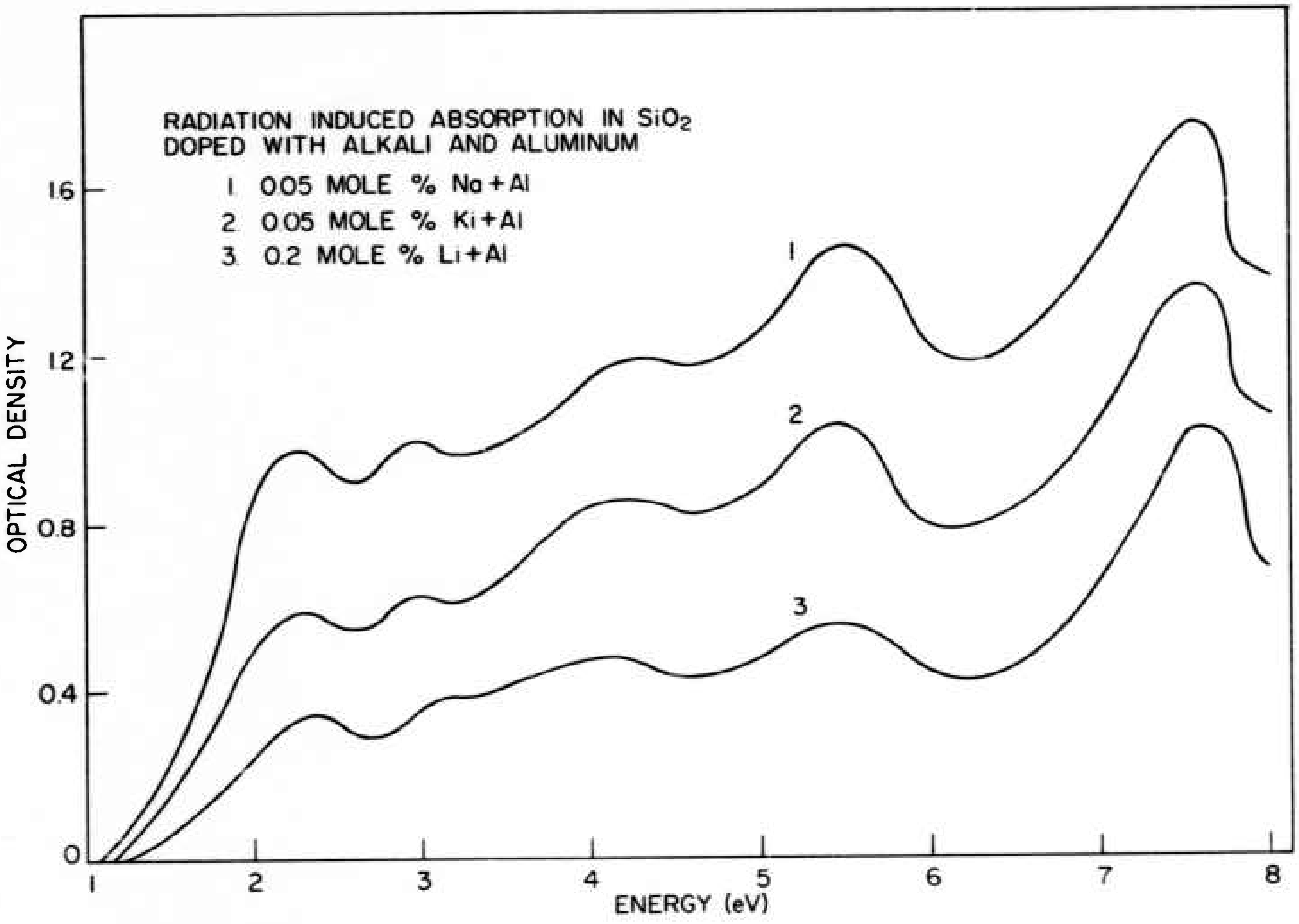

Fig. 11 - The radiation induced optical absorption of SiO_2 doped with alkali and aluminum. The increase in the visible absorption when aluminum is present may arise from an increase in oscillator strength rather than the production of many more defect centers. The radiation dose is approximately 10^6 R.

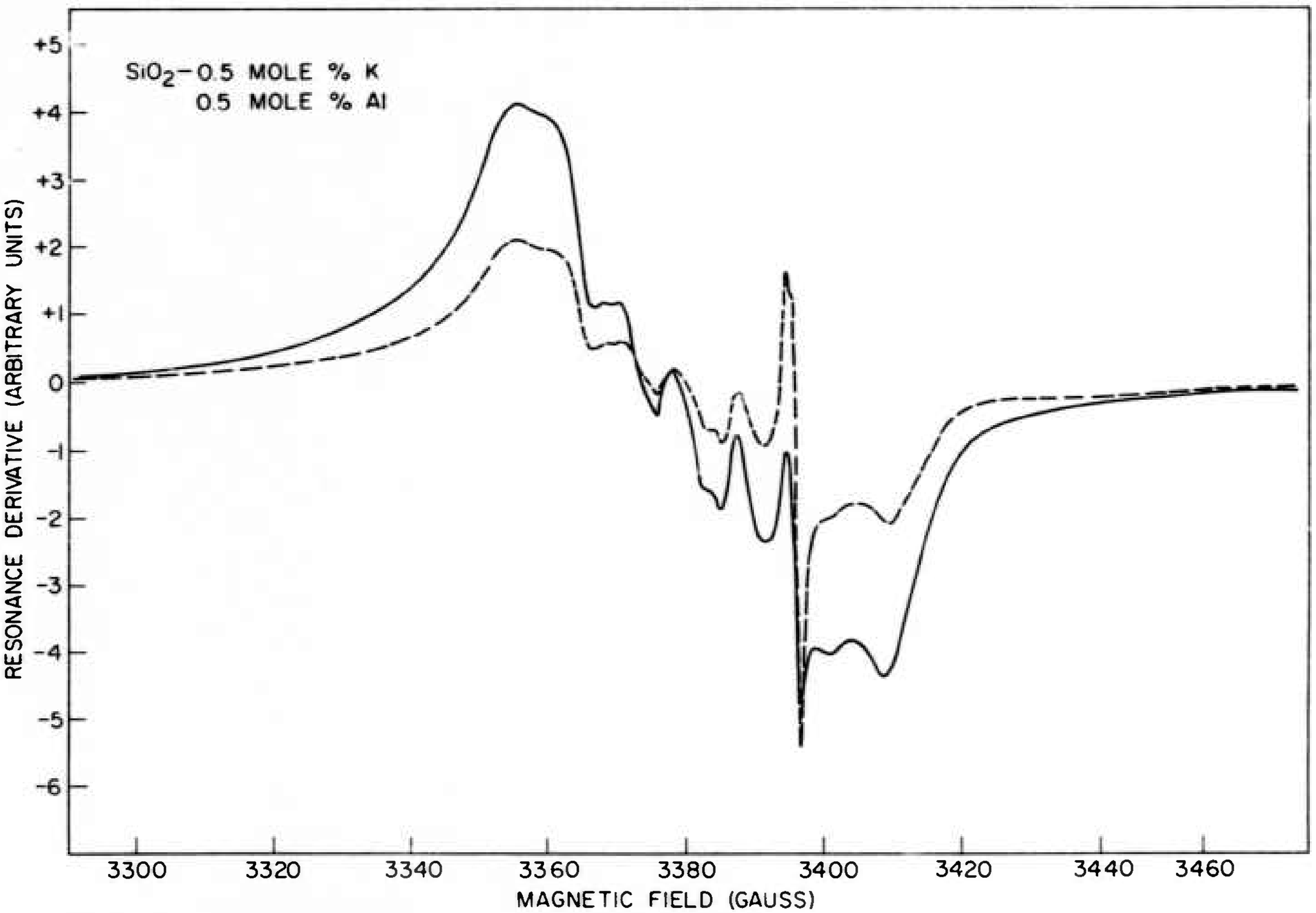

Fig. 12 - The EPR spectrum of an x-irradiated SiO_2 sample doped with 0.5 mole % potassium and 0.5 mole % aluminum. The dotted and solid curves represent the spectrum at 20 milliwatts and 100 milliwatts cavity power respectively. The E' resonance is clearly visible in the low power spectrum. The hyperfine interaction of the hole with the aluminum nucleus of spin 5/2 produces the six line splitting superimposed on the broader resonance.

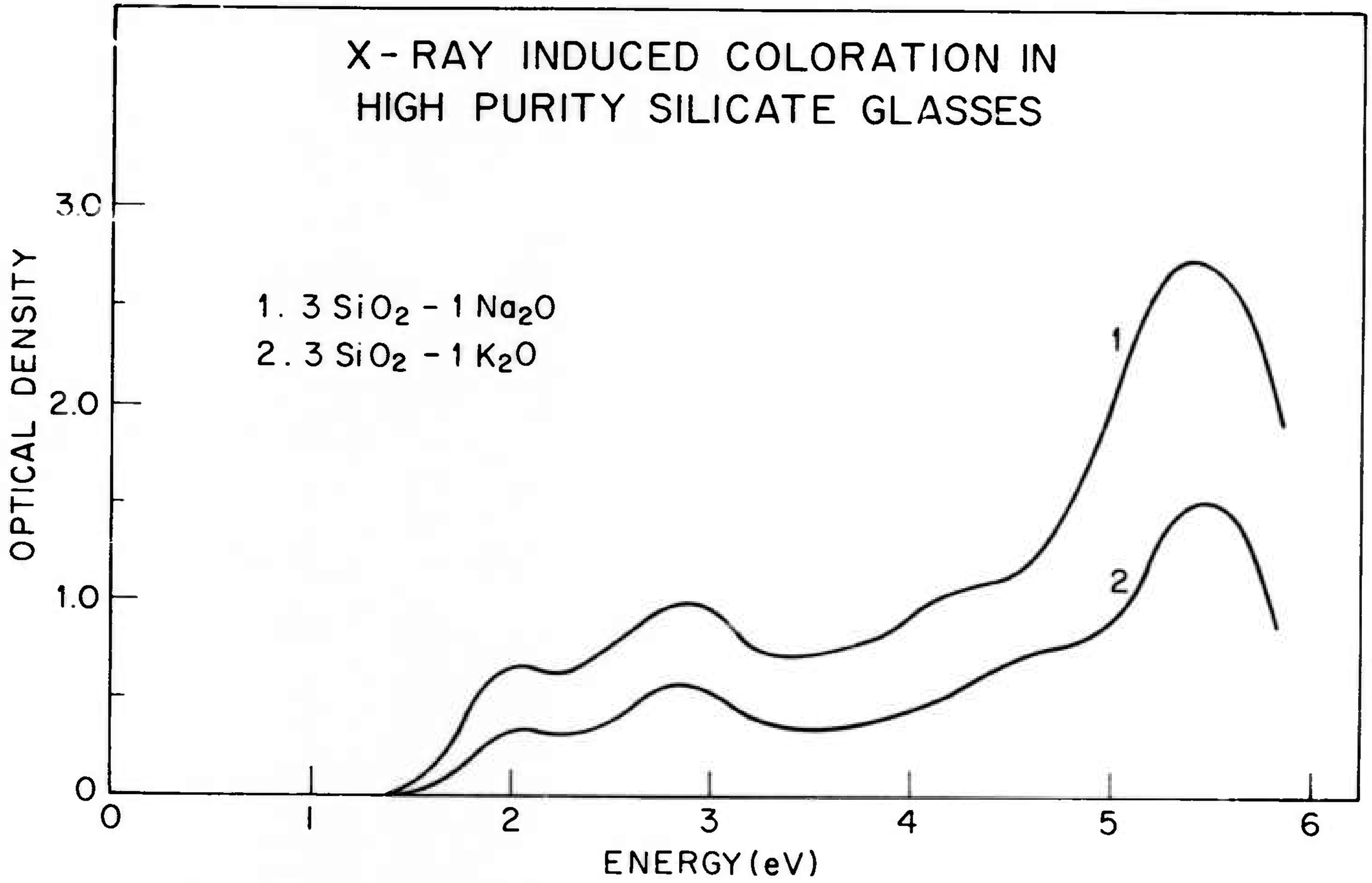

Fig. 13 - The radiation induced optical absorption in two air melted high purity alkali silicate glasses. The strong band at 5.4 eV (230 nm) has been attributed to E_2' type centers which may be a major electron trap in alkali silicate glasses.

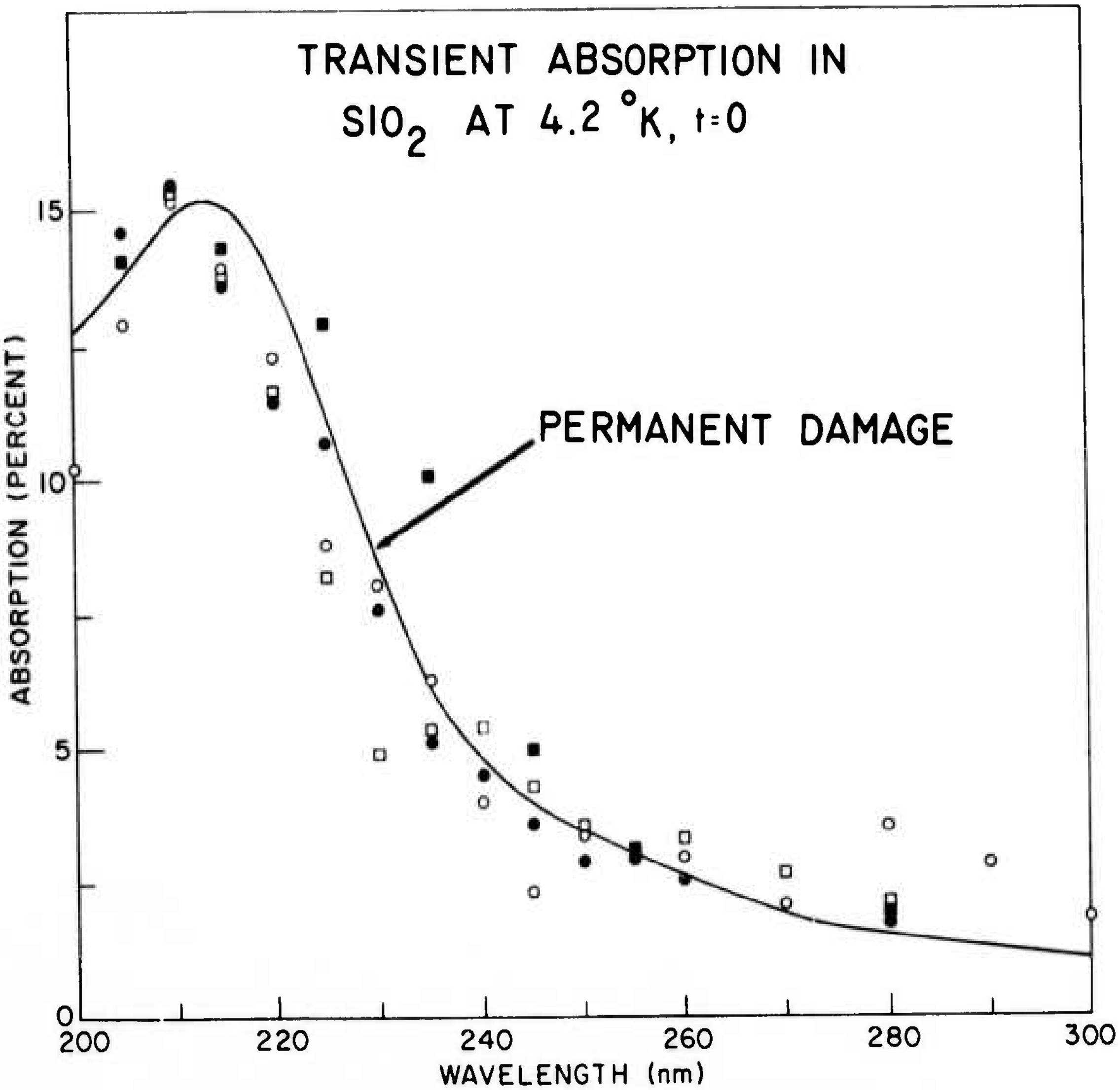

Fig. 14 - A comparison of the permanent damage (solid line) observed in Corning 7943 silica (after Arnold and Compton) with the transient coloration (points) measured immediately following the electron pulse. The band near 215 nm is the E_1' band.

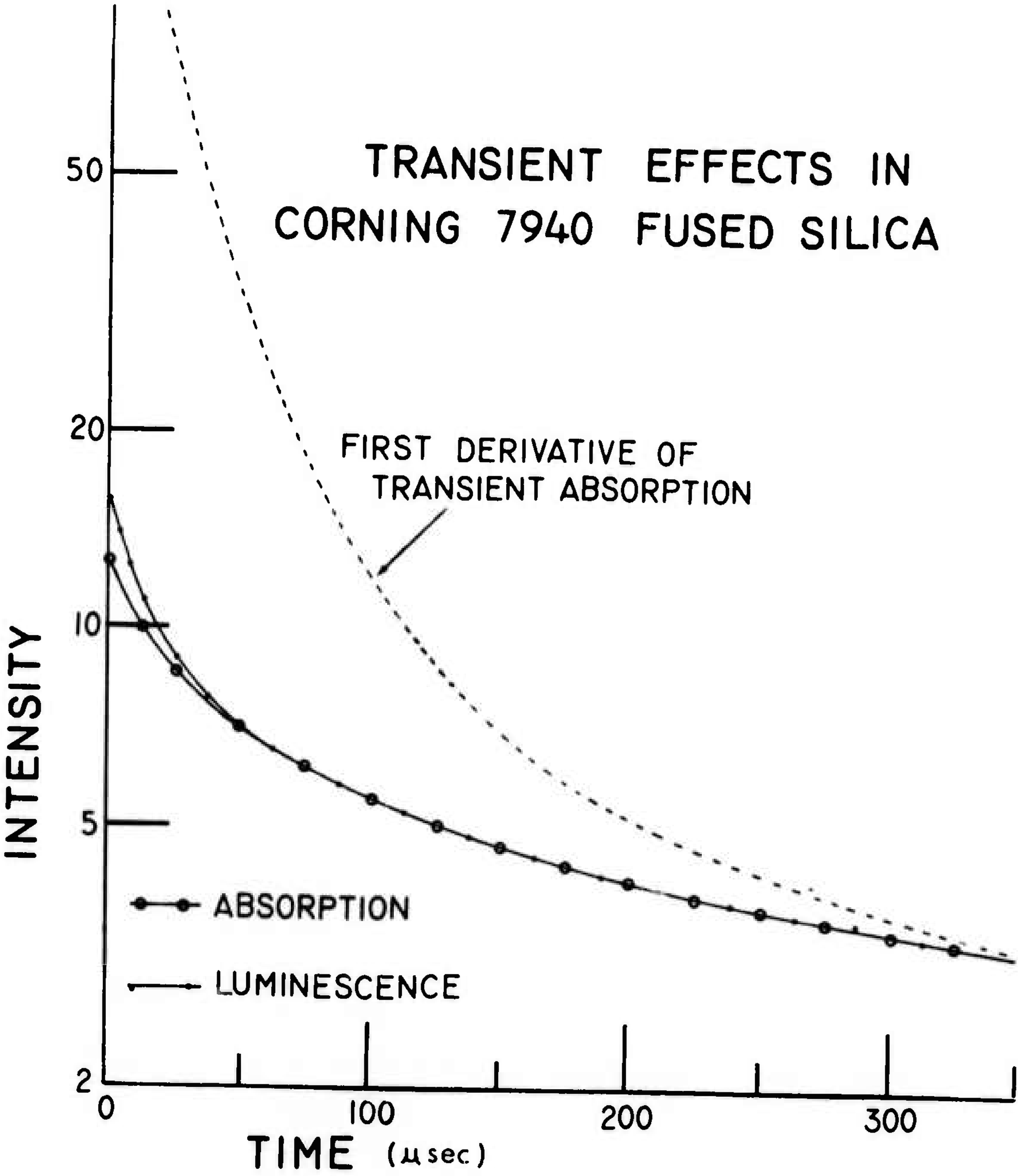

Fig. 15 - The decay rate of the transient emission and absorption at 4.2° K. The luminescence would follow dotted curve if the annihilation of each absorbing center resulted in radiative emission.

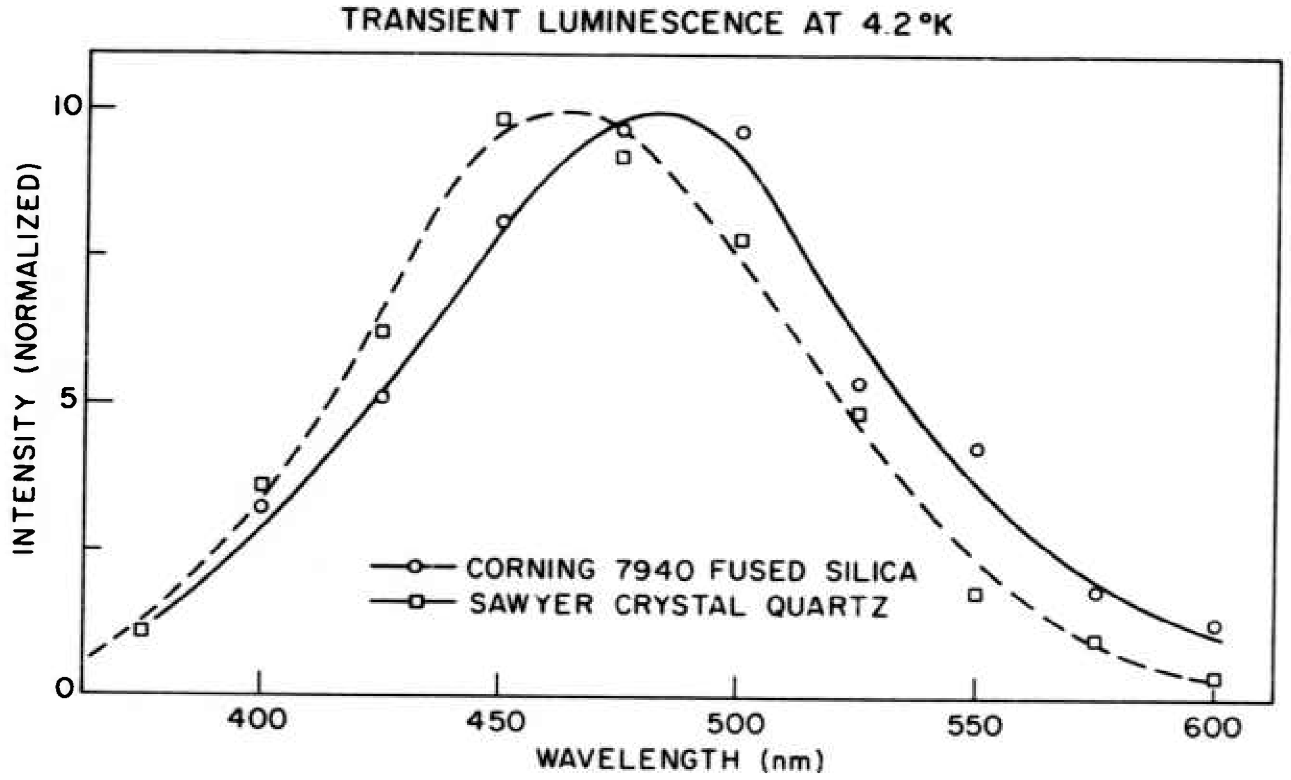

Fig. 16 - Spectra of the low temperature emission of pulse irradiated crystalline quartz and fused silica. At higher temperatures, the emission shifts to shorter wavelengths.

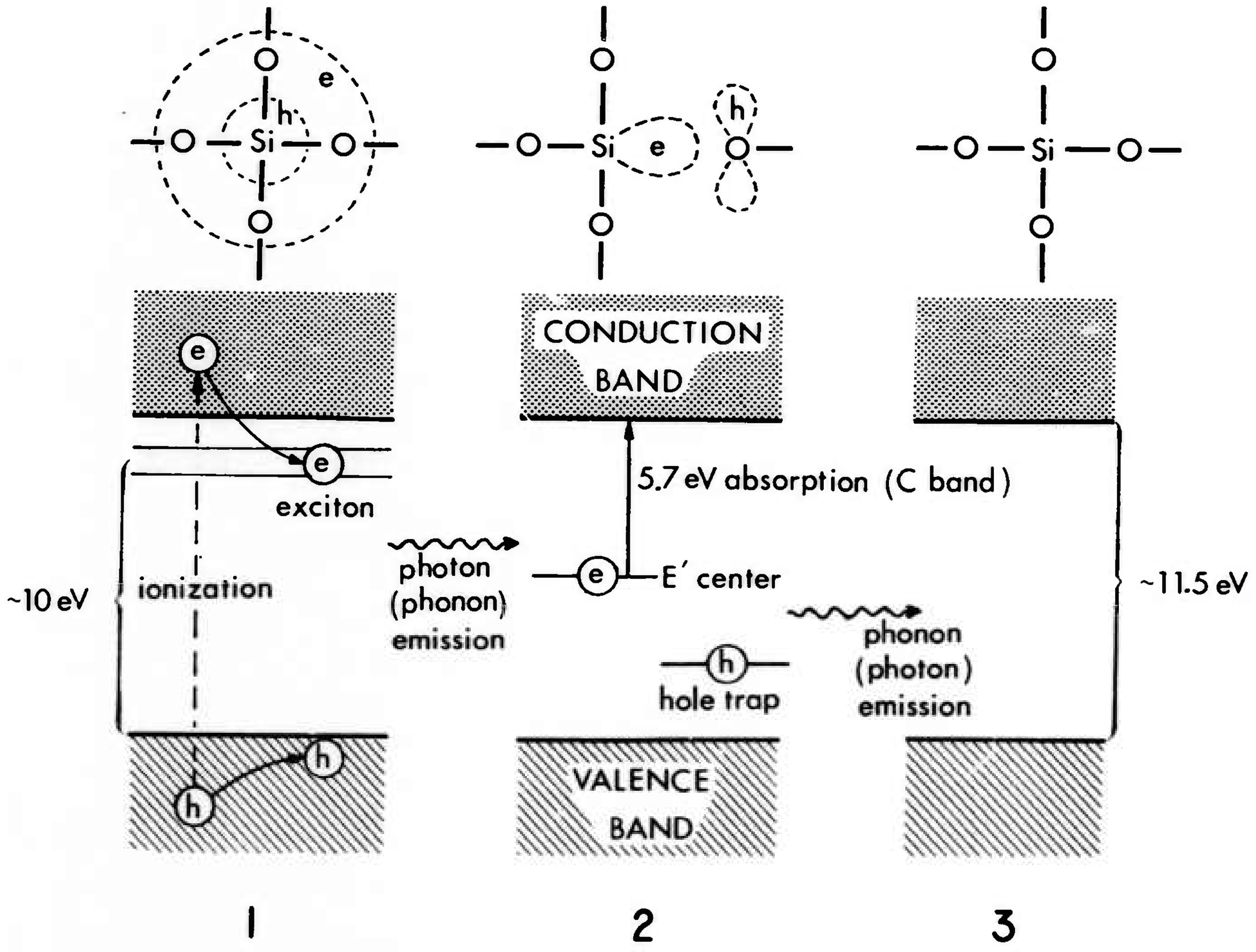

Fig. 17 - Schematic diagram of postulated steps involving the formation and annihilation of transient E′ centers. The impinging radiation can ionize a Si-O bond, resulting in the formation of a defect pair which eventually recombine to reheat the damage.

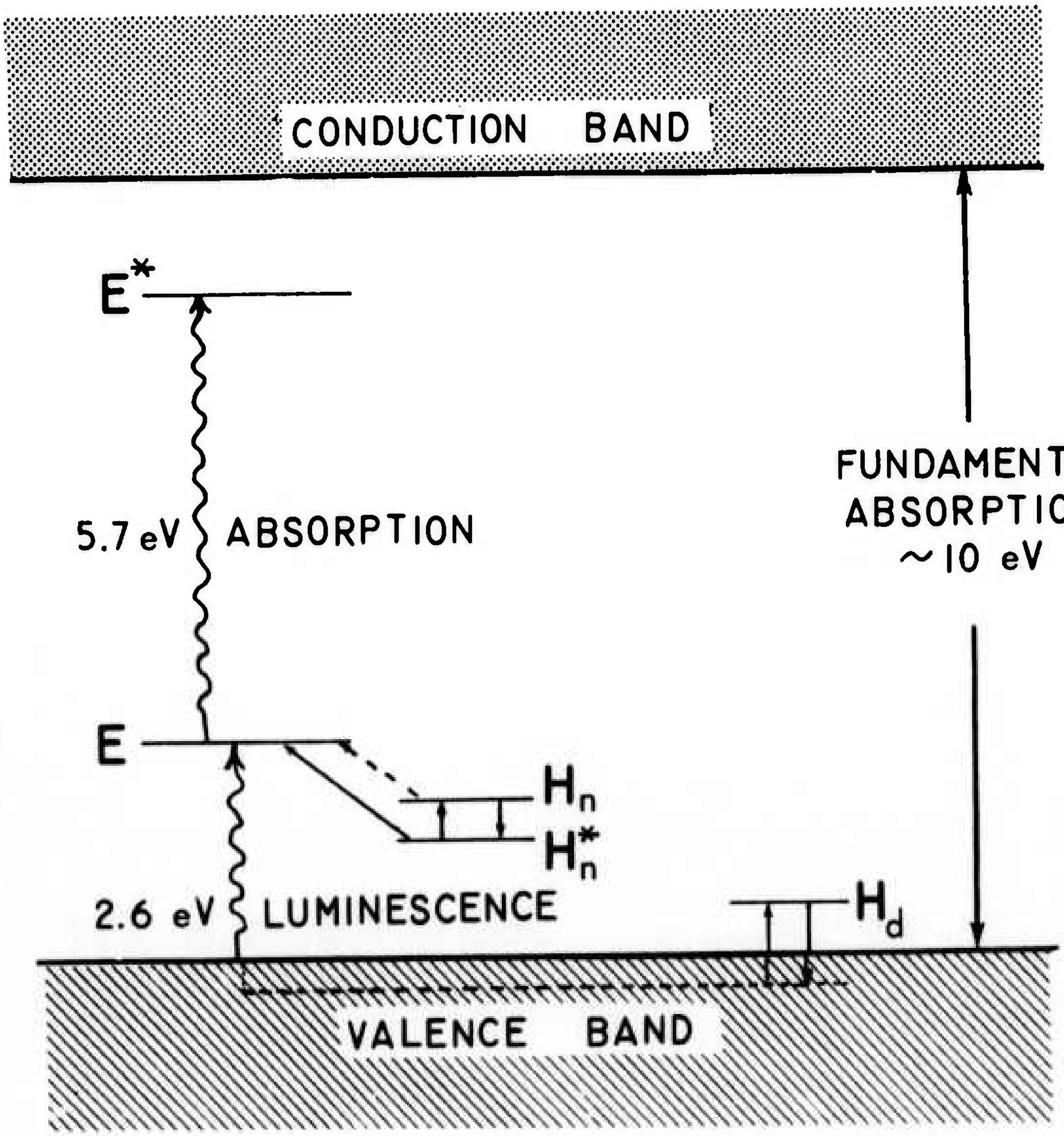

Fig. 18 - The kinetics of the transient radiation effects in SiO_2 are best explained by a model permitting both radiative and non-radiative recombination of holes with E' centers.

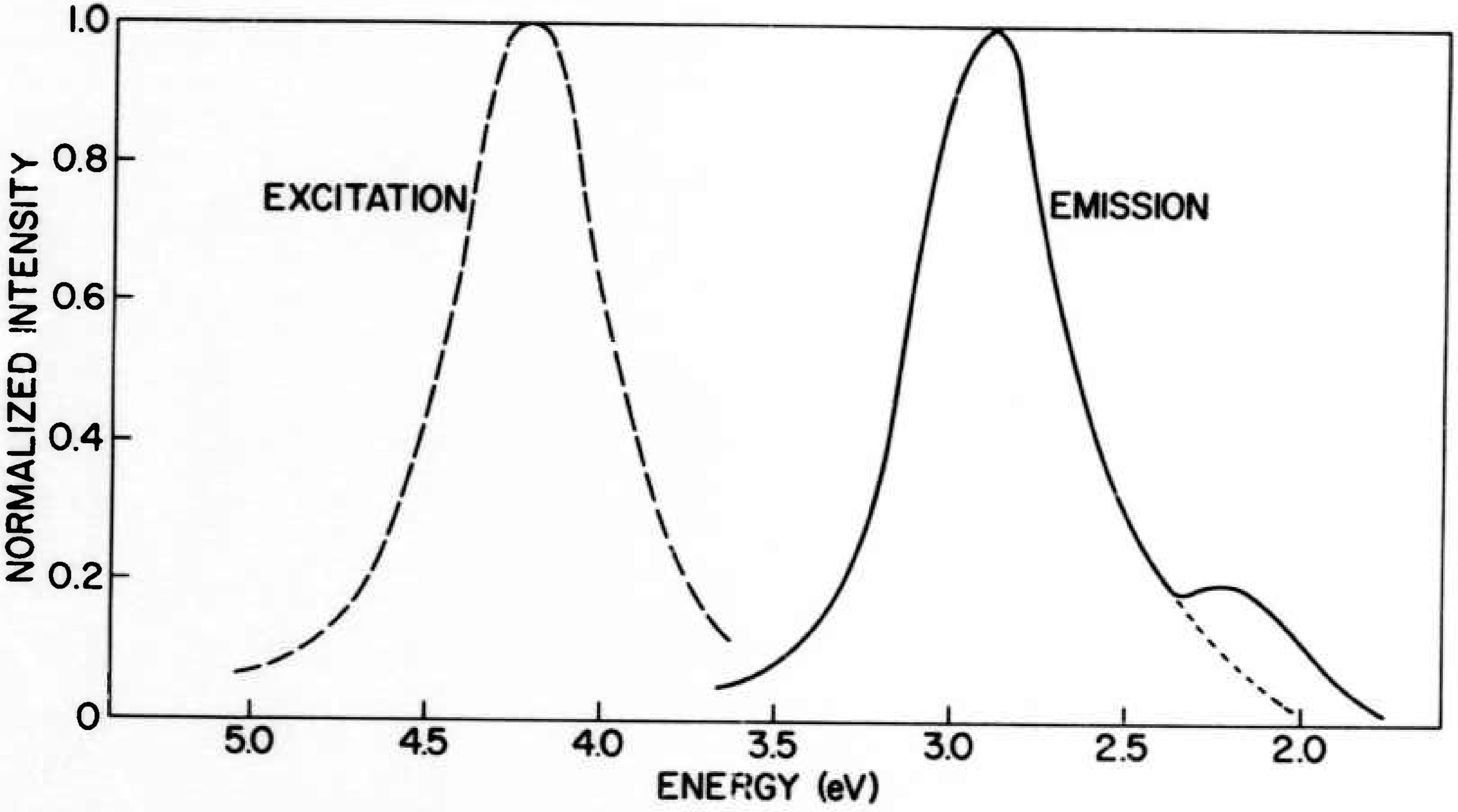

Fig. 19 - Excitation (dashed curve) and Emission (solid curve) Spectra of Corning 7940 and Suprasil at 77°K. The data is identical except for a low energy emission peak observed in 7940 but not in Suprasil (dotted line).

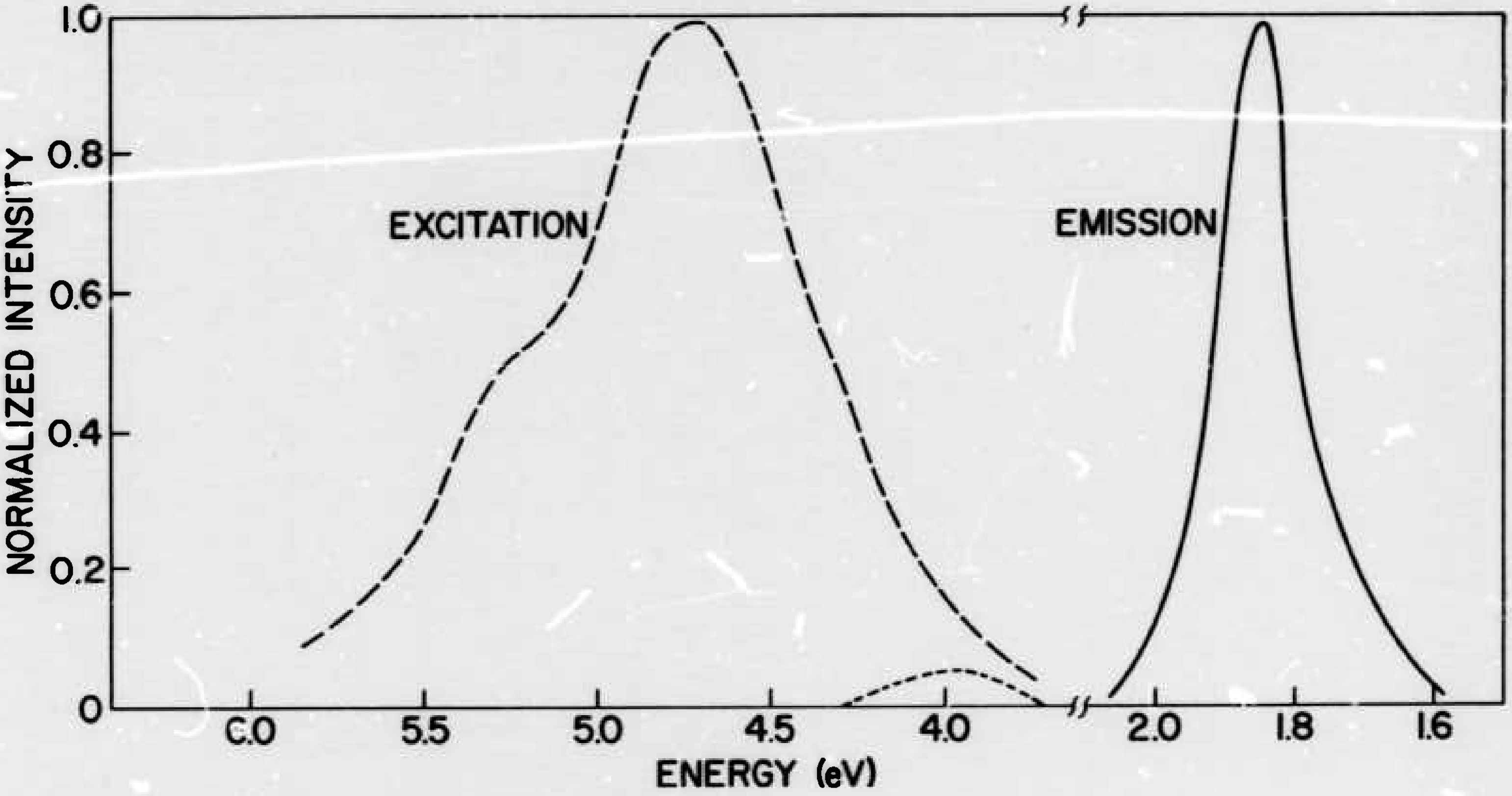

Fig. 20 - Excitation (dashed curve) and Emission (solid curve) of Corning 7940 at 77°K after 2 MeV electron bombardment. The dotted line indicates the relative intensity of the excitation shown in Figure 19.

MODELS FOR ELECTRONIC PROCESSES IN SiO_2

A. R. Ruffa

Naval Research Laboratory
Washington, D.C. 20375

A brief review of theoretical models which have been proposed to describe electronic processes in pure SiO_2 is presented. The models include the valence bond model which allows bond breaking and changes in local environment after an electronic transition, as well as more traditional molecular orbital models. The models are critically compared with experimental data for the pure and glassy materials in order to determine their degree of applicability to the properties involved. Data for the ultraviolet spectrum, the oxygen x-ray emission spectrum as well as that for the intrinsic E_1' defect center are included in the discussion. Further experiments are suggested which may determine in greater detail the range of applicability of the various models.

I. INTRODUCTION

Oxides of silicon are of considerable technological interest because of their important optical and dielectric properties. Vitreous SiO_2, in particular, is interesting from both a theoretical and a practical point of view. Since it possesses one of the simplest structures of any vitreous material, and because many of its properties are so similar to crystalline quartz, a theoretical treatment of its properties is relatively easier. In addition, much practical use is made of vitreous SiO_2 both as a window material and in films in MOS semiconductor devices. More complex silicate glasses possessing the basic short range structure of SiO_2 have widespread application in the optical glass industry, as do thin films of similar chemical composition. A theoretical understanding of the relatively more simple SiO_2 system can hopefully contribute ideas concerning electronic processes in multicomponent glasses and thin films.

With this in mind, the following brief review will concentrate on a critical examination of models which have been proposed for certain electronic processes which are known to take place in pure SiO_2. The review will be fairly narrow in scope, concentrating upon a comparison of the proposed models with available experimental data in order to determine their range of applicability. Thus, the aim is to weed out those parts of the models which are incompatible with the available data, and to use this analysis to suggest experiments which may further sharpen the requirements of the theoretical models.

The first subject which will be taken up in the next section is the question of the structure of fused SiO_2 as compared to its varied crystalline forms. This topic is an important one since many of the properties of vitreous SiO_2 are virtually identical to those of crystalline quartz. The structural evidence will be reviewed as a framework within which the theories must be developed. A topic closely related to the structural evidence, namely the intrinsic E_1' center in SiO_2 will be reviewed in some detail. Next, the outlines of the theories will be presented with an emphasis on the differences in the basic concepts involved. Finally, the theoretical models will be critically compared with some available experimental results. The comparisons demonstrate that some aspects of the competing models are incompatable with observation. On the basis of this analysis, some experiments are suggested whose results may further differentiate between the competing theoretical models. Encouraging further experimentation along these lines is then the primary purpose of this review since only through further experimental results will a fundamental understanding of electronic processes in pure SiO_2 be obtained.

II. THE STRUCTURE OF VITREOUS SiO_2

Crystalline SiO_2 takes on various forms, namely, quartz, cristobalite, tridymite, coesite and stishovite. The first three we will call the low density forms. All of the low density forms with one exception have a common structural feature, the nearly perfect SiO_4 tetrahedron. The high temperature form of tridymite (high tridymite) is somewhat of an exception[1] with O-Si-O bond angles varying between 105.9° and 111.9° as compared to the $109^\circ\ 27'$ angle for the perfect tetrahedron. Of the three polymorphs, quartz has the highest density, some 20% higher than that of fused silica, while the other two have nearly the same density which is only about 4.5% higher than fused silica. The available experimental evidence indicates that fused silica shares the feature of the almost perfect SiO_4 tetrahedron with these crystalline forms although there is some controversy concerning other structural details. Until recently, the most detailed study of the structure of vitreous SiO_2 was that of Mozzi and Warren[2]. On the basis of a careful analysis of their extensive x-ray data, they concluded that each Si atom is tetrahedrally surrounded by four O atoms with a Si-Si-O distance which is virtually the same as that in quartz. In contrast, they concluded that the Si-O-Si bond angle α varies between 120^o and 180^o, with the most probable value being 144^o, only slightly larger than the value 143.5^o in quartz and slightly smaller than the value 146.8^o in low cristobalite. Their distribution of values indicates that α is more likely to be greater than 144^o, partly accounting for the lower density in fused silica compared with that of quartz.

A more recent study by Konnert and Karle[3] has raised the possibility that silica glass may be composed of microcrystallites of the low temperature form of tridymite (low tridymite) having dimensions of approximately 13 Å. Although the structure of low tridymite is not yet known, the radial distribution function indicates that it also features nearly regular SiO_4 tetrahedra. In analogy with low cristobalite, one might expect an Si-O-Si bond angle to be somewhat greater than in quartz. Interestingly enough, high tridymite with its irregular SiO_4 tetrahedra and larger Si-O-Si bond angles has a radial distribution function which is quite different and easily distinguishable from those of fused silica quartz, low cristobalite and low tridymite, whose radial distributions function display a much greater degree of simularity with each other.

Hence the evidence so far indicates that glassy SiO_2 is composed of nearly regular SiO_4 tetrahedra. The question of the Si-O-Si bond angle is still open, but it seems reasonable to assume that the average value is somewhat larger than in quartz. Recently, Philipp[4] has found that certain thin SiO_x films with $x \approx 1.5$ display optical properties similar to those of fused and crystalline quartz, prompting the conjecture that these films also may display the same type of short range order. Verification of this conjecture must await further experimental results, but at this point, it seems reasonable and necessary to incorporate this structural information into the theoretical models.

III. THE E_1' CENTER IN SiO_2

There are two reasons why structural information is important in the development of any theory of SiO_2. First, a knowledge of the atomic positions is quite useful in making any quantum mechanical calculations of electronic energy levels. Second, the details of the structure can give some clues concerning the way in which to construct the bonding orbitals in such a theory. With respect to the second consideration, the tetrahedral structure of the SiO_4 unit surrounding each Si atom, coupled with the fact that the Si atom is in Group IV of the periodic table, gives a strong suggestion that the Si valence orbitals are in the sp^3 hybrid configuration in SiO_2. The sp^3 configuration is the only one in which the orbitals have tetrahedral (or distorted tetrahedral) symmetry without the inclusion of d orbitals. The appreciable admixing of d orbitals appears unlikely since this would require a considerably greater hybridization energy without significantly adding to the bond energies. Calculations such as those of Bennett and Roth[5,6], which will be discussed later, confirm this expectation since they indicate that the Si d orbitals have virtually no involvement in the valence bond states. It is, of course, important to have some experimental confirmation of these inferences. Such evidence is available from the E_1' defect center in SiO_2.

The E_1' center is a radiation-induced paramagnetic defect in both crystalline and glassy SiO_2 which was first reported by Nelson and Weeks[7]. The center was observed to be permanent with an optical absorption peak at about 5.7 eV. While there is some disagreement about the detailed interpretation of the spin resonance data, there seems to be general agreement that the observed paramagnetic resonance is produced by an unpaired Si sp^3 hybrid orbital[8]. This conclusion is based upon the magnitude of the hyperfine interaction of the electron with the Si^{29} nucleus.

Thus the spin-resonance data indicates the presence of the sp^3 hybrid orbitals even if the Si atom is not bonded to four adjacent O atoms. Calculations have shown[9] that a Si atom in the hybrid state and bonded to only three adjacent O atoms is a stable arrangement but that it is unstable if bonded to only two O atoms. Therefore one may reasonably infer from the information concerning the E_1' center in SiO_2 that the environment in both the crystalline and glassy materials favors the tetrahedral arrangement about the Si atoms and the sp^3 hybrid arrangement of the Si valence orbitals. This arrangement is stable enough to survive the removal of an O atom at one of the corners of the tetrahedron.

IV. MODELS FOR ELECTRONIC PROCESSES IN SiO_2

Two different types of quantum mechanical theories have been proposed so far to describe the electronic processes in SiO_2. The first theoretical model which was published[10] attempted to explain the ultraviolet spectrum of SiO_2 by assuming that the ubiquitous SiO_4 tetrahedron results from the sp^3 hybridization of the Si valence orbitals and the formation of Heitler-London type bonds between the Si and O atoms. According to this model, electronic excitation of the system can result in such processes as the breaking of Si-O bonds and the localized rearrangement of atomic valence orbitals. In contrast, the more traditional molecular orbital model as applied in later theories of SiO_2 by Reilly[11] and by Bennett and Roth[5,6] gives a more conservative picture of electronic excitation.

In a molecular orbital approach, the wave function for the N electron system is represented as an antisymmetrized product of one-electron molecular orbitals, each having the form $\Phi_i(j) = \Sigma_n C_n a_n(j)$ where $1 \leq i \leq N$ and the $a_n(j)$ are atomic orbitals centered at each atomic site. The energy eigenvalues or one-electron energies ϵ_i are given by the condition

$$\mathrm{Det}\ (\underset{\sim}{H} - \epsilon \underset{\sim}{S}) = 0$$

where $\underset{\sim}{H}$ represents the matrix elements of the Hamiltonian, and $\underset{\sim}{S}$ the various overlap integrals. The calculated cohesive energy is the difference between the sum of the ϵ_i and one-electron energies for the separated atoms. It is clear that the excited states of the system in this model consist of filling up the unfilled ϵ_i, since for an N electron system, there are N eigenvalues, but in the ground state, only the lowest N/2 are filled, since two electrons having opposite spins can be placed in each of the Φ_i. The wave functions for the excited states of the system differ from that of the ground state only in the values of the C_n in the molecular orbitals. In the work by Reilly, local symmetries about each atom were used to simplify the form of the Φ_i. The sp^3 hybrid orbitals were used for the Si atom, and directed hybrid orbitals, discussed below, were used for the O atom. Estimates of the ϵ_i were made from qualitative considerations in order to arrive at a picture of the nature of the electronic excitation in SiO_2 that gives the first two lines in the ultraviolet spectrum. On the other hand, the ϵ_i were calculated by means of a simplified technique, the Extended Huckel Theory (EHT) by Bennett and Roth. In this method, the off-diagonal matrix elements of the Hamiltonian are given by

$$H_{\lambda\sigma} = 1/2\ K\ (I_\lambda + I_\sigma)S_{\lambda\sigma}$$

where $H_{\lambda\lambda} = I_\lambda$ is the valence state ionization potential, $S_{\lambda\sigma}$ is an overlap integral between atomic orbitals, and K is taken to be a constant, i.e., K = 1.75.

In contrast to the molecular orbital model, the valence bond model proposed by Ruffa[10] takes a quite different conceptual view of both cohesion in the ground state SiO_2 and electronic excitation of the system. The ground state wave function is again represented as a single determinent, but instead of being composed of molecular orbitals, it is instead constructed in the form of a generalized antisymmetric product of Si and O core atomic ions functions. The two electron bonding wave functions Φ_b (1,2) have the form

$$\Phi_b(1,2) = 2^{-1/2}[\Phi_{Si}(1)\Phi_O(2)+\Phi_{Si}(2)](1+S^2)^{-1/2}P(1,2).$$

where P(1,2) is a two-electron singlet spin function, and $S = (\Phi_{Si},\Phi_O)$ is the overlap integral, and as stated earlier, the Φ_{Si} have the form of Si sp^3 hybrid orbitals. The Φ_O are taken to be O_{2p} orbitals, with two of them, say the $2p_x$, paired together as nonbonding lone pair orbitals. The remaining $2p_y$ and $2p_z$ orbitals included in the two electron bonding wave functions, are inclined at angles of 27^o with the bond axes in order to achieve maximum stability[9,10]. There is evidence indicating minimal hybridization of the valence orbitals in the O atom, thus justifying the use of simple 2p bonding orbitals, but this will be discussed in detail later on.

Unlike the molecular orbital model where cohesive energy is represented as the difference between the values of $\sum_i \epsilon_i$ for the material and the separated atoms, cohesion in the valence bond model arises primarily from the Heitler-London bonding mechanism, i.e., the two electron bonding wave functions associated with each Si-O atom pairs. This energy can be calculated quantum mechanically in principle, but it can also be determined from thermochemical data. This has been done for SiO_2 and the bond energy has been found to be 7.9 eV.[10] Excitation of the system is also different in this model. Instead of a filling of the initially unfilled one electron energy levels as is done in the molecular orbital model to describe electronic excitation, the valence bond model allows more drastic changes in the local environment of the material and in the associated wave function. The excited state energy is then calculated accordingly.

Although these energies can in principle be calculated by means of the one electron approximation, the model of excitation used in the molecular orbital scheme has become known in some circles as the one electron approximation. This scheme of using the unfilled one electron energy levels to describe electronic excitation has been used with considerable success in band structure calculations of metals and semiconductors. However, the use of the valence bond model in a material such as SiO_2 presents a picture which is more immediately suited to a description of situations where local changes in environment are brought about by electronic excitation. These changes which include such processes as bond breaking and orbital rotation and rearrangement may very well take place in SiO_2 and other materials which are large band gap insulators and which feature highly localized covalent bonding.

The idea of bond breaking is a rather old one in the study of organic molecules in the gaseous state. The process of photolysis, in which light of a precise frequency is used to break apart molecules has been the physical chemists' tool for a long time in determining bond energies. By studying the products which remain after the molecular decompositions, and knowing precisely the energy associated with the incoming radiation, each of the bond energies in the molecule can be deduced. This information is of considerable importance in reaction rate determinations.

This idea has not received much attention in solid materials, possibly because bond breaking would not in this case lead to decomposition of the material. Instead, bond breaking in the solid material might result in orbital reorientation, exciton creation, and the excitation of electrons into the conduction band. Thus no obvious physical process identifies the breaking of bonds and more subtle analyses must determine whether or not a theoretical model which includes such processes in its description of these materials is valid. Ultimately, experimental observation is the means by which this will be determined, but the nature of the experiments will undoubtedly be suggested by the success or failure of the theoretical models.

V. COMPARISON OF THE MODELS WITH EXPERIMENTAL PROPERTIES OF SiO_2

COMPARISON WITH THE ULTRAVIOLET SPECTRUM

Having sketched the broad conceptual bases for the theoretical models in the last section, we will now make a critical comparison of them with some of the experimental properties of SiO_2. The ultraviolet spectrum of quartz was first examined by Loh[12] who observed a sharp peak at 10.1 eV and a broader peak at about 12 eV. These two prominent features were subsequently confirmed by Philipp[13] in both quartz and fused silica. Philipp extended his data out to 26 eV and observed two other peaks in addition at higher energies with the general features of the results for fused and crystalline quartz being nearly identical. Loh originally suggested that the first peak represented an exciton while the second, he associated with transitions to the conduction band. The shapes of the curves make this speculation attractive, since the first peak is quite sharp and decidely Lorentzian in shape, while the second is broader and more diffuse.

THE VALENCE BOND MODEL

The first model[10] for the ultraviolet spectrum of SiO_2 proposed that the first peak in the spectrum results from the breaking of an Si-O bond with the creation of a Wannier exciton. The binding energy of the hydrogenic orbital associated with such an exciton with respect to the conduction band is $\mu(e^2/K)^2/2h2^2$, where μ is the reduced electron-hole effective mass, and K is the dielectric constant. Using the optical dielectric constant extrapolated to $\lambda = \infty$ and a value $\mu = 0.5$ which is fairly typical for insulators, the binding energy of the Wannier exciton with respect to the conduction band was calculated to be 1.27 eV. The average radius of the orbit is 2.8 eV which is nearly enough to include next nearest neighbors, and hence make the assumption of a relatively large radius orbit reasonable. The second peak then results from the ionization of the exciton into the continuum. This calculated binding energy is also reasonably close to the observed separation between the first two peaks.

The absolute energy placement of the first two peaks, i.e., in this model the energy necessary to create the Wannier exciton, was determined by estimating the energy associated with the bond breaking and orbital rearrangement processes. This was originally accomplished by adding to the energy of the broken bond (7.9 eV) the estimate of the energy lost through the three remaining distorted Si-O bonds associated with the given Si atom. The estimate was made by assuming that the hole would be localized on the Si atom leaving behind the sp^2 hybrid configuration. These orbitals would then be displaced by 19^o from the original bond axes with an estimated reduction in energy by a factor of cos 19^o. This energy reduction approximation is based on the assumption that the Coulomb integral J and the exchange integral K are approximately equal, in the Heitler-London bond energy $E_b = (J+K)/(1+S)$. Since J is nearly independent of orientation and $K \sim \cos^2 \sigma$ where σ is the reorientation angle, then the bond energy varies approximately as $K(1+\cos^2\sigma) \approx E_b \cos \sigma$. Subsequent calculations[9] indicated that this is a fairly good approximation in SiO_2.

However, it is clear that this procedure is a great oversimplification. First, it seems unlikely that the hole would be completely localized on the Si atom. Instead the electron remaining from the broken bond would probably be shared by both the Si and O atoms in order to achieve the lowest energy. Although the large oxygen 2p one electron energy (~ 14 eV) seems to indicate that the electron would be primarily located on the oxygen atom. In addition the process of the reorientation of the other oxygen bonding orbital with respect to the Si-O bond was not considered - a process included in later calculations.[9,14] Finally, the question of the change in energy associated with the change in Si valence orbitals was not considered. Detailed quantitative calculations which properly include all of these processes would be quite difficult and probably not justified until some experimental confirmation of the model takes place. Some suggestions along these lines will be discussed later on.

THE HYBRID MOLECULAR ORBITAL MODEL

Another model for the first two ultraviolet spectral lines in SiO_2 which is quite different conceptually from the first was suggested by Reilly[11]. Using a molecular orbital scheme, Reilly proposed that the oxygen 2s and 2p electrons form the following hybrid orbitals in SiO_2:

$$\Phi_1 = 2^{-1/2}[(2-\cos^2 \alpha/2)^{1/2}\,\varphi_s - \varphi_{py} - (\cot \alpha/2)\varphi_{pz}]$$

$$\Phi_2 = 2^{-1/2}[(2-\csc^2 \alpha/2)^{1/2}\,\varphi_s + \varphi_{py} - \cot \alpha/2)\varphi_{pz}]$$

$$\Phi_3 = (\cot \alpha/2)\varphi_s + (2-\csc^2 \alpha/2)^{1/2}\,\varphi_{pz}$$

$$\Phi_4 = \varphi_{px}$$

where φ_s, φ_{px}, φ_{py}, φ_{pz} are the oxygen atomic orbitals and α is the Si-O-Si bond angle. In this hybrid orbital arrangement, Φ_1 and Φ_2 are orbitals which point in the two Si-O bond directions, Φ_3 is a lone pair orbital in the Si-O-Si plane pointing away from the three atom molecule, and Φ_4 is a lone pair orbital which is perpendicular to the Si-O-Si plane. The last two orbitals contain two electrons each, while the first two contain one each for the total of six oxygen valence electrons.

Reilly associated the first sharp peak in the SiO_2 spectrum with an exciton resulting from an atomic-like transition involving the Φ_4 above, i.e., the oxygen p orbital, and an electronic orbital resembling the oxygen 3s orbital. In similar fashion, he connected the next peak with an oxygen 2p → 3d exciton transition involving the other lone pair orbital Φ_3. Noting Phillip's[13] nearly identical results for fused and crystalline quartz which he observed occur "despite the lack of long range order in the former, characterized by large variations in the Si-O-Si bond angle, he concluded that "the Si influence in the associated excited electron states is secondary". As an example he claimed that excited electron state for the electron hole pair is probably not Si-O antibonding. The reference to the large variations in Si-O-Si bond angle relates to the Mozzi-Warren[2] model of fused silica, where α varies between 120° and 180°.

While Reilly apparently believed that dissociating the excited states from Si atom influence would make his model compatible with both Phillip's[12] results and the Mozzi-Warren model, he appears to have overlooked one serious problem which his hybridization scheme would present. If, in fact, the Mozzi-Warren model is correct, the large variations in α would produce similar variations in associated transition probabilities and one electron energies according to Reilly's hybridization scheme which would predict quite different U.V. spectra for fused and crystalline quartz. Consider the one electron energies, for example, which would determine the positions of the spectral lines. Approximate one electron energies for Reilly's hybrid orbitals can be calculated by noting that if H is the one electron Hamiltonian for the normal oxygen atom, then $\frac{H\varphi_s}{\Phi_s} = \epsilon_s$, and

$\frac{H\varphi_{px}}{\Phi_{px}} = \frac{H\varphi_{py}}{\Phi_{py}} = \frac{H\varphi_{pz}}{\Phi_{pz}} = \epsilon_p$, where ϵ_s and ϵ_p are the one electron energies of the s and p orbitals. We may now calculate approximate one electron energies for the hybrid orbitals by taking the associated expectation values of H:

$$\epsilon_1 =, \epsilon_2 = (\Phi_1, H\Phi_1) = 2^{-1}[(2-\csc^2 \alpha/2)\epsilon_s + (1+\cot^2\alpha/2)\epsilon_p]$$

$$\epsilon_3 = (\Phi_3, H\Phi_3) = (\cot^2 \alpha/2)\,\epsilon_s + (2-\csc^2 \alpha/2)\,\epsilon_p$$

$$\epsilon_4 = (\Phi_4, H\Phi_4) = \epsilon_p$$

We see from this calculation that the value of ϵ_4 is independent of α but that the value of ϵ_3, which according to Reilly's model accounts for the second peak in the U.V. spectrum, is strongly dependent upon α. Using the Herman and Skillman[15] values for ϵ_p and ϵ_s, one quickly finds that the Mozzi-Warren structural model requires that in fused quartz, ϵ_3 varies between 14.1 and 19.1 eV. This wide variation in energy would be matched by the widely ranging values in the transition probabilities for the process $\Phi_3'' \rightarrow 3d$ proposed by Reilly since the various components of Φ_3'' are strongly α dependent. The second spectral line would thus be broadened considerably, probably to the point where it would not be observable. Consequently, this model results in quite different descriptions for the second peak of the U.V. spectra for fused and crystalline quartz and we must conclude that the hybrid molecular orbital (HMO) scheme alone is inconsistent with the Mozzi-Warren model and Phillip's results concerning the similarity of U.V. spectra for crystalline and fused quartz. While the Konnert-Karle model could provide a measure of compatability on this score, since the structure of low tridymite, although it is not known, probably features one or at most a few values of α which are close to that in crystalline quartz, the HMO model also runs into serious problems with the x-ray emission data as will be discussed later. Implied in Reilly's paper, however, is the possibility that further mixing with other orbitals can decouple the s contribution to the bonding orbitals. While this would change the U.V. spectrum interpretation by largely eliminating one of the lone pair orbitals, it would avoid many of the problems discussed above. A nonhybrid model will be discussed further on.

THE EXTENDED HUCKEL CALCULATIONS

Bennett and Roth[5,6] applied the EHT to a calculation of the excited state energy levels and the imaginary part of the dielectric constant of SiO_2 and some clusters representing models of materials in the amorphous series SiO_x, with $0 < x < 2$. They concede that the first sharp peak in the U.V. spectrum may be due to an exciton transition but they do not consider it further. The EHT is generally known to yield useful semiquantitative results for energy levels of small molecules, and, therefore, may be applied to an extended material by considering small clusters of atoms and applying periodic boundry conditions. However, one problem with this method is that the technique is not self-consistent, as is acknowledged by Bennett and Roth, and therefore, the eigenfunctions yielded by the calculations may not realistically represent the system.

The results of the calculations generally confirm these expectations. They are in relatively good semiquantitative agreement with the experimental results of Phillip[4], including the variation of the energy gap with composition and the general shape of the ϵ_2 - vs - frequency curves. However, the EHT has the property that in SiO_2 it yields a nearly ionic configuration, i.e., $S_i^{+4}\ O_2^{-2}$ in connection with the calculated energy eigenvalues. As Bennett and Roth point out, this is a weakness of the method which is a result of its nonself-consistency. Consequently, this method does not appear to be well suited for giving a physical description of the processes involved in the electronic excitation spectrum. Moreover, it does not appear suited to describing an exciton transition, or providing important information concerning the bonding and nonbonding orbitals of the oxygen atom in SiO_2 or the degree of hybridization of the bonding orbitals.

COMPARISON OF THE THEORETICAL MODELS WITH THE OBSERVED OXYGEN X-RAY EMISSION SPECTRUM IN SiO_2

Information concerning the oxygen valence orbitals in SiO_2 can be obtained by examining the oxygen x-ray emission spectrum, since this provides valuable information concerning the nature and degree of hybridization of the valence orbitals as well as their energetic separations. The oxygen Kα emission spectrum arises when an O2p valence electron fills a hole in the K shell caused previously by ionizing x-radiation. It is clear that this process 2p → 1s yields a spectrum whose details (number of lines, relative intensities, energetic separations) are dependent upon the amount of 2p character the various valence orbitals contain, which in turn is determined by the nature and degree of hybridization. The OKα x-ray emission spectrum in SiO_2 was obtained by Ershov and Lukirskii.[16] Their results indicate that the OKα emission spectrum in SiO_2 consists of two primary lines, separated by about 7 eV, with the line corresponding to the higher energy being about three times as intense as the other one.

This spectrum has been analysed[14] within the framework of the valence bond model (VBM). According to this model the more intense line corresponds to the transition 2p (nonbonding)→ 1s, involving the nonbonding lone pair 2p orbitals. The less intense and energetic satellite results from the breaking of an Si-O bond, with the stabilization of the remaining Si-O bond by rotation of the remaining 2p bonding orbital to align it with the bond axis. The calculated energy difference between the two processes is 7.1 eV, in good agreement with observation. The calculated transition probability ratio is also in reasonably good agreement if the electron remaining associated with the broken Si-O bond is not completely isolated on the O atom. As discussed earlier, this possibility appears unlikely.

The observed OKα spectrum may also be compared with other models of SiO_2 in order to determine whether the oxygen valence orbital scheme which they propose is consistent with it. We can quickly see, for example, that Reilly's HMO scheme is not consistent with the OKα spectrum even if we assume a fixed value of α. Setting $\alpha = 143.5^{\circ}$, the value in quartz, the HMO valence orbitals for oxygen take the form,

$$\Phi_1 = 2^{-1/2}(.94403\ \varphi_s - \varphi_{by} = .32975\ \varphi_{pz})$$

$$\varphi_2 = 2^{-1/2}(.94405\ \varphi_s + \varphi_{py} - .32975\ \varphi_{pz})$$

$$\Phi_3 = .32975\ \varphi_s + .94403\ \varphi_{pz}$$

$$\Phi_4 = \varphi_{px}$$

The transition probabilities for the various allowed processes are proportional to the square of the dipole matrix elements $\langle 1s|r|\varphi_n\rangle$ between initial and final states. As a matter of convenience, we will set the relative intensity of the process $\Phi_4 \rightarrow 1s$ equal to unity. The appropriate matrix elements are easily determined, and because the transitions $\Phi_1 \rightarrow 1s$ and $\Phi_2 \rightarrow 1s$ involve the same energy since $\epsilon_1 = \epsilon_2$, then the two processes lumped together would correspond to a single spectral line. The relative transition probabilities are then calculated to be:

$(\Phi_1 + \Phi_2) \rightarrow 1s$	1.09
$\Phi_3 \rightarrow 1s$	0.89
$\Phi_4 \rightarrow 1s$	1.00

Thus we see that the HMO model predicts the existence of three spectral lines in the OKα emission spectrum having nearly equal intensity. Using the Herman and Skillman one electron energies for ϵ_s and ϵ_p, we find that the energetic separations between the lines would be 5.2 eV between the first two lines, and 2.3 eV between the last two. This is obviously inconsistent with the observed spectrum consisting of two lines separated by 7 eV and having an intensity ratio of about 3:1. Consequently, we must conclude that the HMO model is untenable. In addition, the results of this calculation indicates that the two line OKα x-ray spectrum is a fairly strong demonstration of the lack of appreciable hybridization of the oxygen valence orbitals in SiO_2. Figure 1 illustrates the experimental spectrum along with the results calculated using both the HMO and VBM.

The results of the EHT calculations also appear to be incompatible with the OK_α x-ray spectrum. First, the nearly ionic configuration yielded by the EHT presents grave problems in accounting for x-ray satellite lines, since these must be explained in terms of valence orbitals having different one electron energies, and different character in the material (usually bonding and nonbonding). Second, the energy levels associated with the O 2p orbitals obtained using this method are all clustered in a 2-3 eV region. Therefore this model cannot account for the much larger 7 eV separation between lines in the OKα x-ray spectrum. It is not clear whether the Bennett-Roth EHT calculations fail to agree with the OKα x-ray spectrum because of the unrealistic eigenvalues which they yield, or whether in fact, their calculated eigenvalues are fairly accurate, and a simple molecular orbital model which does not differentiate between the ionized and unionized states is incapable of describing the spectrum. Resolution of this question must await more accurate molecular orbital calculations.

A NONHYBRID MOLECULAR ORBITAL MODEL

In order to more nearly complete the discussion, we will now consider a molecular orbital model analogous to the unmodified HMO which avoids the problems associated with using hybridized oxygen valence orbitals in SiO_2. Such a nonhybrid molecular orbital model (NHMO) can be constructed in analogy with the VBM, in which two O 2p orbitals are used in the bonding process, and two nonbonding 2p electrons are placed in lone pair orbitals. In analogy with Reilly's model, the NHMO model can attribute the exciton transition to a $2p \rightarrow 3s$ process involving the lone pair orbitals, while using the sp^3 hybrid orbitals for the valence electrons of the Si atom.

If according to a NHMO model, the first peak in the U.V. spectrum is assigned to a 2p (nonbonding) → 3s transition where the excited state is a narrow band having 3s like atomic character, the question then arises as to the mechanism for the second peak in the spectrum some 2 eV higher in energy. These are two possibilities. One is that the next peak arises from a transition from the narrow 3s band to the conduction band. The other would involve a transition from the 2p bonding level to the conduction band -- a transition which in principle would be allowed in the molecular orbital scheme. The latter assignment would imply that the O 2p bonding and nonbonding energy levels are separated by less than 2 eV in SiO_2. This would be consistent with the results of the Bennett-Roth calculations in which all of these energy levels are clustered within a 2-3 eV region. Moreover, as is illustrated in Fig. 2, this result seems reasonable, since the cohesive energy of SiO_2 of 7.9 eV per Si-O bond means that in the molecular orbital scheme, the total amount by which the eigenvalues of the Si and O bonding orbitals is lowered in the material is 7.9 eV. Since the O bonding orbitals are initially lower in energy than those of the Si-atom by about 6 eV, a minimal lowering of the O bonding orbital eigenvalues seems reasonable. However, this result is completely inconsistent with the OKα spectrum which requires a 7 eV separation between O 2p bonding and nonbonding orbital eigenvalues. This problem is similar to that discussed earlier with respect to the Bennett-Roth EHT calculations. Although it seems unlikely that a more elaborate calculation would significantly change this result, we will allow for this possibility in the discussion which follows.

One is then left with the first possibility for a NHMO model of the second peak in the U.V. spectrum, a transition from a narrow 3s band to the conduction band, with the question of the separation of the bonding and nonbonding oxygen 2p orbitals left open. The participation of the bonding 2p levels could then be assumed to either take place at higher energies, or, in analogy with the case of the lone pair orbitals in the VBM[10], to be prohibited by selection rules. This possibility seems less likely than the one discussed above, but in the absence of more accurate theoretical results which would rule it out, we will consider some of the experimental implications of his model compared with the VBM. In the first place one might expect some similarities as well as differences in behavior between the Wannier exciton of the VBM and the exciton involving the atomic-like transitions of this model as a function of structural detail and density of the material. In the Wannier exciton, the binding energy with respect to the conduction band is inversly proportional to the square of the dielectric constant which, in a microscopic model, is in turn dependent upon the number of polarizable atoms enclosed by the exciton orbit. Thus, in a sample of lower density, the orbit would enclose fewer atoms, with the result that the binding energy of the exciton is increased. This model therefore predicts that in fused quartz, the first peak in the U.V. spectra would be shifted away from the second as compared to crystalline quartz. The same would be true to a lesser extent for cristobalite and tridymite with respect to quartz. The behavior of a 3s atomic-like narrow band would in some respects be similar. The Slater[17] 3s orbital for the oxygen atoms has the form $r^2 \exp(-1.75\ r/3)$. The average value of the radius of this orbital in vacuum is 3.2Å, large enough to enclose next nearest neighbors in SiO_2. In SiO_2, however, the radius would be much larger, due to the dielectric constant of the material, and would enclose many more atoms. In vacuum, the binding energy of the 3s electron is about 4.5 eV with respect to the ionization continuum and about 9.1 eV above the 2p energy level. In quartz the binding energy might be reduced by a factor of the inverse square of the optical dielectric constant to a value of .8 eV. This would make the excitation energy about 13 eV which is much larger than the observed 10.1 eV. On the other hand, one might argue that the one electron energy of the 3s orbital is not so strongly influenced by the dielectric constant and is only slightly increased in SiO_2 to account for the observed transition. The bottom of the conduction band would have to be lowered with respect to the 13.6 eV energy of the ionization continuum in vacuum in order to account for the smaller separation observed between the first two peaks in the SiO_2 U.V. spectra. Energy shifts with respect to changes in the dielectric constant would be similar to those in the Wannier exciton, with the lower dielectric constant in glassy SiO_2 resulting in a shift to lower energies.

It is interesting to note that Philipp's published curves[13] for the U.V. spectrum seem to indicate a small shift to lower energy for the first peak in fused quartz with respect to that for the crystal. The shift is more pronounced in the comparison of the $SiO_{1.5}$ film with crystalline quartz[4], with the shift appearing to be about 0.3 eV. It is not possible to tell whether these shifts are real since the data points are not shown. Such a shift would have to be confirmed either by using a double beam monochromator along with the reflectometer or a continuous U.V. source. Confirmation of such a shift in this manner would strongly indicate that the first peak is the result of either a Wannier or an atomic-like exciton transition.

VI. SUGGESTIONS FOR FURTHER EXPERIMENTAL TESTS

In the absence of further experimental or theoretical evidence, it is not possible at this point to definitely favor either exciton model, although the atomic-like exciton of the NHMO model requires just the right combination of conduction band shift with respect to the vacuum ionization continuum, small effect of the dielectric constant of SiO_2 on the oxygen atomic excitation energy, noninvolvement of the bonding orbitals in the process, and large separation between energy eigenvalues of the bonding and nonbonding oxygen 2p orbitals. The last point is a particularly difficult one, since it seems unlikely that molecular orbital scheme can require an energetic separation between bonding and nonbonding O 2p orbitals which nearly equals the energy per Si-O bond in order to make it agree with the observed OKα spectrum. However, it is possible that this question can be settled by a key experiment involving thin SiO_2 films. It appears to be possible to deposit thermally annealed thin films which display most if not all of the short range order that exists in the bulk glassy material. The films which Philipp studied[4] may have had this property. On the other hand, R.F. sputtered films do not appear to display even short range order since the atoms are deposited one at a time in random fashion. In such a sputtered film, if the structure is truly random, and the SiO_4 tetrahedral structure is largely nonexistent, then the VBM featuring the Wannier exciton and a strong dependence on the details of the Si-O bond would predict that no such exciton transition would occur. Hence, according to this model, such a film would not display the sharp structure which has been observed in the U.V. spectra of glassy and crystalline SiO_4 between 10 and 12 eV. On the other hand, the NHMO model which features the atomic-like 2p → 3s exciton transition predicts that this structure in the spectrum should occur irrespective of short range order, since an atomic-like transition involving nonbonding orbitals is virtually independent of the details of the Si-O bonding mechanisms. A preliminary experiment of this type has already been carried out by Sigel[18] who was unable to observe this structure in the U.V. spectrum of sputtered SiO_2 films. If this result should be confirmed by more extensive studies of various types of films in conjunction with careful local structure determinations by means of x-ray analysis, the VBM featuring the Wannier exciton would be strongly confirmed, while the NHMO model and its atomic exciton would be virtually eliminated from further consideration. The disappearance of this structure in SiO films as observed by Philipp is initial evidence in this direction.

The question of whether or not bond breaking processes takes place in SiO_2 is then quite an important one in the thin film applications. Since the local structural order of such films appears to be quite variable, their optical properties may be amenable to structural "tayloring" if bond breaking is involved in the electronic processes. One example was just given concerning the U.V. spectrum. Another may involve the intrinsic E_1' center. A model for this defect center consistent with the VBM has been given[10] which is in agreement with available experimental data and which predicts that the optical excitation of the center results in the breaking of a Si-O bond. It has been suggested[10] that the bond breaking may be detected by spin resonance techniques. The only other model for this center was set forth by Bennett and Roth[5] who observed in their EHT calculations that an oxygen vacancy resulted in the appearance of an energy level 6.6 eV above the ground state which they associated with the E_1' center. This model does not appear to be tenable, however, since the dangling Si sp^3 hybrid orbital required by the experimental results needs a much larger void in the material than a single O vacancy. As has been pointed out,[10] the overlap between adjacent Si orbitals at an O vacancy is too large to allow anything but a singlet configuration (or a triplet excited state), which is contrary to the doublet paramagnetic property of the center. Moreover, Bennett and Roth recognized that their model gives the wrong intensity of the hyperfine interaction in the ESR spectrum.

Since the E_1' center requires a large void in the material, the question arises as to just where such voids might exist. It is well known that it is difficult to produce these centers in crystalline quartz, but relatively easy in fused silica. Of course, the centers could occur in the crystal at dislocations and other large structural defects. Structural defects and voids would be much more prevalent in the glassy material, possibly explaining its easier coloring property. However, the Konnert-Karle structural model raises a fascinating possibility. If the glassy material is composed of microcrystallites, then the E' centers could occur at their surfaces. In this case, the ease of formation of these centers in thin films could be determined by their structural details. Thus the E_1' band could be made to appear or disappear in a film depending upon the way in which it is deposited.

It has already been suggested[14] that paramagnetic defect centers might be created in SiO_2 by x-radiation on high energy electrons if the bond breaking mechanism for the OKα emission spectrum is correct. It is clear, however, that in a thin film, this mechanism may be structure dependent, so that the susceptibility of a film to the formation of defects may be a function of the way in which the film is deposited. The studying of bond breaking possibilities by x-radiation or high energy electrons create problems because of the structural damage which is done in the material. With the commercial available of U.V. lasers, it may now be possible to conduct experiments which involve only the valence electrons and the Si-O bonds with the avoidance of the undesirable disruption of the inner shell electrons.

VI. SUMMARY AND CONCLUSIONS

In this article, we have examined four different theoretical approaches to the understanding of electronic processes in SiO_2. Three of these, the valence bond model of Ruffa, the hybrid molecular orbital model of Reilly, and the extended Huckel calculations of Bennett and Roth have already appeared in the published literature. The fourth, the nonhybrid molecular orbital model, has been set forth and analyzed in this article in order to surmount some of the problems encountered by the hybrid molecular orbital model and to make for a more complete discussion. A summary of the analyses of these models and suggested experimental tests which appeared in this article are included in Table I.

It is clear that some of the experiments proposed in this article could have wide ranging possibilities concerning the further understanding of the properties of SiO_2, particularly the thin films of this material and its nonstoichiometric variations. Confirmation of a shift to lower energies of the first peak in the U.V. spectrum of glassy composed to crystallic quartz would strongly support the Wannier or atomic exciton transition models. Disappearance of this structural feature in the U.V. spectra in sputtered films, but not in thermally annealed films would strongly confirm the bond breaking and Wannier exciton models. This would imply that the U.V. spectrum could be varied by the way in which the films are deposited or annealed. Similar possibilities exist for the E_1' defect. Particularly if the bond breaking mechanism are confirmed, it would appear that both the pure films as well as those containing atomic impurities could be subject to a wide range of controlled variation in their optical and defect properties.

TABLE I. SUMMARY OF DISCUSSIONS CONCERNING PROPOSED THEORETICAL MODELS OF ELECTRONIC PROCESSES IN SiO_2

VALENCE BOND MODEL (VBM)

1. Associates first peak in U.V. spectrum with breaking of Si-O bond and formation of Wannier exciton. Second peak then results from excitation of electron into conduction band. Fairly good agreement with observed energies.

2. Predicts that first peak changes or disappears if SiO_4 tetrahedra in material are changed or destroyed.

3. Predicts slight shift in first peak to lower energy in quartz compared to position of first peak in fused silica.

4. Associates low energy satellite in OKα x-ray emission spectrum with the breaking of Si-O bond. Gives fairly good agreement with observed energy separation and intensities of two lines.

5. Predicts formation of paramagnetic point defects resulting from x-ray emission and other radiative processes.

HYBRID MOLECULAR ORBITAL MODEL (HMO)

1. Associates first two peaks in U.V. spectrum with atomic-like exciton transitions involving two different sets of lone pair orbitals resulting from hybridization of O valence electron orbitals. Gives results inconsistent with Mozzi-Warren structural model of vitreous SiO_2 and with observed similarity of U.V. spectra of quartz and fused silica.

2. Yields three line OKα x-ray spectrum in SiO_2 with each line having equal intensity, as opposed to observed two-line spectrum with lines having intensity ratio of about 3:1.

EXTENDED HUCKEL THEORY (EHT)

1. Does not appear suited to describing exciton transition.

2. Gives fairly good semiquantitative agreement with observed energy level and ϵ_2-vs-frequency curves.

3. Yields unrealistic ionic eigenfunctions for SiO_2 due to lack of self consistency.

4. Energy level separation of O 2p orbitals inconsistent with $OK\alpha$ x-ray emission data.

NONHYBRID MOLECULAR ORBITAL MODEL (NHMO)

1. Uses nonhybrid O valence orbitals.

2. Associates first peak in U.V. spectrum with atomic-like exciton transition involving lone pair orbitals.

3. Predicts that first peak is virtually independent of nature of short range order, i.e. SiO_4 tetrahedra.

4. May have difficulty agreeing with both U.V. and $OK\alpha$ x-ray spectra.

REFERENCES

1. W.A. Dollase, Acta Cryst., 23, 617 (1967).
2. R.L. Mozzi and B.E. Warren, J. Appl. Cryst. 2, 164 (1969).
3. J.H. Konnert and J. Karle, Nature Phys. Sci. 236, 92 (1972).
4. H.R. Philipp, J. Phys. Chem. Solids 32, 1935 (1971).
5. A.J. Bennett and L.M. Roth, J. Phys. Chem. Solids 32, 1251 (1971).
6. A.J. Bennett and L.M. Roth, Phys. Rev. B4, 2686 (1971).
7. C.M. Nelson and R.A. Weeks, J. Amer. Ceram. Soc. 43, 396 (1960); R.A. Weeks and C.M. Nelson, ibid 43, 399 (1960).
8. R.H. Silsbee, J. Appl. Phys. 32, 1459 (1961).
9. A.R. Ruffa, Phys. Rev. Lett. 25, 650 (1970).
10. A.R. Ruffa, Phys. Status Solidi 29, 605 (1968).
11. M.H. Reilly, J. Phys. Chem. Solids 31, 1041 (1970).
12. E. Loh, Solid State Comm. 2, 269 (1964).
13. H.R. Philipp, Solid State Comm. 4, 73 (1966).
14. A.R. Ruffa, J. Appl. Phys., 43, 4263 (1972).
15. F. Herman and S. Skillman, *Atomic Structure Calculations* (Prentice-Hall, Englewood Cliffs, N.J. (1963)).
16. O.A. Ershov and A.P. Lukirskii, Sov. Phys. Solid State 8, 1699 (1967).
17. J.C. Slater, Phys. Rev. 36 57 (1950).
18. G.H. Sigel, Jr. (private communication).

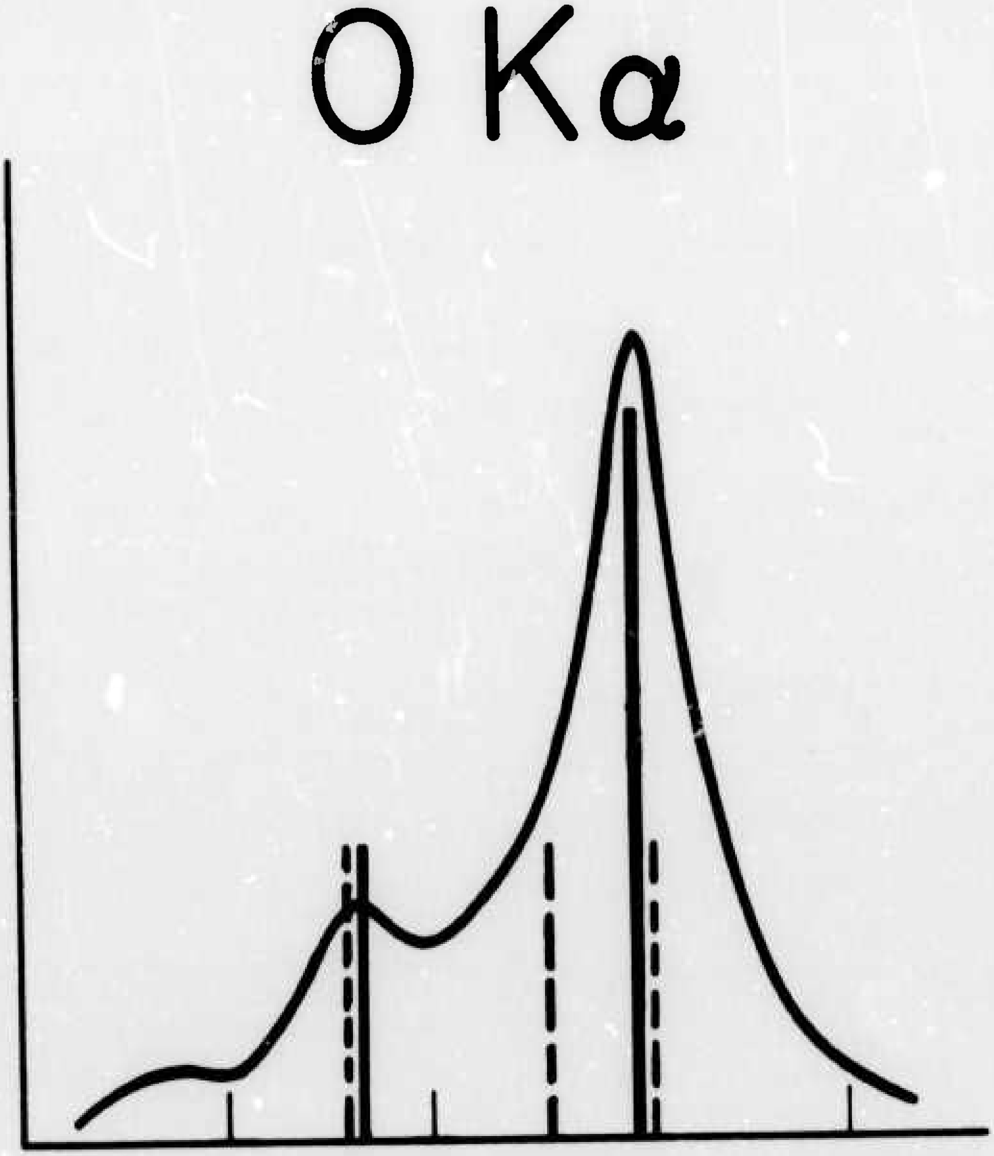

Fig. 1 - Experimental and theoretical OKα x-ray emission spectra for SiO_2. Each graduation on the relative energy scale represents 5 eV, with the energy increasing from left to right. The smooth curve is the experimental result of Ershov and Lukirskii (Ref. 16). The two solid vertical bars represent the result of the valence bond model (VBM) described in the text, with the heights of the bars representing the calculated relative intensities of the two lines. The three dotted vertical lines represent the result of the hybrid molecular orbital model (HMO).

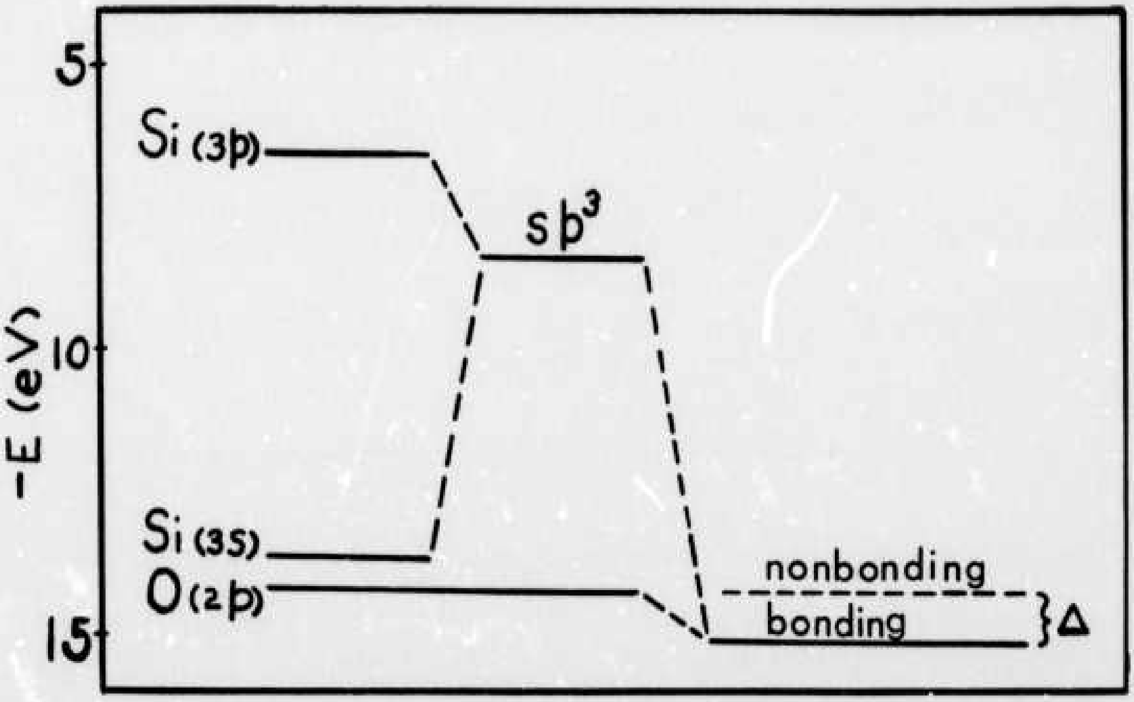

Fig. 2 - Illustration of the energy level shifts associated with the bonding orbitals in SiO_2 in a simple nonhybrid molecular orbital model. On the far left, the one electron energies as given by Herman and Skillman[15] for the Si 3s and 3p and the O 2p orbitals are represented by the three horizontal lines. At the center is represented the one electron energy of the Si sp^3 hybrid orbitals, whose value was calculated from those of the 3s and 3p orbitals by the method described in the text. The one electron energies for the Si sp^3 hybrid orbitals and the O 2p orbitals differ by about 6 eV for the free atoms. On the right, these combine to form a single level associated with a Si -O bond. Since the bond strength is about 7.9 eV, the top level is lowered by about 7 eV and the bottom lowered by about 1 eV in order to produce this bond strength, since the net change in these one electron energies equals the bond strength in this simple approximation. The energy separation between the bonding and non-bonding O 2p one electron energies in SiO_2 is represented by Δ is the illustration, and is about 1 eV. This is the energy separation between peaks which this model would predict for the OKα x-ray spectrum, and it is much smaller than the observed value of 7 eV.

ESR STUDIES OF RADIATION-DAMAGE AND STRUCTURE IN OXIDE GLASSES: A CONTEMPORARY OVERVIEW WITH ILLUSTRATIONS FROM THE ALKALI BORATE SYSTEM

D.L. Griscom

ABSTRACT

Electron spin resonance (ESR) is a particularly powerful method for identifying and characterizing radiation-induced defects in oxide glasses. This paper reviews the fundamental principles and the present state of the art in applying ESR techniques to vitreous materials. A wide variety of generic defect types are discussed in some detail by means of examples from the alkali borate system. Probable analogs in other oxide glasses are pointed out. Special emphasis is placed on the kinds of structural information which can be obtained from these studies.

I. INTRODUCTION

The study of radiation damage in vitreous systems is of interest for two basic reasons: (1) An understanding of the nature of the damage can lead to fabrication of materials in which deleterious effects of radiation can be minimized or the favorable effects can be maximized, and (2) careful study of defect states (trapped electrons or holes) can elucidate certain structural aspects of the glassy state which could not be studied conveniently by other means. The first step of any such investigation must entail the identification of the various defect states which are induced by energetic radiations. The technique of electron spin resonance (ESR) is proving to be the most powerful tool for effecting such identifications. The present paper is a review of the types of radiation defects which have been identified by ESR in oxide glasses, with emphasis on the types of structural information which have been derived. In looking to the alkali borates for examples, the author has afforded himself the luxury of drawing heavily upon his own work. It will be seen that this will entail no loss of generality, for there is ample evidence that analogous defects are (or in principle could be) induced in most other common oxide glass systems. While many of these analogs will be mentioned explicitly, no pretense of completeness is made. The reader wishing a more comprehensive guide to the appropriate literature is referred to several excellent reviews on the general subject of radiation-induced defects in glasses.[1,2]

II. DEFECT STRUCTURE IN RELATION TO GLASS STRUCTURE

Figure 1 presents a schematic view of an oxide glass. Here, a three-dimensional random network, consisting of network forming metal atoms covalently bonded to oxygens, is portrayed as a stylized two-dimensional structure in somewhat the usual manner.[3] It should be understood by this diagram that when four oxygens surround the network former, R, R_A, or R_B, they are in a tetrahedral arrangement with the network former at the center. Silicon is always tetrahedrally coordinated, except when there is an oxygen vacancy as in Fig. 1a. Such oxygen vacancies result in positively charged "point defects" which may trap electrons. When R=Si, this trapped electron center is the E' center,[4] and ESR evidence[4] has shown the wavefunction of the unpaired spin to look something like the dashed "balloon" at the bottom of Fig. 1b.

When glasses are prepared using B_2O_3, P_2O_5, GeO_2, or Al_2O_3 as constituents, other situations can and do occur. Most of these may still be discussed within the framework of Fig. 1 if appropriate conceptual allowances are made. For example, boron is frequently in tetrahedral coordination in complex oxide glasses, although it also occurs in planar triangular units.[3] (The relative numbers of borons coordinated three and four can be ascertained by nuclear magnetic resonance.[5]) Since boron has just 3 valence electrons, when it is found in 4-coordination it has gained another electron from another source (usually a network modifying cation, as discussed below). The same is true of aluminum. Thus, if R_B = B or Al in Fig. 1, the tetrahedral complex $(R_B)O_4$ may be looked upon as a negative point defect whenever it should be isolated from a charge-compensating interstitial cation (the network modifier, again). Such negative defects are hole traps. The approximate wavefunction of a hole trapped at such a site has been learned from ESR[6] to be something like the dashed "dumbell" centered on the oxygen bridging between R_B and an R to the right of Fig. 1b.

Explicit consideration is now given to the effects of additions of network modifying oxides such as alkali or alkaline-earth oxides. As seen above, such additions can lead to the 4-coordination of boron or aluminum. Thus one "molecule" of alkali oxide will provide an oxygen ion with sufficient electrons to form bonds with two borons or aluminums, leaving the two alkali ions in nearby interstitial positions. If, however, a "molecule" of alkali oxide is added to an SiO_2 glass, the effect is to create two "non-bridging" (singly bonded) oxygens. In the absence of nearby charge-compensating cations, these non-bridging oxygens may be looked upon as another type of negatively charged point defect which can trap a hole. The wavefunction for this trapped hole center could not be other than that indicated at the top of Fig. 1b.

Another type of electron trap can result when R_A has the same valency as R, but a greater electron afinity. An example is when Ge($=R_A$) is doped into quartz. For this case an electron can be trapped in a Ge-O antibonding orbital.[7] The stability of such a center would be increased by a nearby interstitial cation. In fact, cations often diffuse to different positions following low temperature irradiation and subsequent warming, thereby stabilizing an otherwise weakly trapped species.[1,7] This situation is illustrated in Fig. 1.

Finally, the interstitial cations themselves may serve as electron traps. Recent ESR evidence for alkali-associated trapped electron centers in alkali borate glasses have been given.[8] Due to the general mobility of interstitial ions, "clusters" may form before, during, or after irradiation, resulting in trapping sites comprising a number of cations.[8] The anti-morph to the cation electron trap is the anion hole trap. Although interstitial anions are a rare situation, there is evidence[9-13] that when alkali borate glasses are prepared with alkali halide additions, the halide ions take up interstitial positions and are often effective hole traps. These effects will be discussed further in later sections.

III. ESR LINE SHAPE ANALYSIS

A. Overview

Crucial to identifying any of the defect sites described above is a careful analysis of the experimental ESR spectra, utilizing the correct theory and the appropriate experimental "tricks" and computational tools. A "flow diagram" illustrating a typical approach to this problem is given in Fig. 2. Many of the steps shown here can themselves be broken up into substeps. For instance, the step "observe induced ESR spectra" should include frequency-dependence studies which themselves may be every bit as valuable as isotopic substitution when it comes to confirming the operating hypothesis. Even more important, the step "infer proper terms in relevant spin Hamiltonian" presumes that the experimenter has some feeling for ESR "powder patterns" and how they are related to the spin Hamiltonian. The powder-pattern concept was originally elucidated by Sands[14] in 1955, and since then numerous contributions on the subject have been scattered throughout the literature. A forthcoming review article[15] will be useful in unifying the latest developments. Introductions to the spin Hamiltonian formalism are provided in many standard texts.[16-19] Finally, the techniques of computer simulating ESR spectra of glasses have been described from several points of view,[20-22] and program listings and user's manuals have been made available upon request (c.f., refs 20 and 21).

For the general reader wishing to understand something of the results of ESR studies of irradiated glasses without consulting all of the original source material, the following simplified discussion is provided.

B. The Spin Hamiltonian

The spin Hamiltonian is an expression for the energy of the particular electron or hole whose ESR is to be observed. It is composed of a number of terms including the Zeeman interaction (the interaction of the electron magnetic moment with the laboratory applied magnetic field), the hyperfine interaction (the interaction of the electron magnetic moment with the magnetic moments of nearby nuclei), and various other terms which won't be enumerated here. The crux of any ESR problem is to single out all of those terms which significantly affect the observed spectrum and to ignore those which don't. As it turns out, the essential aspects of all of the spectra to be described in the following sections derive from the Zeeman and hyperfine interactions only. For the Zeeman interaction, there are just three parameters to be determined experimentally; these are the three principal components of the "g tensor", g_{xx}, g_{yy}, and g_{zz}. (If no "crystal" coordinate system has been defined, these quantities are sometimes written g_1, g_2, and g_3). The "g values" are dimensionless numbers, but they are directly associated with particular values of magnetic field according to

$$g = \frac{h\nu}{\beta H} \qquad (1)$$

where h is Planck's constant, ν is the spectrometer frequency, β is the Bohr magneton, and H is the magnetic field value to be associated with g. By means of Eq. (1), a g value can be defined for any value of H. However, one should not lose sight of the fact that there are only three values of H which correspond to the three principal values of the g tensor.

There are also three parameters associated with the hyperfine interaction for each magnetic nucleus interacting with the electronic "spin": these are the coupling constants A_{xx}, A_{yy}, and A_{zz} (or A_1, A_2, and A_3). Strictly speaking, these have dimensions of energy, but it is common practice to quote "A values" as magnetic fields. When this is done, it should be understood that the quoted numbers are really $A_i/g_i\beta$ (assuming the principal axes of the A and g tensors are coparallel, as it is usually done in the absence of any evidence to the contrary).

C. The Resonance Condition

The reasons that all relevant parameters have a tendency to be converted to magnetic fields is the fact that these parameters can often be scaled directly from an experimental spectrum, which, after all, is a plot of absorption (or more commonly the first derivative of absorption) versus magnetic field. Indeed, while knowledge of the spin Hamiltonian is very useful for getting at the physics of the problem, ESR spectral analysis cannot proceed without knowing the "resonance condition" - an expression which gives the magnetic field at which resonance occurs as a function of , g_1, g_2, g_3, A_1, A_2, A_3, the nuclear magnetic quantum number m_I, and the polar angles of the direction of the applied field with respect to the principal axes of the g and A tensors. The resonance condition derives from the spin Hamiltonian, but is qualitatively a different thing.[16-19] In certain simple cases the resonance condition may be derived exactly. An example is the case when the spin Hamiltonian consists of the Zeeman term only:

$$\mathcal{H}_z = \beta[g_\perp (S_x H_x + S_y H_y) + g_\parallel S_z H_z] \qquad (2)$$

For this case the resonance condition is derived[16] to be

$$H_{res} = \frac{h\nu}{g(\theta)\beta} \qquad (3)$$

where

$$g(\theta) = (g_\parallel^2 \cos^2\theta + g_\perp^2 \sin^2\theta)^{1/2} ,$$

and θ is the angle between the direction of the applied field and the symmetry axis of the g tensor.

An exact resonance condition can also be derived when the spin Hamiltonian consists only of a Zeeman term and the symmetry is orthorhombic. However when the hyperfine interaction is added, perturbation theory must be applied. To first order in perturbation theory the resonance condition for orthorhombic g and hyperfine tensors is[22]

$$H_{res} = \frac{h\nu}{g\beta} - m_I \left(\frac{A}{g\beta}\right) , \qquad (4)$$

where

$$g = [g_{zz}^2 \cos^2\theta + (g_{xx}^2 \cos^2\phi + g_{yy}^2 \sin^2\phi)\sin^2\theta],^{1/2}$$

$$A = [g_{zz}^2 A_{zz}^2 \cos^2\theta + (g_{xx}^2 A_{xx}^2 \cos^2\phi g_{yy}^2 A_{yy}^2 \sin^2\phi)\sin^2\theta]^{1/2}/g ,$$

θ and ϕ are the polar angles of the magnetic field direction with respect to the principal axes of the g and hyperfine tensors, and m_I is the nuclear magnetic quantum number. All of the results to be presented in the following sections are well described by Eq. (4), although small but important improvements are sometimes obtained by appending second-order hyperfine terms.[9,16-19,23]

D. The Powder Pattern: The Effect of Angular Averaging

If the specimen being investigated were a single crystal, the angular dependence of the resonance lines could be fitted by a resonance condition such as Eq. (3) or Eq. (4). But if this same crystal were to be ground into a fine powder, the individual crystallites would describe all possible orientations with the applied magnetic field, and the various resonance lines would be "smeared out" between certain limiting field values derivable from the resonance condition. The resulting absorption curve is known as a "powder pattern". Powder patterns are easily generated on a computer by calculating the resonance condition for each of a large number of orientations corresponding to a uniform grid in $\cos \theta - \phi$ space (equal units of solid angle) and histogramming the results on a magnetic field scale.[21]

The powder pattern pertaining to the simple resonance condition of Eq. (3) is shown in Fig. 3a. Experimentally, one generally observes the first derivative of absorption. The noisy curve in Fig. 3b is an experimental (first derivative) powder spectrum for a species characterized by a axial g tensor (O_2^- in Na_2O_2).[24] The smooth curves in Fig. 3b, including the mathematical divergences (arrows) represent the first derivation of the powder pattern of Fig. 3a. The "discrepancy" in Fig. 3b is only apparent: The way in which the powder pattern was determined involved the (unphysical) assumption that the "single-crystal" linewidth was zero. When the computer is asked to convolute the powder pattern of Fig. 3a with a Lorentzian single-crystal broadening function of an appropriate width, a computed derivative spectrum can be obtained which overlays the experimental spectrum exactly. Thus, using the computer simulation technique as a confirmation, the principal g values, g, $g_{\perp}$, can be determined accurately from this powder spectrum.

The question is frequently asked, how unique are the computer simulation methods? For this there is no simple answer, since every problem is different in one aspect or another. However, it has been the author's experience that, whenever a truly convincing computer fit is made to a powder spectrum which has some distinctive characteristic features, it has involved a very critical choice of spin Hamiltonian parameters--at least some of which could not be varied by more than a few percent without degrading the fit. It may be further remarked that the functional form of the resonance condition is strictly prescribed by theory and hence is not subject to capricious tampering by the experimenter. Thus, trying to computer fit an experimental spectrum with the wrong theory is tantamount to trying to "fit a square peg in a round hole". Of course some ambiguities do arise, and the careful experimenter will be aware of these. For instance a ferromagnetic substance with an isotropic g value and an axial magneto-crystalline anisotropy would also yield a spectrum identical to that of Fig. 3.[25] However, this possibility can be eliminated by obtaining spectra at two frequencies: For the ferromagnetic case the overall linewidth is frequency independent while for the paramagnetic case the field separation between $g_{\parallel}$ and $g_{\perp}$ varies linearly with ν (see Eq. 1). Further remarks on the accuracy of computer-simulation techniques in extracting spin Hamiltonian parameters from powder spectra are presented in Ref. 21.

F. The Difference Between a Powder and a Glass: The Effect of Statistical Variations in Spin Hamiltonian Parameters

The paragraphs immediately preceeding have described the angularly averaged ESR spectra which result when a single crystal specimen is ground to a fine powder. When the sample is a glass -- even a single fragment -- the very same angular averaging will take place. The difference between a powder pattern and a "glass pattern" derives from certain forms of microscopic randomness which distinguish vitreous materials from fine crystalline powders. Regardless of whether one espouses the random network theory[3] or the crystallite theory[3] of the glassy state, it is an inescapable conclusion that there must be some statistical variations in bond lengths, bond angles, cation distributions, and so on. Statistical variations in these quantities lead directly to statistical variations in spin Hamiltonian parameters of an ensemble of paramagnetic defects which are assumed to be randomly distributed spatially in a glass. This "ensemble averaging" modifies the powder patterns which derive from angular averaging alone. Both effects can be simulated by computational methods, as discussed in Ref. 21 and illustrated by examples presented below.

IV. THE OBSERVED SPECTRA AND THEIR INTERPRETATIONS

A. Oxygen-Associated Trapped-Hole Centers

The most commonly observed ESR spectra in irradiated complex oxide glasses arise from oxygen-associated trapped-hole centers. Pioneering studies of this class of defects in the alkali borate system have been reviewed by Griscom, Taylor, Ware, and Bray[26] and explicit evidence that these centers are of the trapped-hole type has been given.[9,26] It has been pointed out[27] that exact analogs of these "boron-oxygen hole centers" (BOHC) probably occur in the alkali silicate system[28] and in many other oxide glass systems as well (see Table I).[29-34] As it is beyond the stated scope of this paper to discuss all of the known or suspected analogous species, the basic structure of the oxygen-associated defect will be illustrated by an exposition of the BOHC.

Figure 4a displays the familiar "five-line-plus-a-shoulder" spectrum obtained at 9 GHz for irradiated alkali borate glasses containing $\lesssim$ 25 molar percent alkali oxide. Parts (b) and (c) of this figure demonstrate the conceptual steps just described in the preceeding section as applied to the computer simulation of the BOHC spectrum. Here it may be noted that a hyperfine interaction with $^{11}B(I=3/2)$ gives rise to four overlapping powder patterns corresponding to the four values of the nuclear magnetic quantum number ($m_I=+3/2, +1/2, -1/2, -3/2$). The hyperfine powder patterns of Fig. 4b are determined from Eq. (4), using the values of g_1, g_2, g_3, A_1, A_2, and A_3 which ultimately provided the best computer fit.[26] It is immediately evident that "bumps" due to the four absorption "edges" determined by g_3 and A_3 are not apparent in the experimental spectrum. This is because there is a statistical distribution of g_3 values whose width W is broader than, and hence obscures, the splittings A_3 (see Fig. 4c).

Several comments, qualifications, and cautions are in order vis-à-vis Fig. 4. It first may be noted that, due to interferences among the four hyperfine powder patterns, it would be virtually impossible to "measure" g_1, g_2, A_1, and A_2 without performing a computer simulation. As it turned out, the computer fit was extremely sensitive to these parameters; thus the values measured with computer assistance are highly accurate.[26] On the other hand, the suggested distribution of g_3 values and the average value of A_3 would be quite problematical were it not for collateral experimental evidence from frequency-dependence studies and from the investigation of polycrystalline compounds in the lithium borate system.[26] Finally, the agreement between the experimental and computed spectra of Fig. 4a is better than that shown in the original publication.[26] Interestingly enough, the improvement was made in the experimental spectrum; the computed spectrum is the very same as shown in Ref. 26. The explanation, very simply stated, is that by irradiating at liquid nitrogen temperature and then bleaching with IR light some spurious underlying resonances were destroyed, leaving behind just the spectrum of interest.[8,25] Underlying resonances are a persistent hazard which can only be overcome by bleaching, annealing, differential microwave saturation, and general circumspection on the part of the experimenter.

When glasses containing $\gtrsim$ 40 molar percent alkali oxide are irradiated and studied at 9 GHz, a "four-line" spectrum is observed.[35] As illustrated in Fig. 5, this has been computer simulated on the basis of a spin Hamiltonian qualitatively the same as that used to explain the "five-line-plus-a-shoulder" spectrum. This indicates that, appearances notwithstanding, varying the composition of an alkali borate glass over a wide range probably does not result in any fundamental changes in the electronic structure of the BOHC.

Knowledge of the spin Hamiltonian parameters g_1, g_2, g_3, A_1, A_2, and A_3 permit the construction of physical models for the BOHC. The ways in which this analysis proceeds are discussed in detail by Griscom, Taylor, Ware, and Bray,[26]. The final model for the BOHC arrived at in Ref. 26 is almost certainly incorrect however.[27,36] The reasons for this probable error are rooted in the fact that only the absolute magnitudes of the hyperfine coupling constants are determined experimentally, while some assumptions must be made about the algebraic signs of these quantities when a model is formulated. Adding to the difficulty is the fact that the exact correspondences between A_1, A_2, and A_3 and A_{xx}, A_{yy}, and A_{zz} are not known a priori, leading to a total of 24 physically distinct solutions.[37] It should be emphasized that these problems can be surmounted. When the identity of the paramagnetic defect is known or suspected, most of the competing possibilities can be eliminated by symmetry considerations[26,27] or by comparisons with isoelectronic species that are well understood.[37] Unfortunately, supporting evidence of the latter type was unavailable at the writing of Ref. 26. More recently, however, a BO_3^{2-} radical has been discovered in calcite[36] and in a potassium borate ceramic[37] and its electronic properties have been elucidated by the methods just mentioned. These studies have shown that it is possible for a trapped hole to be 100% localized in oxygen orbitals while still undergoing a hyperfine interaction of the order of 10 G with an adjacent boron via the mechanism of core polarization.[36,37] On this basis, Symons[36] suggested that the BOHC is probably a "hole on a non-bridging oxygen." Griscom, Taylor, and Bray[27] concurred that this is a reasonable possibility but emphasized that the model of a "hole on a bridging oxygen" is not ruled out. Subsequently, additional evidence for the actual existence of a bridging-oxygen type of center was offered;[38] (see also Section IV H., below, in this contest). Nevertheless, the presently available data and theoretical considerations support, but do not decide between, the two models for the BOHC illustrated in Figs. 6 and 7. The following is a summary of the basic considerations which point to these models.

(1) The boron hyperfine interaction is sufficiently small (~10 G) as to indicate that the hole is primarily located away from the boron.

(2) Simple consideration of the known structural properties[3,5] of borate glasses lead to the conclusion that non-bonding π orbitals on either bridging or non-bridging oxygens provide the lowest energy states for a hole in a boron-oxygen network. (Such a location would be consistent with observation No. 1.)

(3) Since the hyperfine interaction is with a single boron, the model of Fig. 6 is only allowable if R and R' are different structures, i.e., if one is a three-coordinated boron and one is a four-coordinated boron.

(4) Studies of the BO_3^- ion[36,37] indicate that in at least one case a hole which is 100% localized in π-type oxygen orbitals can undergo a boron hyperfine interaction of the proper order of magnitude.

(5) The observed g values can be accounted for on the basis of either of the proposed models according to relations of the type.[26]

$$g_1 \approx g_{\text{free electron}}, \quad (5a)$$

$$g_2 \approx g_{\text{free electron}}\left[1 + \frac{c_2\lambda}{\Delta}\right] \quad (5b)$$

and

$$g_3 \approx g_{\text{free electron}}\left[1 + \frac{c_3\lambda}{\Delta}\right] \quad (5c)$$

where c_1 and c_2 are constants of the order 0.1-1 calculable from theory,[16-19,26] λ is the spin orbit coupling constant for the O^- ion (~0.01 eV),[26] and Δ is the energy splitting (~0.2 eV)[26] shown in Fig. 6. (Similar relations involving Δ_1 and Δ_2 in place of Δ apply to Fig. 7).

In view of the structural differences[3,5] between borate and silicate glasses it seems possible that the BOHC may be a "hole on an oxygen bridging between a three-coordinated boron and four coordinated boron"[26,27] (Fig. 6) while the silicate-glass hole centers[28] may be "holes on non-bridging oxygens" (Fig. 7). As can be seen in Figs. 6 and 7, the electronic structures of these two defects would be quite similar. Indeed, if there exist certain random electrostatic "crystals fields" which determine the splitting Δ_2 and influence the splittings Δ_1, Δ, and E, then the electronic structures of the π orbitals would be virtually indistinguishable, notwithstanding the different numbers of σ bonds. Thus, the listing in Table I may represent both structural types of defects.

In spite of the above ambiguities, the BOHC may be utilized as a probe of borate glass structure. Krogh-Moe[39] has presented considerable evidence for the probable existence in alkali borate glasses of structural units characteristic of the crystalline compounds which are nearest on the phase-equilibrium diagram.[40] As discussed at considerable length elsewhere,[26,38,41] comparisons of BOHC spectra of lithium borate and strontium borate polycrystalline compounds with those of alkali borate and alkaline-earth borate glasses lend strong support for Krogh-Moe's models. Independent of these models, the distributions of g_3 values indicated in Fig. 4c and Fig. 5c are dramatic evidence of randomness in the glass structure. This randomness may result from site-to-site bond angle variations[26] (i.e., the R-O-R' angle in Fig. 6) or random "crystal fields" giving rise to a spread in Δ_2 values in Fig. 7.

B. Dangling-Orbital-Type Trapped-Electron Centers

Perhaps the best known example of a trapped-electron center in oxide glasses is the E' center[4], which is commonly observed in irradiated pure SiO_2 glass[42]. However, the concentrations of E' centers induced by a given radiation dose at room temperature are found to fall off rapidly with the degree of doping with alkalis.[43] In general, complex oxide glasses irradiated near 300°K exhibit ESR spectra due to trapped hole centers (see above) with little or no evidence of spectra due to trapped electrons. This brings up the questions of where the trapped electrons are residing and why they are not detected in complex glasses. Answers to these questions have been found only recently[8,23] by x-irradiating alkali borate glasses in situ at cryogenic temperatures (25 or 77^{o}K) in the dark. One of the trapped-electron centers observed following this treatment has been the boron electron center of "BEC".[23] It will be seen that this is the borate analog of the E' center.

Figure 8 shows the BEC spectra as they appear in relation to the stronger, centrally-located BOHC spectra. The dependences of both resonances on boron isotope can be noted. The BEC spectra can be destroyed completely by warming to room temperature or by exposure to visible light, while the BOHC spectra are reduced in intensity by only 50-70%.[25]

As in the case of the BOHC, the BEC spectrum could only be analyzed by assuming a statistical distribution of spin Hamiltonian parameters. While for the former case it was g_3 which was distributed, for the BEC it turns out to be the isotropic part of the hyperfine tensor, i.e., $A_{iso} = (A_{\parallel} + 2A_{\perp})/3$. The effect of a rather broad, bell-shaped distribution of A_{iso} values is illustrated diagrammatically in Fig. 9. To test this hypothesis and to provide accurate measurements of other spin Hamiltonian parameters, mutually consistent computer simulations were carried out for the BEC spectrum in both ^{11}B- and ^{10}B-enriched samples using Eq. (4) (plus second order hyperfine terms.)[23] The results which are shown in Figs. 10 and 11 confirm the model and demonstrate the power of both the isotopic-substitution and computer simulation techniques.

Once again, accurate determinations of spin Hamiltonian parameters permit the formulation of a detailed model for the paramagnetic defect in question. The measured parameters are given in Table II.[23] The fact that $\langle g_{iso} \rangle$ is smaller than the free-electron g value ($g_o = 2.0023$) is an indication that the BEC is indeed an electron-type center; more substantial evidence for this conclusion is given in Ref. 23. If one makes the (ultimately justifiable) assumption that the wavefunction ψ of the trapped electron has axial symmetry, it follows from elementary theory[26,44] that

$$|\langle \psi | 2s \rangle|^2 = (A_{\parallel} + 2A_{\perp})/3A_s = A_{iso}/A_s \qquad (6)$$

and

$$|\langle \psi | 2p \rangle|^2 = (A_{\parallel} - A_{\perp})/3A_p = A_{aniso}/A_p, \qquad (7)$$

where $|\langle\psi|2s\rangle|^2$ and $|\langle\psi|2p\rangle|^2$ are the densities of the unpaired electron in boron 2s and 2p atomic orbitals, respectively. Here, A_s and A_p are the s-state and p-state coupling constants for atomic boron as determined from theory or gas phase spectroscopy. Values for these parameters found in the literature[18,34,44] vary by as much as 25%; one set which falls approximately in the middle of the range is[44]

$$A_s(\text{atomic } ^{11}B) = 835 \text{ G}$$

and

$$A_p\ (\text{atomic } ^{11}B) = 19.6 \text{ G}.$$

Using these numbers in Eqs. (6) and (7) along with the appropriate quantities from Table II, one calculates

$$|\langle\psi|2s_B\rangle|^2 = 0.13$$

and

$$0 \lesssim |\langle\psi|2p_B\rangle|^2 \lesssim 0.51.$$

Thus it is seen that the unpaired electron of the BEC is considerably more localized on a boron nucleus than is the unpaired spin of the BOHC (Table I). Any model for the BEC is constrained to reflect this localization.

One suitable model is the dangling-orbital-type defect, e.g., the E' center.[4,42] Another possibility is an electron trapped in a boron-oxygen antibonding orbital in the manner of the substitutional boron defect in BeO.[44] On the basis of a number of considerations[23] the Author has concluded that the BEC is most likely an electron trapped in a dangling boron orbital at the site of an oxygen vacancy. While this type of wave-function is conventionally thought to be nonbonding, the possibility of its involvement in a weak three-electron bond with an alkali ion has not been excluded.[23]

If the oxygen vacancy should be at the site of a boron which had been four-coordinated, the steric picture of the BEC would be the same as that for the E' center[4,42] and certain oxygen-vacancy centers in phosphates,[45] i.e., that shown in Fig. 12. It is noteworthy that the energy E, which defines the closest lying excited states, is of the order of 3-4 eV.[42] Thus the g shift, which is generally proportional to λ/E (Eqs. 5), is expected to be small and this is what is observed (Table II). If the oxygen vacancy should be at the site of a boron which had been three-coordinated, a similar energy level scheme would result, except there would be one less B-O bond and the symmetry of the defect structure would be C_{2v} with the dangling orbital lying along the symmetry axis.

The BEC, like the BOHC, serves as a novel probe of borate glass structure. A dramatic illustration of this fact is provided by Fig. 13, which shows that $\langle A_{iso} \rangle$ for the BEC is sensitive both to the type and to the quantity of alkali present. The former sensitivity supports the suggestion that an alkali ion may be bonding to the defect boron, although other explanations[23] are equally plausable. However, the interpretation of the sharp drop in $\langle A_{iso} \rangle$ between 15 and 25 molar % alkali oxide seems less ambiguous. While this behavior does not appear to correlate with either the "boric-oxide anomaly"[3] or the fraction of borons in four-coordination[5], it corresponds nicely with the change-over from pentaborate groups to triborate groups postulated by Krogh-Moe[39] to take place in this composition range. The Author has hypothesized[23] that the BEC is an oxygen vacancy on the periphery of an otherwise intact boron-oxygen ring structure (e.g., a pentaborate group or a triborate group), with the electron trapped in the dangling boron orbital at the vacancy site. The relative proportions of boron 2s and 2p states in the defect wavefunction would then be dependent on the coordination number and bond angles at the apex boron. The ensemble distribution of those bond angles would be responsible for the observed distribution of A_{iso} values (Table II and Fig. 9).

C. Alkali-Associated Trapped-Electron Centers

When the BEC population is compared with the BOHC population by numerical integration techniques, it is found[23] that the BEC can account for only 15±10% of the trapped electrons in the temperature range 20-100°K and none of the trapped electrons at room temperature. At temperatures $\lesssim 77^{\circ}$K it now appears that the majority if not all, of the remaining electrons are trapped on alkalis or alkali "clusters" in sodium and potassium borate glasses.[8] It can be induced that similar trapping sites are effective in other alkali and alkaline-earth borate or silicate glasses.

The fundamental ESR evidence of alkali-associated trapped-electron centers is illustrated in Fig. 14. Here are displayed the X-band ESR spectra for some alkali borate glasses containing 30 molar % alkali oxide. At this composition the BEC spectrum is relatively weak compared with all other principal spectral features. Curve No. 1 in Fig. 14 pertains to a ^{10}B-enriched potassium borate glass which was "annealed" at room temperature after irradiation at $77^{o}K$. Curve No. 2 shows the high-field "edge" of this same spectrum as obtained at 25X gain. Curve No. 3 shows the high-field "edge" for the same glass at 25X gain *before* annealing. The general shape and position of curve No. 3 was found to be relatively insensitive to boron isotopic substitution. However, a glass containing sodium oxide in place of potassium oxide exhibited curve No. 4, when examined at 80X relative gain.

The positions of the "edges" defined by curves Nos. 3 and 4 of Fig. 14 are displaced from the free electron g value, g_o, by amounts virtually equal to 1/2 of the published values[18] for the atomic s-state hyperfine coupling constants for potassium and sodium, respectively. This fact suggests that these "edges" and their low-field counterparts arise from a class of defects involving unpaired electronic spins localized in potassium and sodium s-state atomic orbitals.

The suitability of this hypothesis has been tested by computer simulation techniques.[8] Figure 15 shows several attempts to computer fit the high-field "edge" observed in the potassium borate glass. Due to the overlapping low-field "tail" of the central BOHC resonance, the simulations are not expected to fit in the low-field region, although a "successful" simulation is required to fall *inside* of the experimental envelope. The computed spectrum for the dipotassium molecular ion (K_2^+) fails on the latter count, in addition to providing a poor fit to the high field "edge". (In carrying out each of the simulations, the g values, "single-crystal" linewidths, and *distribution* of A_{iso} values were "juggled" in an effort to optimize the fit.) It can be seen that the four-potassium complex (K_4^{3+}) with 70% of the unpaired spin density equally distributed in the four atomic 4s orbitals appears to provide the best fit, with a value of $\langle g_{iso} \rangle < g_o$. The latter inequality is in agreement with expectation for centers of the trapped-electron type.

Figure 16 illustrates a computer fit of the broad spectrum in a high-sodium glass, assuming 70% of the spin density is distributed equally among 6 sodium 3s orbitals. An improved fit probably could have been obtained by admixing smaller contributions due to complexes of fewer sodium ions along with a small BEC contribution. Again, the average g shift is negative. (The fact that the computed derivative curve crosses the baseline to the low field side of g_o is due to second order hyperfine effects).[9,17-19,23]

The reader may justifiably question the significance of assuming that "70%" of the trapped electron is located in alkali s-state orbitals. The reasoning behind this admittedly arbitrary choice is, first, that the true value should be $< 100\%$, since some fraction of the density is probably in alkali p-states or elsewhere and, second, that a number $< 50\%$ seems physically improbable and, at any rate, leads to poor computer fits.[8] As discussed in Ref. 8, the numbers of alkalis estimated to be involved in the alkali-associated electron centers of Figs. 15 and 16 are proportional to the square of the fractional spin density assumed to be in alkali s-states. Thus, if one believes 100% of the spin density to reside in these states, the best fits of Figs. 15 and 16 would correspond to 8 potassiums and 12 sodiums, respectively, instead of 4 and 6.

Numerical integrations of the best-fit curves of Figs. 15 and 16 were carried out and compared with the integrated intensities of the "central" resonances. It was found that the long-dashed curves of these figures represent intensities which are ~ 1/3 and ~ 2/3 as great as the respective "central' resonances. Thus, at least in the sodium borate case, the majority of the trapped electrons at 77°K have been accounted for. The Author has argued[8] that the remaining trapped electrons in these glasses (and most of those in lithium borate glasses) give resonances which underlie the central BOHC spectrum or else they are trapped in pairs and hence give no resonances at all.

The structural information to be derived from ESR studies of alkali associated centers relates to the apparent "clustering" of the alkali ions. While considerable work remains to be done to elucidate this effect, the present evidence[8] suggests that "cluster" sizes are influenced by radiation exposure and subsequent thermal and bleaching histories. The lower activation energy for diffusion of the smaller lithium ions is probably responsible for the present inability to observed lithium-associated centers by ESR means. Although optical studies are outside the scope of this review, it is noted that the familiar radiation induced band[46,47] in the range 1.5 - 2.4 eV appears[8] to be due to alkali-associated trapped-electron centers whose ESR spectra can be observed.

D. Interstitial-Proton Trapped-Electron Centers

Virtually all oxide glasses that have not been deliberately prepared "water free" contain varying amounts of OH groups and interstitial protons. When these glasses are irradiated at cryogenic temperatures, an almost inevitible result is the formation of some paramagnetic atomic hydrogen by electron trapping at the protons. The consequent hyperfine doublets, split by ~500 G, are in clear evidence in Figs. 10, 11 and 16. A discussion of the atomic-hydrogen defect in fused silica has been given.[48] The only point to be emphasized here is that this type of defect generally plays a minor role in the overall electron trapping scheme. For example, the integrated intensity represented by the hydrogen doublet in Fig. 16 is roughly 10^4 times smaller than the intensity of the sodium-associated centers.

E. Interstitial-Anion Trapped-Hole Centers

As discussed by Weeks[42], there is no substantive ESR evidence for interstitial O^--type defects in alkali borate or silicate glasses.* Indeed, there is no reason to expect the existence of significant numbers of interstitial oxygen ions in glasses containing ≤ 50 molar % alkali oxide. However, when alkali borate glasses are prepared with alkali halide additions, there is ample evidence that the halide ions take up interstitial positions.[9-13] When these halide-loaded glasses are irradiated at room temperature, sizeable numbers of hal_2^- molecular ions are produced, suggesting the reactions[9]

$$hal^- \xrightarrow{h\nu} hal^0 + e^- \tag{8}$$

and

$$hal^0 + hal^- \rightarrow hal_2^-. \tag{9}$$

The second process would depend on thermally activated diffusion of the radiation produced hal^0 to the site of another hal^-. Griscom and Patten[13] have carried out in situ irradiations near 20°K with the object of studying these kinetic effects.

Following irradiation by 50 keV x-rays at 22°K, X-band ESR spectra of high complexity were noted for glasses containing chloride, bromide, and iodide. Parts of these spectra, along with the relatively simpler spectra observed in some fluoride-containing and halide-free glasses, were explainable as superpositions of the now familiar BOHC and BEC spectra. Other portions of the spectra were due to

---

*The situation is quite different for glasses containing lead. There is ample evidence of radiation induced O^--type centers in lead borate, boro-silicate, silicate, and germanate glasses containing $\gtrsim 35$ molar % PbO.[49]

Cl_2^-, Br_2^-, or I_2^- molecular ions: the latter components grew in intensity as the samples were warmed[13] to 200°K and were easily identifiable on the basis of considerations which will be described in Sub-Section F., below.

The chloride and bromide glasses additionally exhibited other distinctive spectral features which were interpreted[12] as arising from Cl^o and Br^o, respectively. The bases for these identifications were:

(1) Each spectrum appeared to comprise a hyperfine quartet consistent with a nuclear spin of 3/2, as for the major isotopes of chlorine and bromine.[50]

(2) The splittings of these quartets were very nearly equal to the values of $A_{\parallel}$ predicted on the basis of published atomic anisotropic hyperfine coupling constants[18,34] for the halogens present in the respective samples.

(3) Additional small splittings were observed in each case which were consistent with the known relative abundances and nuclear-magnetic moments of the appropriate halogen isotopes.[50]

(4) Isochronal annealing experiments[13] show that the paramagnetic species in question are indeed precurso rs of the dihalogen molecular ions observed at higher temperatures, as predicted by Eqs. (8) and (9).

(5) Successful computer simulations of the chlorine and bromine spectra were carried out, utilizing the g-value theory[51] developed for the isoelectronic O^- ion along with published values of the spin-orbit coupling constants[19] for chlorine and bromine.

The ESR spectrum observed immediately after irradiation of the chloride-containing glass at 22°K is shown in Fig. 17a; some distinctive spectral features which are due primarily to the BOHC, the BEC, H^o, Cl_2^-, and Cl^o have been indicated. Figure 17b is a computer simulation of the Cl^o contribution. Figure 18 presents the analogous results for the bromide-containing glass. Here, the computer simulation is indicated by the dashed curve; the "double-bump" structure observed near 4100 G in both the experimental and simulated spectra is an isotope effect. The spin Hamiltonian parameters used in carrying out these simulations are listed in Table III.

The computer simulations of Figs. 17 and 18 are particularly useful in illustrating some of the concepts which have been presented in the preceeding Sub-Sections. If one considers the case of the chlorine atom, the highest occupied energy levels correspond to the 3p orbitals indicated in Fig. 19a. If the atom were in free space, these levels would be degenerate. However, the Jahn-Teller Theorem[16] provides assurance that the same atom when placed in a solid matrix will experience unsymmetric crystal fields such that the orbital containing the unpaired spin will be split upward from the other two. Thus, it is an a priori expectation that there will be some splitting Δ (which need not be large), although the exact mechanism of the interaction must be inferred from the experimental details. As discussed in Section IIIE., there is also an a priori expectation that when the solid matrix is a glass there will be an ensemble distribution of Δ values, such as the Gaussian curve of Fig. 19b, rather than a single well-defined splitting. Since Cl^o is iso-electronic with O^-, one may adapt the g value theory[51] for the latter; this is given to a first order approximation in Fig. 19c. (It can be noted that the form of these equations is essentially the same as Eqs. 5.) It is immediately clear that the symmetrical distribution of Δ values of Fig. 19b leads to the skewed distribution of g values shown in Fig. 19d. The computer simulation of Fig. 17 was performed by computing a separate spectrum for each point in Fig. 19d and then summing them according to the indicated weighting factors.

Once again, the question of uniqueness arises. It is not possible to fit any spectrum with an arbitrary theory by distributing enough parameters? The answer is, no, this does not follow. To see why, one must focus his attention on the constraints of the problem as well as the freedoms. Here, the Author has constrained himself to use (i) a Gaussian distribution of Δ values, (ii) a simple, but unbending, theory (Fig. 19c), (iii) the correct value of λ for the appropriate species, (iv) hyperfine coupling constants in ranges not precluded by published data, and (v) the same assumptions in computing both the Cl^o and Br^o spectra. Moreover, it was found that the high-field features of these spectra were, at any rate, completely insensitive to the g value distribution. (Conversely, the "choppiness" on the low-field side of the computed spectra results from the finite number of points in the $g_\perp$ distribution.) Finally, the "most probable" g values for the two atomic species were found to be related according to

$$\frac{\langle g_\perp(Cl^o)\rangle - g_\parallel(Cl^o)}{\langle g_\perp(Br^o)\rangle - g_\parallel(Br^o)} \approx \frac{\lambda(Cl^o)}{\lambda(Br^o)} \qquad (10)$$

This indicates that the average value of Δ is apparently the same (~1.2 eV) in both cases, suggesting that the glassy matrix is the "common denominator".

Although halide ions are not present in significant numbers in most oxide glasses, it is of value to consider the structural information to be inferred from the above results. The splitting Δ could arise from an electrostatic interaction with two or more positive ions, e.g., alkalis, noncollinearly arranged in the x-y plane (refer to Fig. 19a) or from a weak, three-electron covalent bond directed along the z axis.[12] Symons[52] favors the latter hypothesis, and has suggested that the weak bond may be with an oxygen. In this case, one may visualize defects of the type

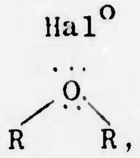

where R would be a borate tetrahedron or triangle.

F. Interstitial Di-Halogen-Molecular-Ion Trapped-Hold Centers

The di-halogen molecular ion, or hal_2^-, is the end product of the reactions specified by Eqs. (8) and (9). It is interesting to note that the Cl_2^- hole-type defects are highly stable at room temperature, while the analogous "V-type" centers in alkali halides are not.[9] This is probably because the glasses contain some very deep electron traps.[13] It seems very likely that the glass-bound Cl_2^- is a true interstitial; the optical and spin Hamiltonian parameters indicate[11] that Cl_2^- in borate glasses is closer to the "free" molecular species than either the V_k center or the H center in KCl. However, hal_2^- in the glasses are constrained not to rotate even up to 500°K.[11] The reasons for this are not clear.

Figures 20 and 21 show, respectively, the X-band and Ka-band spectra of Cl_2^- centers in γ-irradiated alkali borate glasses. Parts (a) of these figures are the experimental spectra and parts (b) are computer simulations based on the set of spin Hamiltonian parameters listed in Ref. 9. The ability to obtain good computer fits at two widely separated frequencies adds a further dimension of confidence to the spin-Hamiltonian analysis which was carried out.[9]

The electronic structure of the hal$_2^-$ defect is illustrated in Fig. 22. The splittings Δ_1 and Δ_2 in this figure determine the shift of $g_\perp$ away from the free electron value g_o,[19] while the energy E_1 designates the principal UV transition at ~ 3.7 eV.[11] Although these parameters do not appear to be terribly sensitive to the glass structure, the present understanding of this defect permits its use as a probe for studying the kinetics of electron and hole trapping in alkali borate glasses by tracing the relative populations of various defect types as functions of post-irradiation thermal treatment[13].

G. O_2^- and Other Peroxy Radicals

Weeks[42] has discussed the possibility of observing O_2^- or other peroxy radicals (RO_2.) in irradiated oxide glasses and has suggested that a familiar structureless, anisotropic resonance with $g_\parallel \approx 2.04$ and $g_\perp \approx 2.002$ observed in irradiated silicate[4,32] and borate[53] glasses may be due to this source. However, this hypothesis has not been confirmed.

An ESR spectrum which definitely arises from a peroxy radical had been obtained from certain alkali peroxyborate preparations which were partially amorphized in the course of a solid-state reaction which can be made to take place below the melting point of the material.[24,54,55] This is the so called "Z resonance"[24,54,55] which has been attributed to either interstitial O_2^- or the radical

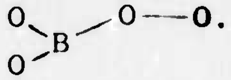

Up until very recently, resonances of this particular type had not been unambiguously detected in alkali borate glasses quenched from a melt.

The Author[56] has studied a quenched glass having the nominal composition 70% Na_2O - 30% B_2O_3 prepared in a manner similar to that described by Kline.[57] It is known from NMR studies[5,57] that all of the borons in glasses of this composition are three coordinated. As indicated in Fig. 23, a strong "Z resonance" was observed[56] in the as-quenched glass; this was not enhanced by x irradiation at 77°K. These findings are consistent with either of the proposed models[24, 54,55] for the "Z resonance" and represent the first confirmed observation of a peroxy-type center in a quenched oxide glass. However, this species may not be a common radiation-induced defect in oxide glasses as previously suggested.[42]

The broad, low-field "humps" in Fig. 23 result from a broad distribution of $g_{\parallel}$ values.[24,54,55] This is in contrast to the case of O_2^- in polycrystalline Na_2O_2, where discrete values of $g_{\parallel}$ and $g_{\perp}$ are represented (see Fig.3).[24] Computer simulations which corroborate the postulated distributions have been carred out[55,58] within the constraints of the g-value theory developed[59] for the O_2^- ion. The physical reason for these distributions could be related to random coordination by Na^+ ions in the O_2^- case, or to random B-O-O bond angles in the RO_2 case.[24,42]

The electronic structure of the O_2^- molecular ion differs from that of the hal_2^- (Fig. 22) in that there are two fewer electrons in the valence orbitals. Thus, O_2^- could be described by Fig. 22 by removing the two uppermost electrons, leaving the unpaired spin in the highest lying π^{AB} orbital, say, the π_x^{AB}. Peroxyradicals RO_2^- would differ only in that the π_y "AB" orbital would be involved in the bond with R. It is the splitting between the π_x^{AB} and π_y^{AB} orbitals which is critical in determining the g shifts.[59]

H. Paramagnetic Oxide-Glass Defect Centers Which Have Not Been Observed in the Alkali Borate System

As mentioned above, interstitial O^- ions have not been detected in alkali borate glasses although they have been observed in glasses of high lead content.[49] Interstitial O_3^- ions have also been suggested[42] as possible defects in oxide glasses, but they have not yet been detected outside of the "amorphized" peroxyborates.[24,54,55] An example of a defect which is probably without any borate analog is the P_2 doublet observed by Weeks and Bray[45] in irradiated phosphate glasses. On the basis of comparisons with a sequence of isoelectronic tetrahedral radicals, Symons[60] has attributed the P_2 doublet to structures comparable to PO_4^{4-}. As discussed by the Author,[23] there is no reason to suspect the existence of structures comparable to the pseudoisoelectronic species BO_4^{6-} in borate glasses.

One defect worthy of special mention in the present context is the H_4^+ center described by Mackey and coworkers[61] in irradiated, reduced sodium silicate glasses. Their model for this center,

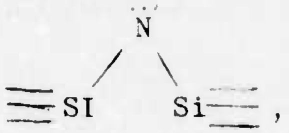

is exactly analogous to one of the models (Fig. 6) proposed for the BOHC, i.e.,

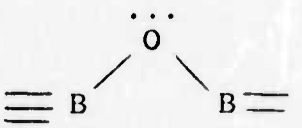

As emphasized in the present paper, the existence of these kinds of analogs in various oxide glass systems appears to be the rule rather than the exception.

What is particularly useful about the H_4^+ center is that it provides a piece of complementary information, namely, the spin density on the bridging species. This is because the abundant ^{14}N nucleus has a nuclear moment--and hence a hyperfine interaction--while ^{16}O does not. Using the values $A_\parallel = 36G$ ($=g_{zz}$ in Fig. 6) and $A_\perp \approx 2G$ given by Mackey et al[61] and assuming that $A_\parallel$ and $A_\perp$ have different algebraic signs, one calculates by means of Eqs. (6) and (7)

$$|\langle\psi|2s_N\rangle|^2 \approx 0.02$$

and

$$|\langle\psi|2p_N\rangle|^2 \approx 0.74$$

assuming values of A_s and A_p for ^{14}N tabulated by Ayscough.[18] These results clearly show that the hole is highly localized on the bridge, while the high p-state-to-s-state ratio (~37) underscores the π-like nature of this defect. (Recall that the π-orbital nature of the BOHC was inferred from less direct evidence.)

The H_4^+ center bears another crucial similarity to the BOHC, that is the broad distribution of g_3 values (Fig.4), attributable to variations in the bond angle at the bridging oxygen[26] or nitrogen[61] sites. On the other hand, $g_1 \approx g_2$ for the H_4^+ center,[61] in contrast with the case for the BOHC (Table I). Assuming the BOHC is indeed described by Fig. 6 (rather than Fig. 7), this difference can be explained as follows: In Fig. 6, the hole is bound to its site in the glass network by the electrostatic attraction of a (negatively charged) four-coordinated boron, at say, R. This may cause one principal axis of the g tensor to lie close to the O-R bond and, as described in Ref. 26, would lead to a value of $g_2 > g_1$. In the case of the H_4^+ center, the hole is bound to the nitrogen site by virtue of the lower nuclear charge of the nitrogen vis-à-vis oxygen. Thus, since R and R' would be identical silicons, the symmetry of the structure dictates that the principal axes of the g tensor would be the x, y, and z axes in Fig. 6, with the consequence that $g_2 \approx g_1$.[61]

V. SUMMARY

It can now be stated that all of the generic types of radiation-induced defects in the more common oxide glasses have probably been identified and characterized by ESR means. Most of these have been illustrated by examples from the alkali borate system. Noteworthy have been the repeated instances of statistical distributions of spin Hamiltonian parameters, stemming from the random nature of the glassy state. The importance of computer simulation techniques in elucidating these results cannot be overemphasized. Examples of useful structural information gained from these ESR studies have been given.

REFERENCES

1. E. Lell, N.J. Kreidl and J.R. Hensler, in: Progress in Ceramic Science, Vol. 4, Ed. J. Burke (Pergamon, Oxford, 1966).

2. A. Bishay, J. Non-Crystalline Solids 3, 54 (1970).

3. H. Rawson, Inorganic Glass-Forming Systems, (Academic Press, New York, 1967).

4. R.A. Weeks, J. Appl. Phys. 27, 1376 (1956); C.M. Nelson and R.A. Weeks, J. Am. Ceram. Soc. 43, 396 (1960); ibid 43, 399 (1960); R. H. Silsbee, J. Appl. Phys. 32, 1459 (1961); F.J. Feigl, J. Phys. Chem. Solids 31, 575 (1970).

5. P.J. Bray and J.G. O'Keefe, Phys. Chem. Glasses 4, 37 (1963); P.J. Bray, in: Interaction of Radiation with Solids, Ed. A. Bishay, (Plenum Press, New York, 1967).

6. M.C.M. O'Brien, Proc. Roy. Soc. (London) A231, 404 (1955).

7. J.H. Mackey, Jr., J. Chem. Phys. 39, 74 (1963).

8. D.L. Griscom, J. Non-Crystalline Solids 6, 275 (1971).

9. D.L. Griscom, P.C. Taylor and P.J. Bray, J. Chem. Phys. 50, 977 (1969).

10. M. Hass and D.L. Griscom, J. Chem. Phys. 51, 5185 (1969).

11. D.L. Griscom, J. Chem. Phys. 51, 5186 (1969).

12. D.L. Griscom, Solid State Comm., in press.

13. D.L. Griscom and F.W. Patten, Am. Ceram. Soc. Bull. 51, 367 (1972); to be published.

14. R.H. Sands, Phys. Rev. 99, 1222 (1955).

15. P.C. Taylor, H.M. Kriz, and J.H. Baugher, Chem. Reviews, manuscript in preparation.

16. G.E. Pake, *Paramagnetic Resonance* (W.A. Benjamin, Inc., New York, 1962).

17. P.W. Atkins and M.C.R. Symons, *The Structure of Inorganic Radicals* (Elsevier, Amsterdam, 1967).

18. P.B. Ayscough, *Electron Spin Resonance in Chemistry*, (Methuen and Co. Ltd. London, 1967).

19. C.P. Slichter, *Principles of Magnetic Resonance* (Harper & Row, New York, 1963).

20. J.H. Mackey, M. Kopp, E.C. Tynan, and T.F. Yen, in: *Electron Spin Resonance of Metal Complexes* (Plenum Press, 1969).

21. P.C. Taylor and P.J. Bray, J. Mag. Res. **2**, 305 (1970).

22. J.D. Swalen and H.M. Gladney, IBM J. Res. Dev. **8**, 515 (1964).

23. D.L. Griscom, J. Chem. Phys. **55**, 1113 (1971).

24. D.L. Griscom, Ph.D. Thesis, Brown University, Providence, R.I., 1966.

25. D.L. Griscom, unpublished results.

26. D.L. Griscom, P.C. Taylor, D.A. Ware, and P.J. Bray, J. Chem. Phys. **48**, 5158 (1968).

27. D.L. Griscom, P.C. Taylor and P.J. Bray, J. Chem. Phys. **53**, 469 (1970).

28. J.W.H. Schreurs, J. Chem. Phys. **47**, 818 (1967).

29. Y.M. Kim and P.J. Bray, J. Chem. Phys. **53**, 716 (1970).

30. T. Purcell and R.A. Weeks, Phys. Chem. Glasses **10**, 198 (1969); Nalamolu Gopalarao, Ph. D. Thesis, Brown University, June 1969.

31. G.O. Karapetyan and D.M. Yudin, Fiz. Tver. Tela **3**, 2827 (1961), [Eng. Transl.: Sov. Phys.-S.S. **3**, 2063 (1962)]; Y. Nakai, Bull. Chem. Soc. Japan **37**, 1089 (1964).

32. S.Lee and P.J. Bray, Phys. Chem. Glasses **3**, 37 (1962).

33. Y.M. Kim, D.E. Reardon, and P.J. Bray, J. Chem. Phys. 48, 3396 (1968).

34. C.M. Hurd and P. Coodin, J. Phys. Chem. Solids 28, 523 (1967).

35. Sook Lee and P.J. Bray, J. Chem. Phys. 40, 2982 (1964).

36. M.C.R. Symons, J. Chem. Phys. 53, 468 (1970).

37. P.C. Taylor, D.L. Griscom, and P.J. Bray, J. Chem. Phys. 54, 748 (1971).

38. P.C. Taylor and D.L. Griscom, J. Chem. Phys. 55, 3610 (1971).

39. J. Krogh-Moe, Phys. Chem. Glasses 3, 101 (1962); 6, 46 (1965).

40. E.M. Levin, C.R. Robbins, and H.F. McMurdie, Phase Diagrams for Ceramists, Ed., M.K. Reser (American Ceramic Society, 1964).

41. P.C. Taylor and P.J. Bray, J. Am. Ceram. Soc., in press.

42. R.A. Weeks, in: Interaction of Radiation with Solids, Ed. A. Bishay, (Plenum Press, New York, 1967).

43. G.H. Sigel, Jr., private communication.

44. A.R. Reinberg, J. Chem. Phys. 41, 850 (1964).

45. R.A. Weeks and P.J. Bray, J. Chem. Phys. 48, 5 (1968).

46. P. Beekenkamp, Thesis, Technische Hochschule, Eindhoven, Netherlands, 1956 [published in Philips Res. Rept. Suppl. No. 4 (1966)].

47. S. Arafa and A. Bishay, Phys. Chem. Glasses 10, 192 (1969).

48. R.A. Weeks and M.M. Abraham, J. Chem. Phys. 42, 68 (1965).

49. Y.M. Kim and P.J. Bray, J. Chem. Phys. 49, 1298 (1968).

50. See, for example, "NMR Table", distributed by Varian Associates, Palo Alto, California.

51. J.R. Brailsford, J.R. Morton, and L.E. Vannotti, J. Chem. Phys. 49, 2237 (1968).

52. M.C.R. Symons, private communication.

53. Sook Lee and P.J. Bray, J. Chem. Phys. 39, 2863 (1963).

54. J.O. Edwards, D.L. Griscom, R.B. Jones, K.L. Watters, and R.A. Weeks, J. Am. Chem. Soc. 91, 1095 (1969).

55. D.L. Griscom and P.J. Bray, to be published.

56. D.L. Griscom, unpublished.

57. D. Kline, Ph.D. Thesis, Brown University, Providence, R.I., 1964.

58. P.C. Taylor, unpublished work.

59. W. Kanzig and M.H. Cohen, Phys. Rev. Letters 3, 509 (1959).

60. M.C.R. Symons, J. Chem. Phys. 53, 857 (1970).

61. J.H. Mackey, J.W. Boss, and M. Kopp, Phys. Chem. Glasses 11, 205 (1970).

TABLE I. Spin Hamiltonian parameters for oxygen associated hole-type centers in a variety of oxide glasses.[27]

Material	nucleus	g_1	g_2	g_3[a]	$\frac{\langle A\rangle}{A_s}$[b]	ref.
borate glass	^{11}B	2.002	2.010	2.035	0.013	26
silicate glass	^{29}Si	2.003	2.009	2.019	0.010	28
titanate glass	^{47,49}Ti	2.003	2.010	2.022	d	29
germanate glass	^{73}Ge	2.002	2.008	2.051	d	30
phosphate glass	^{31}P		2.010[c]	a	0.009	31
aluminate glass	^{27}Al		2.009[c]	a	0.005	32
niobate glass	^{93}Nb		2.01[c]	a	0.002	33

[a] Each of the glass spectra is evidently characterized by a distribution of g_3 values, accounting for the observed low-field shoulders. The "average" g_3 value for borate glasses was determined by computer simulation (Ref. 26); this method has not yet been applied to the other glasses listed.

[b] $\langle A\rangle$ = (average measured hyperfine splitting) $\approx 1/3$ Tr $|A|$. Values for A_s, the atomic Fermi contact coupling, were taken directly, or extrapolated, from the calculations of Hurd and Coodin (Ref. 34).

[c] For phosphate, aluminate, and niobate glasses, the only available g value is that for the centroid of the hyperfine multiplet structure; this should correspond approximately to the values of g_2 listed for the other centers.

[d] Hyperfine structure due to ^{47}Ti (8% abundant), ^{49}Ti (5.5% abundant), or ^{73}Ge (8% abundant), if present, may be obscured by superhyperfine structure or other effects.

TABLE II. Spin Hamiltonian parameters for the boron electron center (BEC).[23]

Parameter and Measured Value[a]	Definition
$\langle A_{iso}(^{11}B)\rangle = 108 \pm 2$ G	Average value of A_{iso}
$\Delta A_{iso}(^{11}B) = 34 \pm 4$ G	Half width of gaussian distribution of A_{iso} values
$\langle A_{aniso}(^{11}B)\rangle \lesssim 10$ G	Average value of A_{aniso}
$\langle g_{iso}\rangle = 2.0018 \pm 0.0009$	Average value of g_{iso}
$\langle g_{aniso}\rangle \lesssim 0.0013$	Average value of g_{aniso}

[a] All measurements pertain to a glass of composition 17.7% K_2O - 82.3% B_2O_3. $\langle A_{iso}(^{11}B)\rangle$ is sensitive to glass composition (See, Fig. 13).

TABLE III. Spin Hamiltonian parameters for Cl^o and Br^o isolated at 22°K in x-irradiated potassium halide-potassium borate glasses.[12]

Isotope	$g_{\parallel}$ [a]	$g_{\perp}$ [b]	$A_{\parallel}(G)$	$A_{\perp}(G)$ [c]	$\Delta H_{p-p}(G)$ [d]	$\lambda(cm^{-1})$ [e]
^{35}Cl	1.997	2.063	122	61	11.5	440
^{81}Br	1.909	2.26	485	229	34.5	1842

[a] Not corrected for effect of nuclear quadrupole interaction.

[b] "Most probable" value, given the assumed value of $A_{\perp}$.

[c] These values do not constitute "measurements"; they were, however, used in carrying out the computer simulations of Figs. 17 and 18.

[d] Peak-to-peak derivative linewidths of the Lorentzian convolution functions used in computing the spectra of Figs. 17 and 18.

[e] Given in Ref. 19 (p. 180).

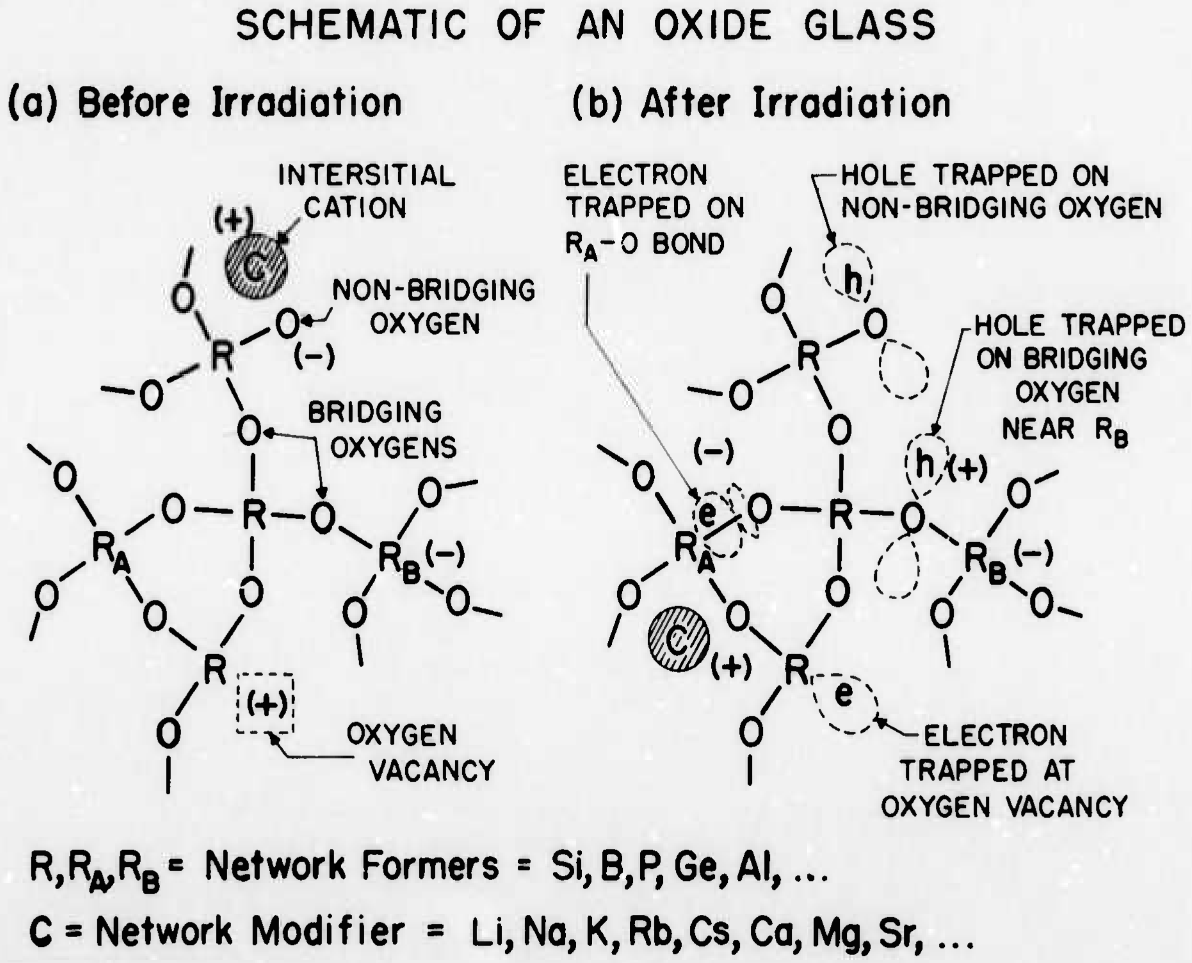

Fig. 1 - Schematic diagram of an oxide glass showing several types of radiation-induced paramagnetic centers in their relationships with pre-existing defects such as an oxygen vacancy, a non-bridging oxygen, and substitutional impurities. Dashed "baloons" enclose regions of high probability density for the trapped electrons (e) or trapped holes (h). This figure illustrates the locally charge-compensated nature of the trapped species. It should be noted, however, that the individual trapped holes and electrons are assumed to be much more distant from one another than shown here.

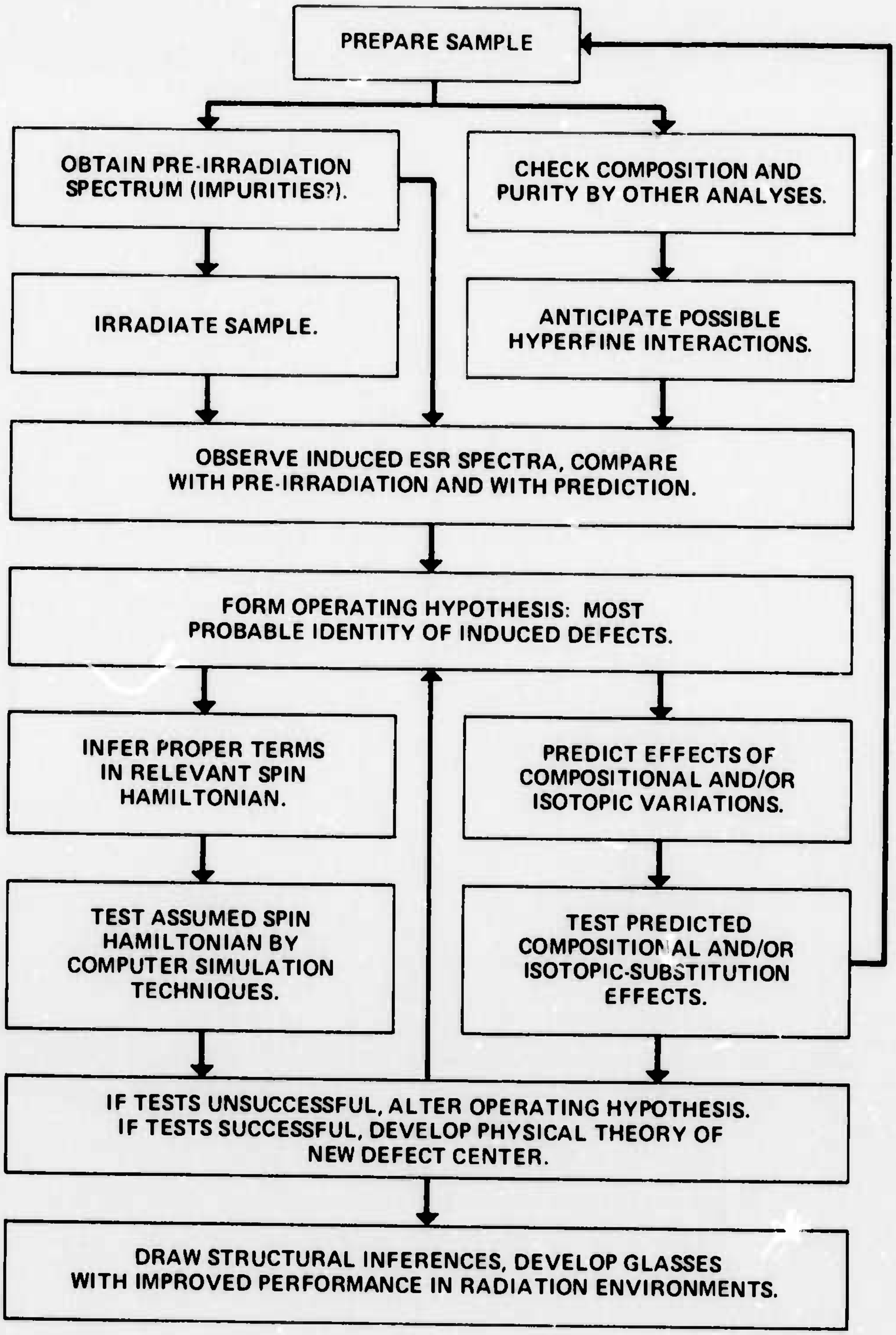

Fig. 2 - "Flow diagram" illustrating a typical approach to the study of radiation damage and structure in glassy materials by means of electron spin resonance techniques.

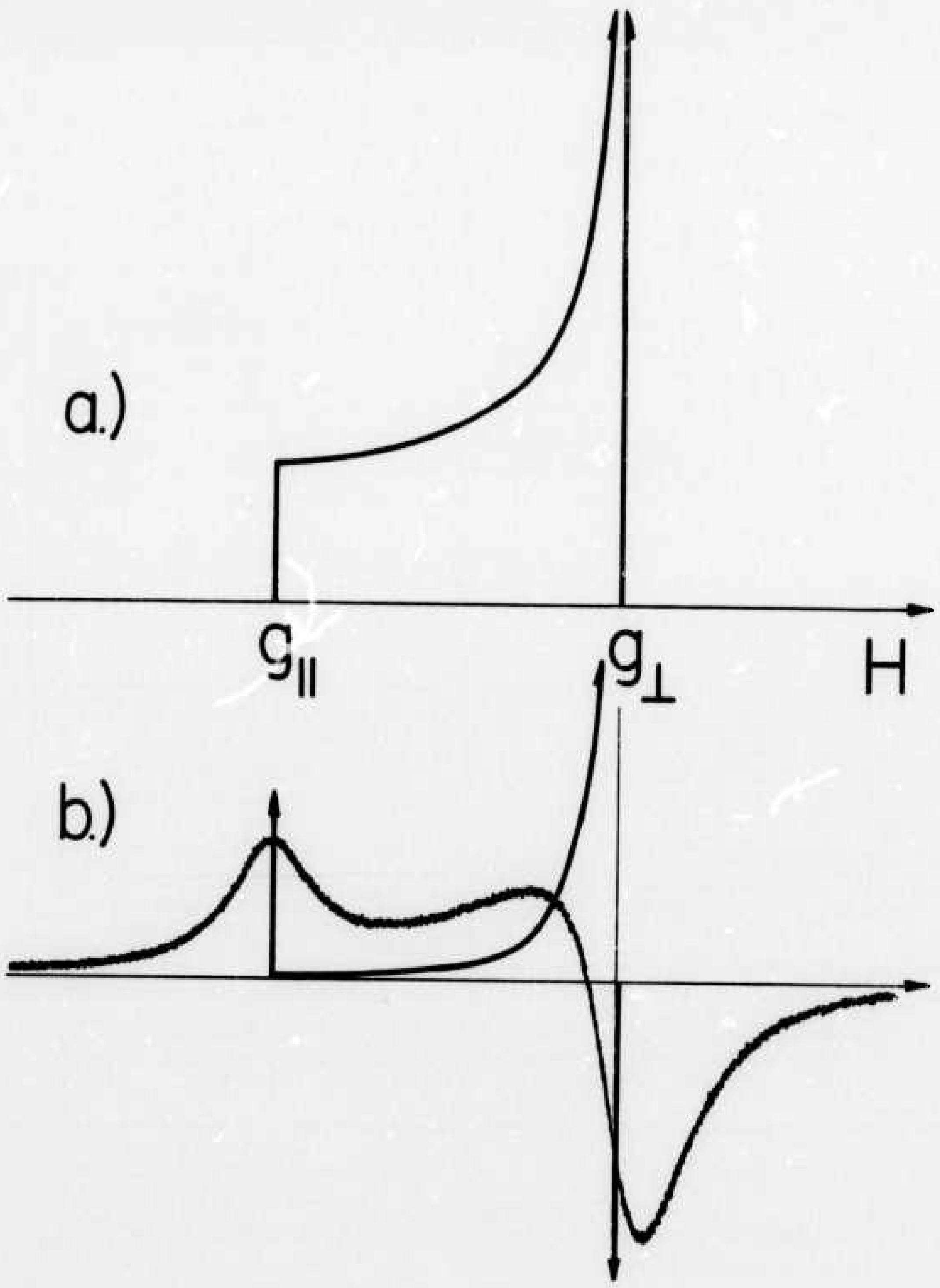

Fig. 3 - ESR "powder pattern" for a paramagnetic center characterized by an axially symmetric g tensor and no hyperfine interactions. (a) Absorption line shape assuming zero single-crystal line-width. (b) First derivative of (a). Noisy curve is an experimental first-derivative spectrum for a sample having a finite single-crystal width.

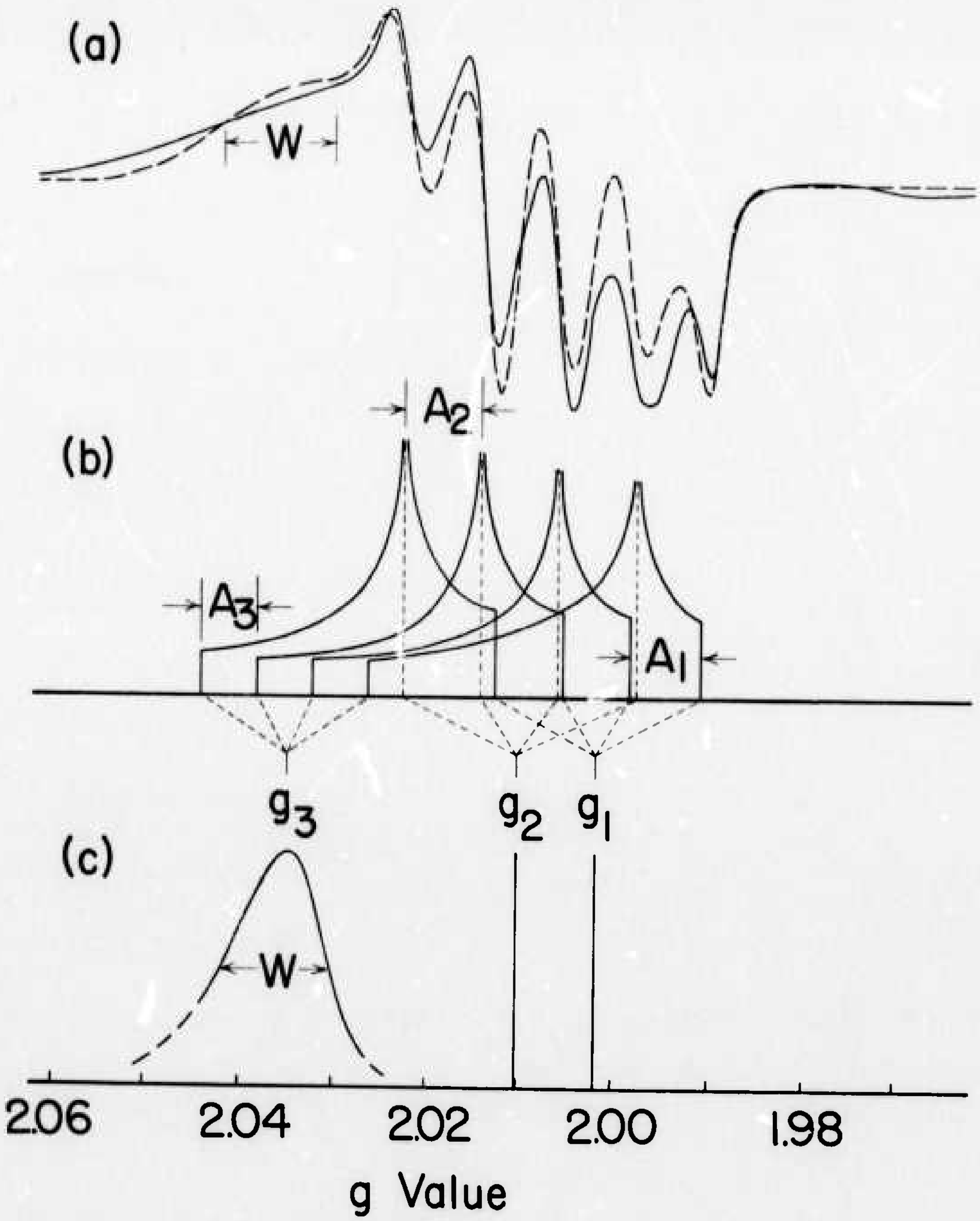

Fig. 4 - An analysis of the X-band (9 GHz) ESR spectrum of the boron-oxygen hole center (BOHC) in irradiated alkali borate glasses. The unbroken curve in (a) is the experimental spectrum for a 20% K_2O-80% B_2O_3 glass x-irradiated at 77° K and bleached with IR light. The dashed curve in (a) is a computer simulation [26] based on the powder patterns shown in (b) and the distribution of g values shown in (c). Because the width W of the g_3 distribution, expressed in units of magnetic field, is greater than the hyperfine coupling constant A_3, no hyperfine structure is discernable on the low-field shoulder in (a).

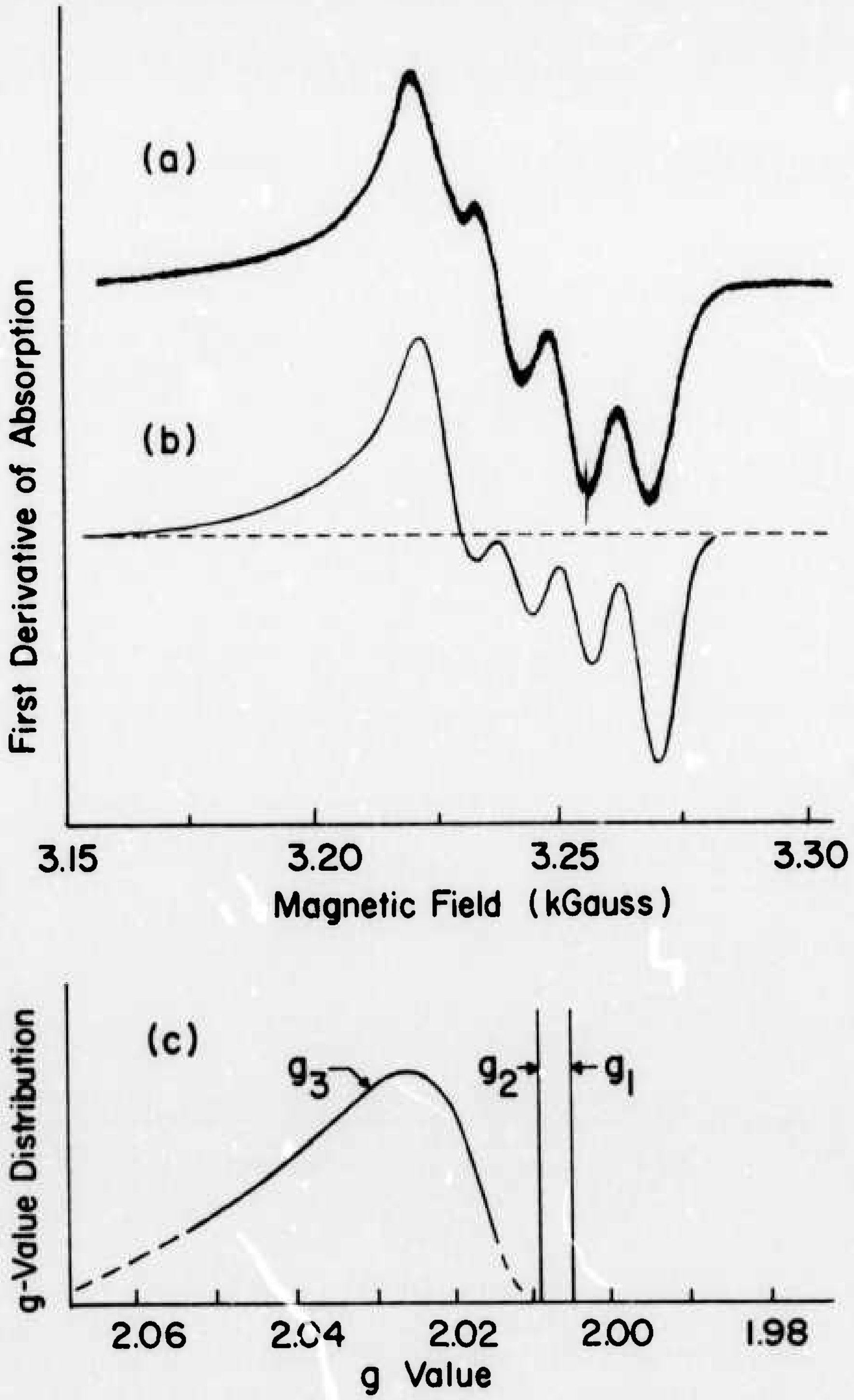

Fig. 5 - X-band ESR spectrum of a 50% Li_2O-50% B_2O_3 glass, γ-irradiated at 77°K. (a) Experimental spectrum. (b) Computed spectrum[26] (c) Distribution of g values used in carrying out the simulation.

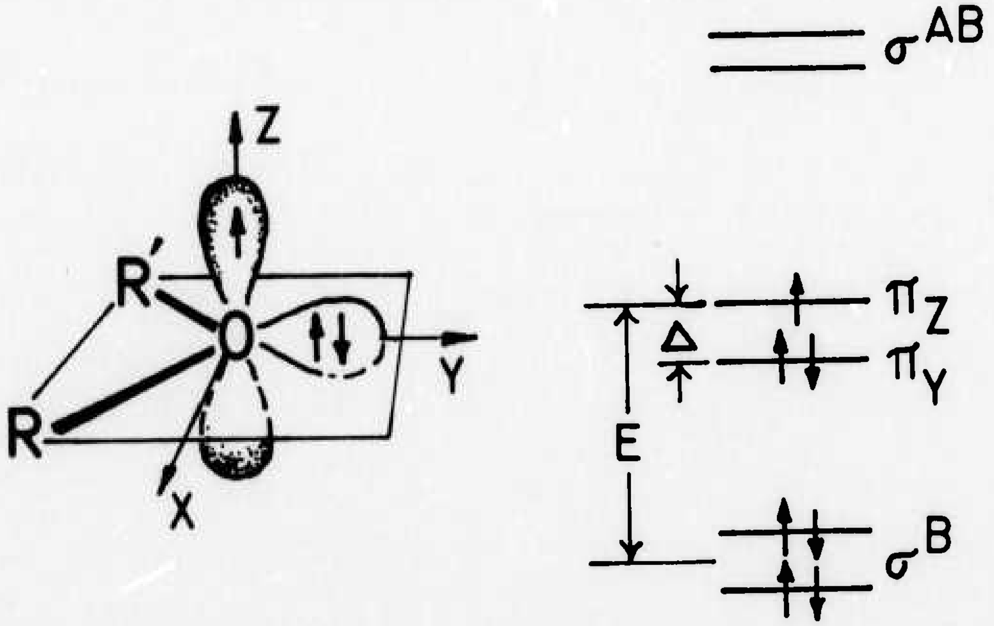

Fig. 6 - Schematic of a bridging-oxygen trapped-hole center. Left: steric picture. Right: electronic energy levels. As indicated, the unpaired spin would be in the non-bonding π_z orbital.

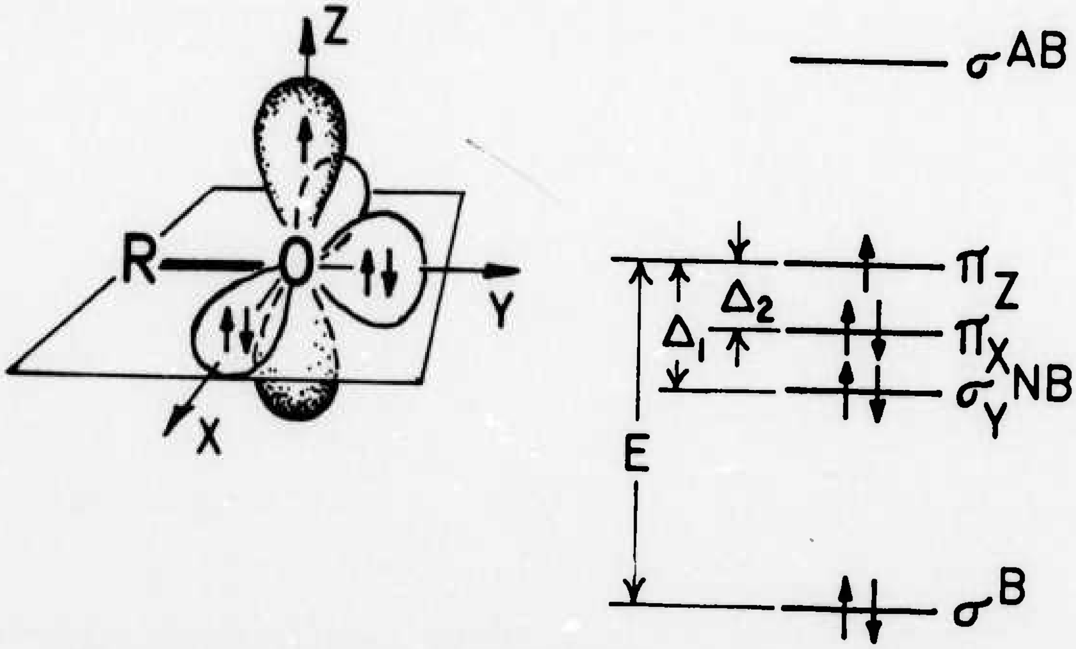

Fig. 7 - Schematic of a non-bridging-oxygen trapped-hole center. Left: steric picture. Right: electronic energy levels. The mechanism responsible for the splitting Δ_2 is not known.

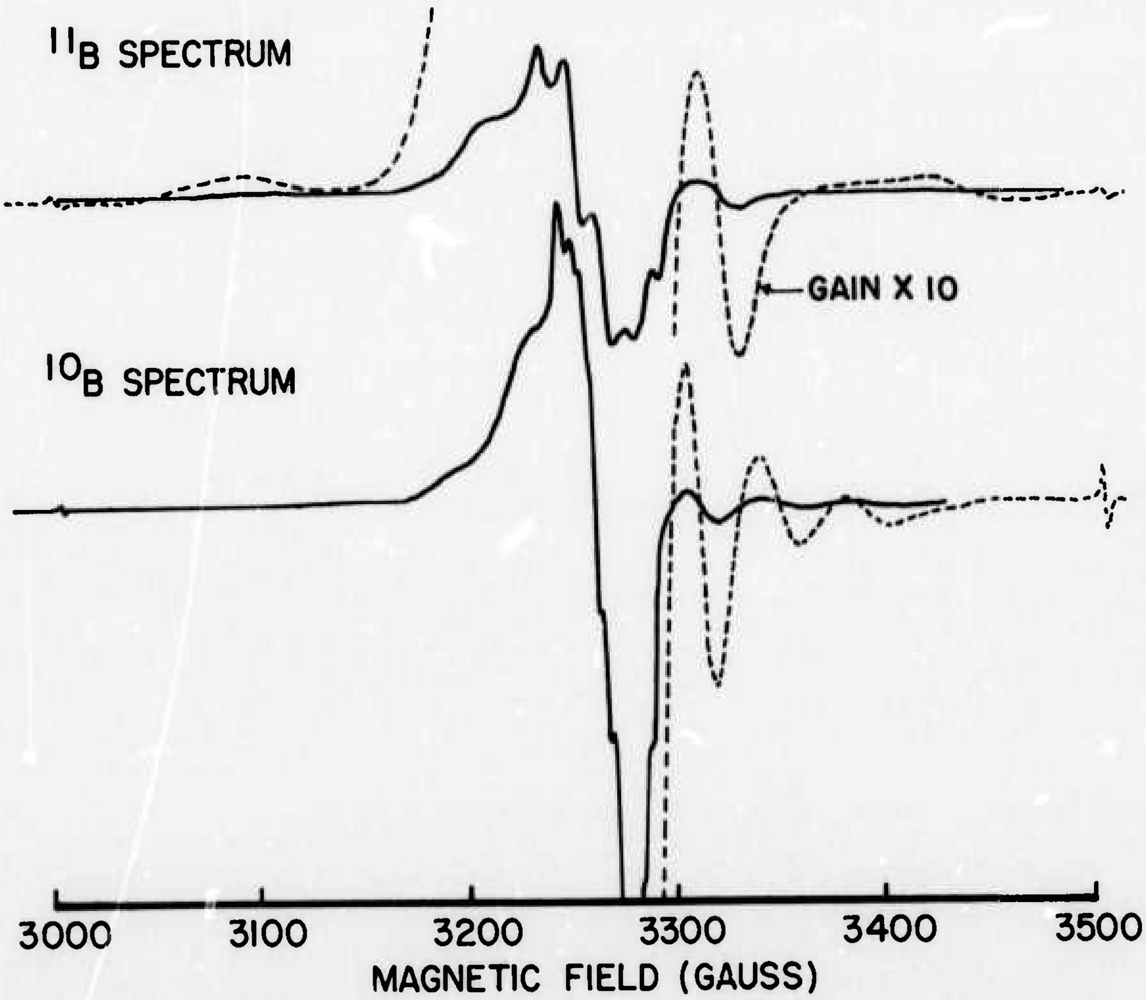

Fig. 8 - X-band ESR spectra for glasses of composition 17.7% K_2O-82.3% B_2O_3 obtained under various conditions. Top spectrum: Glass of normal isotopic abundance, x-irradiated and observed at 22° K. Bottom spectrum: Glass enriched in ^{10}B, x-irradiated at 22° K, warmed to 90° K and observed at 70° K. Dashed curves are portions of the same experimental spectra recorded at high gain. (Qualitatively similar results were obtained at other temperatures below ~100° K.)

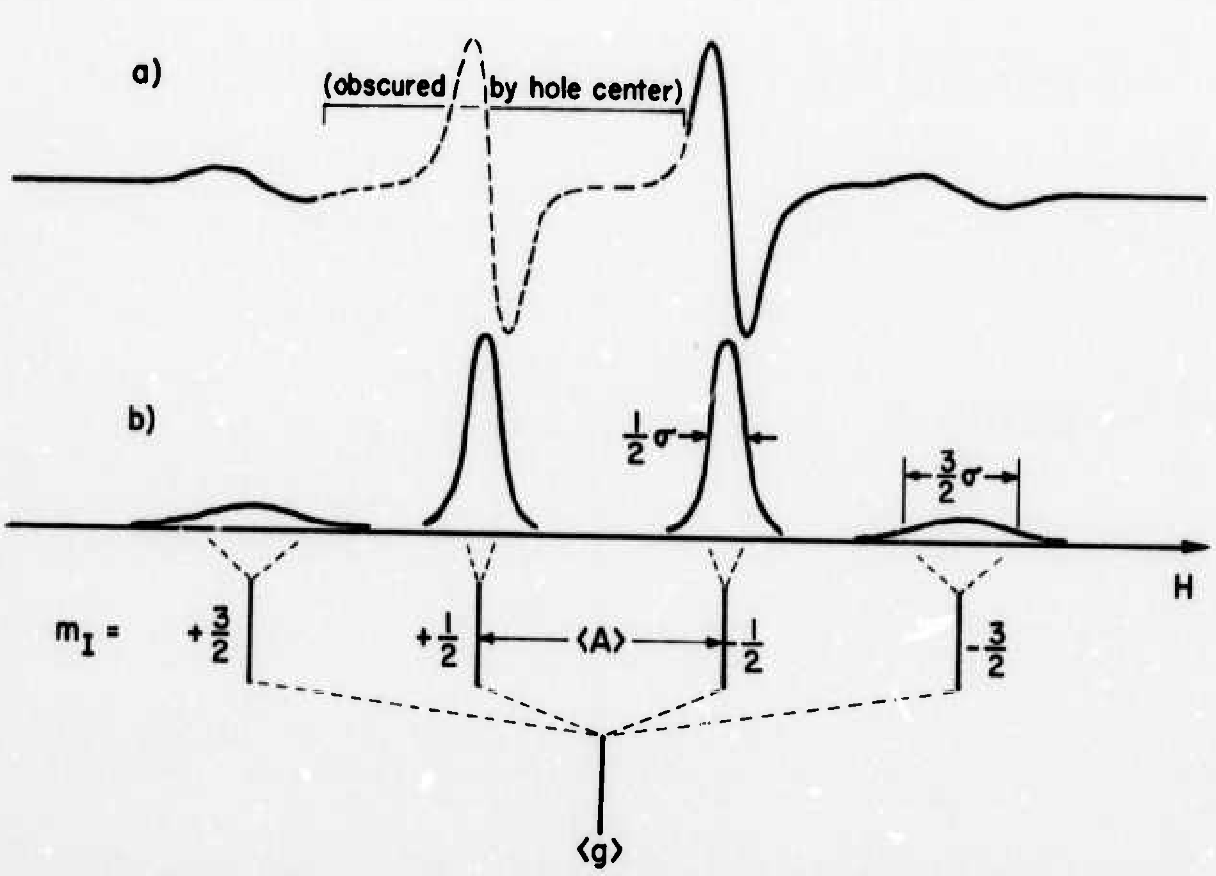

Fig. 9 - A model explaining the qualitative features of the BEC spectrum. (a) Experimental first-derivative spectrum (shape of m_I = +1/2 component is inferred). (b) "Stick Diagram" defining the average g value ⟨g⟩ and the average ^{11}B hyperfine coupling constant ⟨A⟩ . Here, the effect of a distribution of coupling constants is illustrated in terms of its effect on the (undifferentiated) absorption spectrum. A bell-shaped distribution having a width at half maximum equal to σ results in widths for the individual hyperfine lines equal to 1/2 σ for the m_I = ± 1/2 peaks and 3/2 σ for the m_I = ± 3/2 peaks. The latter are accordingly lower in amplitude than the former by a factor of 9 if no other line broadening mechanisms are considered.

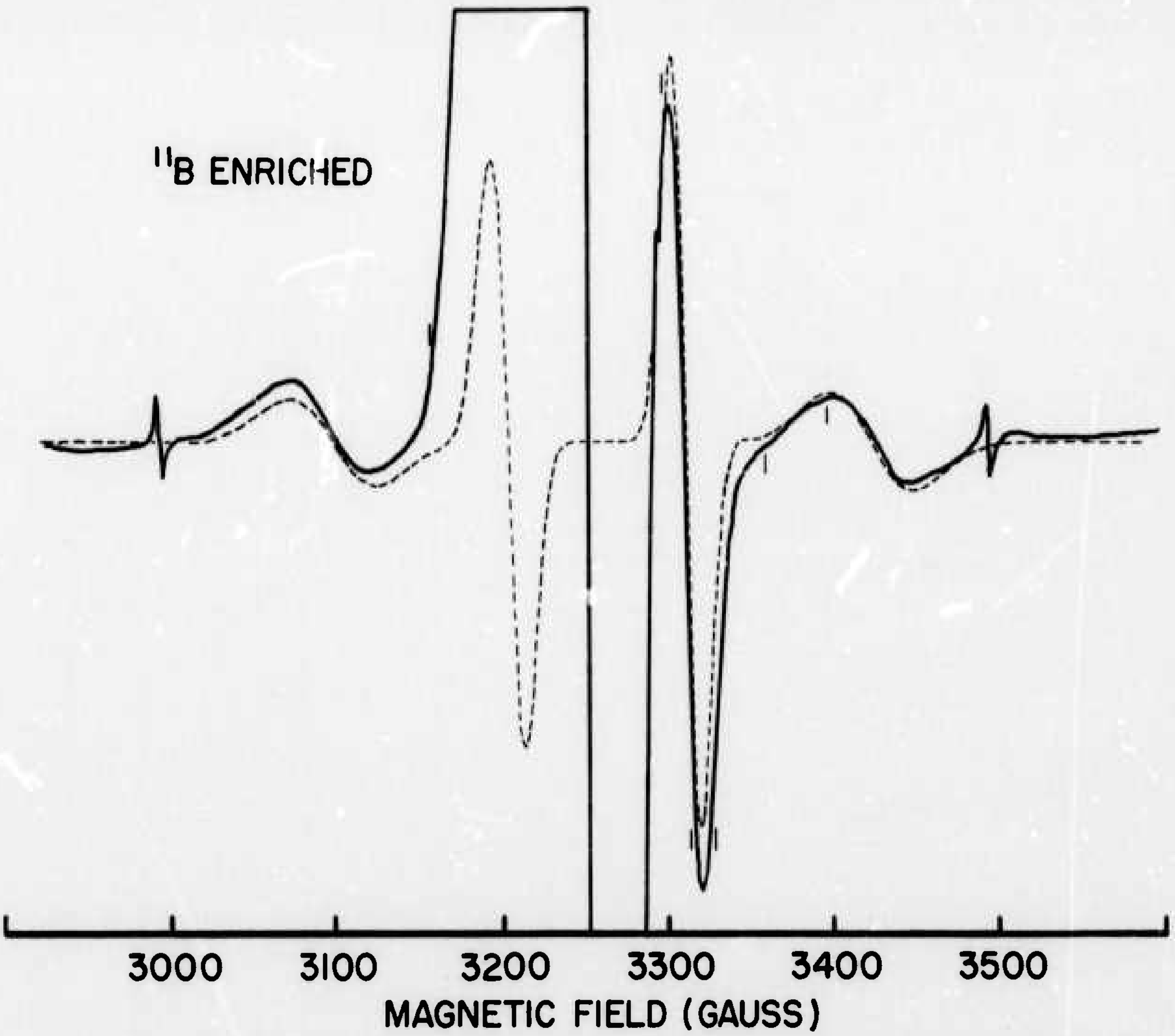

Fig. 10 - X-band ESR spectrum of a 17.7% K_2O-82.3% B_2O_3 glass, enriched to 98.4% ^{11}B, x-irradiated and observed at 77° K. Dashed curve is a computer simulation of the BEC contribution, based on the parameters listed in Table II. (Weak lines split by ~ 500 G are due to atomic hydrogen.)

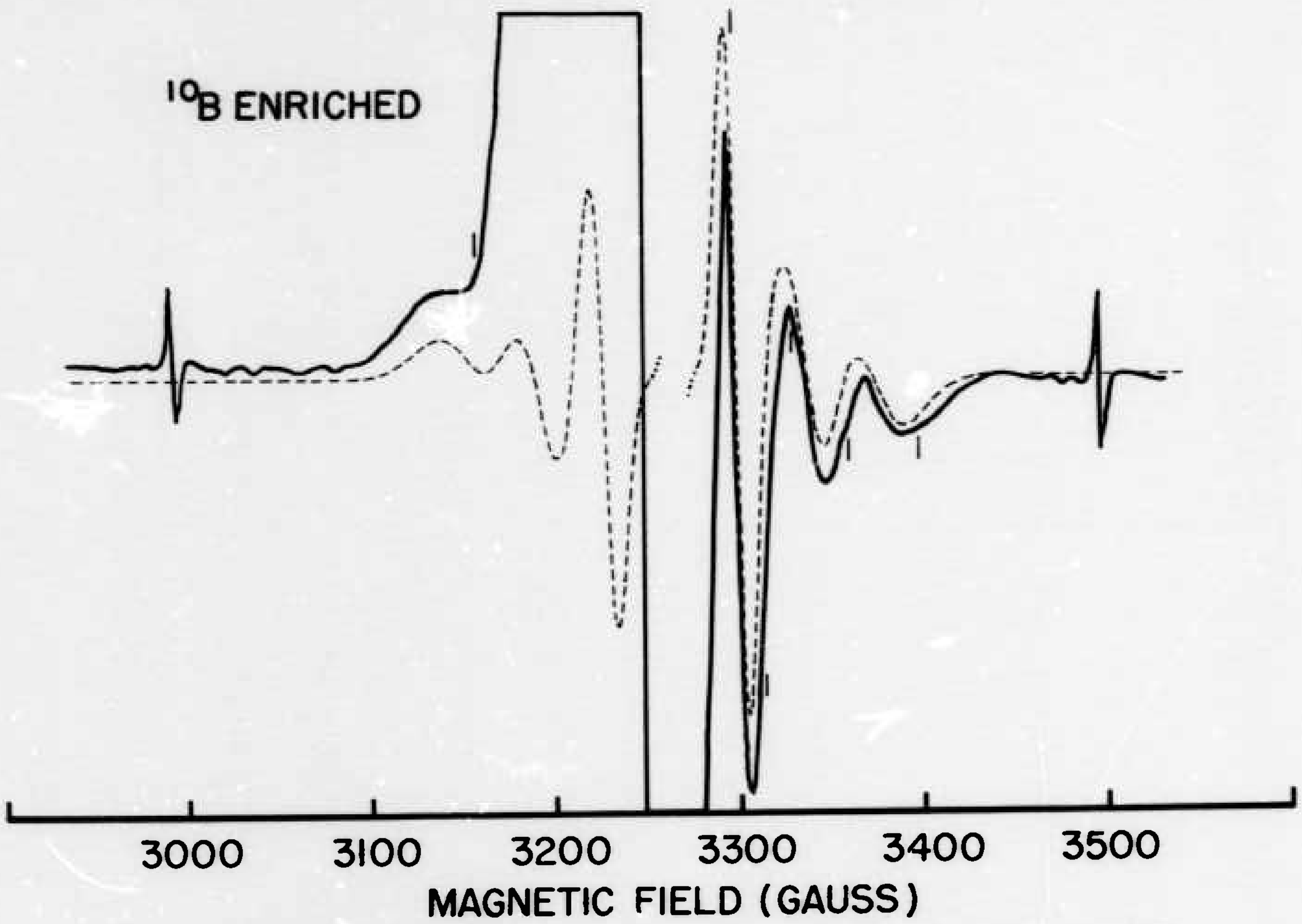

Fig. 11 - X-band ESR spectrum of a 17.7% K_2O-82.3% B_2O_3 glass, enriched to 96.4% ^{10}B, x-irradiated and observed at 77° K. Dashed curve is a computer simulation of the BEC contribution, based on parameters wholly consistent with those used to compute the spectrum of Fig. 10. For simplicity in computation, the central, $m_I = 0$ component was suppressed.

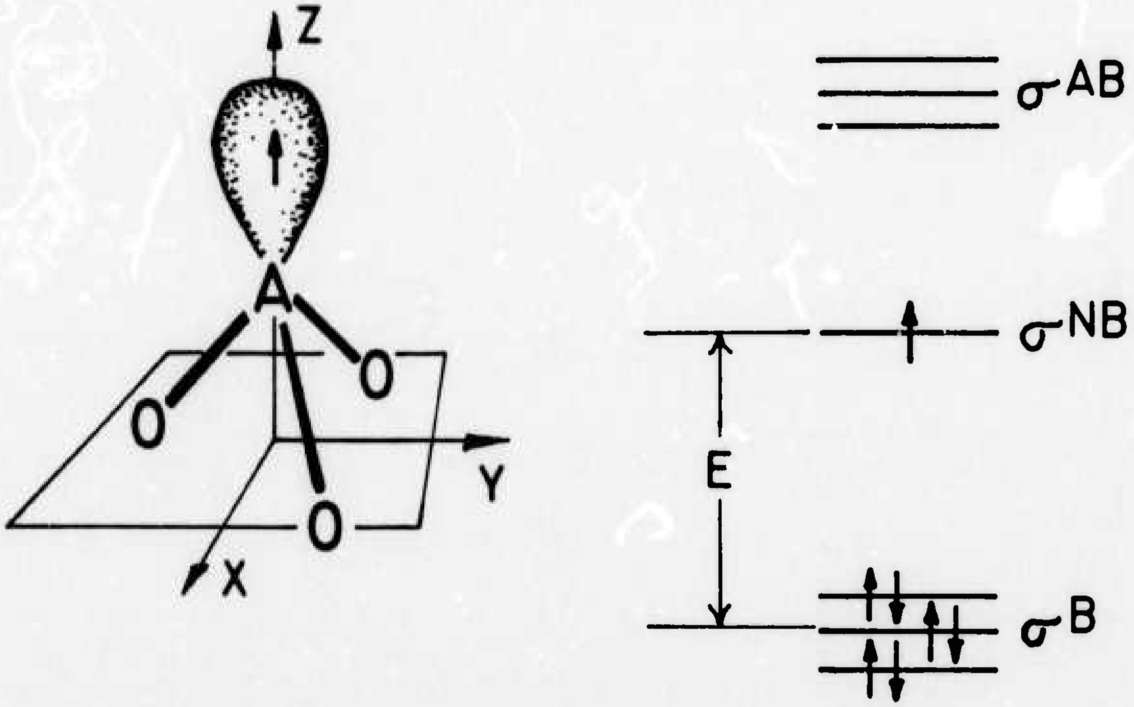

Fig. 12 - Schematic of a dangling-orbital-type trapped-electron center. Left: steric picture. Right: electronic energy levels.

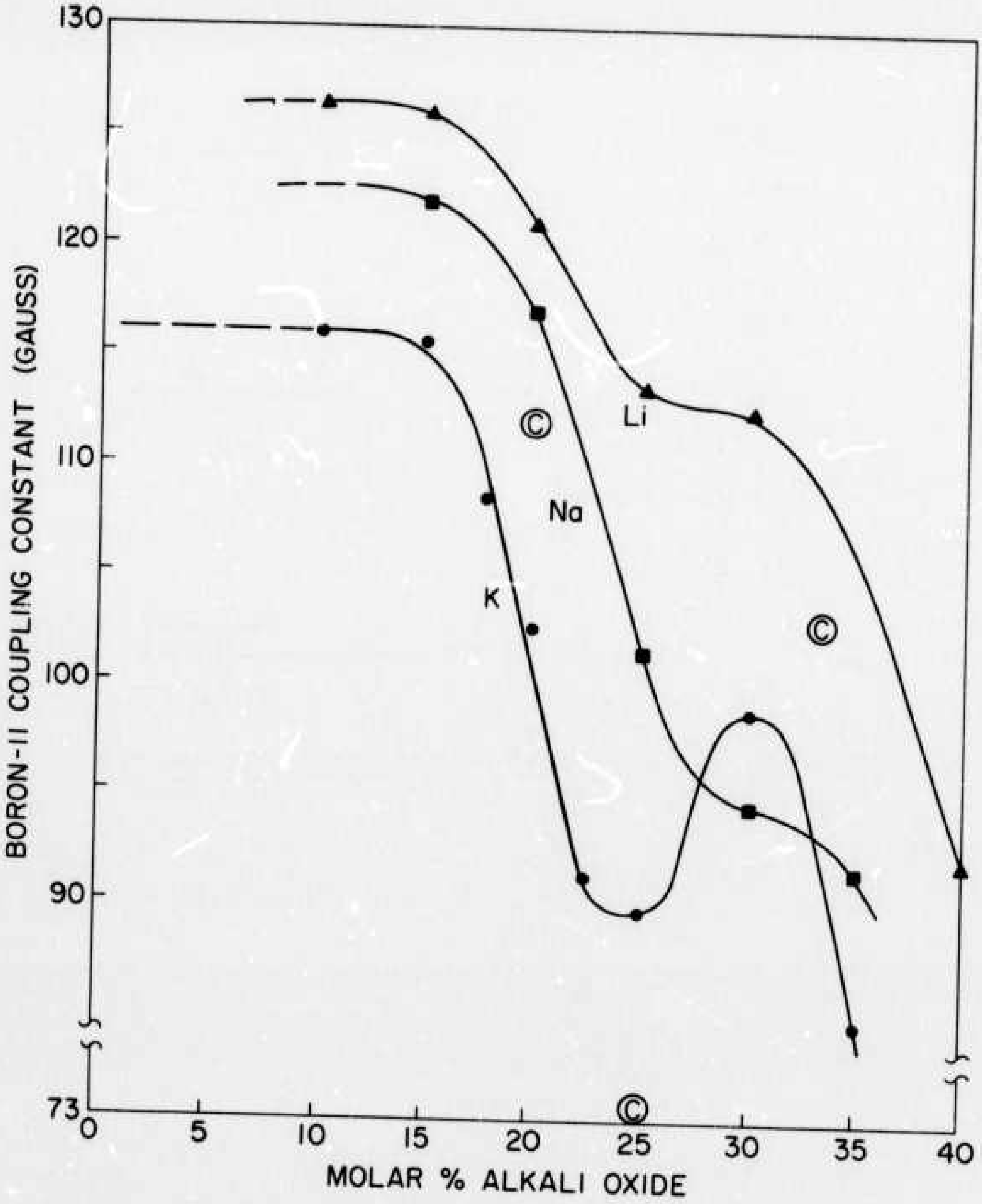

Fig. 13 - Variation of $\langle A_{iso}(^{11}B)\rangle$ with glass composition. Curves pertaining to the BEC in the lithium, sodium, and potassium borate glass systems are indicated by Li, Na, and K. The circles with an inscribed "C" refer to measurements performed on lithium borate polycrystalline compounds. (These data should be treated with certain cautions described in Ref. 23.)

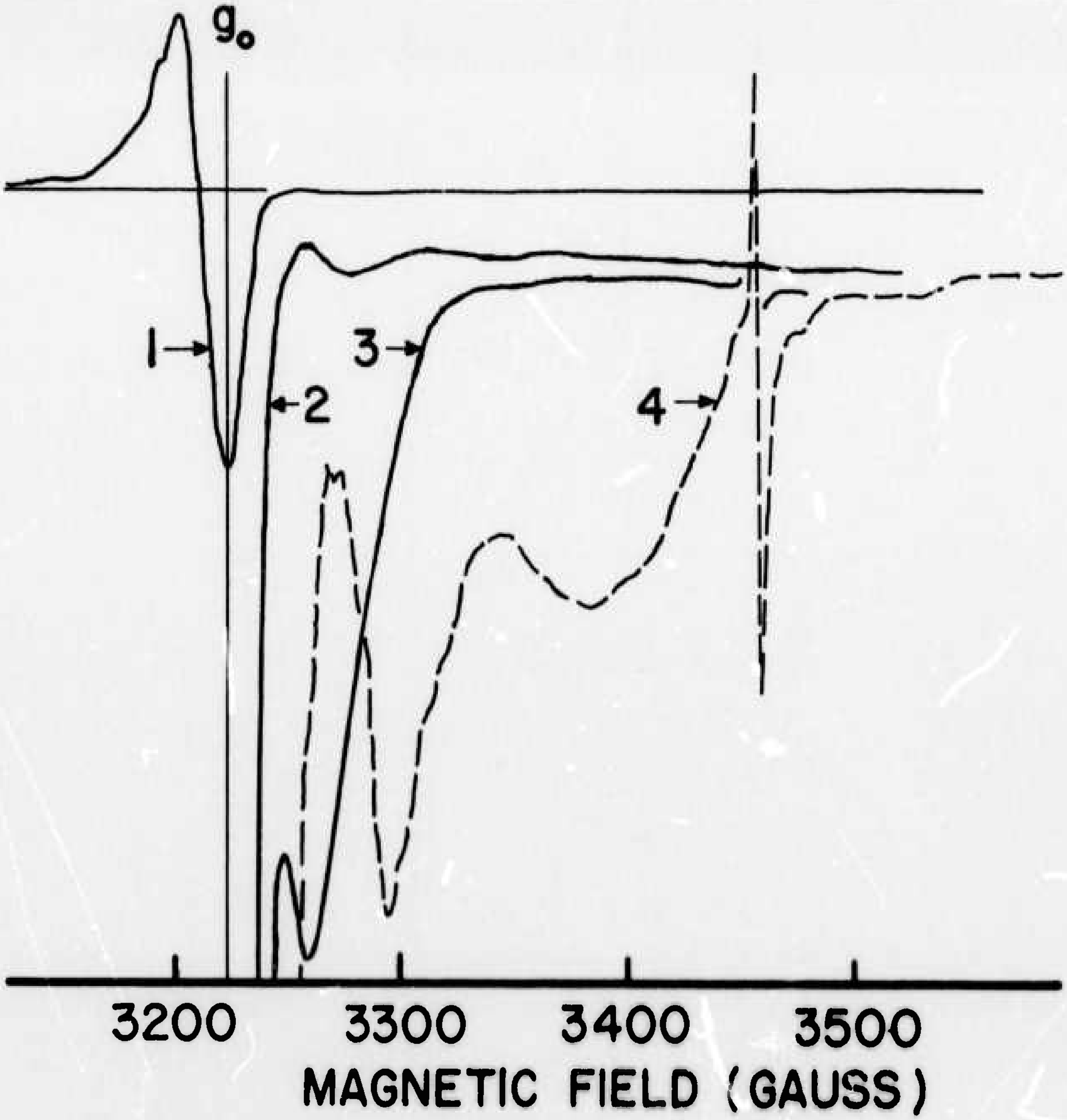

Fig. 14 - X-band ESR spectra of 30% K_2O-70% B_2O_3 (unbroken curves) and 30% Na_2O-70% B_2O_3 (broken curves) glasses following x-irradiation at 77° K. Differences in thermal treatments and spectrometer gains are described in the text. The sharp spike at ~3460G is the high-field member of a doublet due to atomic hydrogen, while part of the undulating character of the dashed curve is due to the boron electron center.

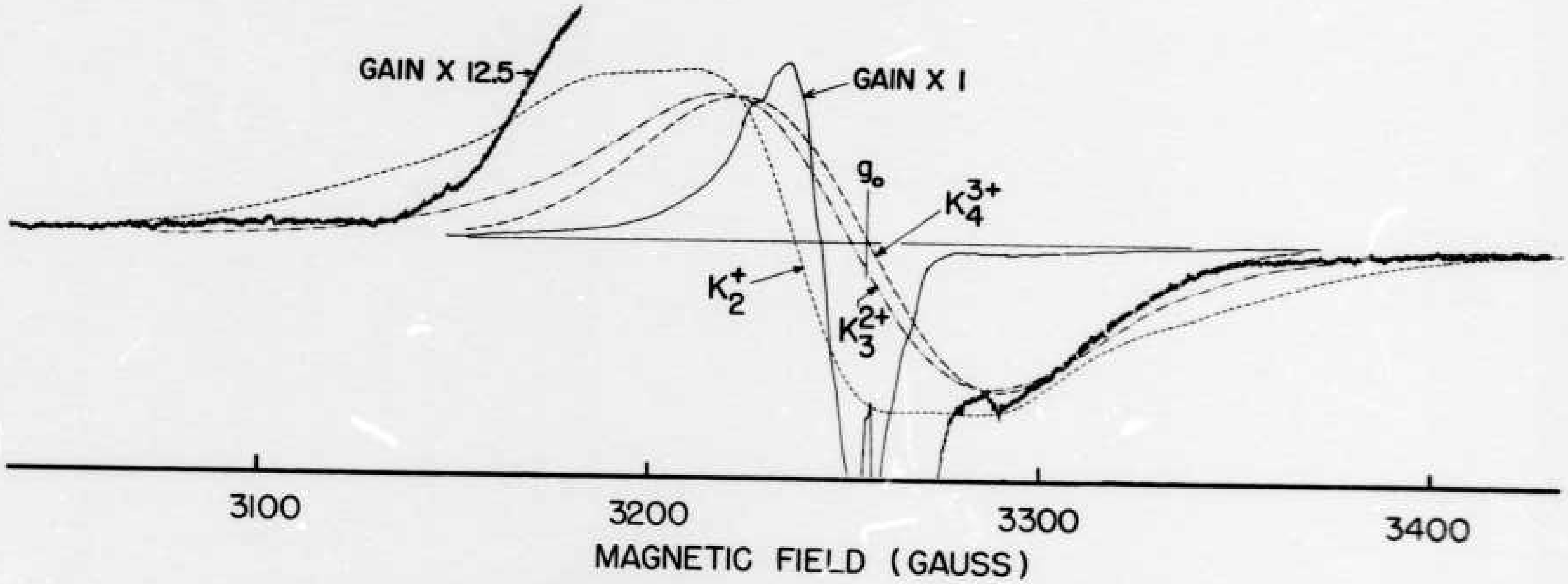

Fig. 15 - X-band ESR spectrum of a 30% K_2O-70% $^{10}B_2O_3$ glass following x-irradiation at 77° K. Dashed curves are computed simulations aimed at fitting the high-field shoulder under the assumptions that 70% of the unpaired spin density is equally distributed among the 4s atomic orbitals of 2, 3, or 4 potassium ions.

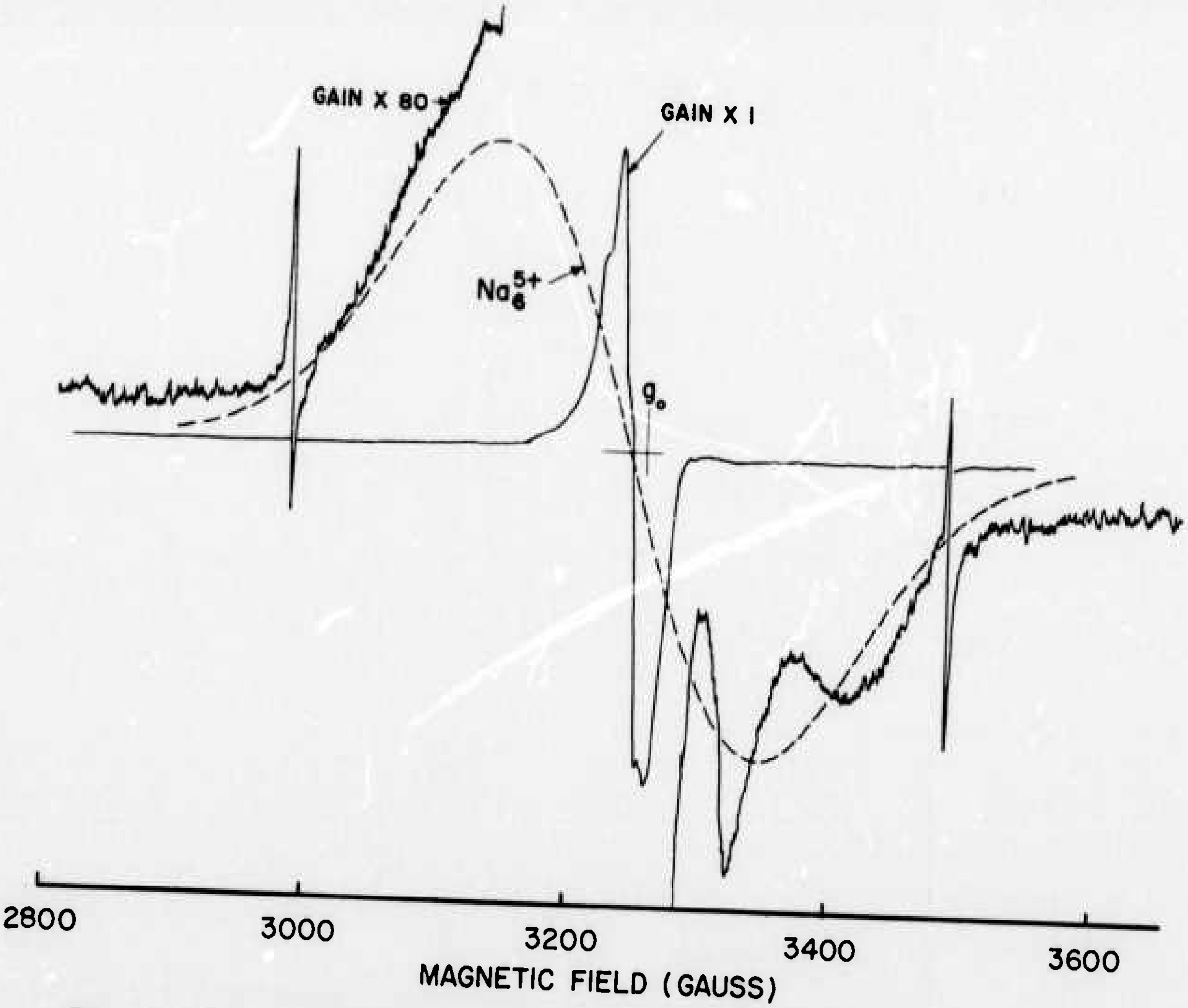

Fig. 16 - X-band ESR spectrum of a 30% Na_2O-70% B_2O_3 glass following x-irradiation at 77° K. Dashed curve is a computer simulation of the broad resonance under the assumption that 70% of the unpaired spin density is equally distributed among the 3s atomic orbitals of 6 sodium ions.

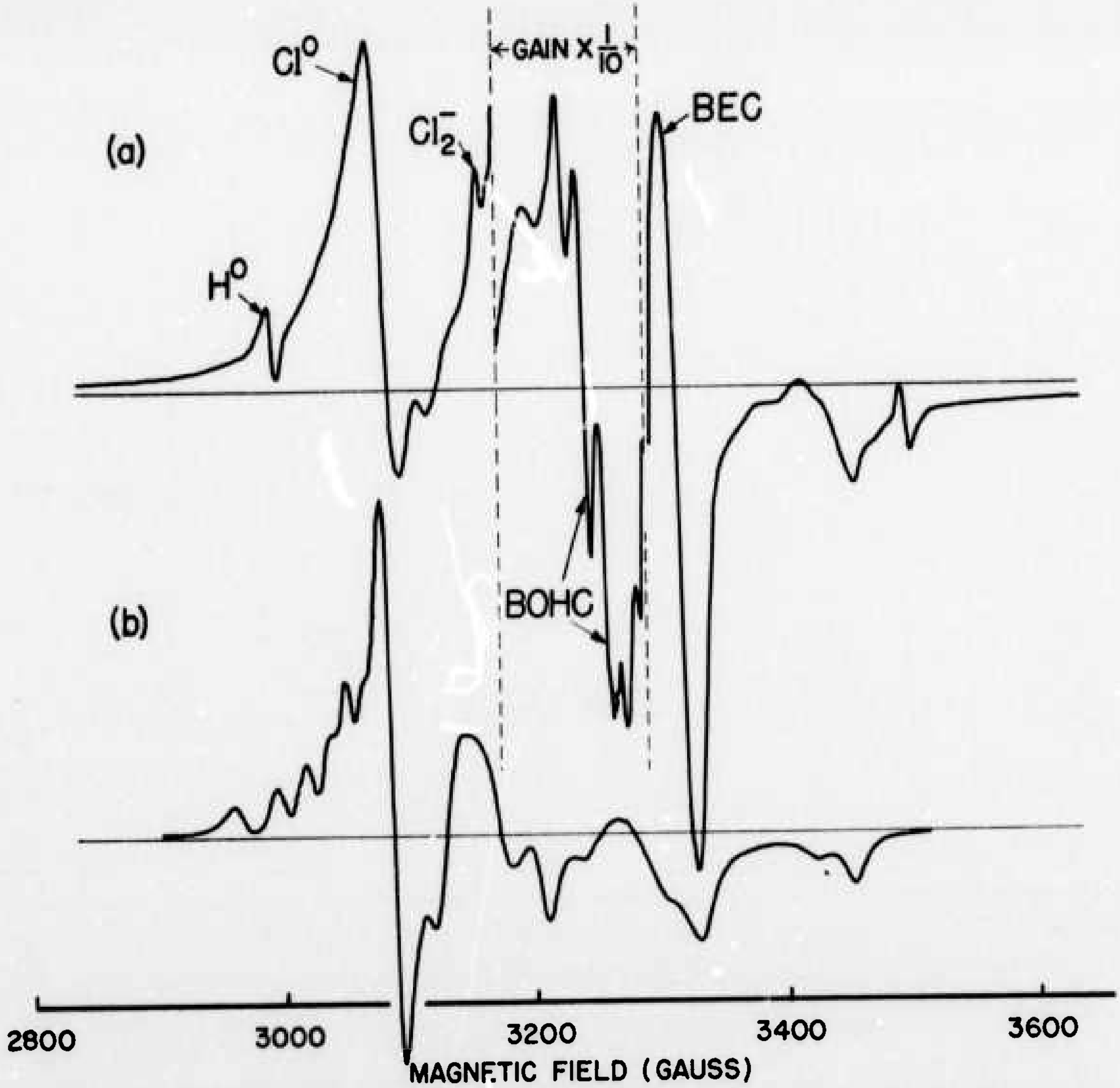

Fig. 17 - (a) X-band ESR spectrum of an 8.3% KCl-12.7% K_2O-79% B_2O_3 glass immediately following x-irradiation at 22° K. (b) A computer simulation of the Cl° contribution to this spectrum.

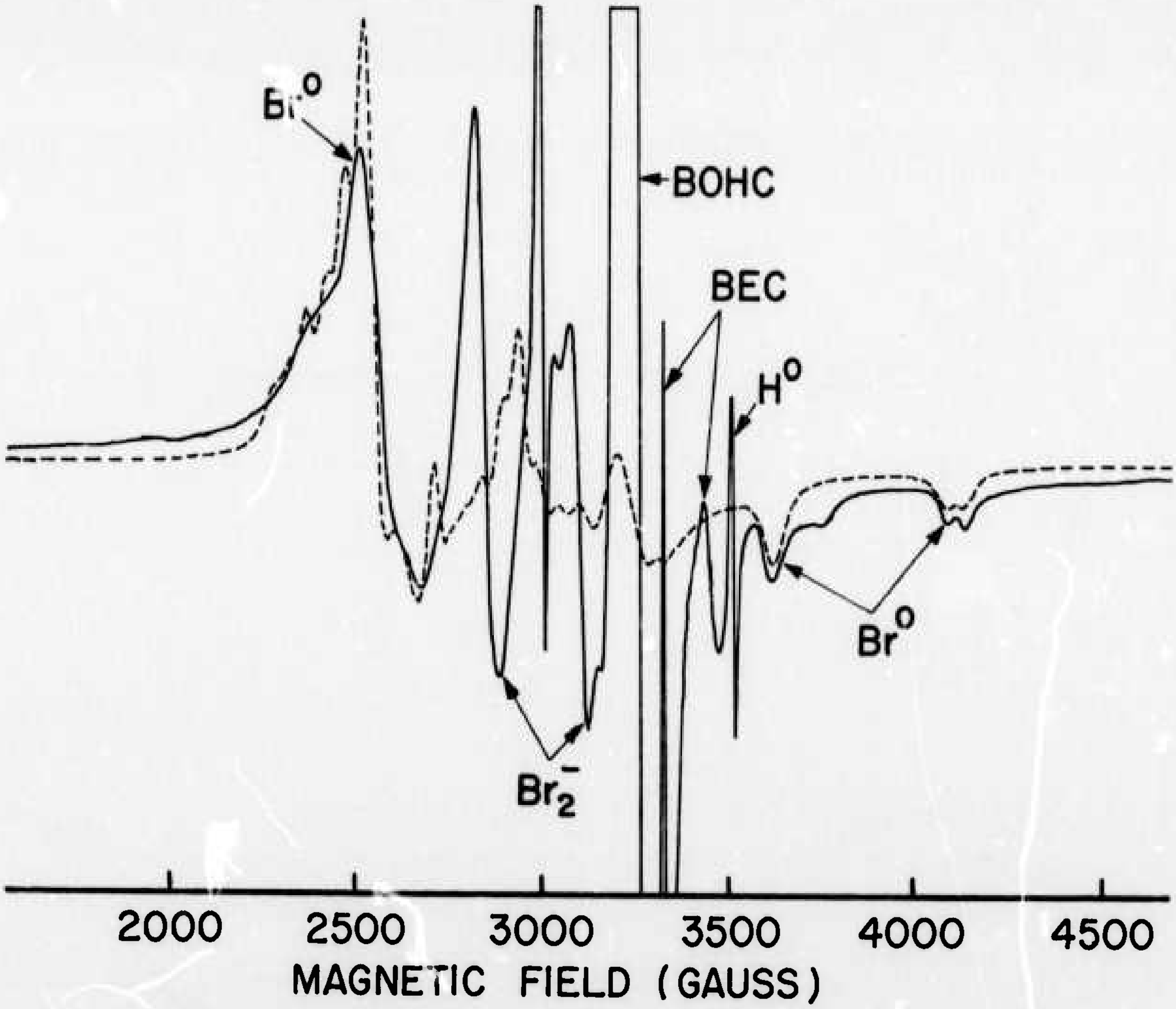

Fig. 18 - X-band ESR spectrum of an 8.3% KBr - 12.7% K_2O - 79% B_2O_3 glass immediately following x-irradiation at 22° K. Dashed curve is a computer simulation of the Br° contribution.

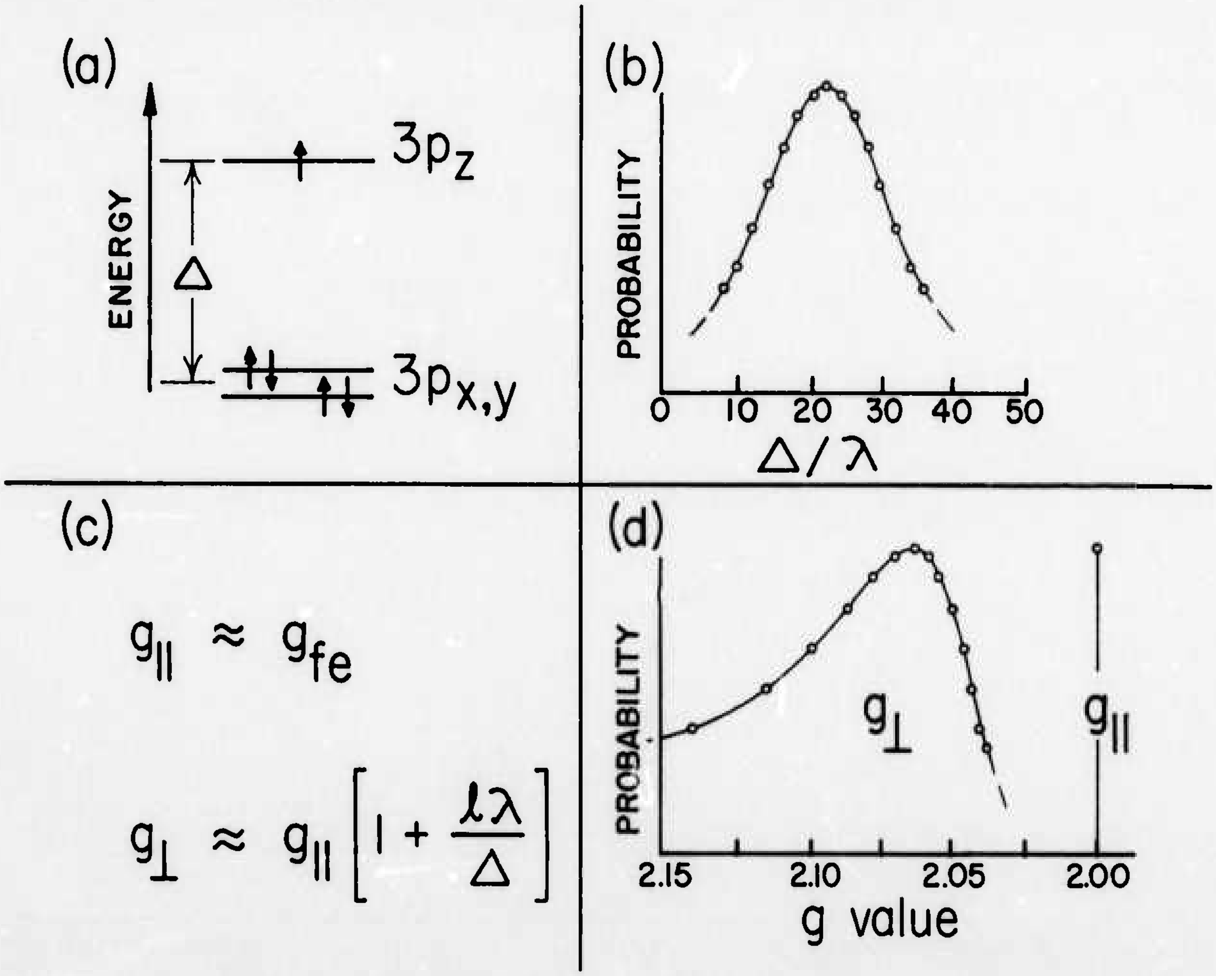

Fig. 19 - (a) Schematic diagram defining the splitting Δ of the $p_x{}^2p_y{}^2p_z{}^1$ ground state of atomic chlorine isolated in a rigid matrix. An environment having nearly axial symmetry about the z axis is assumed. (b) Distribution of Δ values estimated to characterize the ensemble of chlorine atoms contributing to the spectrum of Fig. 17a. (c) First-order expressions for the g values of matrix-isolated halogen atoms, where g_{fe} is the free electron g value, λ is the spin-orbit coupling constant, and ℓ is a constant of the order of unity (determined[12] in this case to be ~0.7). (d) g values and weighting factors ($g_{\perp}$ only) derived from (b) and (c) and used to compute the spectrum of Fig. 17b.

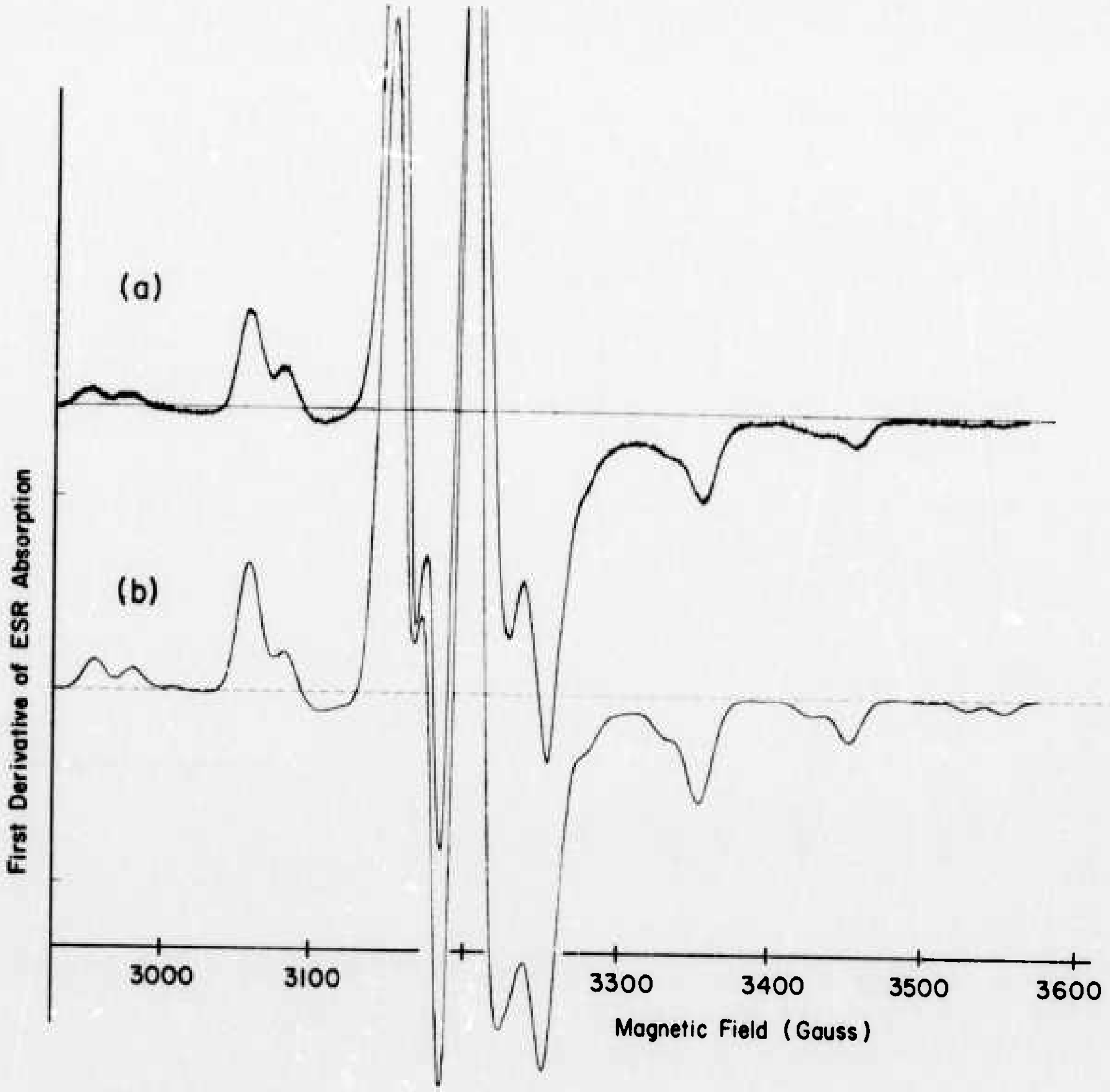

Fig. 20 - X-band ESR spectrum of an irradiated glass prepared from NaCl and B_2O_3.[9] (a) Experimental spectrum. (b) Computed spectrum for Cl_2^- centers.[9]

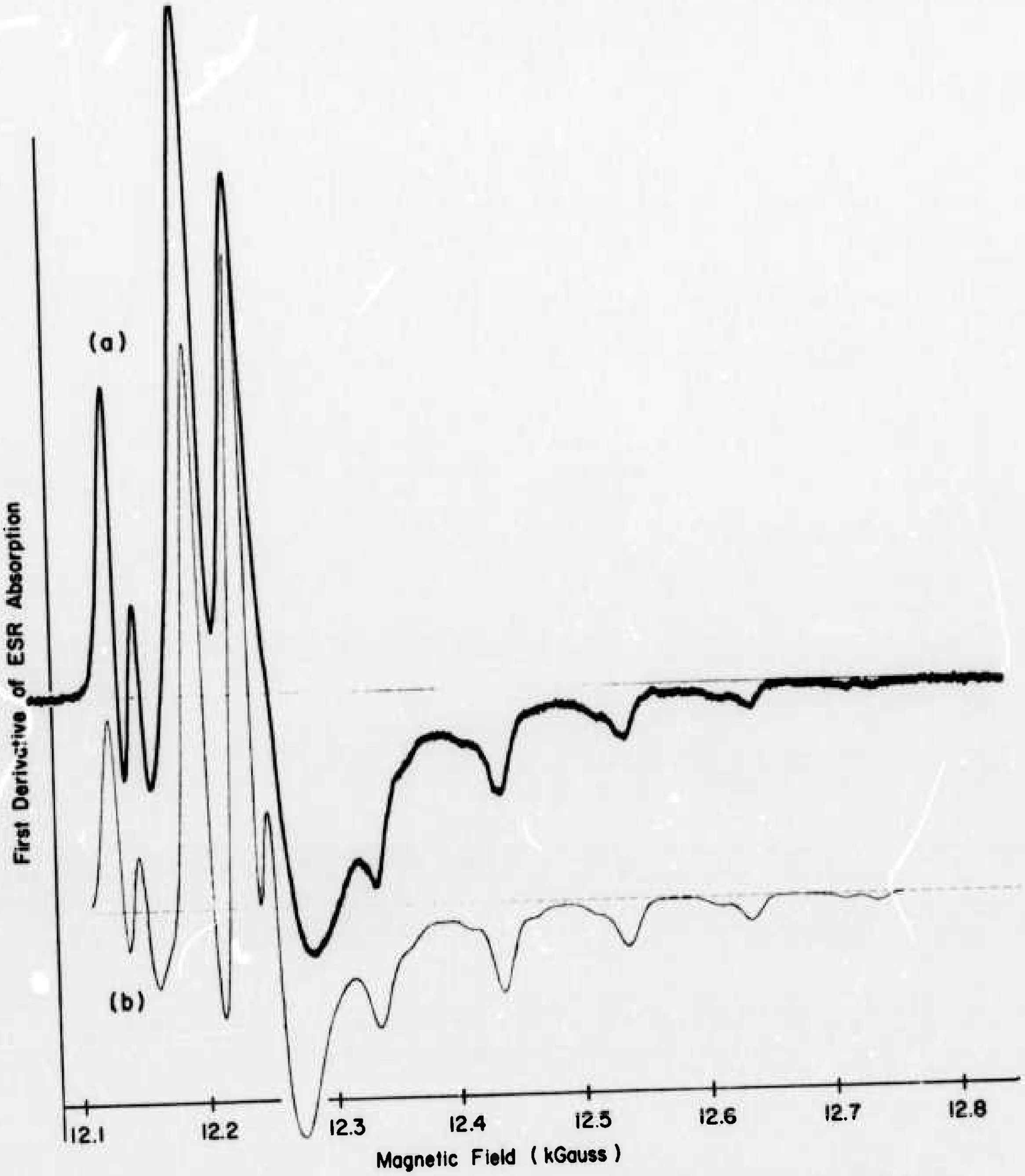

Fig. 21 - Ka-band ESR spectrum of an irradiated glass prepared from KCl and B_2O_3. (a) Experimental spectrum. (b) Computed spectrum for Cl_2^- centers.[9]

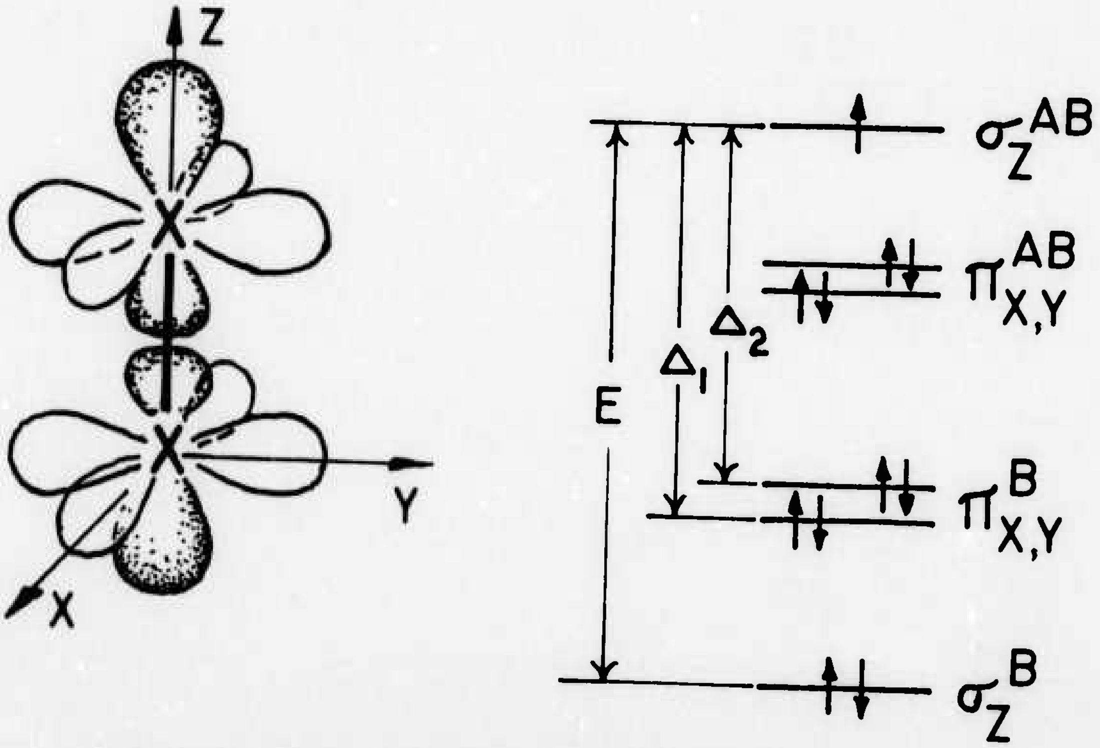

Fig. 22 - Schematic of a hal$_2^-$ molecular ion. Left: steric picture. Right: electronic energy levels. The unpaired spin is located in the σ_z anti-bonding orbital (shaded).

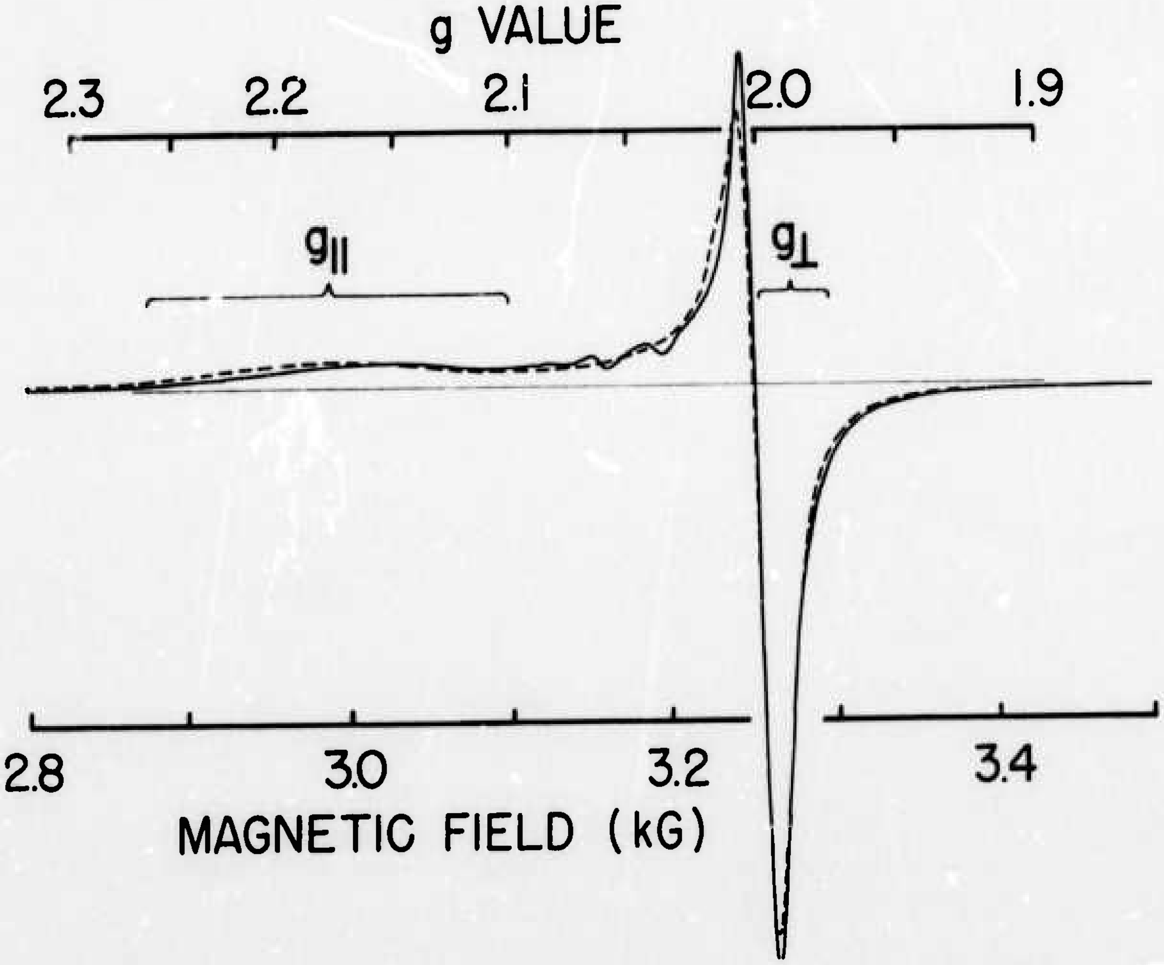

Fig. 23 - ESR spectra obtained at 77° K for amorphous borates. Dashed curve: "amorphized" sodium peroxyborate.[25, 54, 55] Unbroken curve: a quenched, unirradiated glass of nominal composition 70% Na_2O - 30% B_2O_3.[56] Both spectra were obtained at a microwave power level of 100 mW in order to saturate overlapping resonances due to O_3^- in the former case and Cu^{2+} (bumps near 3.2 kG) in the latter. (Due to probable exchange effects, this type of peroxy radical is not itself easily saturable.)[24, 55]

STRUCTURAL AND ELECTRICAL PROPERTIES OF CHALCOGENIDE GLASSES

Structural Properties

P. C. Taylor

S. G. Bishop

D. L. Mitchell

The basic structural properties of vitreous materials remain almost as illusive today as they were before publication of the first X-ray diffraction studies of glasses(1) over four decades ago. Although the coordination numbers of many constituent atoms in glasses can now be determined accurately on the basis of X-ray, electron, and neutron diffraction, nuclear magnetic resonance, and infrared spectroscopy, there is still considerable disagreement over a concept as fundamental as the basic structural unit of any given glass. Is the basic structural unit of vitreous SiO_2 the SiO_4 tetrahedron as suggested by Zachariessen(1) and Warren(2) or is a Trydomite-type unit more appropriate as recently suggested by Konnert and Karle(3)? Is glassy B_2O_3 best represented by an aggregation of BO_3 triangular units(4), by boroxyl groups(2) or by some larger association of boron-oxygen units? The same basic question can be asked concerning the structure of many other glassy materials including the broad class of semiconducting chalcogenide glasses. These glasses, based on the sulfides, selenides, and tellurides of the arsenic group elements, have been the subject of intensive research efforts in recent years related to their possible technological importance. The first half of this review is concerned with the structural properties of selected chalcogenide glasses in both solid and liquid states.

Randomness is of course, fundamental to any description of the structure of glasses. However, the absence of long-range structural periodicity does not preclude the existence of fundamental structural units (local structural order) which may be linked in a random fashion to form the bulk material. The basic questions which arise are how large are these fundamental structural units, are they related to structural units in the crystalline modification, and how are they linked together? Many of the chalcogenide glasses are based on crystalline compounds which have either one-dimensional chain structures or two-dimension layer structures. In such glasses there is perhaps greater hope of unambigiously determining the basic structural units and their relationship to the structure of corresponding crystalline compounds.

In attempting to determine the basic structural properties of glasses three approaches have proved effective. First, the properties of a glass may be compared with its crystalline modification when one exists. Second, the behavior of a glass below the glass transition temperature, T_g, may be compared with its behavior in the liquid phase above T_g and also above the melting point of the corresponding crystalline compound, T_m, when one exists. Third, glasses of different compositions spanning a glass-forming system may be studied, in order to detect changes in physical properties which may be related to structural changes. All three of these approaches have been utilized in the research on the structural properties of chalcogenide glasses described in the present article.

EXPERIMENTAL:

The far infrared studies were performed on a Perkin-Elmer Model 301 grating monochromater and on a Research and Industrial Instruments Corporation interferometric spectrophotometer. Transmission measurements above T_g were made using high temperature cells employing silicon windows(5). Nuclear Magnetic Resonance measurements were performed using a Varian Model 4200 wide line NMR spectrometer in conjunction with a Nicolet Model 1074 signal averager. A gas flow system was used to obtain the high temperature NMR spectra(6). Nuclear quadrupole resonance measurements were obtained with a pulsed NMR spectrometer(7).

RESULTS AND DISCUSSION:

A. Infrared Vibrational Modes in Chalcogenide Glasses

Most chalcogenide glasses display well defined vibrational absorption peaks in their infrared spectra(8-10). In glasses based on layer (two-dimensional) or chain (one-dimensional) structure compounds these peaks are about a factor of ten broader and slightly higher in frequency than those of the corresponding compounds. In addition the lineshapes of these vibrational modes in the glasses are Gaussian and not Lorentzian as observed in crystalline materials. Figure 1 illustrates the Gaussian character of the absorption peaks in two representative glasses, one based on a layer compound (As_2Se_3) and one based on a chain (primarily) compound (Se). Hereafter such glasses will be referred to as layer-type and chain-type. In Figure 1 the natural log of the product of the absorption constant α and the index of refraction n is plotted versus the natural log of the frequency in cm^{-1}. The quantity $n\alpha$ is related to the conductivity, σ in $\Omega^{-1}cm^{-1}$ by the following equation: $n\alpha = 120\pi\sigma$.

Glasses which are entirely tetrahedrally coordinated do not follow the pattern described above. In vitreous SiO_2 the vibrational absorption modes retain the Lorentzian shape (Fig. 1) observed in the various crystalline modifications. In the tetrahedrally coordinated glasses of the system Cd-Ge-As and Cd-Ge-P, no well defined vibrational modes are observed(11).

The Gaussian nature of the vibrational modes in layer and chain-type chalcogenide glasses is a matter subject to some debate. On the basis of reflectivity studies of As_2S_3 and As_2Se_3 and transmission studies of thin evaporated films of As_2Se_3, Lucovsky(12) has interpreted the vibrational modes in these glasses in terms of Lorentzian oscillators with large damping coefficients. However, this interpretation cannot explain the transmission spectra of thicker films (50 - 250 μ)reported by several authors(10,13,14). The situation is summarized for the absorption around 220 cm^{-1} in vitreous As_2Se_3 in Figure 2. In this figure the natural log of the absorption coefficient is plotted versus wave-number. The open circles are the data of Lucovsky on thin evaporated films. The remaining data are due to Taylor, Bishop and Mitchell(10), Zlatkin and Markov(14), and Austin and Garbitt(13). A solid line through the data points indicates the Lorentzian fit obtained by Lucovsky(12) in applying an harmonic oscillator model to the reflectivity spectrum of glassy As_2Se_3. There are two oscillators contributing to the absorption in Fig. 2 centered at 218 and 246 cm^{-1}. The dashed line represents the Gaussian distribution of narrow (small damping constant) Lorentzian oscillators employed by Taylor, Bishop and Mitchell(10,15) in fitting their reflectivity and transmission data. Again, two Gaussian distributions centered at 213 and 252 cm^{-1} have been assumed. It appears that the data can be better accounted for by assuming a Gaussian distribution of

Lorentzian oscillators whose damping coefficients are approximately those of the corresponding modes in the related crystalline compound.

Several parameters of physical significance can be determined by fitting the infrared absorption spectra of chalcogenide glasses. These parameters include the halfwidth at 1/e of the Gaussian line Γ, the contribution to the low frequency dielectric constant $\Delta\epsilon$, the center frequency of the absorption ν_0, and an estimate of the Lorentzian damping coefficient γ. The values of these parameters for several chalcogenide glasses are listed in Table 1.

One will note that the differences between the Lorentzian and Gaussian interpretations are not merely academic. For example, the central frequencies of the two As_2Se_3 lines of Figure 1 are 213 and 252cm^{-1} in the Gaussian fitting and 218 and 246 cm^{-1} in the Lorentzian scheme. In addition, the contributions to the dielectric constant are substantially different for the two interpretations(10,12).

The physical significance of the Gaussian halfwidth remains an open question. The most plausible explanation is that the removal of translational symmetry allows internal electric fields to develop in glasses composed of chains or layers with anisotropic polarizabilities. In a simple classical picture, these internal electric fields create an ensemble of force constants which in general would be stiffer than the force constants in the structurally periodic case (Lyddane-Sachs-Teller effect(16)). The slight shift to higher frequency of the vibrational modes in glasses is in agreement with the predictions of the model.

The increase in width and shift to slightly higher frequency of the vibrational modes in As_2S_3 and As_2Se_3 glasses with respect to the modes in the crystalline phases is evident in Figure 3. Figure 3a shows the reflectivity spectra of crystalline As_2S_3 (orpiment) in the two in-plane and one out-of-plane polarizations(17) compared to glassy As_2S_3(12). Figure 3b shows the corresponding spectra for crystalline(18) and glassy(10) As_2Se_3 where the out-of-plane polarization spectrum for the crystal has not yet been measured. In analogy to the As_2S_3 results one would expect an out-of-plane mode occurring in crystalline As_2Se_3 at about 275 cm^{-1}. One will note from this figure that the out-of-plane crystalline mode is strongly suppressed in the glassy phase, if it is present at all.

The vibrational absorption spectra of glassy As_2S_3 and As_2Se_3 are very similar. In fact a simple scaling relation exists between the central frequencies of the vibrational peaks in these two materials. This fact is not entirely surprising because the two crystalline compounds are isomorphic. An harmonic oscillator model provides a simple explanation of the scaling relation between glassy As_2S_3 and As_2Se_3. In the harmonic oscillator approximation the frequency of a vibrational mode is proportional to $\sqrt{k/\mu}$ where k is an effective force constant and μ a reduced mass. If the force constants in As_2S_3 and As_2Se_3 are nearly identical, then the frequencies will scale as $\mu^{-1/2}$ in these two materials. In this fashion, one predicts $\nu_o(As_2Se_3)/\nu_o(As_2S_3) = 0.8$ while the experimental value is ~ 0.7.

The structure of crystalline As_2Te_3 consists of puckered layers or ribbons and is not isomorphic with As_2S_3 and As_2Se_3(19). Glassy As_2Te_3 can be formed in the bulk only by rapid quenching techniques(20), and the glass crystallizes easily on polishing or heating. However, glasses in the range of compositions As_xTe_{1-x} $(0.45 < x < 0.55)$ can be formed in bulk and are relatively stable. The infrared spectra of As_xTe_{1-x} glasses are essentially independent of x and surprisingly similar to those of As_2S_3 and As_2Se_3(21). Figure 4 compares the vibrational peaks in $As_{55}Te_{45}$ with those in As_2Se_3. The peaks in $As_{55}Se_{45}$ are generally shifted to lower frequency and the two peaks near 200 cm^{-1} are better resolved. Using the same scaling relation as developed above for As_2S_3 and As_2Se_3, one obtains $\nu_o(As_{55}Te_{45})/\nu_o(As_2Se_3) = 0.75$ while the experimental value is ~ 0.8. The applicability of the simple scaling hypothesis to the As_xTe_{1-x} glasses is remarkable, and suggests that the structure of these glasses resembles more the layers of As_2S_3 and As_2Se_3 than the ribbons of As_2Te_3. This conclusion may partially explain the difficulty in forming glassy As_2Te_3.

The compositional dependence of the vibrational modes in several chalcogenide glass systems has also provided some useful structural information. In the $As_2S_xSe_{3-x}$ system, a single vibrational mode is observed for the end compositions, As_2S_3 and As_2Se_3, and two modes with unshifted frequencies are observed for all intervening compositions(22). The intensities of these two modes are proportional to the amount of end constituent (As_2S_3 or As_2Se_3) present in the mixed glass. In the more complicated system $Tl_2Se_xTe_{1-x}As_2Se_yTe_{3-y}$ two vibrational modes are present in all glasses and shift to lower frequencies with increasing Te content(8). In the all-Se glass of this system $(x = 0, y = 3)$ the two features appear at 213 and 255 cm^{-1}(See Table I).

In mixed crystalline chalcogenide alloy systems, the vibrational peaks follow one of two characteristic modes of behavior(23). They either remain constant in frequency and change in intensity, or they remain essentially constant in intensity and gradually shift in frequency. Mixed vitreous systems also exhibit one of these two modes of behavior. The $As_2Se_xS_{3-x}$ glass system shows the first mode of behavior while the $Tl_2Se_xTe_{1-x}As_2Se_yTe_{3-y}$ glass system displays the second. Which mode a system obeys depends on the band structure and vibrational dispersion characteristics of the end compositions(24). A necessary condition for the first mode of behavior is the occurrence of an effective energy gap in the phonon dispersion curves of the end constituent with the lighter mass (i.e., As_2S_3 in the $As_2Se_xS_{3-x}$ system). Thus knowledge of the compositional dependence of the vibrational modes can in principal yield information about the band structure of chalcogenide glasses.

B. Temperature Dependence of Vibrational Modes

The vibrational modes in layer- and chain-type chalcogenide glasses exist essentially unchanged in the molten phase not only above the glass transition temperature, T_g, but also above the melting point of the crystalline phase, T_m, when one exists(5,10) The vibrational absorption spectrum for glassy As_2Se_3 is displayed in Fig. 5 at several different temperatures. The strongest peak at 217 cm^{-1}, which is actually a superposition of two Gaussian peaks as described above, is unchanged from 4^oK up to 673^oK. The values of T_g and T_m for As_2Se_3 are 460 and 633^oK, respectively.

In glassy $Tl_2SeAs_2Te_3$ the vibrational modes also exist unchanged well into the liquid phase. However, in this material there exists a temperature T_s above which the vibrational modes abruptly disappear(5) ($T_s = 480^oK$, $T_g = 359^oK$). The disappearance of the vibrational modes at T_s indicates that there is an abrupt change in the local structural order at this temperature in glassy $Tl_2SeAs_2Te_3$ which should be reflected in other experimental measurements such as specific heat and X-ray or neutron diffraction.

There is an abrupt change in the slope of the viscosity curve ($\ln\eta$ vs. $1/T$) in many chalcogenide glasses near $\eta = 1000$ poise(25). This break in viscosity is attributed to a change in bonding configuration because there are distinctly different activation energies for dissociation above and below the abrupt change in slope(25). The temperature T_s for glassy $Tl_2SeAs_2Te_3$ occurs very near this break in viscosity, and the two phenomena may very well be related. If there is indeed a relation between the change in the dissociation energy and the change in local structure order, then one would predict a disappearance of the characteristic vibrational modes in many chalcogenide glasses at elevated temperatures. In particular, from viscosity measurements(5,20) one would anticipate the temperature T_s to occur near 725°K for liquid As_2Se_3 although no measurements have as yet been made near this temperature.

Many of the infrared results discussed above suggest that remnants of the layer or chain structures of specific chalcogenide compounds are retained in the corresponding glasses and that these vitreous materials are not well described by a three dimensional random network model as has been suggested(12,26). Suppression of only the out-of-plane vibrational mode in glassy As_2S_3 suggests the presence of warped layers in this material. The shift of vibrational modes to higher frequencies in As_2S_3 and As_2Se_3 glasses is consistent with the assumption of locally anisotropic polarizabilities which could result only from the presence of layers and not from an isotropic random network. Retention of the vibrational modes above the crystalline melting point T_m in As_2Se_3 suggests that remnants of layers are even present in the liquid phase but may well disappear abruptly at some elevated temperature as one could infer from the abrupt disappearance of the vibrational modes in liquid $Tl_2SeAs_2Te_3$ at T_s.

Several additional experimental results lend support to the layer and chain hypothesis. The structures of Vitreous S and Se have long been described as mixtures of rings and chains(27). Layers(28) and chains(29) have also been invoked to explain the low glass transition temperature of many chalcogenide glasses. According to this interpretation the abrupt change in viscosity at T_g is due to the breaking of the weak van der Waals forces between chains or layers while the change in slope of the $\ln\eta$ vs. $1/T$ plot below $\eta = 10^3$ poise is attributed to the break-up of the layers themselves(25,28,29). Optical properties of glassy As_2S_3 and As_2Se_3 in the 1 - 14 eV range show that the effect of disorder on the electronic structure is very slight and again support the existence of layer segments in these glasses(30,31). X-ray(32) and neutron(33) diffraction studies have been interpreted as indicating that the local structure of As_2Se_3 glass looks very much like crystalline, layered As_2Se_3 out to at least 20Å. As will be seen in the following section nuclear magnetic resonance (NMR) results in both the glassy and liquid phases also support the presence of layers and chains in many chalcogenide glasses.

C. Nuclear Magnetic Resonance in Chalcogenide Glasses

Early investigations of the extent of glass-forming regions in glass systems containing As-S or As-Se and a third element showed that particularly large regions exist for the addition of Tl(34). The thallium nuclei are particularly well-suited for nuclear magnetic resonance studies, and the existence of As-Se-Tl glasses over large ranges of compositions makes it possible to apply NMR techniques to the study of local bonding configurations in these materials. NMR spectra provide information concerning short range (primarily nearest-neighbor) structural configurations, and in contrast to X-ray diffraction spectroscopy, the NMR technique is not hampered by the absence of long range structural periodicity in glasses and liquids. There are two resonant isotopes of thallium, Tl^{203} and Tl^{205}, both with spin $I = 1/2$. Because of the large nuclear charge, the NMR spectra of Tl^{203} and Tl^{205} exhibit large chemical shift effects which serve as a sensitive measure of the relative covalency or ionicity of the thallium chemical bonds. Spectra of only the more abundant Tl^{205} nuclei need be considered here. NMR studies of Tl^{205} in the glass system Tl-As-Se provide direct evidence both of strong covalent bonding of Thallium in the glass network and of preservation of the local order well into the liquid state.

One component of the chemical shift arises because the resonant nucleus Tl^{205} is affected not only by the externally applied magnetic field but also by the local magnetic field produced at the nuclear site by the diamagnetic response of the orbital electrons to the applied field. The second component of the chemical shift is a second order paramagnetic contribution which arises from the interaction of the applied field with excited paramagnetic states of the free ion mixed into the ground state by the electrostatic interaction with neighboring ions. It is this paramagnetic contribution to the chemical shift which provides a measure of the relative covalency of the Tl chemical bonds. Tl^{205} chemical shifts were measured relative to the resonance position of Tl^{205} in a 2.5 molar solution of Thallium acetate in water(35).

Measured values of the isotropic chemical shift ($|\Delta H|/H$) are plotted in Fig. 6 for seven glasses in the pseudo-binary system $(Tl_2Se)_x(As_2Se_3)_{1-x}$ with x ranging from 0.1 to 0.67. Two facts are evident from this figure. First, the large paramagnetic chemical shift of Tl^{205} in all glasses of the system indicates that the thallium atoms are strongly covalently bonded to the network. Second, the abrupt change in the magnitude of the chemical shift at $x = 0.3$ indicates that the thallium atoms are undergoing an abrupt change in local environment near this composition. The thallium sites in glasses with $x \lesssim 0.3$ are somewhat less covalent than those for $x \gtrsim 0.3$.

Additional evidence for identifying the chemical shifts for $x \lesssim 0.3$ as somewhat less covalent is provided by a comparison with chemical shifts measured in thallium halides. In largely covalent thallic chloride ($TlCl_3$) the chemical shift is nearly identical with that observed in the $(Tl_2Se)_x(As_2Se_3)_{1-x}$ glasses with $x>0.3$. In ionic thallous chloride (TlCl) the absolute value of the chemical shift is only slightly less than that in the glasses for $x<0.3$. One might conjecture from these comparisons that the thallium atoms enter the glass as Tl^{+1} ions for low thallium content ($x<0.3$) and as Tl^{3+} ions for high thallium content ($x>0.3$).

The observed change in thallium chemical bonding near $x = 0.3$ is reflected in at least one other physical property. Data do to Flaschen et al.(36) on the temperatures at which the viscosity of glasses in this system reach 30 poise (30 poise points) also show a distinct drop above $x \sim 0.3$. The data are not detailed enough to determine how abrupt this change in 30 poise temperatures is, but the implication is that the depression of the melt viscosity for $x>0.3$ is associated with the occurrence of Tl^{3+} - like bonding configurations in this composition range.

Se^{77} and Te^{125} nuclei can also be observed by NMR in chalcogenide glasses although their responses are much weaker than the Tl^{205} signal(37,38). The two Se^{77} lines in Fig. 7 represent 48 hours of signal averaging(38). The chemical shift is again useful in distinguishing between Se or Te bonding configurations(38). In solid glassy selenium the NMR spectrum is paramagnetically shifted (lower magnetic field) relative to that of Se in glassy As_2Se_3 as indicated in Fig. 7. The substantial difference between the isotropic chemical shifts of the Se^{77} NMR in glassy Se and As_2Se_3 should make it possible to distinguish between Se-Se and As-Se bonds in mixed glass systems containing As and Se.

D. Temperature Dependence of NMR Spectra

Tl^{205} NMR in vitreous $Tl_2SeAs_2Se_3$(6), $(Tl_2Se)0.2(As_2Se_3)_{0.8}$ and $Tl_2SeAs_2Te_3$(39), and Se^{77} NMR in glassy Se and As_2Se_3(37,38), have been studied well into the liquid phases. In all of the layer-type materials (i.e. excluding Se) there is no apparent change in the lineshape or the chemical shift on passing through T_g. These results indicate that the nearest neighbor environments of the thallium or selenium nuclei, including the covalencies of the bonds, are unaltered on passing into the liquid phase.

NMR results for Se^{77} in Se glass above T_g indicate that the behavior of molten chain-type glasses is markedly different from the layer-type materials. The Se^{77} NMR line is observed to motionally narrow in liquid Se in sharp contrast to the unchanged Se^{77} lineshape observed in liquid As_2Se_3. The observation of the motional narrowing of the NMR spectrum in liquid selenium means that the spectral broadening caused by the site-to-site variation in the chemical shift interaction in solid glassy Se has been averaged essentially to zero by the atomic motion or reorientation in the melt. The occurance of motional narrowing implies that, in addition to the breaking of weak interchain bonds, the intrachain bonding configurations are being disrupted with correlation times on the order of 10^{-7} to 5×10^{-5} (37)sec. Because the Se^{77} NMR line is unnarrowed in As_2Se_3 at temperatures up to 400°C, the correlation times for local bonding configurations are greater than 10^{-5} seconds up to at least 400°C. At 400°C the viscosity of As_2Se_3 is equivalent to that of Se at 220°C. Thus there are substantially different correlation times or atomic reorientation rates in layer-type and chain-type chalcogenide liquids even when the (macroscopic) viscosities are equivalent.

The intensity of the motionally narrowed Se^{77} NMR line in molten selenium is shown in Fig. 8 where T_m represents the melting temperature of trigonal selenium (217°C). Above T_m all of the spins are contributing to the narrow Se^{77} NMR line, but below this temperature the intensity decreases monatonically. It is inferred that the missing intensity at temperatures below 220°C is transferred to a broad line characteristic of the static situation which occurs in the solid glass. This broad line is unobservable in the measurement configuration used to study the narrow line at elevated temperatures. The gradual transfer of intensity from a broad to a narrow line with increasing temperatures is characteristic of a nuclear spin system described by a distribution of correlation times(40). The solid line of Fig. 8 is a fit to the data assuming a log normal distribution of correlation times(38). At 220°C the median correlation time obtained from this fit is 5×10^{-5} sec.

E. Nuclear Quadrupole Resonance in Chalcogenide Glasses

The recent observation of As^{75} pulsed nuclear quadrupole resonance (NQR) is vitreous As_2Se_3(7) has provided an additional tool for studying the local bonding properties of semiconducting chalcogenide glasses. In addition to the many As-containing chalcogenide glasses, those glasses containing Sb should also be good candidates for study using pulsed NQR techniques.

In crystalline As_2S_3 (orpiment) two narrow (~ 50 kHz half width) As^{75} pulsed NQR lines are observed near 70 MHz. In glassy As_2S_3 at 4.2°K one extremely broad line (3.5 MHz) is observed near 70 MHz. From the width and position of this broad line compared to the two narrow crystal lines, one may calculate the deviations in local bonding configurations surrounding the As sites in this glass. Specifically, each As atom is bonded to three sulfur atoms in a pyramidal configuration and the As^{75} NQR results demonstrate that these pyramidal units are very well preserved in the glass. The average deviation of pyramidal apex bond angles (S-As-S bond angles) is less than 2^o in glassy As_2S_3 and less than 4^o in glassy As_2Se_3. In addition to these structural implications, the NQR experiments also provide a useful probe of the low frequency phonon modes in glasses(7,41).

Although magnetic resonance (NMR and NQR) studies of chalcogenide glasses generally probe only nearest neighboring interactions, they lend support to the hypothesis that remnants of the layer or chain structures of specific chalcogenide compounds are retained in the glassy state. The different characteristic motions occuring in molten Se and As_2Se_3 at equivalent viscosity attest to a difference in the dimensionality of the long range order in these two glasses. Well defined pyramidal units in As_2S_3 and As_2Se_3 are partial confirmation of the x-ray and neutron diffraction results which indicate that the local order in these glasses is very similar to that of the associated layered crystalline compounds.

ELECTRICAL PROPERTIES

The conductivity spectra of chalcogenide glasses generally exhibit four distinct regions in the frequency range from dc to the optical band edge. In order of increasing frequency, beginning at dc, they are: Region I in which the conductivity is frequency independent and thermally activated with an activation energy (in some temperature range) approximately equal to one-half the optical energy gap; Region II in which the conductivity increases monotonically with frequency and is relatively temperature insensitive (in most cases the frequency dependence is approximated by a power law with the exponent $s \leq 1$): Region III in which the conductivity exhibits sharp vibrational absorption bands; Region IV in which the conductivity has approximately the same frequency and temperature dependences as in Region I but is larger in magnitude by a multiplicative factor β ; and Region V in which the conductivity again increases monotonically due to band edge absorption.

These regions are illustrated in Fig. 9 for the well-studied low conductivity glass (As_2Se_3) and a high conductivity glass ($Tl_2SeAs_2Te_3$). For convenience, the vertical scale in Fig. 1 is labeled in both conductivity units (σ in Ω^{-1} cm^{-1}) and optical absorption units ($n\alpha$ in cm^{-1} where n is the index of refraction and α is the absorption coefficient in cm^{-1}).

Extensive experimental studies of the conductivity of chalcogenide glasses have been carried out in the microwave and infrared (10^9 to 10^{13} Hz). The results of these studies will only be summarized in this review. The restriction to this fixed frequency range is somewhat artificial. As can be seen in Fig. 9, Region I for the $Tl_2SeAs_2Te_3$ glass extends from dc to 10^{10} Hz, and there is no Region II. Region II for As_2Se_3 extends from a few Hz to well into the microwave range. Since the dc conductivity (Region I) and the band edge absorption (Region V) have been discussed extensively elsewhere, they will not be discussed here. Region III has been discussed in the previous section on structural properties.

CONDUCTIVITY IN REGION II:

Several physical mechanisms have been suggested to explain the rising conductivity observed in a large number of solids which are disordered in some way. These mechanisms include electronic hopping, tails of vibrational bands and the Maxwell-Wagner effect(42). Although current experimental results appear to favor the hopping mechanism, the available evidence is not yet conclusive. The nature of the problem is illustrated in Fig. 10 which shows the frequency dependence of the room temperature conduction for As_2Se_3 measured in a number of laboratories(10,43-47). The large differences at low frequencies may well be due to contamination by common electrode materials (Cu, Au and Ag) which dissolve easily in the chalcogenides(48). The uppermost curve (ref. 47), is, in fact, for a sample intentionally doped with 0.2% Ag.

The discrepancy among the microwave measurements is much smaller (only one order of magnitude). However, critical differences remain. For example, the data of Lakatos and Abkowitz(46) show a saturation or peak in the conductivity in the range 10^9 to 10^{10} Hz, while the data of Crevecoeur and De Wit(43) and Taylor, Bishop, and Mitchell(10) have slopes in the microwave region of approximately the same value as at lower frequencies. Precise measurements in this range are particularly important since the three possible physical mechanisms lead to conductivities with quite different behavior at high frequencies. Hopping conductivity would exhibit a maximum and then decrease at higher frequencies(49), vibrational tails would increase monotonically to the vibrational bands; and the Maxwell-Wagner conductivity would saturate and approach a plateau(42). Further experimental measurements of the frequency and temperature dependences of the conductivity for well characterized samples are clearly needed in the microwave and millimeter wave regions.

CONDUCTIVITY IN REGION IV:

A frequency independent (approximately) and thermally activated optical absorption in the region between the vibrational absorption bands and the optical band edge (see Fig. 9) has been reported(50) for glassy and liquid $Tl_2SeAs_2Te_3$. As seen in Fig. 11, the room temperature activation energies for the dc and infrared conductivities are equal ($\Delta E = 0.35$ eV) to within experimental error and have a value of approximately one-half the optical energy gap ($E_g \sim 0.75$ eV). The equivalence of the activation energies for the infrared and dc conductivities is strong evidence that the dc and infrared conduction mechanisms both involve carriers thermally activated to extended states in the conduction and valence bands. The relative frequency independence of the infrared conductivity (free carrier absorption) implies extremely short relaxation times τ ($\omega\tau < 1$ for $\omega < 10^{14}$ Hz, where ω is the angular frequency of the radiation).

A similar temperature dependent optical absorption has been observed(51) and analyzed(50), in liquid As_2Se_3 at high temperatures. In this case the conductivity does exhibit a pronounced frequency dependence which could arise from a tail in the band edge optical absorption superposed on the free carrier absorption. Analysis of the As_2Se_3 data likewise yields a value for the infrared activation energy in good agreement with the dc value(50). This equivalence again supports the identification of this process in As_2Se_3 as free carrier optical absorption.

Although the dc and infrared activation energies are equal for both $Tl_2SeAs_2Te_3$ and liquid As_2Se_3 the magnitudes of the conductivities differ by a factor β ($\beta = \sigma_{ir}/\sigma_{dc}$)

which can be quite large ($Tl_2SeAs_2Te_3$, $\beta \simeq 8$ at 300°K; As_2Se_3, $\beta \simeq 20$ at 800°K). The physical origin of the factor β has not been identified. Possible mechanisms include strong in-plane electron-phonon coupling which leads to a large polaronic effective mass, or inhomogeneous electronic conductivity which gives rise to a generalized Maxwell-Wagner effect.

The fact that the vibrational and electronic properties of these glasses do not change noticeably as the temperature passes through T_g suggests that these properties are determined by the in-layer or in-chain bonding and that the layers or chains themselves may be ordered over a significant distance.

ACKNOWLEDGEMENTS:

The authors thank D. Treacy for the use of his infrared reflectivity data on crystalline As_2Se_3 prior to publication.

REFERENCES

1. W.H. Zachariasen, J. Amer. Chem. Soc. 54, 3841 (1932).

2. B.E. Warren, Sov. Phys. Cryst. 16, 1106 (1972) [Kristallografiya 16, 1264 (1971)].

3. J.H. Konnert and J. Karle, Nature (Physical Science) 236, 92 (1972).

4. B.E. Warren, H. Krutter and O. Morningstar, J. Am. Ceram. Soc. 19, 202 (1936).

5. P.C. Taylor, S.G. Bishop and D.L. Mitchell, Phys. Rev. Letters 27, 414 (1971).

6. S.G. Bishop and P.C. Taylor, Phys. Rev. B, in press.

7. Mark Rubinstein and P.C. Taylor, Phys. Rev. Letters 29, 119 (1972).

8. D.L. Mitchell, S.G. Bishop and P.C. Taylor, J. Noncryst. Solids 8-10, 231 (1972).

9. P.C. Taylor, S.G. Bishop and D.L. Mitchell, in Proceedings of the International Conference on Phonons, Rennes, France (1971), p. 197.

10. P.C. Taylor, S.G. Bishop and D.L. Mitchell, Solid State Commun. 8, 1783 (1970).

11. L.B. Zlatkin, Yu. F. Markov, A.I. Stekhanov and M.S. Shur, J. Phys. Chem. Solids 31, 567 (1970).

12. G. Lucovsky, Phys. Rev. B6, 1480 (1972).

13. I.G. Austin and E.S. Garbett, Phil. Mag. 23, 17 (1971).

14. L.B. Zlatkin and Yu. F. Markov, Phys. Stat. Solidi (a) 4, 391 (1971).

15. P.C. Taylor, S.G. Bishop, D.L. Mitchell and D. Treacy, Bull. Am. Phys. Soc. (1973) in press, and to be published.

16. M. Born and K. Huang, Dynamical Theory of Crystal Lattices (Oxford Univ. Press, London, 1954) p 87.

17. D. Treacy and P.C. Taylor, to be published.

18. R. Zallen, M.L. Slade and A.T. Ward, Phys. Rev. B3, 4257 (1971).

19. G. Carron, Acta Crystallogr. 16, 338 (1963).

20. A. Hrubý and L. Štourač, Mat. Res. Bull. 6, 465 (1971).

21. P.C. Taylor, L.A. Rauber, S.G. Bishop and D.L. Mitchell, Bull. Am. Phys. Soc. 17, 114 (1972) to be published.

22. E.J. Felty, G. Lucovsky and M.B. Myers, Solid State Commun. 5, 555 (1967).

23. R.C. Keezer, G. Lucovsky and M.L. Slade, Solid State Commun. 6, 765 (1968).

24. G. Locovsky, M.H. Brodsky and E. Burstein, in Localized Excitations in Solids (R.F. Wallis, ed.) Plenum Press, New York (1968), p. 592.

25. B.T. Kolomiets and V.P. Pozdnev, Sov. Phys. Solid State 2, 23 (1961) [Fiz. Tverd. Tela 2, 28 (1960)].

26. G. Lucovsky and R.M. Martin, J. Non-Cryst. Solids 8-10, 185 (1971).

27. G. Gee, Trans. Faraday Soc. 48, 515 (1952).

28. S.V. Nemilov, Sov. Phys. Solid State 6, 1075 (1964) [Fiz. Tverd. Tela 6, 1375 (1963)]

29. K. Ueberreiter and H. Orthmann, Koll. Z. 123, 84 (1951).

30. R.E. Drews, R.L. Emerald, M.L. Slade and R. Zallen, Solid State Commun. 10, 293 (1972).

31. R. Zallen, R.E. Drews, R.L. Emerald and M.L. Slade, Phys. Rev. Letters 26, 1564 (1971).

32. A.A. Vaipolin and E.A. Porai-koshits, Sov. Phys. Solid State 5, 178 (1963) [Fiz. Tverd. Tela 5, 246 (1963)].

33. J.H. Konnert, J. Karle and G.A. Ferguson, Science 179, 177 (1973), and to be published.

34. N.A. Goryunova, B.T. Kolomiets and V.P. Shilo, Soviet Phys. Solid State 2, 258 (1960).

35. H.S. Gutowsky and B.R. McGarvey, Phys. Rev. 91, 81 (1953).

36. S.S. Flaschen, A.D. Pearson and W.R. Northover, J. Am. Ceram. Soc. 43, 274 (1960).

37. S.G. Bishop and P.C. Taylor, Solid State Commun. 11, 1323 (1972).

38. S.G. Bishop and P.C. Taylor in *Proceedings of the 11th International Conference on the Physics of Semiconductors*, Warsaw, Poland, 1972, to be published.

39. S.G. Bishop, P.C. Taylor and D.L. Mitchell, J. Noncryst. Solids 8-10, 106 (1972).

40. H.A. Resing, J. Chem. Phys. 43, 669 (1965).

41. P.C. Taylor and Mark Rubinstein, Bull. Am. Phys. Soc. (1973), to be published.

42. L.K.H. Beek, Progress in Dielectricts, Ed. J.B. Birks (CRC Press, Cleveland, 1967) p. 69.

43. C. Crevecour and H.J. de Wit, Solid State Commun. 9 (1971) 445.

44. E.B. Ivkin and B.T. Kolomiets, J. Non-Crystalline Solids 3 (1970) 41.

45. M. Kitao, F. Araki and S. Yamada, Phys. Status Solidi 37 (1970) K 119.

46. A.I. Lakatos and M. Abkowitz, Phys. Rev. B3 (1971) 1791.

47. A.E. Owen and J.M. Robertson, J. Non-Crystalline Solids 2 (1970) 40.

48. M.H. Brodsky and D. Turnbull, Bull. Am. Phys. Soc. 16, (1971) 304.

49. N.F. Mott, Festkörperprobleme 9, (1969) 22; M.

Pollak, Phil. Mag. 23 (1971) 519.

50. D.L. Mitchell, P.C. Taylor and S.G. Bishop, Solid State Commun. 9 (1971) 1833.

51. J.T. Edmond, Brit. J. Appl. Phys. 17, (1966) 979.

TABLE I

GAUSSIAN LINESHAPE OPTICAL PARAMETERS FOR SELECTED VITREOUS MATERIALS

Glass	ν_o (cm^{-1})	Γ^a (cm^{-1})	γ^b (cm^{-1})	$\sigma_{max}{}^c$ (Ω-cm)$^{-1}$	$\Delta\epsilon^f$
Se	493	32.5	$\lesssim$ 10	0.06	--
	365	d	d	0.06	--
	254	~13	d	0.99	d
	235	d	d	0.58	d
	135	~15	d	0.55	d
	120	d	d	d	--
	95	d	d	0.32	d
As_2Se_3	213	13	$\lesssim$ 5	27.9	0.79
	252	15	$\lesssim$ 5	9.3	0.30
	156	12	d	0.7	0.03
	102	19	d	3.2	0.57
$Tl_2SeAs_2Se_3$	255	20	$\lesssim$10	11.9	
	213	25.5	d	19.3	
	86	53	d	12.6	
$Tl_2SeAs_2Te_3$	246	18.5	$\lesssim$10	6.6	0.39
	189	29	d	7.1	
	80	47.5	d	17.2	
$As_{55}Te_{45}$	235	17	d	3.4	d
	183	19	d	1.1	d
	102	24	d	5.3	d
	70	32	d	1.8	d
SiO_2	1070	$\lesssim$10	32	196	0.16
	800	$\lesssim$10	50	28.1	0.07
	450	$\lesssim$10	80	70.8	0.84
$CdGeAs_2$	~ 250	~125^e		~ 20	d

a Half width at 1/e peak value.
b Full width at half height.
c Peak value of conductivity.
d Not measurable due to overlapping absorptions.
e Full width at half height, line shape not determined.
f Contribution of absorption peak to low frequency dielectric constant.

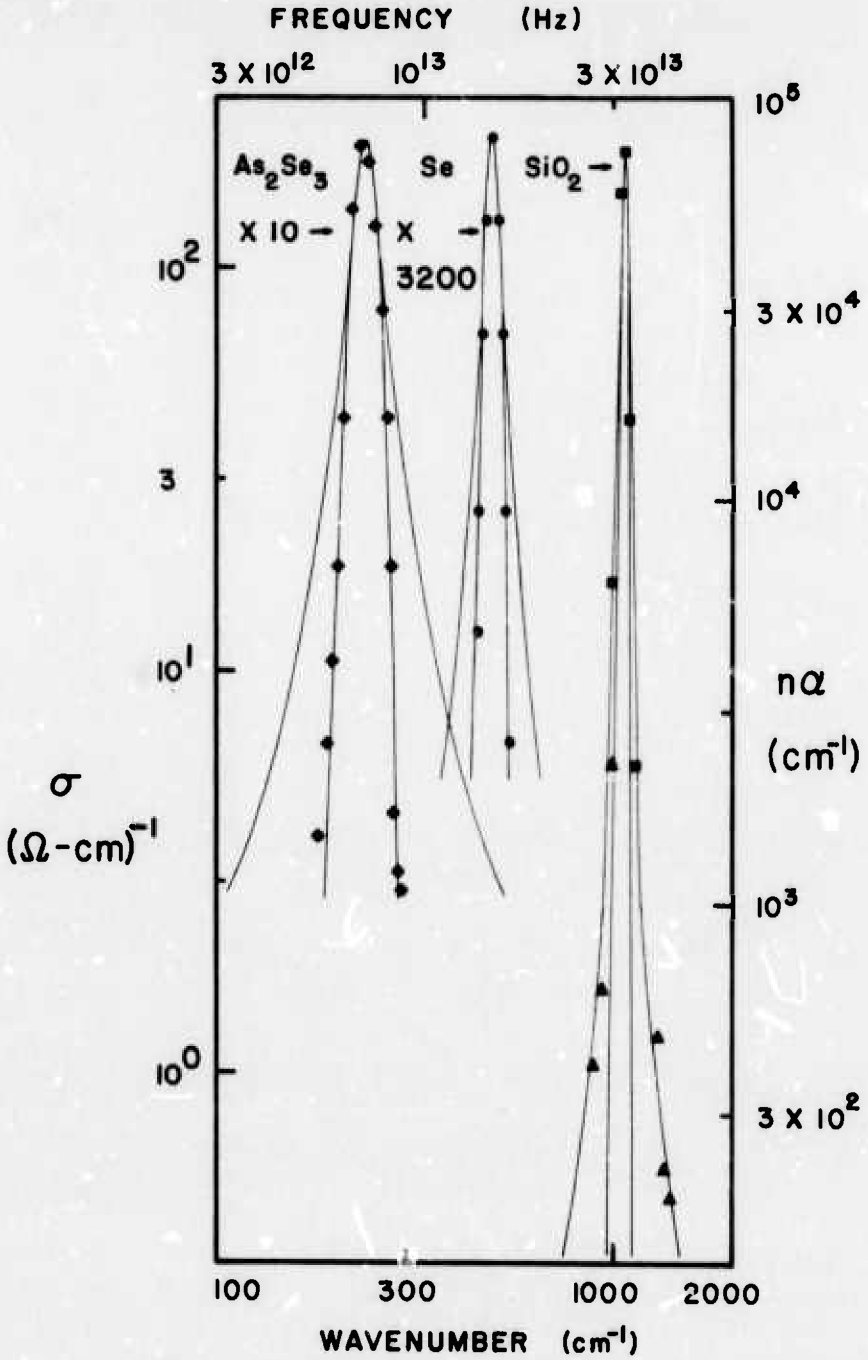

Fig. 1 - Conductivity σ (or index of refraction times absorption constant $n\alpha$) versus wave number for three representative absorption peaks in glasses based on one-dimensional (Se), two dimensional (As_2Se_3) and three-dimensional (SiO_2) compounds. Steeply falling solid lines are Gaussian lineshapes; less steeply falling solid lines represent Lorentzian lineshapes. Both lineshapes are fit to the width of the absorption at half height. (After ref. 9.)

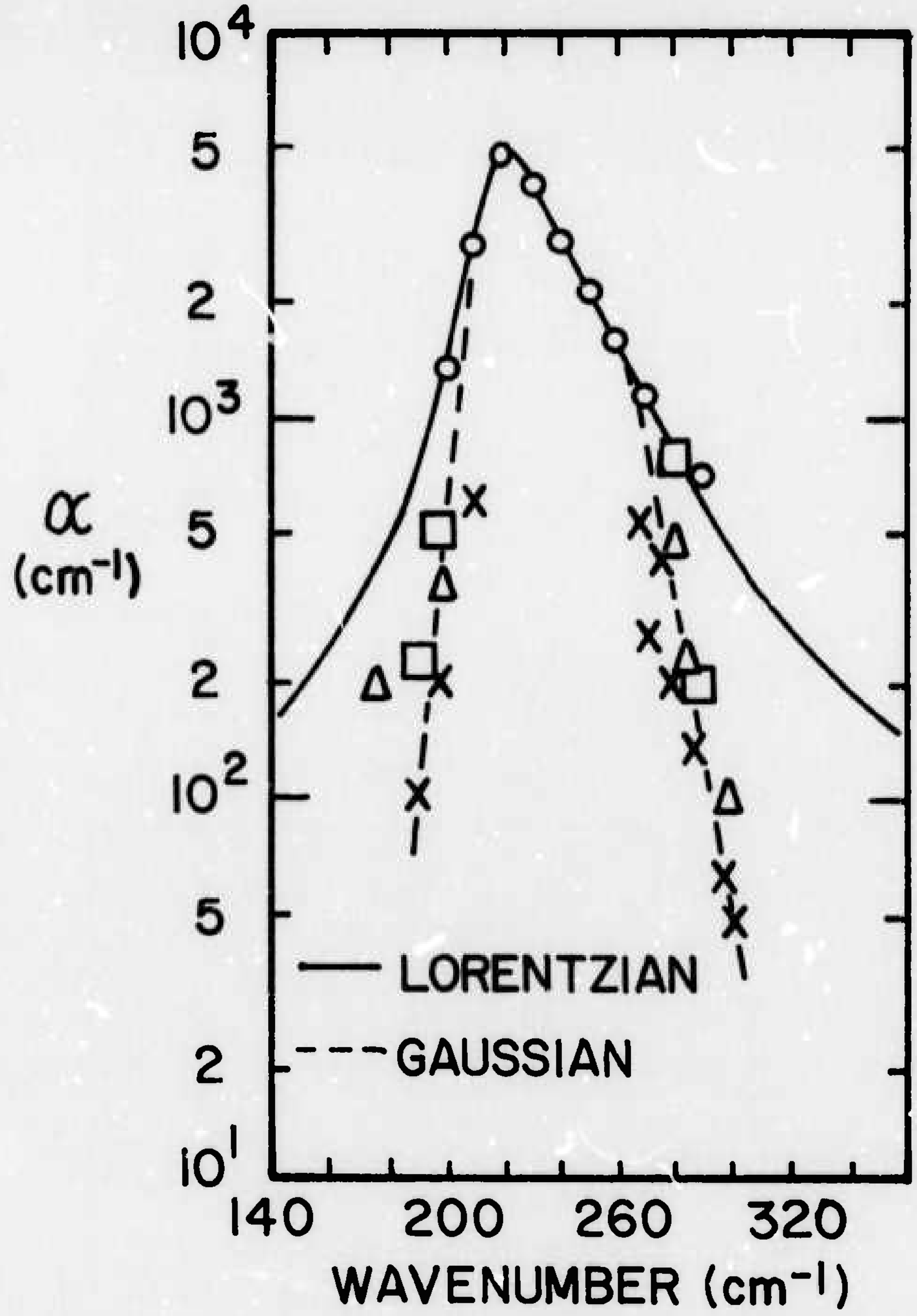

Fig. 2 - Absorption constant (on a log scale) versus wavenumber in glassy As_2Se_3 as abstracted from transmission data of the following sources: circles from ref. 12 on thin evaporated films, squares from ref. 11 on bulk samples, triangles from ref. 13 on bulk samples and crosses from ref. 10 and the present work on bulk samples. The solid line is a fit using two Lorentzian oscillators (after ref. 12). The broken line is a fit using two Gaussian absorption peaks.

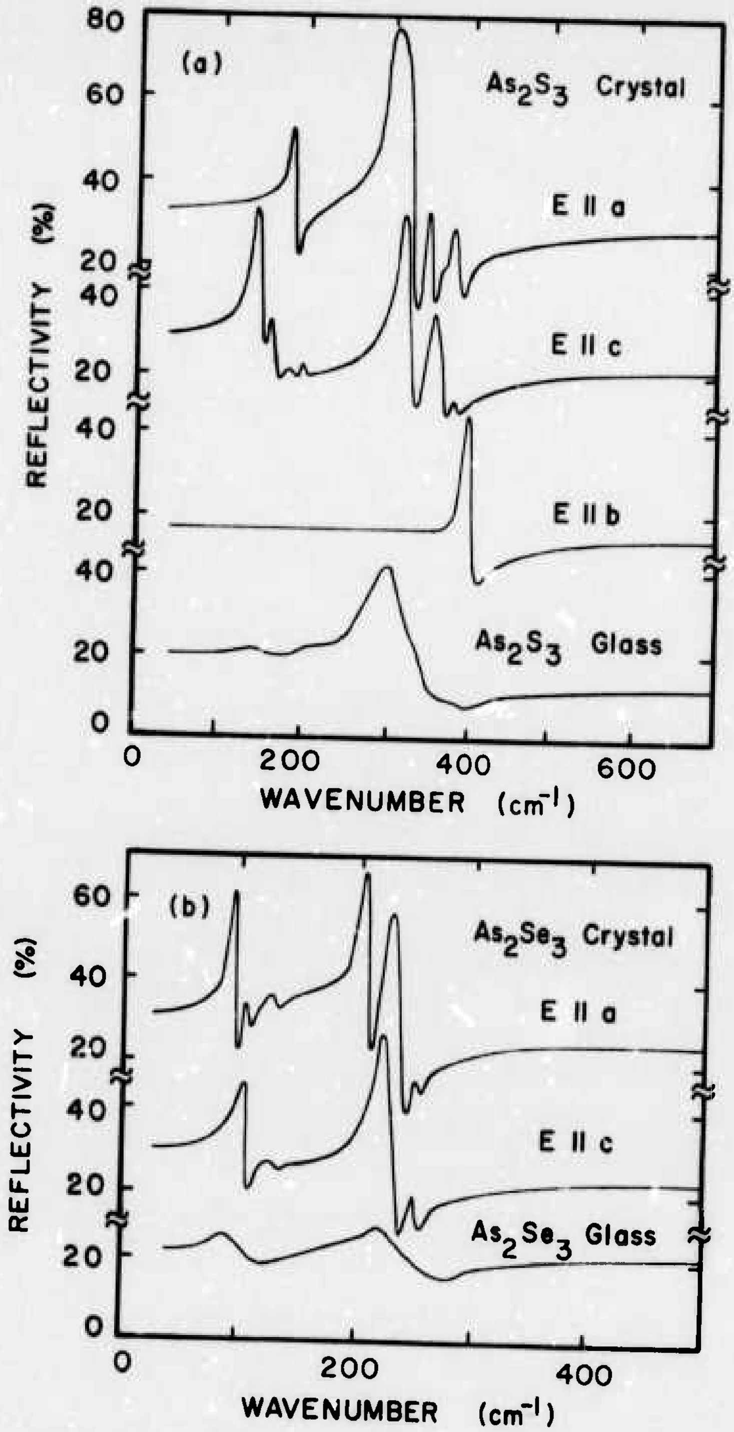

Fig. 3 - Comparison of the crystal and glass reflectivity spectra in (a) As_2S_3 and (b) As_2Se_3. The crystal data for As_2S_3 and As_2Se_3 are taken from refs. 17 and 18, respectively. The glass data are from refs. 22 and 10.

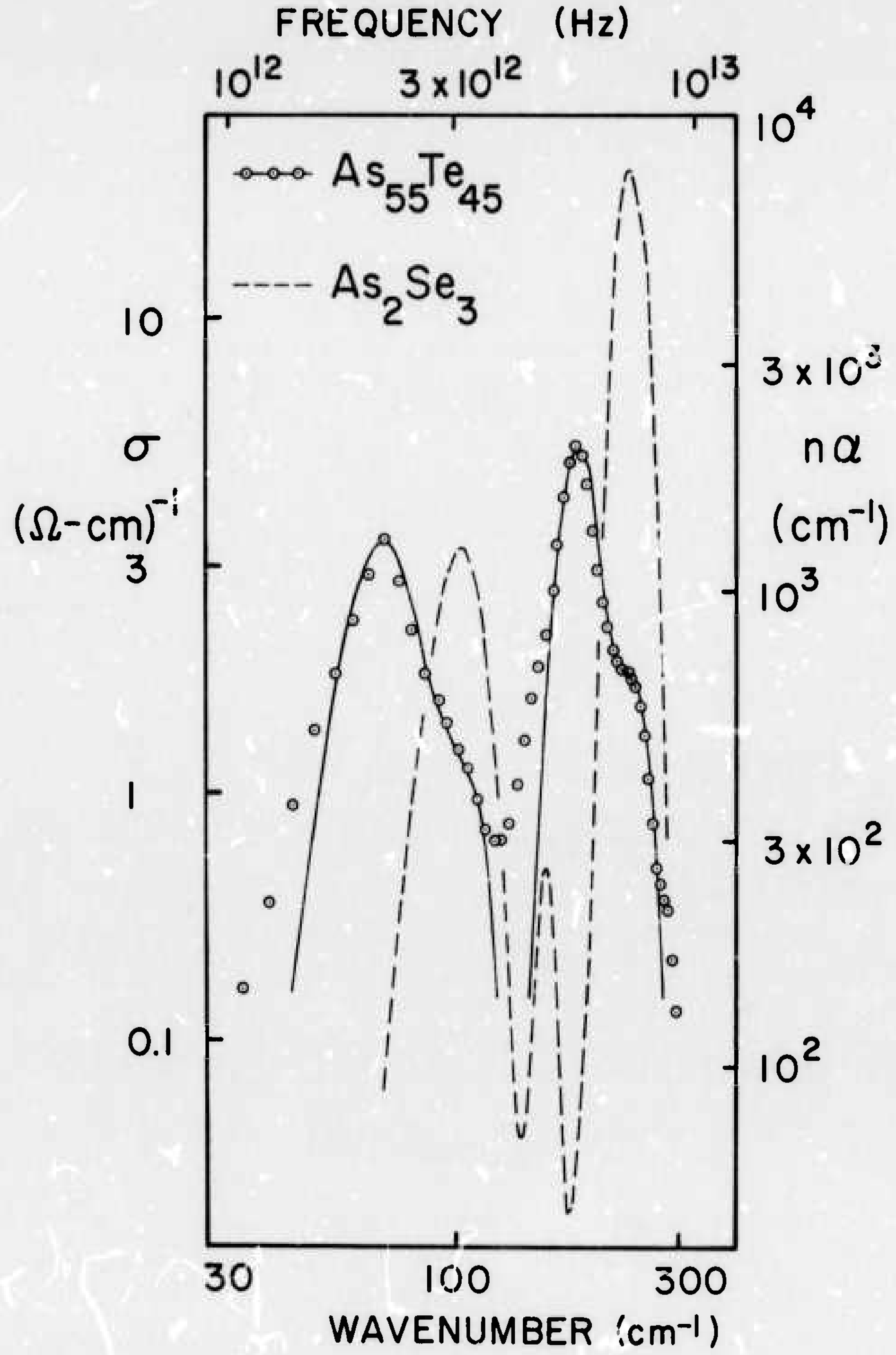

Fig. 4 - Absorption peaks in glassy $As_{55}Te_{45}$ and As_2Se_3 (log-log scale). The solid line is a fit to the data assuming Gaussian absorption peaks whose parameters are listed in Table I.

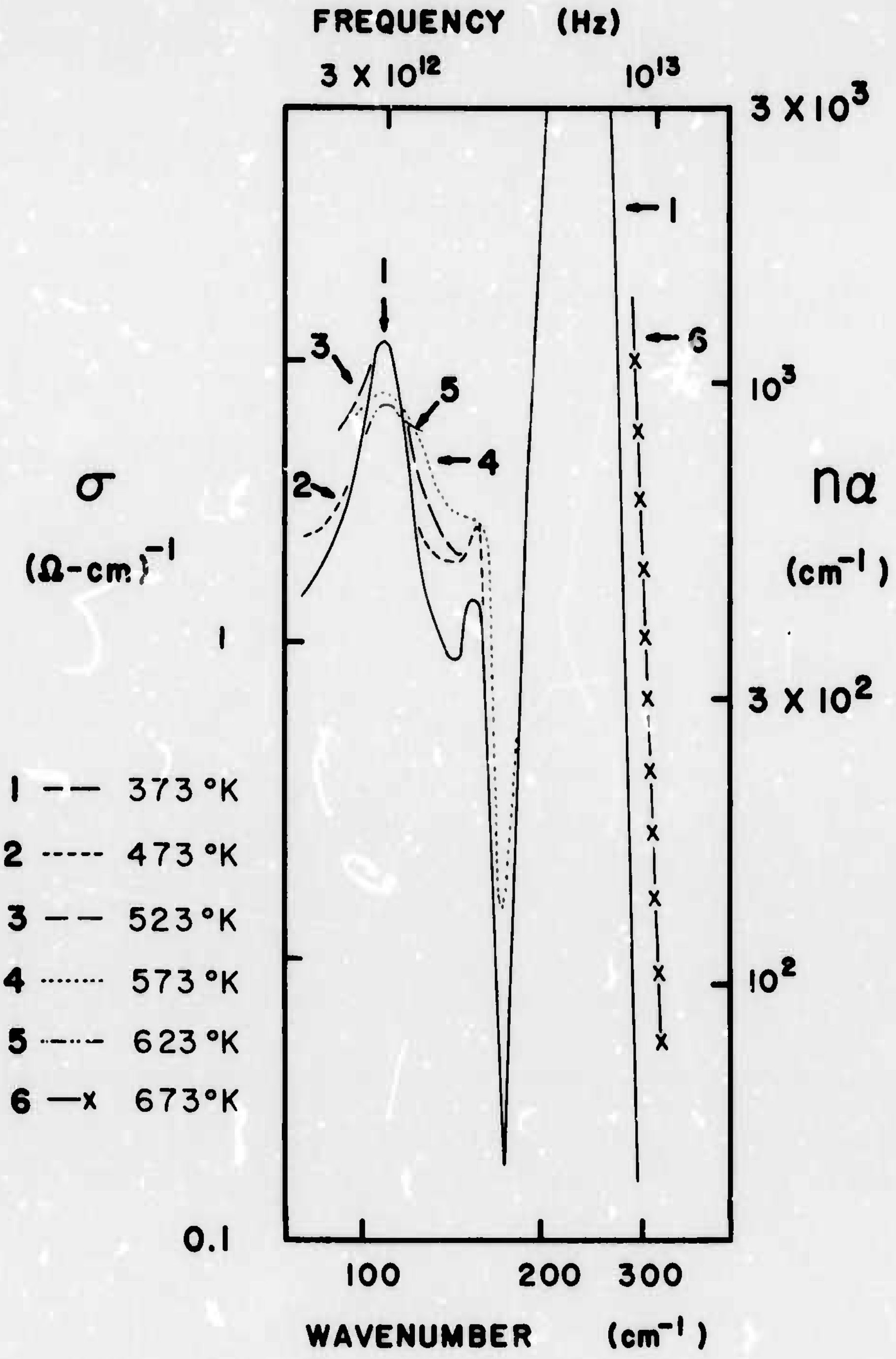

Fig. 5 - Temperature dependence of the absorption peaks (log-log scale) in glassy As_2Se_3 (after ref. 5). Data at 623° K extend only from 90 to 110 cm^{-1}; data at 673° K extend only from 290 to 305 cm^{-1}. At all other temperatures data extend from approximately 40 to 300 cm^{-1}.

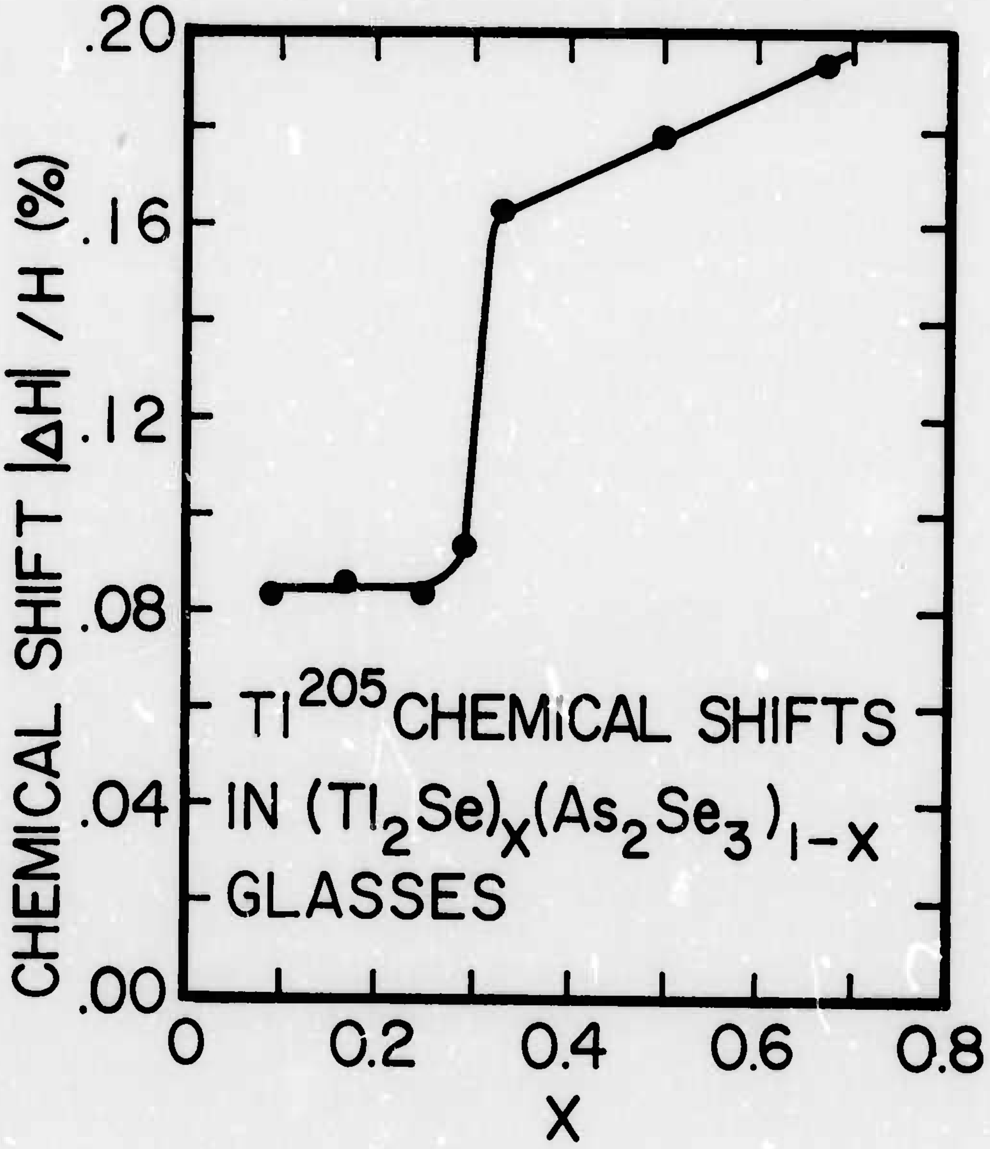

Fig. 6 - Magnitude of the Tl^{205} NMR chemical shift in $(Tl_2Se)_x$ $(As_2Se_3)_{1-x}$ glasses versus composition after ref. 6).

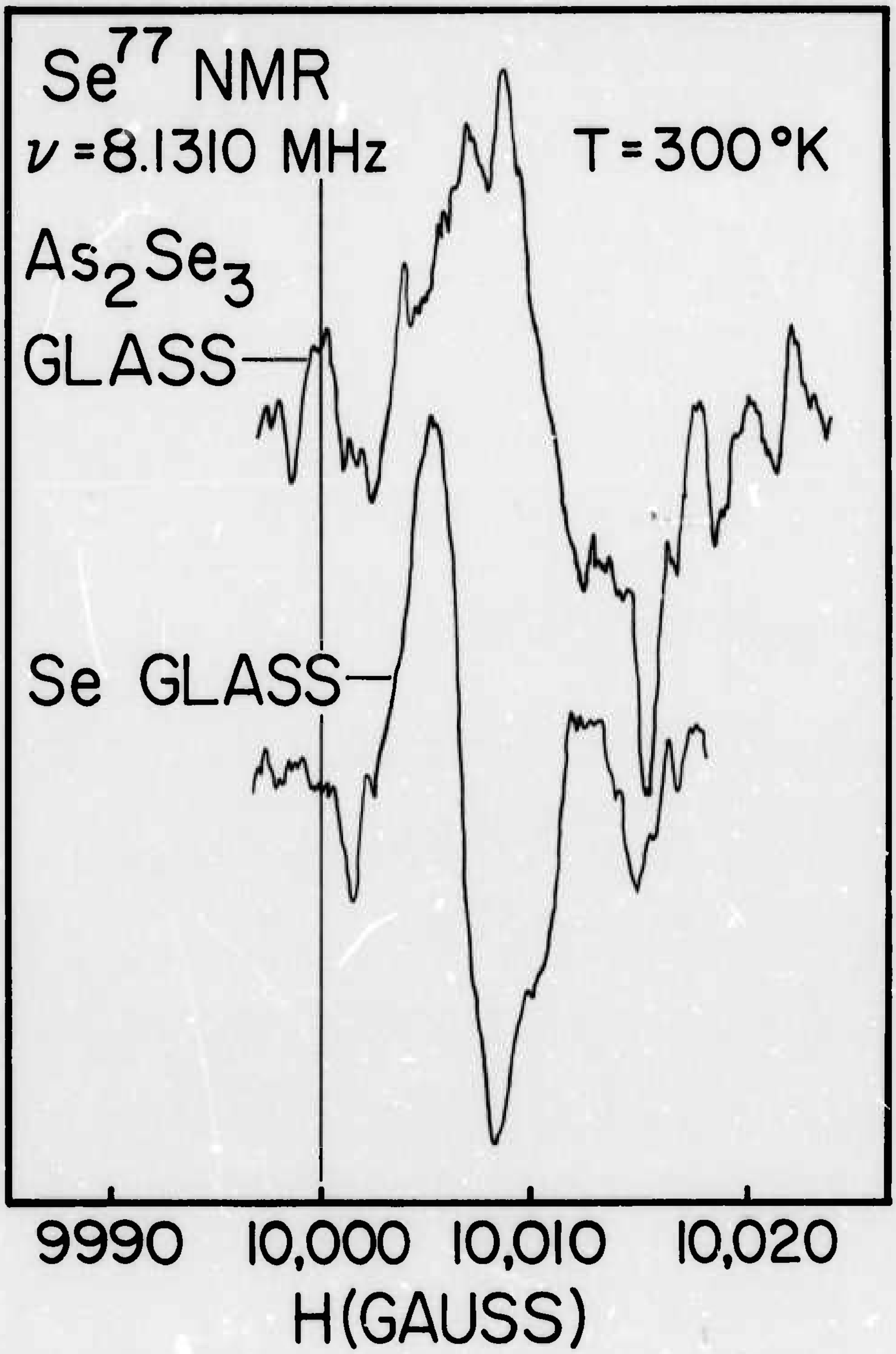

Fig. 7 - Se'' NMR spectra in solid vitreous As_2Se_3 and in molten Se. The vertical line indicates the Se^{77}NMR in an H_2SeO_3 reference sample[35] (after ref. 38).

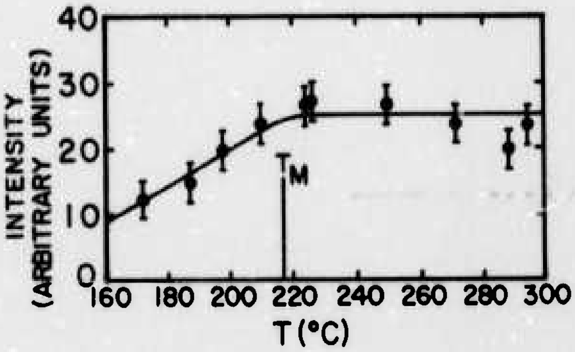

Fig. 8 - Intensity of the narrow Se^{77} NMR line in Se as a function of temperature (after ref. 38). The intensity has been corrected for the temperature dependence of the population distribution in the nuclear Zeeman levels.

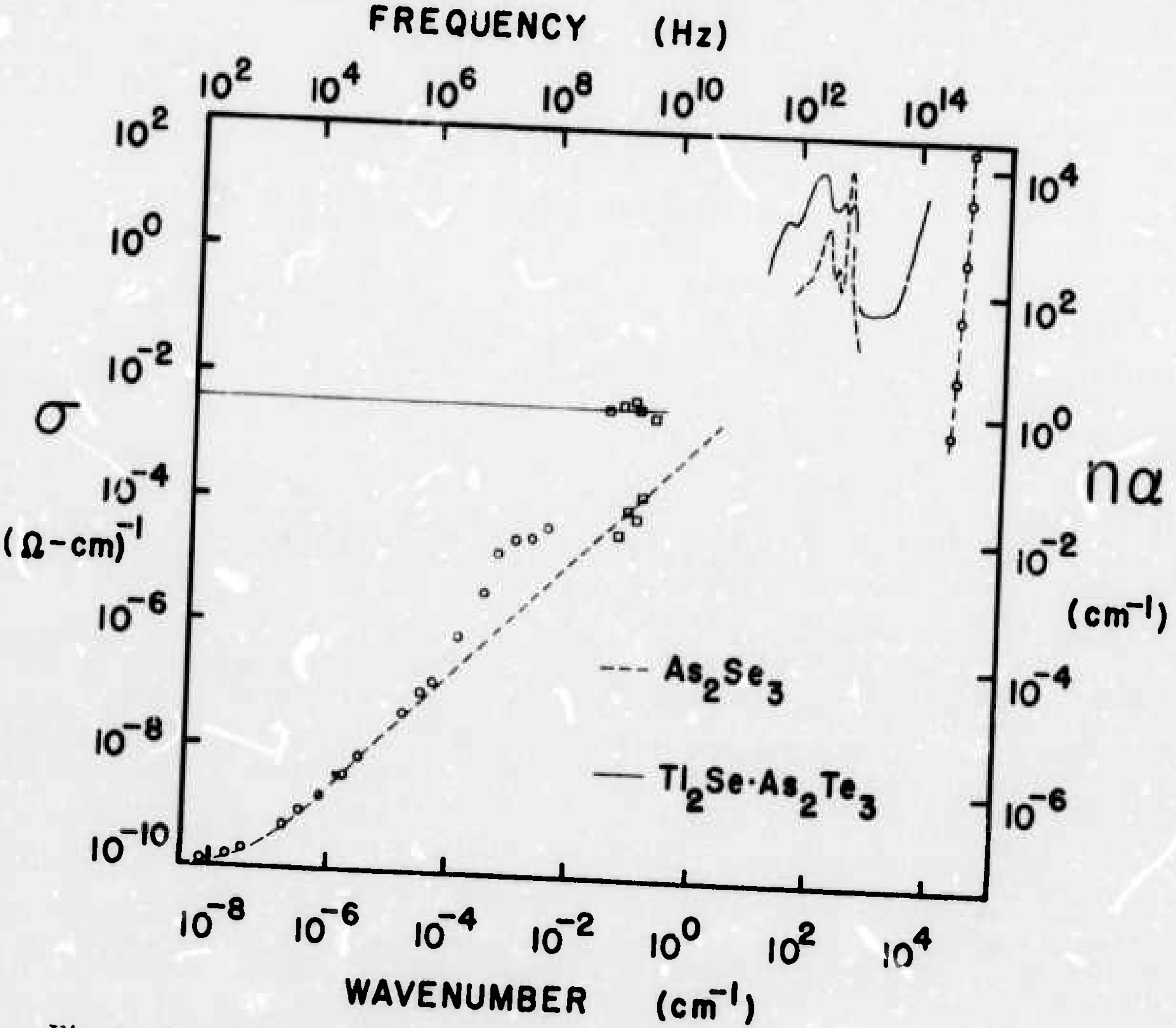

Fig. 9 - Room Temperature conductivity in vitreous As_2Se_3 (dashed curve) and $Tl_2SeAs_2Te_3$ (solid curve) from 10^2 to 10^{15} Hz. The data from 10^2 to 10^8 Hz for As_2Se_3 are the bridge measurements of Owen and Robertson[47]; those from 1 to 6 GHz are slotted wave guide measurements[10]; those from 10^{12} to 10^{15} Hz are reflection and transmission results[10].

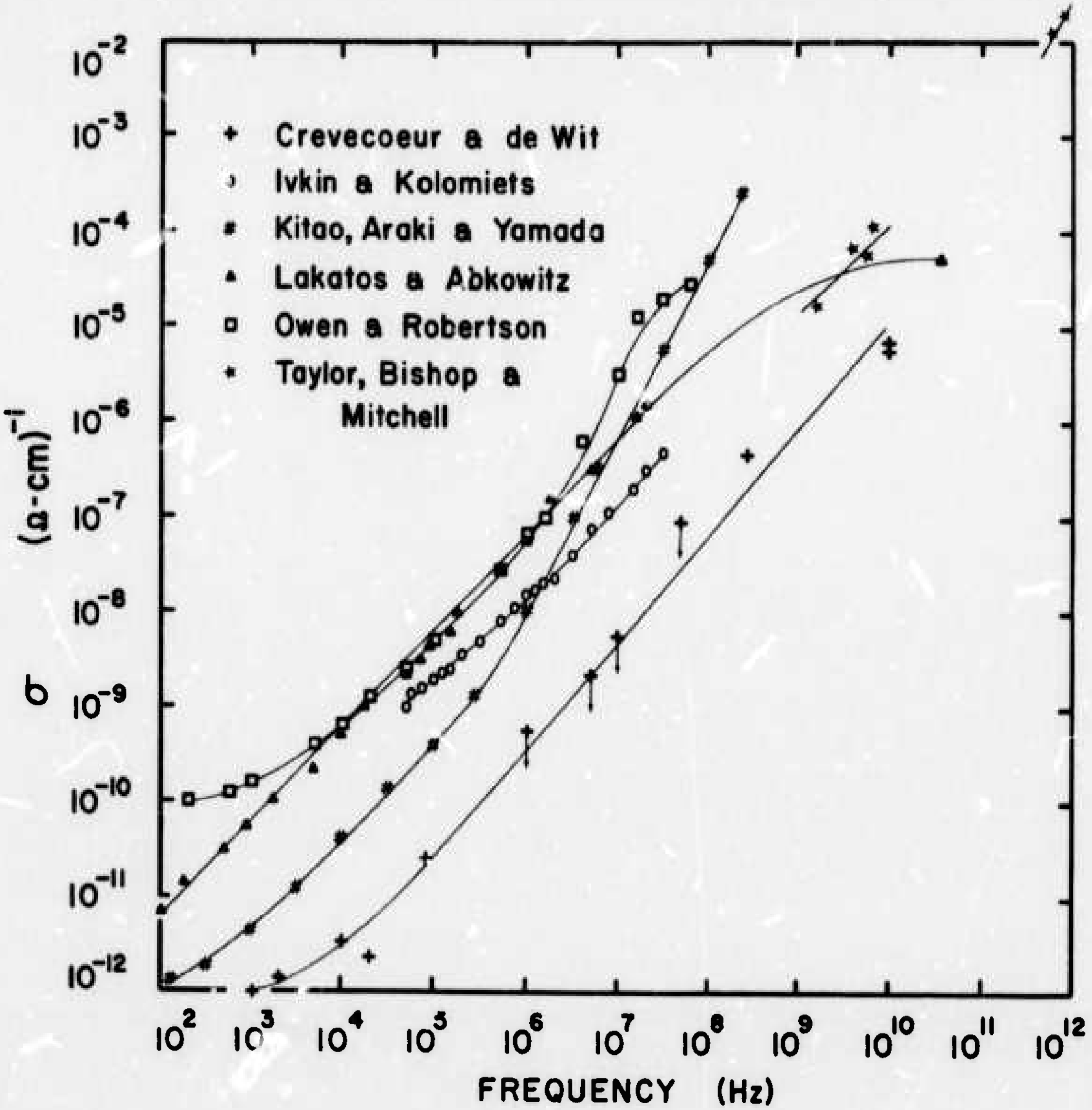

Fig. 10 - A compendium of room temperature conductivity measurements for vitreous As_2Se_3 from 10^2 to 10^{12} Hz.

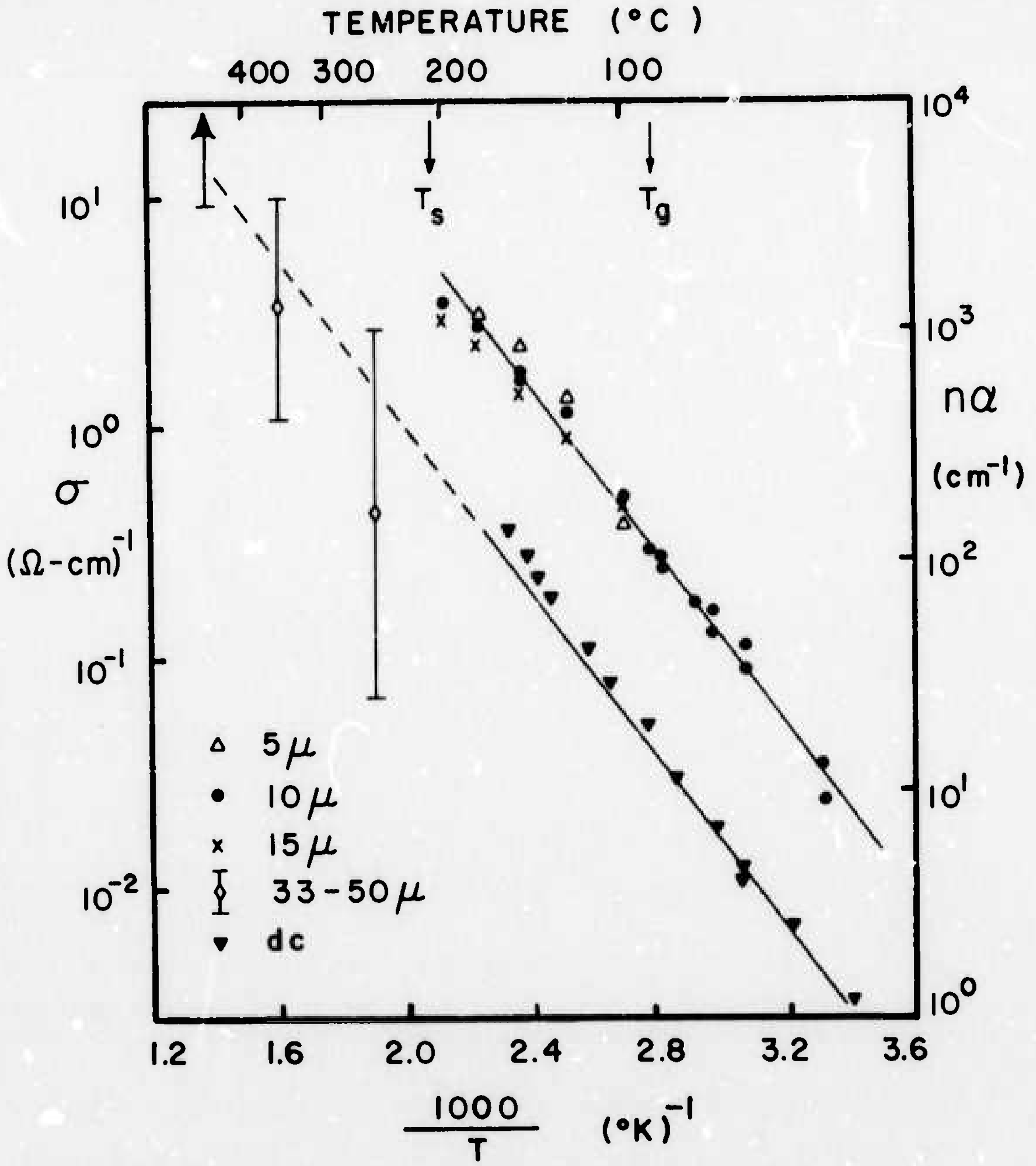

Fig. 11 - Conductivity at dc and optical (infrared) frequencies versus reciprocal temperature in glassy and liquid $Tl_2SeAs_2Te_3$[50]. The open triangles, circles and crosses represent data taken at 5, 10 and 15μm (2000, 1000 and 666 cm^{-1}) respectively. The solid triangles represent dc measurements. The slope of the two solid lines corresponds to an activation energy $\Delta E = 0.35$ eV. Sample thickness varied from 25 to 860 μm.

THE EFFECTS OF ION IMPLANTATION ON THE STRENGTH OF FUSED SILICA

G.H. Sigel, Jr.

ABSTRACT

An investigation has been made into the possibility of using ion implantation to achieve high strength glass. Optical and ESR measurements have been made to study the radiation damage which accompanies the implantation. In spite of the shallowness of the ion penetration, biaxial tensile tests indicate a strength increase in fused silica following irradiation.

INTRODUCTION

In many ways fused silica resembles the ideal, isotropic elastic solid. Failure is believed to occur almost entirely by brittle fracture with little or no plastic flow taking place. Theoretically SiO_2 glass should exhibit a cohesive strength in excess of 10^6 psi, but in practice rarely approaches this value. Griffith(1) was the first to account for this discrepancy in a quantitative manner. It was postulated that failure originated at the glass surface because of the presence of microscopic flaws and cracks which can concentrate the stress. The specimen fails when stress at the crack tip exceeds the cohesive strength of the material. The successful strengthening of glasses depends then on the removal and/or control of these surface flaws.

One of the most successful methods for controlling propagation of surface cracks has been the surface compression strengthening technique. Cracks normally propagate inward from the glass surface at right angles to the maximum tensile stress. By placing the surface in compression, the surface flaws are pushed closed and crack tip stresses are reduced. This technique can greatly increase the strength of a glass. Thermal tempering(2) chemical ion exchange(3-5), surface cladding, surface crystallization(6) are among the specific techniques which have been utilized.

One method that had not been investigated which seemed to hold some promise was implantation of ions into the glass surface using high energy accelerators. The object was to force as many ions as possible into the surface, thereby creating a large surface compressive stress. The method has several obvious advantages: 1) A very high concentration ($10^{20}/cm^3$) can be stuffed into the surface, 2) a wide lattitude of species can be implanted ranging from protons to inert gases, 3) any host glass can be used, which is not the case for example with ion exchange, and 4) the profile can be controlled rather precisely by the variation of the accelerating potential. On the minus side for the technique is the shallowness of the penetration depth (a few microns) and the possibility of a degradation in strength due to radiation damage. The implanted layer tends to be highly damaged since the ions lose energy both by ionization and nuclear collisions. Linhard et al(7) have developed the so called LSS theory to explain the energy loss of high energy ions travelling through a material. Because of the high defect densities, both optical and ESR spectroscopy can be utilized to study the radiation centers in a layer of a few microns.

In the present work fused silica samples have been implanted with boron, nitrogen and neon ions. The nature of the radiation damage was determined, and tensile strength measurements were made using both three point bending and biaxial 3 ball and piston techniques.

EXPERIMENTAL

Suprasil, Infrasil and GE 125 fused silica were used in the investigation. Samples were both disks and rectangles of 1 mm thickness.

Irradiations were performed using both a small 60-kV and the NRL 5-mV Van de Graaff accelerator. On the larger samples, the beam spots were electrostatically scanned over the samples to obtain uniform irradiations. Surface charge buildup which can produce crazing of a dielectric surface was eliminated by the production of secondary electrons at the target plate. Samples were implanted with 60 keV B^{11} and N^+, and 1 and 3 MeV $^{20}Ne^+$. Doses ranged from 2×10^{14} to

7.7×10^{16} ions/cm^2. Sample temperatures during irradiation were below 100°C. Since the irradiations could be made only on a space available basis, the ionic species used here were not chosen by design but were those available at the time.

Optical absorption measurements were performed with a Cary model No. 14 MR spectrophotometer and a McPherson Model 235 Seya Namioka vacuum ultraviolet spectrometer. ESR data was taken on a Varian E-9 spectrometer operating at X band with 100 kc modulation. All measurements were made at room temperature. A weak pitch sample was used as a calibration source to estimate the number of spins in the implanted samples.

Tensile strength measurements were made using a 3 ball and piston technique developed by Wachtman et al(8). The sample rests on three steel balls spaced equidistant and at 120° with respect to one another. The stress is applied from above by a steel piston centered on the sample. Specimens were silica disks of 1" diameter and 1/16" thickness. This technique eliminates edge effects and does not require critical flatness for test specimens. It can therefore produce reliable data when a limited number of specimens are available.

Conventional 3 point bending tests were made on the smaller specimens.

RESULTS AND DISCUSSION

A) Radiation Effects

The basic structural unit of fused silica is the SiO_4 tetrahedron. Two fundamental defect centers are thought to be produced in the radiation damage process of silica. The breaking of a strained Si-O results in the creation of two complementary centers (1) an electron trapped on a dangling sp^3 silicon orbital (the E' center)(9) and a hole trapped in a non-bonding p orbital of a singly bonded oxygen(10). The trapped electron center produces an optical absorption band near 5.9 eV, and in addition is paramagnetic. The hole absorption band lies at 7.6 eV near the absorption edge.

The damage expected in an ion implanted solid results from electronic and nuclear energy loss mechanisms associated with the particle slowing down as it penetrates the surface. The electronic stopping proceeds by ionization while nuclear stopping can produce displacements. Linhard et al(8) have developed a theory which provides a universal nuclear stopping power curve. From this curve one can obtain a theoretical profile of the implanted species in a given target material. In general nuclear stopping is most important at low energies while electronic stopping is linear with energy over a wide range. Profiles of the implanted species have not been determined experimentally for the implanted SiO_2 samples used in this study. However projected range corrections can be made on the LSS theory to estimate penetration depths. A 60 keV B^{11} implant into SiO_2 will lie in the first micron of the surface. A 2 MeV^{20}Ne ion will penetrate about 2 microns and a 3 MeV^{20}Ne$^+$about 4 microns.

High purity fused silica such as Suprasil exhibits very little permanent damage in the presence of ionizing radiation. Defect centers are only transient in nature, annihilating in a few milliseconds(11). Doses of 2.5×10^{15} 60 keV B^{11} ions/cm^2 and 2×10^{14} $^{20}Ne^+$ did not produce any measureable absorption bands in Suprasil at room temperature. There was however evidence of increased absorption near the ultraviolet edge. By choosing a less pure silica material (Infrasil), permanent damage was obtained from a dose of 1×10^{15} 60 keV B^{11} ions/cm^2. The optical absorption is shown in Figure 1. The band near 210 nm appears similar to the E' band although shifted slightly to higher energy. The shift may result from the high density of centers in the implanted layer. The higher energy band near 160 nm also seems to be present as a shoulder on the edge of the glass. The up turn shown in Figure 1 near 160 nm is probably an artifact resulting from the subtraction of two large numbers to obtain a small one.

ESR measurements confirm the presence of E' centers in the ion implanted Infrasil. Figure 2 shows the isotropic resonance measured following irradiation by 1.3×10^{15} 60 keV B^{11} ions/cm^2. The g value and line shape are almost identical to that observed for the E' resonance in bulk material. A rough estimate of the concentration in the sample was obtained by comparison with a weak pitch standard. A sample of 0.33 cm^2 cross section contained approximately 3×10^{12} spins. This indicates a defect center concentration in the 10^{18} -10^{17}/cm^3.

Annealing studies showed that temperatures of 400°C were sufficient to anneal out most of the damage. This temperature is sufficiently low to rule out the migration of the implanted species over large distances within the silica.

measurements have been made to measure a damage profile using diluted HF etching and the repeated measurement of the ESR signal of the E' resonance. The less pure material exhibits a profile characteristic of the combined electronic and nuclear stopping curve. This is consistent with the observation mentioned earlier that in pure material, broken bands reheal quickly because of the absence of permanent trapping sites, normally produced by impurities.

STRENGTH OF ION IMPLANTED SAMPLES

The initial irradiation of SiO_2 produces a change in density(12) which is responsible for a tensile stress on the surface. Density changes in neutron irradiated materials reach saturation at about 2×10^{20} nvt. It is this initial densification that makes ion implanted silica useful as optical waveguides. This is the equivalent dose of about 10^{15} ions/cm^2. Once this is achieved, the compressive stress produced by the ion stuffing will begin to dominate. In the present work doses up to 7.7×10^{16} $^{20}Ne^+$ were obtained.

The stresses produced by the 3 ball and piston biaxial flexure test at the lower center of the specimen can be calculated exactly by use of Equation 1 developed by Kirstein and Woolley.(13)

STRESS EQUATION FOR PISTON-ON-3-BALL BIAXIAL FLEXURE TEST

$$S = -3/4\pi \frac{p}{d^2} (x-y) \tag{1}$$

$$x = (1+\nu) \ln(\frac{b}{c})^2 + \frac{(1-\nu)}{2} (b/c)^2 \tag{2}$$

$$y = (1+\nu)\ 1+\ln(\frac{a}{c})^2 + (1-\nu) (\frac{a}{c})^2 \tag{3}$$

where S = tensile stress at center of lower surface, p = applied load, d = thickness of specimen, a = diameter of support circle, b = diameter of piston, c = diameter of specimen and ν = Poisson's ratio.

Samples of optically polished GE 125 silica were tested for strength prior to irradiation. Tests on 25 samples indicated an average failure stress of 2.8×10^4 psi with a fractional deviation of ±10.7%. The highest stress recorded was 3.6×10^4 psi.

Disks from the same batch of GE 125 silica were implanted with doses of $7 \times 10^{16}/cm^2$ 1MeV $^{20}Ne^+$ and 60 keV N^+. The average failure stress was 4.35×10^4 psi with a fractional deviation of ±13.5%. This represents an average strength increase of 52.4%.

Three point bending measurements on smaller pieces indicate average strength increases ranging from 16 to 130%. but these show much more scatter.

A control group of 25 samples which irradiated with low energy 2 keV electrons was observed to slightly decrease in strength with an average failure stress of 2.1×10^4 psi and a fractional deviation of ±16.1%.

Thus in spite of the initial contraction of SiO_2 to radiation, the shallow depth of the implant, and the radiation damage produced, there is some evidence that SiO_2 may be strengthened by ion implantation. More data is required to settle this question. At present, our access to the Van de Graaff accelerators is extremely limited, but plans have been made to perform a series of tests on Pyrex samples if machine time becomes available.

CONCLUSION

Optical and ESR measurements of ion-implanted fused silica have indicated the presence of both trapped electron and hole centers. The damage anneals at sufficiently low temperatures that the implanted profile should not be affected. Tensile stress measurements indicate some strength increase in ion implanted samples which have received doses in excess of 10^{15} ions/cm^2. Further experimental work is required to confirm this observation.

ACKNOWLEDGMENTS

The author is indebted to Dr. J. Comas, Dr. W. Lucke and Dr. P. Malmberg of the NRL Nuclear Sciences Division for the irradiation of the samples, and to R. Rice of the Chemistry Division for both the use of the mechanical testing facilities and many helpful discussions on the mechanical properties of glasses.

REFERENCES

1. A.A. Griffith, Phil. Trans. Roy. Soc. (London) 221A, (1920) 163.
2. G.M. Bartenev, J. Tech. Phys. USSR 19, (1949) 1423.
3. S.D. Stookey and J.S. Olcott, Advances in Glass Technology, Plenum Press, New York (1962) 400.
4. H.P. Hood and S.D. Stookey, U.S. Patent 2 779 136 (1957).
5. A.J. Burggraaf, Philips Research Reports, Supplements.
6. S.S. Kistler, J. Am. Ceram. Soc. 45, (1962) 59.
7. J. Lindhard, M. Scharff and H.E. Schiott, Kgl. Danske Videnskab. Selskab, Mat. Fys. Medd. 33, (1963) 14.
8. J.B. Wachtman, Jr., W. Capps and J. Mandel, paper presented at American Ceramic Society Pacific Coast Regional Meeting, San Francisco (1970).
9. R.A. Weeks, J. Appl. Phys. 27, (1956) 1376; Phys. Rev. 130, (1963) 570.
10. E.W. Mitchell and E.G. Paige, Phil. Mag. 1, (1956)1085.
11. G.H. Sigel, Jr. and D.L. Griscom, Bull. Am. Ceram. Soc. 48, (1969) 447.
12. W. Primak, L.H. Fuchs, and P. Day, Phys. Rev. 92, (1953) 1064; J. Am. Ceram. Soc. 38, (1955) 135.
13. A.F. Kirstein and R.M. Woolley, J. Res. NBS, 71C (1967) 1.

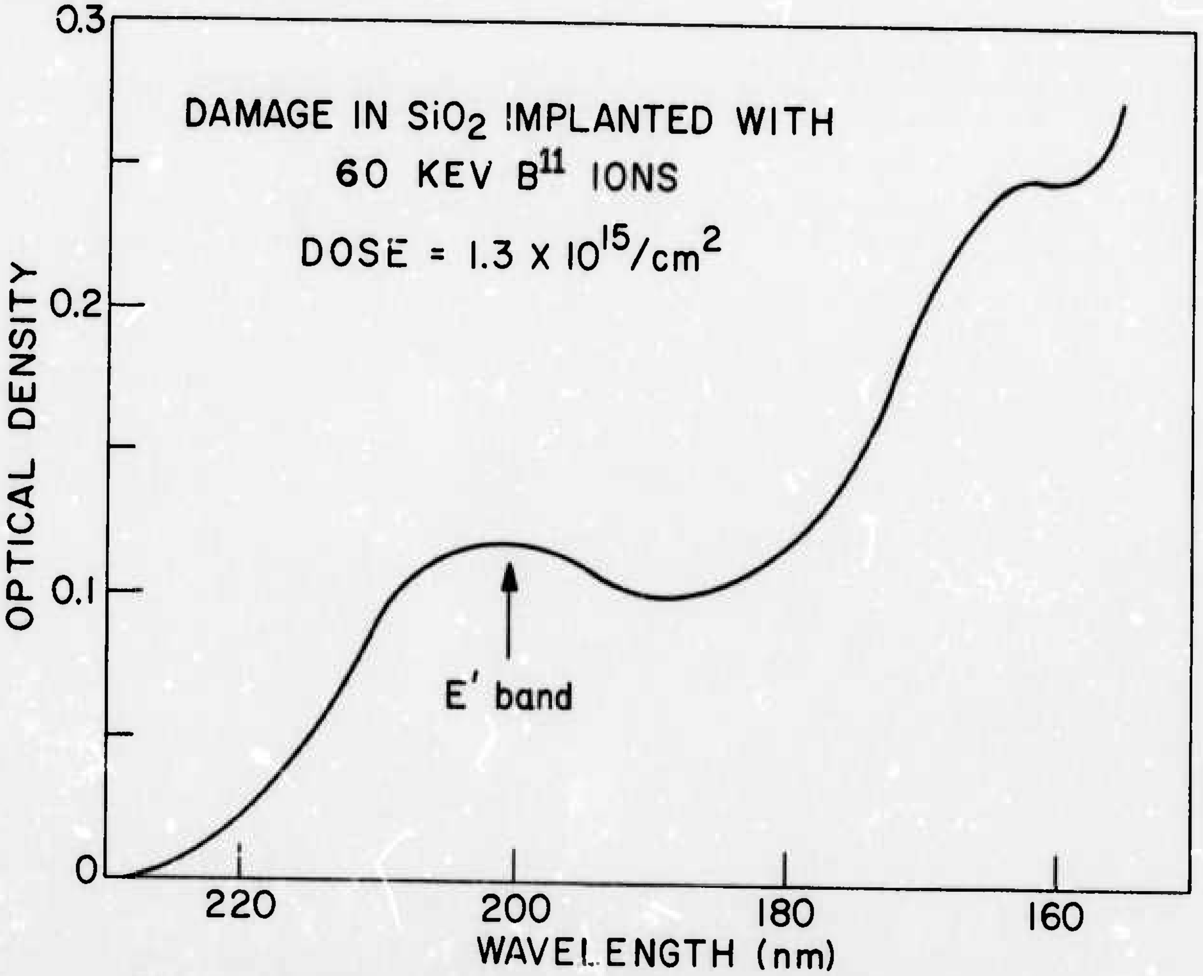

Fig. 1 - Optical absorption produced in Infrasil fused silica. High purity materials showed little measureable absorption at this dose level.

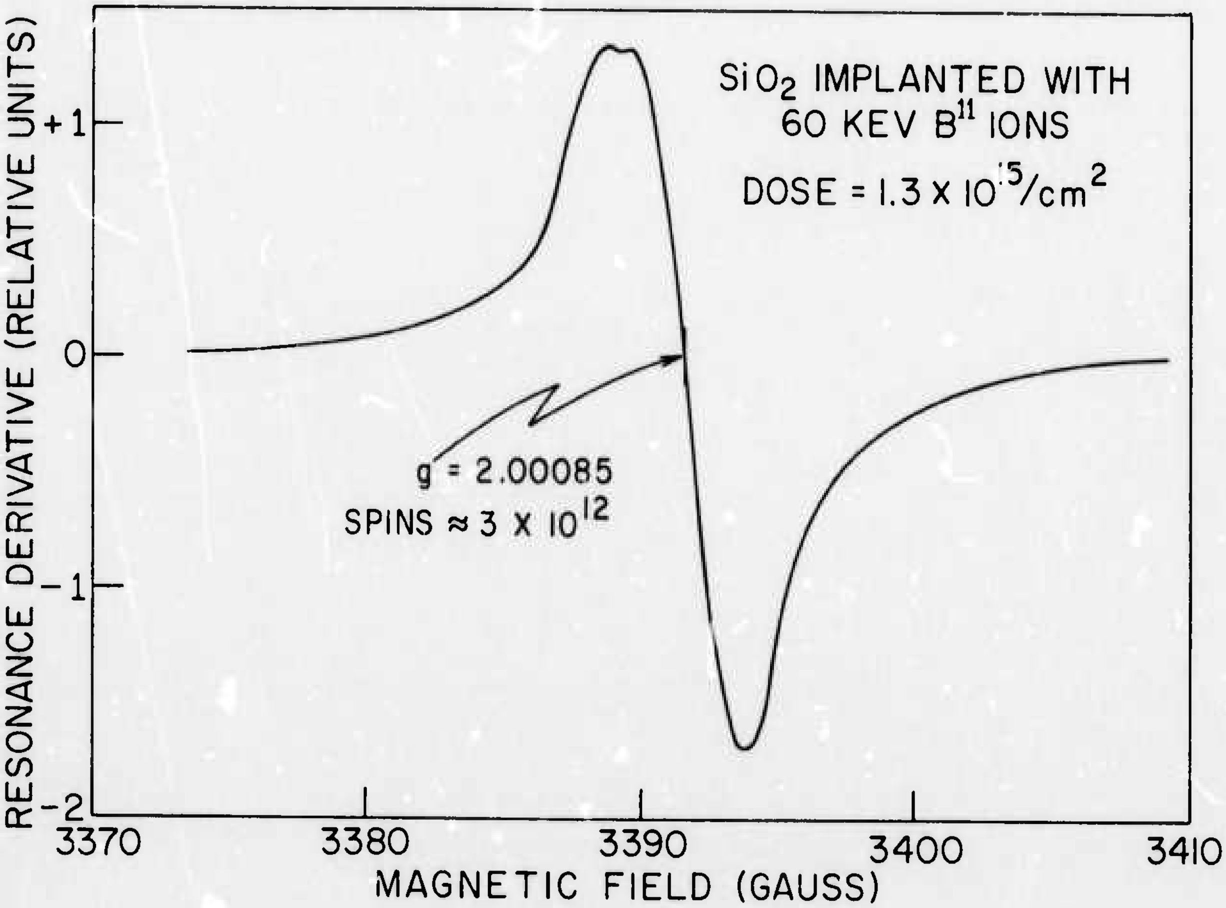

Fig. 2 - ESR signal sample as shown in Figure 1. The resonance is due to E' centers, electrons trapped on dangling silicon orbitals.